

# **Gravel-bed river behaviour: modelling and analysis of process feedbacks over spatio-temporal scales**

by

David Lawson Adams 

B.Env(Hons), The University of Melbourne, 2016

A THESIS SUBMITTED IN PARTIAL FULFILLMENT OF  
THE REQUIREMENTS FOR THE DEGREE OF

**DOCTOR OF PHILOSOPHY**

in

THE FACULTY OF GRADUATE AND POSTDOCTORAL STUDIES

(Geography)

THE UNIVERSITY OF BRITISH COLUMBIA

(Vancouver)

December 2022

© David Lawson Adams  2022

---

The following individuals certify that they have read, and recommended to the Universities for acceptance, the thesis entitled:

**Gravel-bed river behaviour: modelling and analysis of process feedbacks over spatio-temporal scales**

submitted by **David L. Adams** in partial fulfillment of the requirements for the degree of **Doctor of Philosophy in Geography** at the University of British Columbia (UBC), and **Doctor of Philosophy in Science** at the University of Melbourne (UoM).

**Examining Committee:**

Ian D. Rutherford, Professor, Geography, Earth & Atmospheric Sciences, UoM  
*Co-supervisor*

Brett C. Eaton, Professor, Geography, UBC  
*Co-supervisor*

Michael A. Church, Professor, Geography, UBC  
*University examiner*

John S. Richardson, Professor, Forestry, UBC  
*University examiner*

**Additional Supervisory Committee Members:**

Marwan A. Hassan, Professor, Geography, UBC  
*Supervisory Committee member*

# Abstract

Alluvial rivers arise through process interactions between water and a deformable boundary. These processes are poorly understood in gravel-bed rivers as they are difficult to measure, and are often described using simple conceptual models. Perhaps the simplest is the 'fluvial trinity' which describes the feedback between sediment transport, morphology, and hydraulics. There are two aspects of channel dynamics not explicated by this model: (1) the spatial distribution of channel feedbacks, and (2) interactions between processes across spatial-temporal scales. This thesis examined the effect of these two aspects using a recirculating stream table, from which conceptual frameworks and analytical tools were developed.

First, I modelled the response of a channel to successive increases in discharge and identified stage-dependent feedbacks that controlled the adjustment of the system towards a steady-state. Notably, at low flows, transport capacity was modulated by the spatial concentration of shear stress and channel deformation was controlled by larger-than-average grains. The following chapters focused on two components of the fluvial trinity. I combined recent advances in fluid dynamics, statistics, and remote sensing to estimate how roughness length varied across different physical scales. The novel technique provided an intuitive representation of how morphology and hydraulics vary across different scales and affirmed the importance of bar-scale roughness in pool-riffle settings.

I evaluated the performance of 1D and 2D bedload transport functions under high relative shear stress conditions. The results clarified that although the spatial distribution of shear stress may be required to predict transport under low stresses, 1D simplifications may be effective under high stresses. Despite being similarly accurate, the 1D and 2D approaches provided substantially different estimates of critical dimensionless shear stress, suggesting that the estimate and interpretation

## *Abstract*

---

of critical shear stress may depend on whether it is averaged or considered a distribution.

Finally, I reviewed hierarchical conceptual frameworks based on ideas of self-organisation or 'emergence' and their potential application to explain the relationship between processes occurring across different spatio-temporal scales within fluvial systems. These conceptual frameworks provide testable hypotheses about the relationship between process scales and may have implications for understanding sediment transport and approaching physical modelling of rivers.

# Lay Summary

River change occurs via the movement of water and sediment as they interact with the shape of the channel. The interplay between these three components ('the fluvial trinity') is poorly understood as natural rivers are difficult to measure, especially in mountain settings. This thesis aims to understand the fluvial trinity by physically modelling mountain rivers and developing the analyses and concepts required to interpret their behaviour. The results highlight how interactions between the fluvial trinity determine the amount of sediment that is moved and demonstrate that these interactions are different at the scale of individual grains versus the overall channel.

# Preface

This dissertation is formatted in accordance with the regulations of the University of Melbourne and submitted in partial fulfillment of the requirements for a PhD degree awarded jointly by the University of Melbourne and the University of British Columbia. Versions of this dissertation will exist in the institutional repositories of both institutions.

The dissertation presents research conducted by David L. Adams under the co-supervision of Professor Ian D. Rutherford and Professor Brett C. Eaton. David Adams was the primary researcher and was responsible for the main study design, data collection, analysis, interpretation, and writing of the content. Sections of this dissertation have been published in peer-reviewed journals as listed below. These publications are attached at the end of this thesis in an appendix.

A portion of Chapter 2 has been published: Adams, D.L. (2020) Towards bed state morphodynamics in gravel-bed rivers. *Progress in Physical Geography: Earth and Environment* 44(5), pp. 700–726.

A version of Chapter 4 has been published: Adams, D.L. (2021) Morphodynamics of an erodible channel under varying discharge. *Earth Surface Processes and Landforms* 46(12), pp. 2414–2420.

A version of Chapter 5 has been published: Adams, D.L., Zampiron, A. (2020) Short communication: Multiscalar drag decomposition in fluvial systems using a transform-roughness correlation (TRC) approach. *Earth Surface Dynamics* 8, pp. 1039–1051. David Adams developed the approach, conducted the experiment and analysis, and wrote the manuscript. Andrea Zampiron provided expertise in open-channel hydraulics and helped refine the analysis and communication.

A version of Chapter 6 has been published: Adams, D.L., Eaton, B.C. (2022) A comparison of 1D and 2D bedload transport functions under high excess shear

## *Preface*

---

stress conditions in laterally-constrained gravel-bed rivers: a laboratory study. *Earth Surface Dynamics*. David Adams conducted the experiment, performed the analysis, and wrote the manuscript. Brett Eaton provided expertise.

This dissertation was supported by a Research Training Program (RTP) Scholarship from the Australian Government and a Four-Year Fellowship (4YF) from the Canadian Government.

# Table of Contents

<b>Abstract</b> . . . . .	iii
<b>Lay Summary</b> . . . . .	v
<b>Preface</b> . . . . .	vi
<b>Table of Contents</b> . . . . .	viii
<b>List of Tables</b> . . . . .	xi
<b>List of Figures</b> . . . . .	xii
<b>Acknowledgments</b> . . . . .	xviii
<b>1 Introduction</b> . . . . .	1
1.1 Modelling . . . . .	3
1.2 General research questions and thesis organisation . . . . .	4
<b>2 Literature review</b> . . . . .	6
2.1 Introduction . . . . .	6
2.2 Space: 2D processes . . . . .	8
2.2.1 Flow resistance . . . . .	9
2.2.2 Bedload transport . . . . .	12
2.3 Scale: space and time . . . . .	13
2.4 Conclusion and specific research questions . . . . .	14

*Table of Contents*

---

<b>3</b>	<b>Methodology</b>	16
3.1	Approach	16
3.2	Runs	17
3.2.1	Scaling	17
3.2.2	Run design and data collection	20
3.2.3	Data processing	23
3.3	Data usage in Chapters	26
<b>4</b>	<b>Adjustment of the fluvial trinity in response to varying discharge</b>	28
4.1	Introduction	28
4.2	Data analysis	30
4.3	Results	31
4.4	Discussion	37
4.5	Conclusion	40
<b>5</b>	<b>Multiscalar roughness-length decomposition</b>	43
5.1	Introduction	43
5.2	Practical considerations	45
5.3	Application of TRC approach in gravel-bed rivers	48
5.3.1	Stream table experiment	48
5.3.2	The transform-roughness correlation approach	50
5.4	Results and Discussion	51
5.4.1	Estimates of total $k_s$	52
5.4.2	Application of TRC approach	55
5.5	Implications, applications, and limitations	60
5.6	Conclusions	62
<b>6</b>	<b>A comparison of 1D and 2D bedload transport functions under high excess shear stress conditions</b>	64
6.1	Introduction	64
6.2	Data analysis	66
6.2.1	Determining a representative sediment transport rate	66

*Table of Contents*

---

6.2.2	1D and 2D excess shear stress . . . . .	69
6.3	Results . . . . .	71
6.4	Discussion . . . . .	79
6.4.1	Comparison between prediction errors . . . . .	79
6.4.2	Comparison between 1D and 2D approaches . . . . .	81
6.5	Conclusions . . . . .	84
<b>7</b>	<b>The trinity, emergence, and river behaviour . . . . .</b>	<b>85</b>
7.1	Introduction . . . . .	85
7.2	Fluvial trinity . . . . .	88
7.3	Emergence . . . . .	91
7.4	Bedload transport . . . . .	96
7.5	Modelling morphodynamics . . . . .	98
7.6	Conclusion . . . . .	102
<b>8</b>	<b>Conclusion . . . . .</b>	<b>103</b>
8.1	Summary . . . . .	103
8.2	Synthesis . . . . .	104
8.3	Future work . . . . .	106
8.4	Contributions . . . . .	109
	<b>Bibliography . . . . .</b>	<b>111</b>
 <b>Appendices</b>		
<b>A</b>	<b>Publication: Chapter 2 . . . . .</b>	<b>133</b>
<b>B</b>	<b>Publication: Chapter 4 . . . . .</b>	<b>161</b>
<b>C</b>	<b>Publication: Chapter 5 . . . . .</b>	<b>169</b>
<b>D</b>	<b>Publication: Chapter 6 . . . . .</b>	<b>183</b>

# List of Tables

3.1	Summary of average mechanical and geometrical parameters for distorted Froude-scaling modeling across model runs. . . . .	19
3.2	Summary of unit discharges ( $Q/W$ ) used in each phase (P) of Runs a-c. . . . .	20
3.3	Summary of runs conducted in the A-BES. . . . .	20
3.4	Summary of mean flow model results . . . . .	25
3.5	Runs and data products used in each empirical chapter. . . . .	27
5.1	Summary of hydraulic measurements from experiments. . . . .	48
6.1	Summary of mean experimental and flow model results . . . . .	69
6.2	Optimised values of $\tau_c^*$ and goodness-of-fit statistics for excess shear stress and observed bedload transport using four different approaches. . . . .	71

# List of Figures

1.1	The ‘trinity’ of channel morphology, water flow, and sediment transport in a feedback loop (from Leeder, 1983). . . . .	3
2.1	Interactions between channel morphology, channel flow, and sediment transport (from Ashworth and Ferguson, 1986). . . . .	7
2.2	Schematic longitudinal profiles of alluvial channel morphologies. . . . .	11
3.1	Adjustable-Boundary Experimental System (A-BES) at the University of British Columbia. . . . .	19
3.2	Measured versus modelled mean hydraulic depth $h$ (i.e. reach-averaged) at the end of each run phase, featuring 16 percent bounds. Error bars are based on the measurement precision of the stream gauges. . . . .	26
4.1	Variation in flow resistance, topographic variability, and bedload transport over the duration of the multi-phase experiment, and absolute percentage change in these variables over time. . . . .	32
4.2	Reach-averaged morphologic activity over the duration of the multi-phase experiment, presented as both raw values and values normalised by time. . . . .	34
4.3	Comparison of flow resistance, topographic variability, and bedload transport values at each successive point of the experiment. . . . .	35
4.4	Change in $f_{sys}$ and $q_b$ at each successive point of the experiment, separated by experimental phase. . . . .	37

*List of Figures*

---

5.1	Comparison of CWT and MODWT applied to example experimental data. . . . .	47
5.2	Relationship between total $k_s$ estimated by a roughness correlation and Colebrook-White equation. . . . .	53
5.3	Relationship between $k_{s,rc}^*$ and $\Sigma k_{s,rc}$ for the A-BES and Hohermuth and Weitbrecht (2018) experiments. . . . .	55
5.4	Evolution of the form size distribution during Experiment 1a. . . . .	56
5.5	Effective slope and skewness of each topographic wavelength during Experiment 1a. . . . .	57
5.6	Drag size distribution over the course of Experiment 1a. . . . .	58
5.7	Plot of $(8/f)^{1/2}$ against relative submergence for A-BES and Hohermuth and Weitbrecht (2018) data, using four different roughness lengths. . . . .	60
6.1	Width-averaged bedload transport over time in two runs with different widths but similar reach-averaged shear stress. . . . .	68
6.2	The goodness-of-fit for $q_b$ and excess shear stress with varying critical dimensionless shear stress for each approach. . . . .	72
6.3	Channel area at the conclusion of Experiment 3b showing elevations, flow depths, and shear stresses based on the flow model. . . . .	73
6.4	a) Relationship between unit discharge and mean shear stress using depth-slope product and modelled shear stresses, and b) Relationship between unit discharge and the proportion of the wetted channel area. . . . .	74
6.5	a) Cumulative distribution functions of mean-normalised modelled flow depth and shear stress, and b) cumulative distribution function of non-normalised modelled shear stresses in experimental phases with highest and lowest mean shear stress. . . . .	76
6.6	Relationship between local mean-normalised flow depth and shear stress across all experiments. . . . .	77

*List of Figures*

---

6.7	Regression of excess shear stress and observed bedload transport using 1D and 2D approaches. . . . .	78
7.1	Components of the fluvial system (A - catchment, B - planform, C - bend, D - bedform, E - patch, and F - grain), from Schumm (1985) . . . . .	90
7.2	Simplified hierarchical representation of dynamically decoupled scales in fluvial systems. . . . .	95

# Nomenclature

$g$	gravity [m/s]
$\rho$	density of water [kg/m <sup>3</sup> ]
$\rho_s$	density of sediment [kg/m <sup>3</sup> ]
$\nu$	kinematic viscosity [m <sup>2</sup> /s]
$S_v$	mean valley gradient [m/m]
$S$	mean channel gradient [m/m]
$Q$	discharge [L/s]
$W$	maximum channel width [m]
$q = Q/W$	unit discharge [L/s/m]
$D_x$	grain diameter percentile of the bulk mixture [mm]
$D_{max}$	maximum grain diameter [mm]
$A$	cross-sectional flow area [m <sup>2</sup> ]
$w$	mean wetted width [m]
$P$	wetted perimeter [m]
$d$	flow depth [m]
$h = A/w$	mean hydraulic depth [m]

## NOMENCLATURE

---

$R = A/P$	hydraulic radius [m]
$Fr$	Froude number [-]
$U$	velocity [m/s]
$\tau$	shear stress [Pa]
$Re$	Reynolds number [-]
$U^*$	shear velocity [m/s]
$Re^*$	boundary Reynolds number [-]
$k$	representative roughness height [m]
$k_s$	equivalent sand roughness parameter [m]
$f = 8gRS_v/U^2$	Darcy-Weisbach friction factor [-]
$f_{sys} = 8gRS/U^2$	Darcy-Weisbach friction factor for entire system [-]
$\sigma_z$	standard deviation of elevations [m]
$ES$	effective slope of surface [m/m]
$Sk$	skewness [-]
$\lambda$	wavelength [m]
$k_s^*, rc$	roughness length estimated by roughness correlation [m]
$k_s^*, CW$	roughness length estimated by the Colebrook-White equation [m]
$k_s, rc$	roughness length estimated by roughness correlation for a given $\lambda$ [m]
$M_{raw}$	volumetric change (morphologic activity) [m <sup>3</sup> ]

## NOMENCLATURE

---

$M$	volumetric change per unit time [m <sup>3</sup> /min]
$\sigma_\tau$	standard deviation of shear stress [Pa]
$q_b$	bedload transport rate [kg/m/min]
$Q_b$	width-averaged bedload transport rate [kg/min]
$\tau_c^*$	critical dimensionless shear stress [-]
$\tau_c = \tau_c^* g(\rho_s - \rho)D$	critical shear stress [Pa]

# Acknowledgments

This thesis began as something in Melbourne, Australia and around five years later, ended in Vancouver, Canada as something entirely different. Thankyou to the professional staff, professors, and graduate students at UBC and UoM for their support and encouragement throughout this process. I would especially like to thank UBC staff Sandy Lapsky and Danny Wong for their exemplary work behind the scenes. I deeply appreciated fellow graduate and postdoctoral researchers William Booker, Lucy MacKenzie, Kevin Pierce, and Conor McDowell for their engagement with my research and for sharing theirs too.

Each of my advisors made substantial contributions to the thesis and to my development, which I would like to briefly acknowledge. Ian Rutherford has supervised both my Honours and PhD research and is largely responsible for imparting the research skills that have made this research possible under challenging conditions. Since arriving in Vancouver in 2018, Brett Eaton has granted me the freedom and the resources to pursue my research interests and when needed, provided the expertise necessary to bring them to fruition. I would like to thank Marwan Hassan for his mentorship in research, and also his friendship during the most difficult phases of my graduate school experience.

At various points during the prodigious examination process, each member of my supervisory and examination committees has served a critical role in improving the thesis and ensuring my graduation. In particular, Greg Pasternack, Michael Church, and John Richardson made important contributions to the communication of the thesis as a whole.

My parents, Peter and Sheryl, cultivated my interest in natural science from an early age and provided me with the best opportunities I could hope for. They provided unwavering help and encouragement, even as I decided to move 13,200 km

## *Acknowledgments*

---

away! In addition to my friends who have always been there, I would like to thank Priya whose tolerance and support throughout 2022 were truly mammoth.

# Chapter 1

## Introduction

Rivers are natural ‘machines’ that function to transmit water and sediment towards base level (Ferguson, 1981). Alluvial rivers, with boundaries comprised of erodible and transportable sediment, have many available modes of adjustment or ‘degrees-of-freedom’ to accommodate changes in the volumes of material delivered from upstream (Phillips, 1991). These degrees of freedom may be described in various complementary ways, for example, using hydraulic variables (i.e. width, depth, velocity, slope, and frictional resistance), or process scales (catchment, planform, bedform, and grain). In channels that receive a mixture of sediment calibers which are typically transported as bedload (as opposed to suspended load), generally characterising rivers in steep mountainous areas, the spatial organisation of grain sizes represents an additional degree-of-freedom available to adjust transport rates to changes in sediment supply (Dietrich et al., 1989). Given that these gravel-bedded rivers have only been the subject of concentrated research within the past half-a-century, they remain poorly understood relative to lowland rivers (Wohl, 2014). This thesis is concerned with the dynamics of steep gravel-bed rivers, focusing on planform and bedform scales.

River change is highly varied in nature. On timescales that are observable by humans, it may be driven by extreme events such as volcanic eruptions (Zheng et al., 2014), glacial outburst floods (Desloges and Church, 1992), or landslides (Davies and Korup, 2007), and may occur following alteration of land cover or hydrology due to anthropogenic activity (e.g. Schumm, 1968; Millar, 2000; Green and Westbrook, 2009; Polvi and Wohl, 2012; Collins et al., 2012). However, it must be noted that large geomorphic effects need not be driven by large external perturbations (Schumm, 1973, 1979), and researchers have failed to quantify a

direct, proportional relationship between causes (events) and geomorphic effects (responses) in the field (see Lisenby et al., 2018). Even explaining river behaviour – why they change or do not change in response to intrinsic and extrinsic forces – is a fundamental challenge in geomorphology.

River behaviour is often conceptualised as the outcome of feedbacks between channel flow, morphology, and sediment transport (Figure 1.1) – termed the ‘fluvial trinity’ (Leeder, 1983; Ashworth and Ferguson, 1986; Best, 1986). As I review in Chapter 2, researchers have elaborated on this simple explanatory model by incorporating the spatial variation in these feedbacks (Lane and Richards, 1997; Eaton et al., 2006), as well as their variation across different spatio-temporal scales (de Boer, 1992; Werner, 1999). Second, an understanding of the feedbacks between these channel characteristics is hindered by difficulties associated with measuring rivers in nature. Our inability to predict geomorphic change, and the dangers associated with floods, erosion, and mass-wasting, means that researchers typically obtain data before and after an event, but not during. As a result, conceptual frameworks surrounding channel adjustment (of which the fluvial trinity is one) are applied retrospectively or using deductive reasoning. Consequently, physical and numerical models that reproduce natural processes are important tools in geomorphology.

## 1.1. Modelling

---

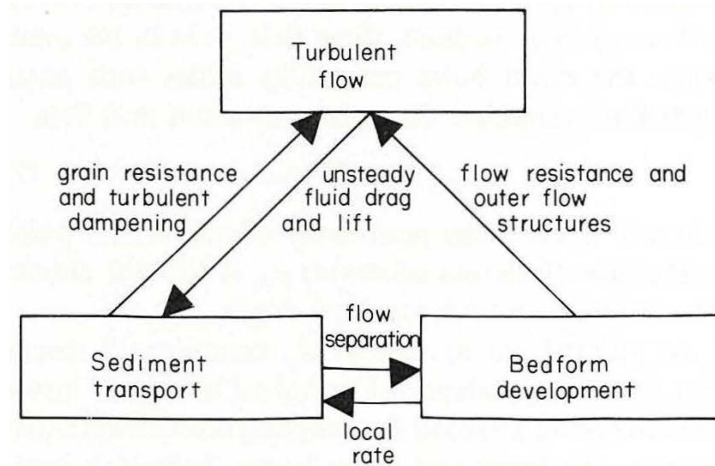


Figure 1.1: The ‘trinity’ of channel morphology, water flow, and sediment transport in a feedback loop (from Leeder, 1983).

## 1.1 Modelling

Models are inherently simplified versions of reality, whether they are numerical, conceptual, or physical. In fluvial geomorphology, numerical and physical models encompass *a priori* assumptions and convenient simplifications, such as the elimination of certain processes that are considered secondary or tertiary, the reduction of system dimensions (i.e. one- or zero-dimensional representations), and removal of larger spatio-temporal scales (i.e. findings are later extrapolated or ‘upscaled’) (Rhoads, 2006). These simplifications reduce the degrees-of-freedom available to the model, which may suppress process feedbacks as well as spatially- and temporally-dependent dynamics (Peirce et al., 2018). Given there is a reliance on laboratory models to understand river processes, these limitations are not trivial. Without systematic comparisons to natural rivers, or hierarchical approaches in which ideas are tested in models with different degrees-of-freedom (e.g. Werner, 1999), assumptions and simplifications that are left unverified become self-reinforcing. The potential consequence is ascientific; insights gained from models can be mistaken for truth instead of unproven working hypotheses of

natural processes, which are potentially determined by formulation of the model itself.

Physical and numerical models are equally susceptible to these shortcomings. The growth of computer processing speed and memory capacity has enabled the development of 2D models with coupled sediment transport and morphological change, however, these models are far from complete and researchers remain wary of their validity (Church and Ferguson, 2015). Notably, despite improvements over 1D models, process simplification, averaging, and arbitrary parameterisation make it difficult to accurately replicate process feedbacks and predict system trajectories (Hardy, 2012; Church, 2015). Geomorphologists have embraced physical modelling for over a century (Gilbert, 1914; Friedkin, 1945; Schumm and Khan, 1972), although most resemble 1D systems and replicate only a subset of processes that occur in natural alluvial rivers. This limitation is potentially alleviated in larger-scale physical models of rivers that embrace more degrees-of-freedom (Peakall et al., 1996), which provides an opportunity to investigate river behaviour. This thesis leverages these larger-scale models to investigate channel processes, rather than upscaling findings from the grain or bedform-scale.

## **1.2 General research questions and thesis organisation**

This thesis tests two general sets of research questions which surround the fundamental concepts of space and scale in geomorphology. Subsequent hypotheses are critically tested using scaled stream table experiments based on steep gravel-bed rivers.

- Does the spatial distribution of channel processes mediate river adjustment?
- What is the direction (i.e. upwards or downwards) of the relationship between channel processes that are superimposed over different spatio-temporal scales?

## 1.2. General research questions and thesis organisation

---

In the literature review (**Chapter 2**), I elaborate on the general research questions to develop a series of more specific questions to be tested. The thesis comprises four original research chapters, three of which leverage physical modelling of steep gravel-bed rivers to provide empirical data. The approach surrounding this physical modelling, detailed in **Chapter 3**, comprises a Froude-scaled fixed-bank stream table under recirculating conditions. I utilise a range of channel widths and discharges to provide a suite of channel conditions, which provides the appropriate data for addressing the empirical questions in the subsequent chapters.

In **Chapter 4**, I investigate the evolution of the three components of the fluvial trinity in response to successive increases in discharge. In **Chapters 5 and 6**, I examine the spatial distribution of morphology and process in the experiment; first hydraulics (and specifically flow resistance), and then sediment transport. In **Chapter 7**, I review the application of fluvial trinity and emergence concepts in alluvial channels, and develop testable hypotheses regarding how scale-dependent process interactions in rivers drive overall system behaviour. In **Chapter 8**, I outline overall conclusions, implications, and further research opportunities.

# Chapter 2

## Literature review

### 2.1 Introduction

The notion that rivers arise via feedbacks between morphology, hydraulics, and sediment transport is a foundational idea in fluvial geomorphology. This idea underpinned the work of early researchers (e.g. Gilbert, 1876, 1914; Rubey, 1931), but was formalised in the 1980s by several British geomorphologists and sedimentologists. In a review of bedform theory, Leeder (1983) suggested that a complete understanding of bedforms required an understanding of the ‘trinity’ of turbulent flow, sediment transport, and bedform morphology that interact in a continuous feedback loop (Figure 1.1). Using this model, Leeder highlighted a key insight: individual components (i.e. hydraulics or sediment transport) cannot be studied in isolation if the system is to be understood as a whole. In a study of a proglacial braided river, Ashworth and Ferguson (1986) presented a more complex interpretation of these interactions to explain dynamics at the planform scale, including an input from the river discharge (Figure 2.1). Ashworth and Ferguson (1986) described a subset of the interactions within the fluvial system to accompany their conceptual model:

Unsteady discharge through a system of highly non-uniform channels with rough beds produces a complicated spatial pattern of water velocity that also changes over time. The vertical velocity gradient at any point determines the shear stress on the bed and this together with sediment availability governs the size and amount of bed material that can be moved as bedload. In turn, bedload transport either maintains the existing size, shape and pattern of channels or alters the



## 2.2. Space: 2D processes

---

(e.g. Figure 2.1) express the direction, type (i.e. positive or negative), or magnitude of the feedback. These conceptual models provide a basis for many investigations of morphodynamics associated with bedforms (Rhoads and Welford, 1991), river confluences (Best, 1986), bedload transport (Church and Ferguson, 2015), channel planform (Lane and Richards, 1997; Eaton et al., 2006), and biogeomorphic interactions (Tal and Paola, 2010). However, it is especially obvious to researchers that the simplicity of this model belies the enormous complexity of the feedbacks between channel processes in nature (Leeder, 1983). In addition, studies have identified how additional (i.e. non-fluvial) processes modulate these feedbacks, such as vegetation, (Tal and Paola, 2010), large wood (Comiti and Mao, 2012), instream biota (Fremier et al., 2018), landslides (Davies and Korup, 2007), and geomorphic history (Church and Ryder, 1972).

The fluvial trinity provides a solid foundation which may be built upon to better explain channel dynamics. In this literature review I examine areas where researchers have elaborated on the fluvial trinity, focusing on two aspects: space and scale. I then identify research opportunities to examine or build on these ideas.

## 2.2 Space: 2D processes

Fluvial trinity models identify channel processes and the relationships between them, commonly expressed as feedbacks. In its simplest form this model is a truism; that there is interaction between channel form, flow, and sediment transport is obvious. It is also typically a one-dimensional representation of a two-dimensional set of processes, as noted by early proponents (Best, 1986; Ashworth and Ferguson, 1986). Several areas of the literature emphasise that incorporating the spatial variation in processes into conceptual models is essential in understanding the system. I will now discuss two of these areas: flow resistance and bedload transport.

### 2.2.1 Flow resistance

The ability to predict *a priori* the flow resistance generated by a surface, based purely on its geometric characteristics, is of great interest to fluid research and practice. It is particularly important in gravel-bed rivers where the measurement of hydraulic variables is subject to practical limitations (Miller, 1958). However, roughness correlations have traditionally been concerned with reach-averaged flow characteristics rather than its spatial pattern.

Between the First and Second World Wars, the minimization of wing frictional drag was a major challenge for airplane design, and necessitated the development of boundary layer equations for both laminar and turbulent flow to estimate aerodynamic efficiency (Eckert, 2007). This problem was addressed by several German scientists, notably, Johann Nikuradse (1933) and Hermann Schlichting (1936), who examined the effect of uniform roughness elements on the surface of pipes. In 1938, American government scientist Garbis Keulegan extended the theoretical investigations of Ludwig Prandtl and Theodore von Kármán, and the experimental work of Nikuradse, from pipes to open channel flow. In gravel-bed rivers, researchers have advanced this theory to account for the ratio of roughness height (e.g. grain size, bedform amplitude) to flow depth which varies greatly across flow stages. Notably, Ferguson (2007) presented the variable-power flow resistance equation accounting for the influence of relative roughness

$$(8/f)^{1/2} = \frac{a_1 a_2 (d/k)}{(a_1^2 + a_2^2 (d/k)^{5/3})^{1/2}} \quad (2.1)$$

where  $f$  is the Darcy-Weisbach friction factor,  $a_1$  and  $a_2$  are empirically-derived coefficients,  $d$  is a metric of flow depth, and  $k$  is a representative roughness length. The value of  $k$  may take the form of a representative grain diameter (a relic of Nikuradse's experiments that used sand), but recent work has suggested that the standard deviation of bed elevations  $\sigma_z$  may account for the influence of larger-scale bed features (Smart et al., 2002; Aberle and Smart, 2003; Cadol and Wohl, 2013; Yochum et al., 2014).

These reach-averaged approaches provide little insight into the spatial varia-

## 2.2. Space: 2D processes

---

tion of flow resistance in gravel-bed rivers. Several researchers have identified and classified a range of channel reach morphologies (Figure 2.2), each with their own spatial pattern and hierarchy of roughness elements (Grant et al., 1990; Montgomery and Buffington, 1997; Hassan et al., 2007). Some studies have attempted to disaggregate the roughness length into grain and form contributions by correlating bar geometry with flow resistance (Davies and Sutherland, 1980; Prestegard, 1983). Advances in remote-sensing and statistics have enabled researchers to develop multiscalar decompositions of geometric roughness using analyses such as variograms (Robert, 1988; Clifford et al., 1992) and transforms (Nyander et al., 2003). Although multiscalar roughness correlations have not yet been developed for rivers, this approach has been proposed for aeolian surfaces using Fourier transform (Nield et al., 2013; Pelletier and Field, 2016; Field and Pelletier, 2018), which may serve as a proof-of-concept. Methods that explicate the spatial variation or scaling characteristics of flow resistance (research question in Section 2.4) may contribute to a more two-dimensional understanding of the interplay between hydraulics, sediment transport, and morphology.

2.2. Space: 2D processes

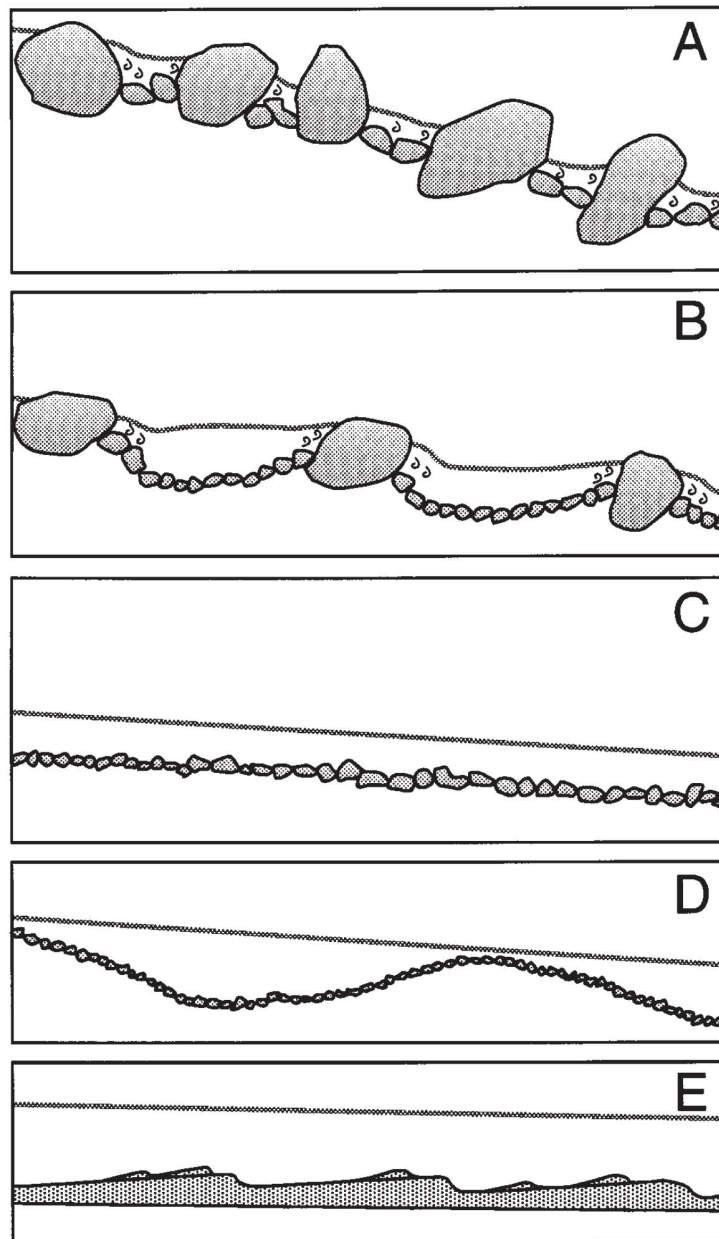


Figure 2.2: Schematic longitudinal profiles of alluvial channel morphologies at low flow: (A) cascade; (B) step pool; (C) plane bed; (D) pool riffle; and (E) dune ripple, from (Montgomery and Buffington, 1997).

### 2.2.2 Bedload transport

To predict bedload transport, researchers have proposed mechanistic equations – typically empirically-calibrated – that relate the rate of movement to a force-balance between the flow and individual particles. One of the most simple and widely used relations is the Meyer-Peter and Müller (1948) equation, a reach-averaged or one-dimensional (1D) equation that estimates bedload transport as a function of excess bed shear stress, which are non-linearly related:

$$q_b = k(\bar{\tau} - \tau_c)^{1.6} \quad (2.2)$$

where  $q_b$  is width-averaged bedload transport,  $k$  accounts for flow resistance and the relative density of sediment,  $\bar{\tau}$  is reach-averaged bed shear stress,  $\tau_c$  is the critical shear stress for a given grain diameter, and the exponent 1.6 is based on the empirical evaluation Wong and Parker (2006). This approach is typically referred to as 1D as it reduces the spatial variation in shear stress to a simple average. The extension of this approach to gravel-bed rivers, typically characterised by a wide range of grain sizes, necessitated several modifications that accounted for the differential mobility of grain sizes, hiding and exposure (Parker and Klingeman, 1982; Parker, 1990; Recking, 2013a; Wilcock and Crowe, 2003).

The application of 1D bedload transport equations to channel morphologies with complex spatial patterns of processes (e.g. braided channels) indicated that they may under-estimate bedload volumes (Paola and Seal, 1995; Paola, 1996; Nicholas, 2000). Subsequent research emphasised that at conditions where  $\bar{\tau} \approx \tau_{c50}$  ( $\tau_c$  for the median grain size), bedload transport is affected by the variance in shear stress, not just its mean value (Ferguson, 2003; Bertoldi et al., 2009; Francalanci et al., 2012; Recking et al., 2016). There is strong evidence that under a wide range of flow conditions in gravel-bed rivers, accounting for the spatial distribution of channel processes is necessary to predict bedload transport.

A considerable limitation of the above studies is that there is an abundance of empirical data surrounding rivers at low to moderate flows, and a paucity at high relative shear stress conditions  $\bar{\tau} \gg \tau_{c50}$ , where most channel change oc-

curs. Thus, the inverse notion of the above studies – that bedload transport in rivers collapses to a more simple function (i.e. with mean shear stress and median grain size) under high excess shear stress conditions – is yet to be conclusively demonstrated (research question in Section 2.4). Critically, there is insufficient data collected at high excess shear stresses due to field data collection limitations. Recently proposed 2D bedload transport functions that integrate across the frequency distribution of shear stresses Monsalve et al. (2016, 2020) provide an opportunity to test this hypothesis should the appropriate data become available.

## 2.3 Scale: space and time

The form and functioning of geomorphic systems is the end product of processes interacting across a range of spatial and temporal scales. Thus, researchers are presented with a fundamental problem of scale (Rhoads, 2006), which has stimulated the development of terminology and concepts to interpret these interactions. Based on the apparent similarity between geomorphic and ecologic (or other complex) systems (Allen and Starr, 1982; Graf, 1988; Haken, 1983; Schweber, 1993; Goldenfeld and Kadanoff, 1999), several contributions have developed and promoted nested, hierarchical representations of geomorphic systems (Sugden and Hamilton, 1971; Trudgill, 1976; Allen and Starr, 1982; Werner, 1995, 2003; Murray, 2003; Harrison, 2001; Phillips, 2016), including a comprehensive review and synthesis of earlier contributions by de Boer (1992). Most of this work is predicated upon the notion that scales of form and process are connected (Jackson, 1975; Douglas, 1976), and that spatial and temporal scales of process are linked (Haigh, 1987; Graf, 1988). The central proposition across these studies is that processes and forms at a given scale *emerge* from processes and forms at a finer scale but are constrained by processes and patterns at a coarser scale (Schumm and Lichty, 1965; Walsh et al., 1998; de Boer, 1992; Werner, 2003). A classical example of such a top-down process is a sand dune, where the trajectories of individual particles who compose the bedform are ultimately constrained by the bedform itself. Most contributions surrounding hierarchical processes have been concerned

## 2.4. Conclusion and specific research questions

---

with geomorphology generally, with only some examples of fluvial processes.

In contrast to the concept of emergence, the concept of the fluvial trinity is a gross simplification of the process interactions that drive river behaviour because it is agnostic to scale. Fluvial processes occur across a wide range of spatial and temporal scales, ranging from instantaneous sediment entrainment in the turbulent boundary layer (Ancy, 2020a), to landscape denudation occurring over geological timescales (Davis, 1899). The concept of scale is frequently acknowledged in the literature surrounding rivers, although the hierarchical frameworks describing how different scales interact are seldom referenced or utilised. For example, according to Google Scholar in June 2022, the synthesis of de Boer (1992) has been cited 216 times, with one notable usage in fluvial processes (Fryirs et al., 2018). Another significant contribution – Werner (2003) – has been cited 95 times with one notable citation (Hajek and Wolinsky, 2012). There are studies that embrace hierarchical theories of fluvial processes without referencing foundational work mentioned above (e.g. Kleinhans, 2010), although the lack of connectivity across the literature means that important theory is potentially missed. This theory is likely essential in interpreting how processes across different scales contribute to channel adjustment.

The hierarchical theory of geomorphic processes, concerned with the process of emergence, provides two key opportunities. First, the terminology and concepts within this theory may be extended to fluvial geomorphology and the interpretation of channel behaviour (research question in Section 2.4). Second, these concepts may guide physical modelling of channel processes given that this research involves isolating a subset of fluvial processes.

## 2.4 Conclusion and specific research questions

In this literature review, I identified two areas of research that elaborate on the fluvial trinity. First, researchers have emphasised the importance of the spatial dimension over which process feedbacks occur. Notably, processes associated with flow resistance and bedload transport are highly spatially variable. I also identified

## 2.4. Conclusion and specific research questions

---

opportunities to resolve these theoretical and analytical problems based on existing literature. Second, there is a fundamental problem of scale in geomorphology whereby processes interact across multiple spatial and temporal scales. There is an opportunity for hierarchical (i.e. scale-explicit) theories of geomorphology to be integrated with the fluvial trinity to better interpret channel adjustment. I will now present specific research questions based on the literature review:

### Chapter 4

- Do nonlinear feedbacks between sediment transport, channel morphology, and hydraulics disrupt the temporal pattern of adjustment proposed by Graf (1977)? This pattern involves an initially rapid rate of change in processes, which decreases asymptotically towards zero.

### Chapter 5

- What is the relative contribution of different scales of river bed topography to the total roughness length?

### Chapter 6

- What is the relative effectiveness of 1D and 2D bedload transport functions under high relative shear stress conditions?
- What is the conceptual difference between 1D and 2D conceptualisations of excess shear stress and bedload transport?

### Chapter 7

- How do fluvial trinity and emergence perspectives intersect?
- What are the potential implications for understanding sediment transport and morphodynamics?
- What are the potential implications for how we physically model rivers?

# Chapter 3

## Methodology

### 3.1 Approach

In Chapter 1.1, I identified that larger-scale physical models of rivers provide an opportunity for investigating channel adjustment as they incorporate more degrees-of-freedom (Peakall et al., 1996). The empirical data collection harnesses a stream table that models reach-scale processes (i.e. spanning several bar wavelengths) in laterally-constrained gravel-bed rivers. Consequently, the channel has been constrained to various widths to prevent significant lateral adjustment. Throughout the runs, sediment is recirculated to model capacity-limited channels, whereby the upstream supply of sediment is simply determined by the channel's ability to convey it under the imposed discharge. The runs model flood disturbance across a range of discharges capable of reworking the bed surface and transporting large volumes of sediment (Ashworth and Ferguson, 1989; Wolman and Miller, 1960).

Runs have been selected for each chapter based on two considerations: 1) the most appropriate dataset for the research question at hand (justified in each chapter), and 2) the available runs at the time of production given laboratory closures and renovations at various times over the COVID-19 pandemic. Following a detailed description of the run methodology and data products, I detail their usage in each chapter (Table 3.5).

## 3.2 Runs

### 3.2.1 Scaling

Laboratory models of channels lie on a spectrum defined by two end-members of mechanical similarity: 1) 1 : 1 scale models, which maintain the kinematic (flow) properties of Froude and Reynolds numbers observed in the field prototype (e.g. Fenton and Abbott, 1977; Ancey et al., 2006), and 2) analogue or ‘toy’ models with geometrical (physical) similarity, resembling a reduced complexity version of nature in which flow properties are distorted compared to the field-scale but illuminate larger-scale processes (Hooke, 1968; Peakall et al., 1996). Subsequently, model scale is necessarily a trade-off between maintaining flow mechanics and allowing for various scales of processes that occur in the field. For example, if grain-scale processes are of interest (notably, sediment transport and hydraulics) kinematic similarity is typically prioritised to maintain flow properties, notably, the particle Reynolds number (Church, 2021). At the same time, the geometric similarity is relaxed, whereby a small vertical-to-horizontal scale ratio helps to maintain adequate flow depth (Peakall et al., 1996). The corresponding reduction in width-depth ratio suppresses emergent patterns such as bedforms, bars, and planforms, and at its most narrow states culminates in a one-dimensional or ‘1D’ river (e.g. Wilcock and McArdell, 1993; Masteller and Finnegan, 2017).

This thesis is concerned with channel-scale processes in natural gravel-bed streams, which necessitates a model with greater geometrical similarity. To this end, the most appropriate laboratory approach is a Froude-scale model whereby the Reynolds number is compromised whilst the Froude number of the field prototype is maintained (Peakall et al., 1996). Runs were performed in the Adjustable-Boundary Experimental System (A-BES) at the University of British Columbia (Figure 3.1). The A-BES comprised a 1.5 m wide by 12.2 m long tilting stream table with a length scale ratio of 1:25 and a reach-averaged gradient of 2 percent. The model parameters were based on a generic prototype rather than a specific field channel. At the 0.3 m channel width, the A-BES had formative discharge  $Q$  of approximately 1.5 L/s, and  $D_{50}$  of 1.6 mm ( $D_{84} = 3.2$  mm,  $D_{90} = 3.9$  mm).

### 3.2. Runs

---

The lower end of the model sediment mixture was truncated at 0.25 mm to maintain a hydraulically rough boundary. The mixture comprised natural clasts with a density of around 2,500 kg/m<sup>3</sup>.

Based on 2D hydraulic modelling detailed in Section 3.2.3, I outline the relevant parameters for both geometrical and mechanical similarity in Table 3.1. Model width-depth ratios varied between 15–32, except for two narrower experiments where  $w/d \approx 5$ . This range of values is typical for steep gravel-bed channels. Froude numbers varied between 0.80–1.03 with a median of 0.87. Runs were characterised by flow within the upper end of the sub-critical regime, which is typical of gravel-bed channels undergoing flood discharges (Wahl, 1993). Reynolds numbers ranged from 2528–6118 with a median of 3918. Based on the range for transitional flow being approximately 2300 to 3500, eight runs were within the transitional regime, and twelve were within the turbulent regime. Particle Reynolds numbers ( $Re^* = U^*k/\nu$ , where  $U^*$  is shear velocity,  $k$  is  $D_{84}$ , and  $\nu$  is kinematic viscosity) across all runs ranged from 111–142, meaning that all were within the fully rough regime defined by  $Re^* \geq 70$  (Buffington and Montgomery, 1997; Schlichting, 1979). Given that channel geometry and Froude number of the generic prototype were maintained, and the Reynolds number was only partially distorted, the runs serve as an excellent model for steep gravel-bed river processes.

### 3.2. Runs

Table 3.1: Summary of average mechanical and geometrical parameters for distorted Froude-scaling modeling across model runs.

Run	$w/d$	Fr	Re
2a	4.4	0.92	4431
2b	5.4	0.85	4431
1a	17.2	0.92	4117
1b	15.9	0.83	3132
1c(1)	15.0	0.80	2528
1c(2)	16.6	0.81	2995
1c(3)	16.5	0.87	4116
1c(4)	15.1	1.03	6118
3a	25.3	0.87	3869
3b	20.0	0.87	3609
3c(1)	17.9	0.83	3010
3c(2)	22.1	0.83	3173
3c(3)	23.6	0.89	4083
3c(4)	23.5	0.97	5405
4a	32.2	0.89	3966
4b	29.6	0.81	3194
4c(1)	23.5	0.84	3114
4c(2)	28.2	0.85	3398
4c(3)	29.9	0.93	4390
4c(4)	32.1	0.97	5660



Figure 3.1: Adjustable-Boundary Experimental System (A-BES) at the University of British Columbia, featuring cameras (top-right) and bank control system at a width of 30 cm.

### 3.2. Runs

Table 3.2: Summary of unit discharges ( $Q/W$ ) used in each phase (P) of Runs a-c.

	unit discharge $q$ [L/s/m]			
	P1	P2	P3	P4
Run a	5.00			
Run b	3.33			
Run c	2.22	3.33	5.00	7.50

Table 3.3: Summary of runs conducted in the A-BES. Length refers to the median length of digital elevation models (DEMs), which generally varies by  $\pm 0.1$  m, and does not include approximately 20–30 cm of bed at the upstream end. DEM count excludes screeded bed which has no associated hydraulic data.

Run	W [m]	L [m]	Q [L/s]	Dur. [hrs]	DEMs
2a	0.08	8.7	0.40	16	24
2b	0.08	8.6	0.27	16	24
1a	0.30	10.8	1.50	16	24
1b	0.30	10.7	1.00	16	24
1c	0.30	10.8	0.66, 1.00, 1.50, 2.25	8, 4, 4, 4	20, 16, 16, 16
3a	0.45	10.8	2.25	16	24
3b	0.45	10.8	1.50	16	24
3c	0.45	10.7	1.00, 1.50, 2.25, 3.37	8, 4, 4, 4	20, 16, 16, 16
4a	0.60	10.8	2.00	16	24
4b	0.60	10.8	3.00	16	24
4c	0.60	10.7	1.33, 2.00, 3.00, 4.50	8, 4, 4, 4	20, 16, 16, 16

#### 3.2.2 Run design and data collection

The runs utilised interlocking landscaping bricks to constrict the channel to various widths  $W$  between 0.08–0.60 m. The narrowest setting was selected based on preliminary runs where the channel was narrowed until bar formation was suppressed entirely. In addition to the various channel widths, four different unit discharges ( $q = Q/W$ ) are used across the runs (i.e. discharge is scaled by width) that increase by a factor of 1.5 (Table 3.2). There are two constant-discharge runs that use the middle two discharges, and one multi-discharge run consisting of the four discharges in increasing order. A full list of runs is provided in Table 3.3.

At the beginning of each run the bulk mixture was mixed by hand to minimise

### 3.2. Runs

---

lateral and downstream sorting, and then the in-channel area was screeded to the height of weirs at the upstream and downstream end using a tool that rolled along the brick surface. The flow was run at a low rate with little-to-no movement of sediment until the bed was fully saturated, and was then rapidly increased to the target flow.

Three different types of data were collected throughout each run; surface photos, stream gauge measurements, and sediment output. A rolling camera rig positioned atop the A-BES consisted of five Canon EOS Rebel T6i DSLRs with EF-S 18–55 mm lenses positioned at varying oblique angles in the cross-stream direction to maximise coverage of the bed, and five LED lights. Photos were taken in RAW format at 0.2 m downstream intervals, providing a stereographic overlap of over two-thirds. Ten water stage gauges comprised of a measuring tape (with 2 mm intervals) on flat boards were located along the inner edge of the bricks every 1 m (but every 0.8 m for the 0.08 m runs due to the slightly shorter length). To minimise edge effects, gauges were not placed within 0.60 m of either the inlet or the outlet. The gauges were read at an almost horizontal angle which, in conjunction with the dyed blue water, minimised systematic bias towards higher readings due to surface tension effects. Based on the measurement precision of the stream gauge readings, errors of 6–11 percent could be expected for mean hydraulic depths ( $h = A_c/w$ , where  $A_c$  is flow cross-sectional area and  $w$  is wetted width).

The data collection procedure was designed to maximise measurement accuracy as much as reasonably possible. Given that stream gauge data would later be paired with topographic data, the timing of gauge readings needed to closely coincide with surface photography. Every time photos were taken the bed was drained, as the surface water would distort the photos. These constraints necessitated a procedure in which manual stream gauge readings (to the nearest 1 mm) were taken 30–40 seconds before the bed was rapidly drained, around the minimum time it would take to obtain the readings. There was minor re-working during the drain-down process, although the specific amount could not be quantified. Visually, the amount of re-working during this period is considerably less than the amount of

### 3.2. *Runs*

---

morphologic change over the time-step, so its effect is negligible. In other words, any minor alterations of the bed surface during the draw-down and re-wetting procedure was quickly re-worked by the target flow. The bed was then photographed and gradually re-saturated before resuming the run, approximately 10 minutes.

Each run phase was divided into a series of segments between which the data were collected. The procedure occurred in 5, 10, 15, 30, 60, and 120 minute segments with four repeats of each (i.e. 4 x 5 min, 4 x 10 min), which was designed to reflect the relatively rapid rate of morphologic change at the beginning of each phase. For example, in wider channels, alternate bars developed within an hour, and there was relatively little morphologic change in the following hours (Adams and Zampiron, 2020; Adams, 2021).

Throughout the runs, sediment falling over the downstream weir was collected in a mesh bucket, drained of excess water, weighed damp to the nearest 0.2 kg, placed on the conveyor belt at the upstream end, and gradually recirculated at the same rate it was output, as opposed to a ‘slug’ injection. Based on the measurement precision and output volumes, transport rates were measured with reasonable accuracy for sediment transport analysis. With the exception of Runs 2a and 2b, which have lower sediment volumes and are not included in sediment transport analysis (Chapter 6), the transport rate of the run with the lowest output rate (Run 1c(1)) was within 12.5 percent of the exact value. In all other cases transport rate was within 5 percent of the exact value. Based on a range of samples collected across the runs, I determined the weight proportion of water to be approximately 5.8 percent and applied this correction factor to obtain approximate dry weights. There was no initial feed of sediment, although this no-feed period was only 5 minutes. The runs are best described as pseudo-recirculating as sediment was fed at the end of each segment, and every 15 minutes, regardless of whether the bed was drained.

### 3.2.3 Data processing

Using the images, point clouds were produced using structure-from-motion photogrammetry in Agisoft MetaShape Professional 1.6.2 at the highest resolution, yielding an average point spacing of around 0.25 mm. Twelve spatially-referenced control points and additional unreferenced ones were distributed throughout the A-BES, which placed photogrammetric reconstructions within a local coordinates system and aided in the photo-alignment process. Using inverse distance weighting, the point clouds were converted to digital elevation models (DEMs) at 1 mm horizontal resolution.

Despite the use of control points, the DEMs contained a slight arch effect in a downstream direction whereby the middle of the model was bowed upwards, which was an artefact of the photogrammetric reconstruction (see doming: James and Robson, 2014). This effect was first quantified by applying a quadratic function (on average:  $p < 0.001$ ,  $r^2 = 0.9992$ ,  $RMSE = 0.0017$  mm) along the length of the bricks, which represent an approximately linear reference elevation (brick elevations vary randomly by  $\pm 2$  mm). The arch was then removed by determining correction values along the length of the DEM using the residuals, which were then applied across the width of the model. The final least-squares linear fit along the brick surface was homoscedastic with an average RMSE of 0.0018 mm (around the maximum height difference between adjacent bricks), indicating that the DEM was successfully corrected. When performing geomorphic change detection (i.e. differencing between DEMs) this method has a volumetric error ranging from 1 to 16 percent with a median value of 6 percent (Booker and Eaton, 2022). All other analyses presented herein (e.g. flow modelling, channel profiles) treat DEMs individually and are even less sensitive to alignment or correction errors.

I estimated the position of the channel thalweg by manually locating pool centroids and using Gaussian kernel regression to smooth the vertices between the centroids. In the case of the 0.08 m channel which featured a plane-bed morphology, the thalweg was assumed to be the channel centreline. For each DEM, ten wetted cross-sections were reconstructed using the water surface elevation data,

### 3.2. Runs

---

which were then used to estimate reach-averaged hydraulics. For more detailed spatial analysis, the flow conditions of water depth, and shear stress were reconstructed using a 2D numerical flow model (Nays2DH) to the final DEM of each discharge phase. Nays2DH is a two-dimensional, depth-averaged, unsteady flow model that solves the Saint-Venant equations of free surface flow with finite differencing based on a general curvilinear coordinate system (further details can be found in Nelson et al., 2016). Key input boundary conditions are the channel DEM, an initial estimate of reach-averaged Manning's  $n$ , cell resolution, and the water discharge. I selected an  $n$  value of 0.045 based on the channel conditions, a cell resolution equivalent to 5 mm, and a flow duration of 200 s was sufficient to establish convergence. After initially estimating  $n$ , I back-calculated a spatially variable value using the flow resistance law presented by Ferguson (2007), and ran the solver again.

To minimise rounding errors associated with the relatively shallow depths in our runs, the DEM size and discharge were adjusted to the prototype scale (i.e. using a length scale ratio of 25). The estimated water depths, shear stresses and velocities from Nays2DH were then back-transformed to the model scale (Table 3.4). Cells with relatively shallow flows defined as depths less than  $2D_{84}$  were removed as they contributed a large peak in the frequency distribution of flow depths and likely account for a small proportion of bedload activity. Areas of the bed with flows above this threshold are defined as 'wetted'. The mean-normalised frequency distributions of flow depths and shear stresses were fitted with gamma and Gaussian distributions (coefficients presented later in Table 6.1), where the goodness-of-fit was assessed using both Kolmogorov-Smirnov and Anderson-Darling tests.

### 3.2. Runs

Table 3.4: Summary of mean flow model results from Nays2DH. Parameters  $w$  = wetted width [m],  $d$  = flow depth [m],  $U$  = velocity [m/s], Fr = Froude number, Re = Reynolds number ( $Ud/\nu$ , where  $\nu$  is the kinematic viscosity),  $\bar{\tau}$  = mean shear stress [Pa].

Run	$w$	$d$	$w/d$	$U$	Fr	Re	$\bar{\tau}$
2a	0.07	0.016	4.38	0.36	0.92	4431	2.47
2b	0.07	0.013	5.38	0.30	0.85	4431	2.18
1a	0.26	0.015	17.2	0.36	0.92	4117	2.65
1b	0.21	0.013	15.9	0.31	0.83	3132	2.34
1c(1)	0.18	0.012	15.0	0.28	0.80	2528	2.04
1c(2)	0.21	0.013	16.6	0.30	0.81	2995	2.25
1c(3)	0.26	0.016	16.5	0.34	0.87	4116	2.81
1c(4)	0.28	0.018	15.1	0.44	1.03	6118	3.36
3a	0.37	0.015	25.3	0.34	0.87	3869	2.69
3b	0.28	0.014	20.0	0.33	0.87	3609	2.45
3c(1)	0.23	0.013	17.9	0.30	0.83	3010	2.17
3c(2)	0.29	0.013	22.1	0.31	0.83	3173	2.35
3c(3)	0.36	0.015	23.6	0.35	0.89	4083	2.69
3c(4)	0.40	0.017	23.5	0.41	0.97	5405	3.21
4a	0.48	0.015	32.2	0.35	0.89	3966	2.74
4b	0.40	0.013	29.6	0.31	0.81	3194	2.28
4c(1)	0.31	0.013	23.5	0.31	0.84	3114	2.11
4c(2)	0.39	0.014	28.2	0.32	0.85	3398	2.33
4c(3)	0.46	0.015	29.9	0.37	0.93	4390	2.80
4c(4)	0.57	0.018	32.1	0.42	0.97	5660	3.15

The results of the flow model were quantitatively validated by comparing measured reach-averaged depths to modelled reach-averaged depths (Figure 3.2). Most readings fall within 10–15 percent of the line of equality, although the linear fit has a different slope whereby the flow model estimates a narrower range of mean flow depths across the runs. The flow model is likely a more accurate esti-

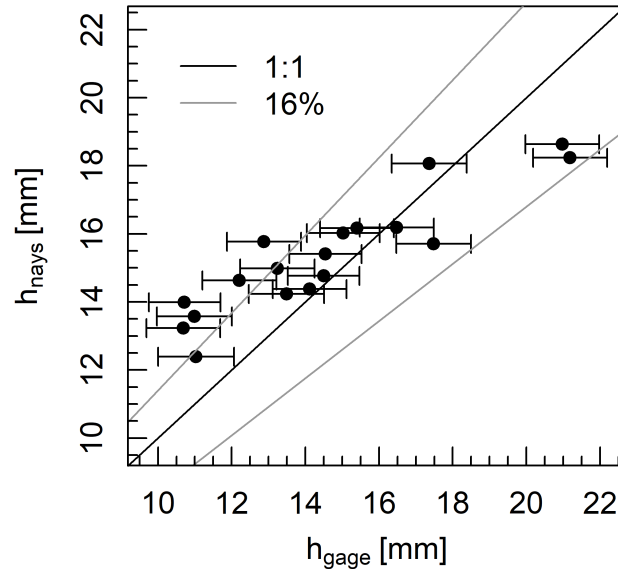


Figure 3.2: Measured versus modelled mean hydraulic depth  $h$  (i.e. reach-averaged) at the end of each run phase, featuring 16 percent bounds. Error bars are based on the measurement precision of the stream gauges.

mate of flow depths compared to the stream gauge measurements. Gauge readings are easily biased towards either large or small values due to the relatively small sample size, and assume that the water surface is horizontal at the cross-section.

### 3.3 Data usage in Chapters

The above section detailed the range of stream table runs conducted and the general data products. The runs were designed to provide a suite of data which constitute tests of specific hypothesis. It is following their usage as tests when they

### 3.3. Data usage in Chapters

---

are referred to as experiments.

I will now describe the usage of these data in the three empirical chapters (Table 3.5). Chapter 4 utilises run 1c, which was the only multi-phase run available at the time of production due to COVID-19. This chapter uses three data products: DEMs, sediment output data, and stream gauge measurements to monitor channel adjustment over the discharge phases. Chapter 5 uses runs 1 and 2 (all discharges), the available runs at the time of production. Stream gauge data and DEMs form the basis of the analysis of channel hydraulics. Chapter 6 utilises all runs besides run 2 ( $W = 0.08$  m), which were excluded due to them having a different morphology (plane-bed), as well as sidewall effects on the shear stress (energy losses to the channel boundary). This chapter utilised sediment output data and 2D flow modelling to examine the relationship between shear stress and bedload transport.

Table 3.5: Runs and data products used in each empirical chapter.

	Runs	Data products
Chapter 4	1c	DEMs, sediment output, stream gauge
Chapter 5	1, 2	DEMs, stream gauge
Chapter 6	All, except 2	Sediment output, 2D flow model

# Chapter 4

## Adjustment of the fluvial trinity in response to varying discharge

### 4.1 Introduction

River behaviour varies across a wide range of temporal scales, such that the notion of system stability is intrinsically time-dependent (Schumm and Lichty, 1965; Lane and Richards, 1997; Phillips, 2006). Over relatively short timescales where climate and geology are fixed, river behaviour may be broadly classified into two conditions; unsteady, where channel form and process are evolving, and steady, where these characteristics oscillate around a mean state ('steady-state'). For example, Graf 1977 proposed that following disturbance the rate of change in processes (e.g. sediment transport rate) is rapid at first and decreases asymptotically towards zero. The concepts of unsteady and steady conditions are often framed through the notion of the fluvial trinity (Ashworth and Ferguson, 1986; Best, 1986), which describes the feedbacks between morphology (form), hydraulics (flow), and sediment transport (flux).

Recent work has emphasised how river behaviour, and particularly the relationship between causes (events) and the magnitude, timing, and manner of geomorphic effect (response), may be highly complex and nonlinear (Schumm, 1973; Phillips, 1992; Lisenby et al., 2018). These nonlinear dynamics may be more generally prevalent in systems with multiple modes of adjustment (e.g. alluvial channels) and threshold mechanisms (Phillips, 2003), for example, channels where bed material transport is restricted to conditions near the threshold of motion ('threshold' channels; Church, 2006). Notably, a key model of channel adjustment is the

#### 4.1. Introduction

---

Concepts surrounding the fluvial trinity, and the nonlinear dynamics that arise from its interactions, have served as general explanations for river behaviour. However, for philosophical and methodological reasons, there has been a lack of quantitative evidence available to interrogate them. A Newtonian paradigm has driven researchers to increasingly small spatio-temporal scales of inquiry and to isolate processes of hydraulics and sediment transport where conservation laws and force-balance relations may be more readily applied (Rhoads and Thorn, 1993; Church and Ferguson, 2015; Ancy, 2020*b*). In practice, this approach has manifested in various simplifications, notably, physical and numerical models that lack degrees-of-freedom available for adjustment in most natural channels, and narrow grain size distributions that may not replicate important processes in prototype streams (Booker and Eaton, 2020). By reducing the number of modes of adjustment, and removing the potential for threshold-dependent transport (in the case of threshold channels), these simplifications may significantly reduce the potential for nonlinear behaviour that may be expected in nature (Phillips, 1993). It is also worth noting a lack of available field data and remote sensing technology, which has historically made quantitative investigations of channel behaviour difficult.

As geomorphologists become increasingly aware of philosophical blind spots and methodological oversimplifications, and have access to improved data collection techniques, there is an opportunity to examine and revise ideas surrounding river behaviour. These investigations need not be exhaustive and elaborate, but rather, should first seek to examine process feedbacks, steady-state conditions, and nonlinear dynamics under relatively straightforward experimental scenarios.

To this end, I physically model the adjustment of an erodible channel under varying discharge to answer the following research question: Do nonlinear feedbacks between sediment transport, channel morphology, and hydraulics disrupt the temporal pattern of adjustment proposed by Graf (1977)? The experiment has fixed banks but is sufficiently wide to allow for the development of alternate bars, and it has a relatively broad distribution of grain sizes (0.5–8.0 mm). The results highlight a time-dependent interplay between form, flow, and flux towards

steady-state conditions, as well as the presence of nonlinear dynamics such as internal thresholds that mediate channel adjustment. The findings have implications for physical and numerical modelling of rivers, and suggest that the spatial distribution of channel processes is necessary for understanding channel adjustment.

## 4.2 Data analysis

To test these hypotheses, I employed a generic Froude-scaled model of a steep gravel-bed river. Specifically, I selected Run 1c (Section 3.3, Table 3.3) as it was the only multiple-discharge experiment available at the time of writing. The experiment models the adjustment of the channel to successive increases in discharge under pseudo-recirculating conditions (i.e. material was recirculated at the same rate it was output, with a brief time-lag). The channel was fixed at a width of 30 cm and comprises four experimental phases of increasing discharge (by 50 percent each time): 1) 0.67 L/s for 8 hours, 2) 1 L/s for 4 hours, 3) 1.5 L/s for 4 hours, and 4) 2.25 L/s for 4 hours. These times were selected based on preliminary runs that indicated approximate times for each flow to reach a steady morphology and sediment output rate. The fluvial trinity is indexed using reach-averaged flow resistance, topographic variation, and bedload flux, which are commonly used parameters that are readily available from the experiment (as opposed to being fully representative of the trinity). Flow resistance is estimated by a variant of the Darcy-Weisbach equation  $f_{sys} = 8gRS_v/U^2$ , where  $g$  is gravity,  $R$  is the hydraulic radius (or mean hydraulic depth),  $S_v$  is the valley gradient (almost identical to channel gradient here), and  $U$  is velocity (Eaton et al., 2004). Topographic variation and bedload flux are indexed by the standard deviation of the thalweg elevation profile  $\sigma_z$  and width-averaged bedload transport  $q_b$ , respectively. In addition, volumetric morphologic activity  $M_{raw}$  is calculated using the height difference between successive digital elevation models (DEMs). The height difference in each cell is multiplied by cell resolution and average porosity (0.46), and summed to provide the total volumetric change.

## 4.3 Results

In phase 1 the channel developed a set of alternate bars over four hours, and which then rapidly re-arranged in response to a spontaneous shift in the bar at the upstream end, yielding 7 complete bars (and a half-bar at each end). The riffles widened and bar-heads eroded in response to the first increase in flow (phase 2), although the previous morphology was largely inherited as larger-than-average grains (4.0–5.6 mm) could not be entrained from the bar-heads. The next phase almost immediately eroded the bars and rapidly deposited a set of 4 complete longer-wavelength alternate bars. Following the final increase in flow (phase 4), the increased discharge immediately planed off the bars to form a flat bed, and slowly redeposited a set of 3 complete alternate bars over four hours.

Each change in discharge yielded different combinations of adjustments between the three variables (Figure 4.1, see arrows). Following an initial increase in the system's frictional resistance during the first phase, there was a general decrease with increasing discharge as flow depth increased. The standard deviation of bed elevations increased throughout the first phase, associated with the development of the pool-bar-riffle sequence. Topographic variability peaked in phases two and three as the pools deepened, but rapidly decreased in the final phase as the bed was planed. There was an approximately exponential increase in bedload transport with increasing discharge. Bedload transport rates were typically higher at the beginning of each phase and decreased towards a relatively constant value. The notable exception is the first phase where bedload transport was negligible prior to the development of morphology.

### 4.3. Results

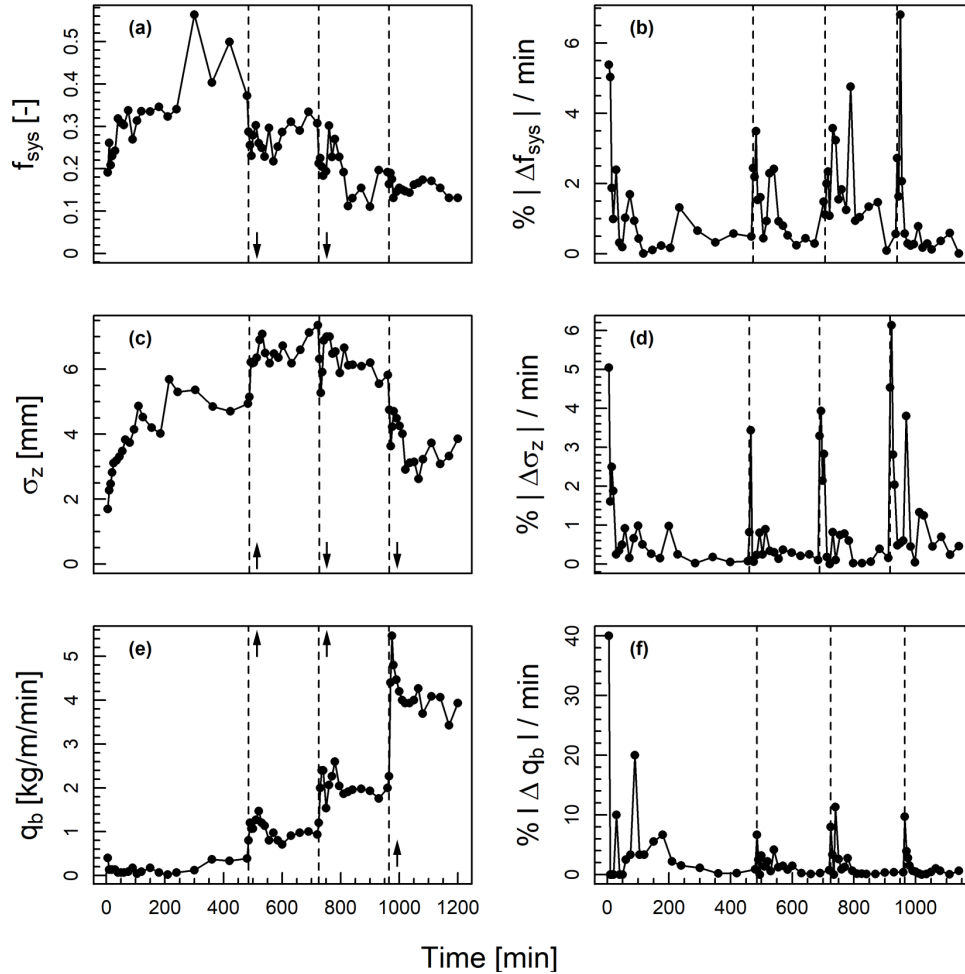


Figure 4.1: **a, c, e**) Variation in flow resistance, topographic variability, and bed-load transport over the duration of the multi-phase experiment, and **b, d, f**) absolute percentage change in these variables over time (expressed as change per minute). Vertical dashed lines represent the final measurement of each phase, and arrows indicate the direction of adjustment from the previous phase (no arrow indicates no change).

Morphological activity is typically presented as a volumetric change per unit

### 4.3. Results

---

time  $M$ , given that physical change is intrinsically a time-dependent process. I also present raw values that are not normalised by time ( $M_{raw}$ ) given that relatively long measurement intervals in the latter portion of each phase tend to under-represent morphologic activity (Figure 4.2). There was relatively little morphologic activity prior the first bar re-arrangement, where there was a rapid increase (indicated by  $\alpha$ ). For the remainder of the experiment  $M_{raw}$  oscillated around a relatively constant value (visually identified and annotated with a horizontal line), except for the periods at the beginning of phases three and four. These two bar reorganisation events are well reflected in periods of higher morphologic activity ( $\beta$  and  $\gamma$ , respectively). The rate of morphologic activity  $M$  follows a similar trend to other variables whereby change tends to be greatest immediately after each increase in discharge, before asymptoting towards zero. The relatively low rate of change at the beginning of the first phase, compared to subsequent increases in discharge, highlights the relatively small amount of volumetric change.

### 4.3. Results

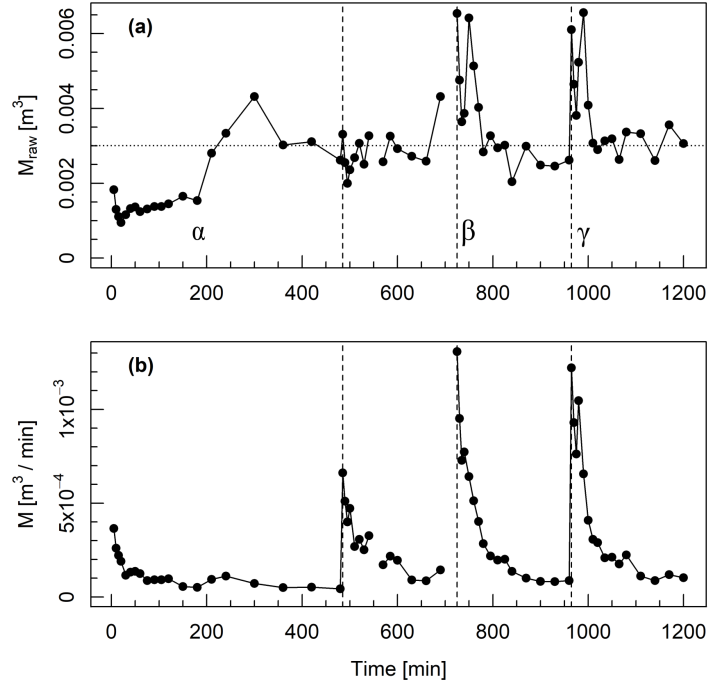


Figure 4.2: Reach-averaged morphologic activity over the duration of the multi-phase experiment, presented as both **a**) raw values ( $M_{raw}$ ), and **b**) normalised by time ( $M$ ). Bar reorganisation events associated with high morphologic activity are indicated by Greek letters, and steady-state  $M_{raw}$  is indicated by a horizontal line.

Flow resistance and bedload transport most effectively discriminate between the experimental phases and indicate four relatively distinct channel characters (Figure 4.3a). With increasing discharge, there was a stepped transition from low bedload flux and high flow resistance (phase 1), to high flux and low resistance (phase 4). Topographic variability and bedload transport also distinguish between the four phases fairly well, although there is little difference in topographic variability between phases 2 and 3 (Figure 4.3b).

### 4.3. Results

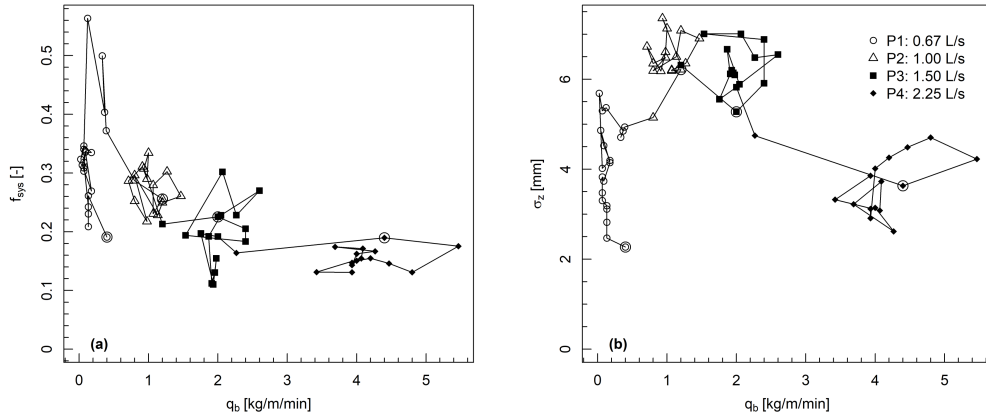


Figure 4.3: Comparison of flow resistance, topographic variability, and bedload transport values at each successive point of the experiment, combined in two different ways. Circled points represent the first measurement taken during each phase.

Changes in flow resistance, topographic variability, bedload flux, and morphologic activity were most rapid at the beginning of each phase (Figure 4.1b–f, 4.2b). Bedload transport exhibited the fastest rates of change during this period. Following the initial adjustment period spanning the first few observations (the first 10–30 minutes), all variables reached a relatively constant rate of change. There were some exceptions to this trend;  $\Delta f_{sys}$  in phase 3, and  $\Delta q_b$  in phase 1. In the latter, the high rate of change was an artefact of the very small volumes of sediment output relative to measurement precision. In other cases, following the initial adjustment period,  $\Delta f_{sys}$  and  $\Delta q_b$  stabilised at relatively similar values, approximately  $< 3$  percent change per minute. Also, the magnitude of the adjustment for each variable generally increased with increasing discharge, except for the initial change from the screeded bed in phase one.

To further explore the patterns of adjustment towards and within steady-state conditions, the rates of change in  $f_{sys}$  and  $q_b$  in each phase are presented in Fig-

### 4.3. Results

---

ure 4.4. Following each successive increase in discharge, there is generally an initial period during which flow resistance and flux change at a relatively rapid rate. Following this adjustment period, there is oscillation around a more constant rate of change. These patterns vary across the different phases, in two notable ways. First, there was only a relatively minor adjustment in sediment transport and flow resistance at the beginning of the second phase. Second, during the steady-state period in phase four there was a very small rate of change, whereby sediment transport and flow resistance varied by less than 1 percent per minute.

#### 4.4. Discussion

---

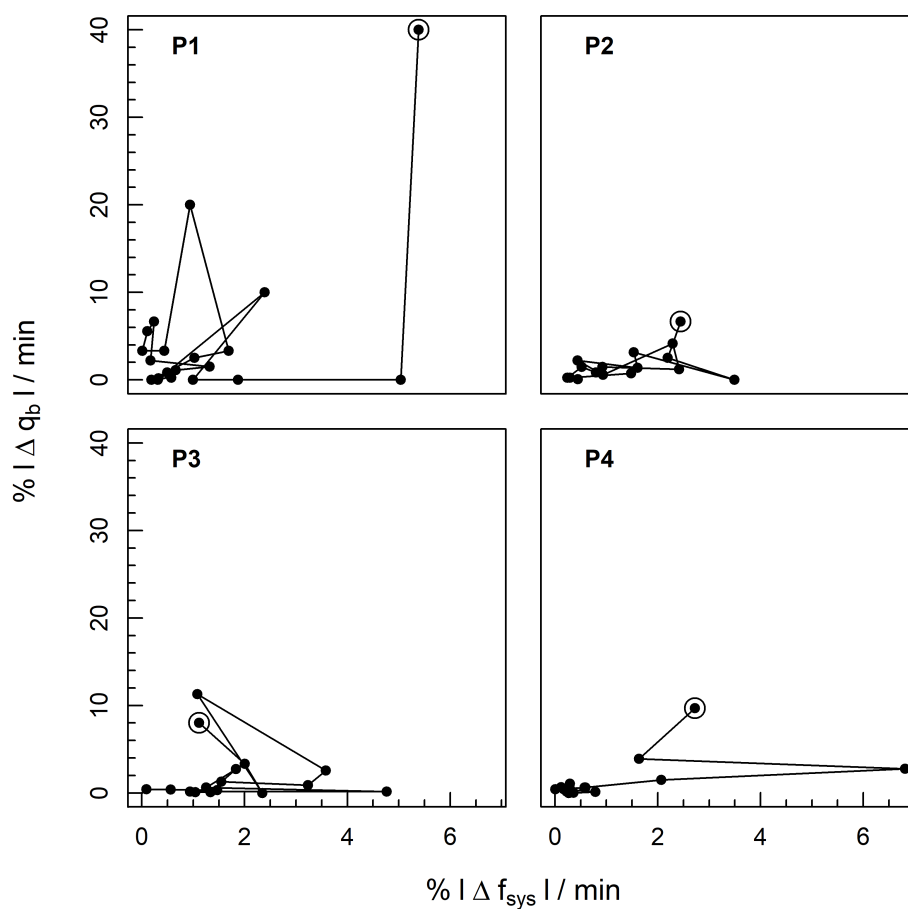


Figure 4.4: Change in  $f_{\text{sys}}$  and  $q_b$  at each successive point of the experiment, separated by experimental phase. Circled points represent the first measurement taken during each phase.

## 4.4 Discussion

The experimental results show an adjustment to the imposed changes in discharge that involves the time-dependent evolution of flow resistance, bed mor-

#### 4.4. Discussion

---

phology, and bedload transport towards conditions where these characteristics become time-independent. The experiment comprises a test of these general temporal trends, rather than a predictive model of the specific timing, magnitude, or character of specific adjustments.

The adjustment of the three parameters was nonlinear within each phase such that the rate of change was rapid at first but decreased toward zero, although fluctuations continued within a finite envelope. This temporal pattern of response is consistent with general models describing the nonlinear adjustment of geomorphic systems towards a constant variance around a mean value (Langbein and Leopold, 1964; Graf, 1977; Rhoads, 2020, Fig. 6.20). Given the fluctuation in flow, form, and flux variables despite constant flow conditions, one could speculate that in a real river system where discharge changes continuously the system may be considerably less stable (Howard, 1982). The system may be even more unstable if the rate of change in external conditions is rapid relative to the adjustment time, as it may never fully adjust to the change in conditions (Rhoads, 2020, Fig. 6.20). Based on high levels of temporal resolution and measurement accuracy, the channel adjustment provides strong evidence for the approximately exponential approach toward steady-state and the potential for transiency if disturbance frequency exceeds the recovery time.

Channel adjustments (i.e. bar reorganisation events) were well reflected by changes in morphologic activity, indicating the magnitude of physical change occurring between time-steps. Subsequently, rapid changes in morphologic activity clearly indicated points in time where the system passed intrinsic thresholds (Schumm, 1973, 1979), or where increases in discharge were geomorphically effective. The system crossed an intrinsic threshold in the first experimental phase (event  $\alpha$ ), where a significant morphologic reorganisation (characterised by an increase in topographic variability and pool depth) led to an increase in bedload transport. The specific magnitude or timing of this adjustment may vary according to initial conditions (say, in the case of a repeated experiment), although these characteristics are not being tested.

Similar feedbacks between the spatial distribution of shear stress and bedload

#### 4.4. Discussion

---

dynamics have been observed in the field and incorporated into models of sediment transport (Paola and Seal, 1995; Paola, 1996; Nicholas, 2000; Ferguson, 2003; Monsalve et al., 2020). The concentration of flow in preferential paths constitutes a fundamental feedback between channel morphology and sediment transport (Church, 2010; Church and Ferguson, 2015).

As discharge was increased the system demonstrated a variety of adjustments. In the second phase, the previous morphology was largely inherited from the previous phase. Visual observations of selective removal of finer grains from the bar-heads, resulting in coarser lag deposits, indicate that these larger-than-average grains acted as keystones that maintained the bar positions. This effect is consistent with studies that have identified larger-than-average grains controlling sediment transport and thresholds for channel deformation, rather than the average grain size (MacKenzie and Eaton, 2017; MacKenzie et al., 2018; Booker and Eaton, 2020). The entrainment threshold for larger-than-average grains was crossed as the discharge was increased again (event  $\beta$ ), suggesting that the influence of these grain size fractions is greatest at threshold and partial transport conditions (Wilcock and McArdell, 1993, 1997). Moreover, the lack of morphologic response to the first increase in discharge is inconsistent with the concept of geomorphic effectiveness (Wolman and Miller, 1960; Lisenby et al., 2018) and the temporal pattern of channel response proposed by Graf (1977).

In the final phase, the increase in shear stress exceeded the entrainment threshold above which bars could be maintained through deposition (event  $\gamma$ ). Here, shear stress was relatively higher than what could be expected in some natural alluvial channels as the discharge was contained within fixed banks, i.e. no widening nor over-bank spill could occur. The beginning of this phase was characterised by a rapid change in morphology and bedload transport as the pool-bar-riffle sequence was planed, and bar redevelopment occurred far slower than in the previous phase due to a low rate of deposition.

There was a nonlinear response of morphology and sediment transport to the regular increases in discharge throughout the experiment, and each aspect of the fluvial trinity followed strongly inter-related but differing trajectories. There was

#### 4.5. Conclusion

---

a negative parabolic trend in topographic variability and an approximately exponential increase in bedload transport, whilst flow resistance decreased relatively steadily. Combinations of these two variables distinguish between channel characters that correspond to each phase of the experiment. In other words, each steady-state condition was achieved via different combinations of form, flow, and flux. The diverging trajectories of these parameters represent distinct manifestations of morphodynamic interplay that facilitates the emergence of a constant variance condition for each flow regime. Interestingly, the adjustment of the fluvial trinity appeared to maintain a relatively constant level of morphological activity across the different steady-state periods (i.e. even when discharge was increased).

For each discharge, each component of the fluvial trinity adjusted towards a constant variance state, suggesting that in practice system stability could be defined in various ways. Indeed, there are several definitions of channel stability that have been proposed, relating to mass-balance ('grade', e.g. Mackin, 1948), energy-balance (Nanson and Huang, 2017), and a constancy of channel morphology ('dynamic' or 'pattern' stability, e.g. Hey and Thorne, 1986; Schumm, 1985). These concepts provide a useful means of classifying channel dynamics into 'stable' and 'unstable' states by isolating a single aspect of the fluvial system. The steady-state conditions observed in the experiment were characterised by different degrees of variation, and there were also marginal departures from steady-state conditions (secondary adjustments following the initial perturbation). These results support a spectrum of system stability that is not reflected in binary representations of behaviour and highlight the importance of determining historical patterns of variability (Brierley and Fryirs, 2005; Wohl, 2011; Fryirs et al., 2012).

## 4.5 Conclusion

The adjustment of the channel to varying discharge highlighted several important aspects of channel behaviour. As discharge was increased, each component of the fluvial trinity exhibited a nonlinear adjustment towards a steady-state characterised by fluctuations around a constant mean. Steady-state conditions were

#### 4.5. Conclusion

---

achieved through the mutual adjustment between these components, suggesting that the investigation and explanation of channel behaviour requires an appreciation of all three. The experiment provides quantitative evidence for conceptual models describing exponential approaches towards steady-state. This evidence is only partial given that volumes of morphologic activity did not always follow the exponential decay trend proposed by Graf (1977). The results also highlight how in natural rivers, particularly those with greater degrees-of-freedom for adjustment, continuous changes in discharge may lead to nonlinear rather than steady-state behaviour.

Particularly at relatively low discharges, the feedbacks between the fluvial trinity underscored the importance of geomorphic thresholds. Under these conditions, channel adjustments comprised feedbacks between morphology and sediment transport, and channel deformation was controlled by larger-than-average grain size fractions. These two processes occurred at the bar scale and were highly spatialised, being associated with the lateral concentration of shear stress and grain patchiness, respectively, which has two important implications. First, reach-averaged representations of process provide only partial insight into channel behaviour. Second, models of rivers that suppress feedbacks between the fluvial trinity, and size-dependent transport, may not replicate important process feedbacks that typically occur in field conditions.

There are, however, several challenges in studying river behaviour in nature. Practical difficulties associated with the collection of field data often mean that only short-term or temporally sporadic data are available. These data may be misleading given the typically nonuniform rates of adjustment and relatively constant changes in channel conditions (i.e. discharge) observed in nature. Given continual advances in field methods, and in particular remote sensing (Kasvi et al., 2019; Dietrich, 2017), we can expect that historical approaches to assessing river behaviour may become increasingly realistic. Especially in natural rivers with greater degrees-of-freedom available (notably, lateral adjustment and meandering) and greater potential for nonlinear behaviour, more holistic assessments of channels that embrace different aspects of the system are critical in understanding

#### 4.5. Conclusion

---

the direction, magnitude, and timing of adjustments. Meanwhile, laboratory experiments may provide further insights into nonlinear channel behaviour, where researchers may take a ‘forensic’ approach to identify processes both temporally and spatially.

The spatial dependence of feedbacks between the fluvial trinity may suggest that understanding channel behaviour requires more spatially explicit representations of processes, rather than reach-averaged ones. In the following chapters, I develop analyses that capture the scale-dependence of hydraulics and morphology.

# Chapter 5

## Multiscalar roughness-length decomposition

### 5.1 Introduction

Understanding flow resistance is of great interest to river research and practice. The estimation of flow resistance is important for determining flood magnitudes, predicting ecological habitat, estimating rates of sediment transport, and understanding channel behaviour. However, the hydraulics of gravel-bed channels, in particular, are relatively poorly understood (see Ferguson, 2007). Given that most of the foundational work in fluid dynamics, upon which conventional approaches to predicting flow resistance are based, was conducted using regular (e.g. Schlichting, 1936) or uniscalar (e.g. Nikuradse, 1933) bed geometry, the multiscalar topographic characteristics of these rivers presents a major challenge. In particular, individual grains and assemblages of grains ('forms') on the bed surface, spanning orders-of-magnitude of scale (ripples, dunes, bars), have variable contributions to the total flow resistance across different channel types. Thus, moving forward, mainstream empirical approaches to estimating flow resistance based solely on grain diameter would ideally be replaced by approaches that explicitly account for multiple nested spatial scales. Decomposing roughness lengths into different scales may contribute to an understanding channel processes given that energy dissipation is increasingly recognised as a condition governing river adjustment (Eaton and Church, 2004; Nanson and Huang, 2018; Church, 2015). Also, the partitioning of bed stresses between grain and form scales is an important step in predicting bedload transport (Ancey, 2020*b*). More fundamentally, as discussed

## 5.1. Introduction

---

in the previous chapter, understanding how channel processes vary spatially is important in understanding channel adjustment.

Inspired by early work in fluid dynamics (Schlichting, 1936; Keulegan, 1938) and subsequent work in fluvial hydraulics (Einstein and Banks, 1950; Nowell and Church, 1979), some geomorphologists sought to disaggregate the roughness length into grain and form contributions by correlating bar geometry with flow resistance (Davies and Sutherland, 1980; Prestegard, 1983). However, further work was likely hindered by limitations associated with the collection of topographic data in rivers (Furbish, 1987; Robert, 1988). Advances in remote-sensing and statistics have since allowed researchers to explore detailed scaling characteristics of gravel-bed surfaces using analyses such as variograms (Robert, 1988; Clifford et al., 1992) and transforms (Nyander et al., 2003). Topographic analyses have led to multiscale decompositions of geometric roughness in rivers, although full decompositions of hydraulic roughness have not yet been presented. The latter approach has been developed for complex aeolian surfaces using transforms (Nield et al., 2013; Pelletier and Field, 2016; Field and Pelletier, 2018), which serves as a proof-of-concept for a multiscale roughness length decomposition.

A recent publication (Adams, 2020b) identified two relatively recent advancements in the fields of statistics and fluid dynamics that could contribute to a multiscale roughness length decomposition tool. The first advancement is the wavelet transform, which is generally superior to the Fourier transform when analysing the underlying structure of complex and aperiodic signals. This is due to the use of a finite (rather than a continuous) wavelet function, that gives rise to a family of wavelets that are dilated (stretched and compressed) and translated (shifted) along the signal (Torrence and Compo, 1998). There are now various types of wavelet transform suited to different applications, some of which have been applied in rivers (Kumar and Foufoula-Georgiou, 1997; Nyander, 2004; Keylock et al., 2014). The second advancement is the development of roughness correlations for irregular surfaces (e.g. Forooghi et al., 2017; De Marchis et al., 2020), which estimate the roughness length of a surface based purely on its geometric characteristics.

In this chapter, I develop a novel technique to answer the question: What is the relative contribution of different scales of river bed topography to the total roughness length? The general approach consists of: 1) a wavelet transform in which the channel surface is decomposed into a set of more simple components each at a different wavelength, and 2) a roughness correlation that estimates the roughness length associated with each wavelength, which is expressed as the equivalent sand roughness parameter  $k_s$  (Nikuradse, 1933; Schlichting, 1936). By modifying the specific roughness correlation that is used, the transform-roughness correlation (TRC) approach may be applied across a wide range of channel types and hydraulic conditions. To demonstrate the TRC analysis, I apply it to a series of original laboratory experiments with high-resolution digital elevation models (DEMs), as well as some additional published data. The proposed technique has important implications for understanding the spatial distribution of channel morphology and hydraulics.

## 5.2 Practical considerations

The transform-roughness correlation approach is a generic tool that should be adapted based on the hydraulic conditions and the purpose of its application. These considerations should span the dataset, the type of wavelet transform, and the specific roughness correlation that is selected. I first discuss these general considerations to provide important context for the TRC approach, prior to introducing the experimental data and the Forooghi et al. (2017) roughness correlation.

First, the minimum resolution and spatial extent of the topographic dataset should be informed by the scale of the features of interest. The data should have a sufficiently high spatial resolution such that it can capture the range of in-channel features that produce drag. Also, to capture the characteristic geometry of bed features (notably, height and spacing) and estimate a reach-averaged roughness length, the spatial extent of the dataset should be at least the length of the largest features that influence the flow, for example, it should span a series of dune crests or pool-riffle pairs.

## 5.2. Practical considerations

---

Second, given that the hydraulic roughness of in-channel features is of interest, the channel topography can be reduced to a one-dimensional profile extending along the thalweg, representative of the primary flow path. It is important to note here that this approach ignores resistance elements such as channel planform, and three-dimensional interactions between flow and in-channel topography. If both hydraulic and topographic data are available, this assumption may be validated by comparing the roughness length estimated using the roughness correlation to a measured roughness length. If the range of interactions between the flow and the surface is of interest, multiple parallel elevation profiles could be analysed.

Third, the choice between discrete and continuous wavelet transforms (DWT and CWT) is a trade-off between the resolution of the decomposition and the physical resemblance to the original profile. Compared to the DWT, the CWT extracts more intricate structural characteristics from the signal and yields a greater number of wavelengths between which information is shared (Addison, 2018). However, the redundancy in the CWT generates a more abstract representation of the topographic variation at a given wavelength. In Figure 5.1, I compare wavelengths extracted using a maximal overlap discrete wavelet transform (MODWT) and a CWT using the same elevation profile. At the wavelength corresponding to the spacing of a pool-bar-riffle sequence ( $\lambda \approx 2$  m), the oscillations output by the MODWT are aligned with the pool-riffle undulations (i.e. the position of peaks and the general shape are similar), but the CWT oscillations do not appear to align with the original profile. Given that they do not resemble the channel surface, it may be invalid to infer hydraulic behaviour from CWT wavelengths.

## 5.2. Practical considerations

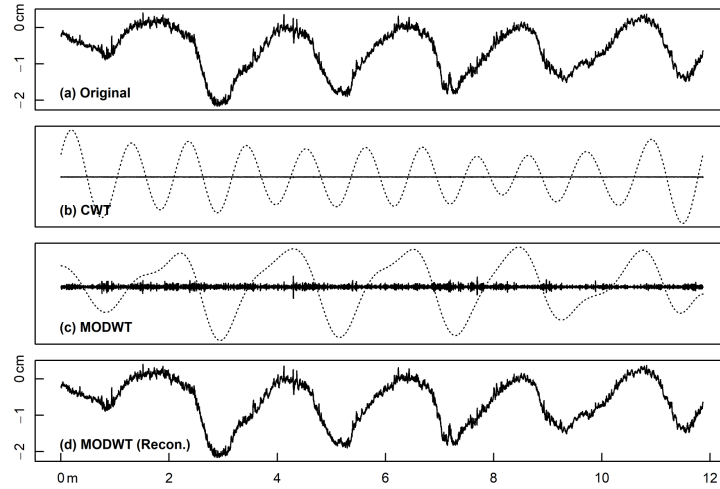


Figure 5.1: **a)** Thalweg elevation profile at end of run 1a featuring a prominent pool-riffle sequence, where the x-axis represents distance upstream, **b)** grain ( $\lambda = 4$  mm) and form ( $\lambda \approx 2$  m, dashed line) wavelengths derived from CWT, **c)** the same two wavelengths derived from a MODWT, and **d)** the original signal reconstructed from the MODWT by recombining wavelengths.

Fourth, the specific roughness correlation that is used should match the regime of the channel's boundary Reynolds number  $Re^* = U^*k/\nu$ , where  $U^*$  is shear velocity,  $k$  is some representative roughness scale, and  $\nu$  is kinematic viscosity. For example, given that gravel-bed rivers tend to be within the fully rough regime where  $Re^* \geq 70$  (Buffington and Montgomery, 1997; Schlichting, 1979), it may only be valid to apply roughness correlations obtained for that regime specifically. Also, the flow should be turbulent, and it should be two-dimensional, which may be indicated (although not guaranteed) by flow aspect ratios or width-depth ratios greater than 5 (Nezu and Nakagawa, 1993).

Last, roughness correlations in fluid dynamics tend to be developed for flows sufficiently deep to have logarithmic velocity profiles, which should be considered when they are applied to flows with less developed profiles. Jimenez (2004) suggested that logarithmic layers develop where relative submergence  $h/k$  is greater than 40, although Cameron et al. (2017) observed a logarithmic layer in rough

### 5.3. Application of TRC approach in gravel-bed rivers

Table 5.1: Summary of A-BES experimental data collected during the final portion of each experimental phase. Values represent the mean of the last 12 measurements using stream gauge data. The reported  $\sigma_z$  values were calculated following the detrending process detailed in Section 5.3.2, and  $Re^*$  was calculated with the roughness length  $k = k_{s,rc}^*$ , which is defined in Section 5.3.1. Units:  $h$  [m],  $U^*$  [m/s],  $\sigma_z$  [mm],  $k_s$  [m].

Run	$h$	$U^*$	$U/U^*$	$\sigma_z$	$h/D_{84}$	$h/\sigma_z$	$Re^*$	$k_{s,rc}^*$	$k_{s,CW}^*$
2a	0.015	0.053	6.85	1.55	4.53	9.35	213	0.005	0.008
2b	0.013	0.051	5.35	1.18	4.11	11.16	181	0.005	0.017
1a	0.015	0.053	6.74	6.06	4.56	2.41	619	0.015	0.011
1b	0.012	0.048	6.19	5.17	3.74	2.31	479	0.014	0.006
1c(1)	0.011	0.047	4.55	4.94	3.50	2.27	453	0.013	0.019
1c(2)	0.013	0.051	5.31	7.35	4.11	1.79	762	0.019	0.019
1c(3)	0.014	0.053	7.15	5.82	4.43	2.44	671	0.016	0.013
1c(4)	0.018	0.060	7.23	3.86	5.71	4.74	1034	0.023	0.008

open-channel flow at submergences as low as 1.9. During most flow conditions, it is common for gravel-bed rivers to have relative submergences of less than 10, and in some cases, as low as 0.1 (Lee and Ferguson, 2002; Ferguson, 2007), where no logarithmic layer can develop because roughness elements are not submerged. However, if one is interested in channel-forming flows capable of reworking the bed surface (Ashworth and Ferguson, 1989; Wolman and Miller, 1960) where relative submergence may be two orders-of-magnitude higher (Limerinos, 1970; Bray, 1982), the logarithmic assumption should be satisfied for most rivers.

## 5.3 Application of TRC approach in gravel-bed rivers

### 5.3.1 Stream table experiment

To demonstrate the TRC approach, I required a large set of DEMs and associated hydraulic data for validation, and ideally straight channels where in-channel features represent the dominant source of drag. I utilised all runs available at the time

### 5.3. Application of TRC approach in gravel-bed rivers

---

of writing, which were conducted at widths of 0.3 and 0.08 m (i.e. 1a,b,c and 2a,b in Table 3.3) which feature relatively simple pool-bar riffle (or alternate bar) and plane-bed morphologies, respectively. These runs were appropriate for testing the TRC approach as they maintained relatively rough flow whilst they also reproduced multiple scales of bed features (notably, grains and a pool-riffle sequence). A summary of hydraulic data is provided in Table 5.1, and data and code for the TRC approach are available online (see Adams, 2020a, for link). In addition to the estimate of  $k_s$  obtained using the roughness correlation, I estimate  $k_s$  using the hydraulic data ( $k_{s,CW}^*$ ), using a Colebrook-White type formula defined as

$$\frac{1}{\sqrt{f}} = -K_1 \log \left( \frac{k_s}{K_2 h} + \frac{K_3}{4Re\sqrt{f}} \right) \quad (5.1)$$

where  $K_1 = 2.03$ ,  $K_2 = 11.09$ , and  $K_3 = 3.41$  as determined by Keulegan (1938) and  $Re$  is the Reynolds number. I neglect the second term within the logarithm as it represents the contribution of viscous forces to friction, which is likely small for hydrodynamically rough conditions. The Darcy-Weisbach friction factor  $f$  is defined as

$$\sqrt{\frac{f}{8}} = \frac{\sqrt{ghS}}{U} \quad (5.2)$$

In addition to the runs conducted for this study, I obtained topographic and hydraulic data for 86 step-pool runs published by Hohermuth and Weitbrecht (2018). The runs were conducted in a 1:20 nays-scaled model of a mountain stream, utilizing a range of bed slopes (8–11 percent), channel widths (0.15–0.35 m), and unit discharges (0.019–0.167 m<sup>2</sup>/s). Four different grain size distributions were used, where  $D_{50}$  varied from 2.1–7.0 mm, and  $D_{90}$  remained around 58 mm. For a given run, a range of potentially usable elevation profiles were identified based on criteria for erroneous values, then the profile closest to the channel centreline was selected. Of the 86 runs conducted, 83 are used in this study. Thus, there is a total of 247 DEMs with associated hydraulic data when combined with the

A-BES runs, which span three morphologic types; step-pool (SP), pool-bar-riffle (PBR), and plane-bed (PB).

### 5.3.2 The transform-roughness correlation approach

Here I specifically tailor the TRC approach to the geometric and hydraulic characteristics of gravel-bed channels. First, a MODWT was applied to the thalweg elevation profiles of each DEM, yielding a set of simplified profiles representing topographic variation occurring at different wavelengths. Second, I selected a roughness correlation developed by Forooghi et al. (2017) that predicts  $k_s$  from surface geometry in the fully rough regime, which was applied to each wavelength. The relation was developed by conducting 38 direct numerical simulations in closed channels with an array of systematically varied roughness geometries, both regular and irregular. By correlating surface and flow properties, Forooghi et al. (2017) proposed the following empirical relation

$$\frac{k_s}{k_{ref}} = F(Sk, \Delta) \cdot F(ES) \quad (5.3)$$

where  $k_{ref} = 4.4\sigma_z$ , and  $Sk$  is the skewness of the probability distribution of elevations. The functions  $F(Sk, \Delta)$ ,  $F(Sk)$ , and  $F(ES)$  are defined, respectively, as

$$F(Sk, \Delta) = \begin{cases} F(Sk), & \Delta \geq 0.35 \\ F(Sk)(1 + m(Sk) \cdot (\Delta - \Delta_0)), & \Delta \leq 0.35 \end{cases} \quad (5.4)$$

$$F(Sk) = 0.67Sk^2 + 0.93Sk + 1.3 \quad (5.5)$$

and

$$F(ES) = 1.05 \cdot (1 - e^{-3.8 \cdot ES}) \quad (5.6)$$

where  $\Delta$  is a measure of variability in the elevation of the peaks of roughness elements (height range divided by the mean,  $\Delta = 0$  if peak heights are identical),

#### 5.4. Results and Discussion

---

$\Delta_0 = 0.35$  (not related to the critical  $ES$  value introduced below), and  $m(Sk) = 1.47Sk^2 - 1.35Sk - 0.66$ . The parameter  $ES$  is the effective slope, given by

$$ES = \frac{1}{L} \int_L \left| \frac{dz(x)}{dx} \right| dx \quad (5.7)$$

where  $z(x)$  is the height array,  $x$  is the streamwise direction, and  $L$  is the surface length in  $x$ . Effective slope may be interpreted as the mean gradient of the local roughness elements (Napoli et al., 2008), and therefore represents the aspect-ratio of roughness elements rather than their vertical height. With other surface parameters kept equal, the roughness length is strongly dependent on  $ES$  within the range  $0 < ES < 0.35$  (Napoli et al., 2008; Schultz and Flack, 2009). I calculated values of  $\Delta$  for each wavelength by identifying peaks of the oscillations, and found  $\Delta > 1$  for almost all cases. Values of  $\Delta$  could not be estimated for the longest few wavelengths as they typically contain very few (or even one) complete oscillations that could be interpreted as roughness peaks. As a result, I simply used the  $F(Sk)$  term in Equation 5.4. The roughness length for each wavelength is expressed as  $k_{s,rc}$ .

In addition to applying the roughness correlation to each wavelength, I applied it to each thalweg elevation profile to obtain an estimate of  $k_s$ , expressed as  $k_{s,rc}^*$ . Each profile was first detrended using the least-squares approach, which is not necessary with the wavelet transform as the overall trend is represented by a single wavelength and removed from all others. In the following section, I present the results of the TRC approach applied to the runs.

## 5.4 Results and Discussion

In this section, I first seek to validate the TRC approach, and then focus on the multiscale roughness-length decomposition of run 1a, which features a well-developed pool-bar-riffle sequence under a formative discharge. First, I compare the topographic- and hydraulic-based estimates of  $k_s$ . Second, I demonstrate

the relationship between estimates of  $k_s$  with and without the wavelet transform. Third, I show how the key parameters of the roughness correlation (standard deviation, effective slope, skewness) vary across each wavelength. Fourth, I estimate the relative contribution of different scales of bed topography to the total roughness length and explain how the estimated values relate to the key parameters and the characteristics of the experiments. Fifth, I compare the performance of different roughness lengths in estimating flow resistance. Finally, I discuss the significance, limitations, and potential applications of the TRC approach.

### 5.4.1 Estimates of total $k_s$

The relationship between the estimates of  $k_s$  from the roughness correlation  $k_{s,rc}^*$  and the Colebrook-White equation  $k_{s,CW}^*$  differs between the three different channel morphologies (Figure 5.2). Here, I consider  $k_{s,CW}^*$  to be a ‘measured’ quantity which the roughness correlation may be tested against. The pool-bar-riffle experiments ( $W = 0.3$  m) exhibit the closest relationship between the two  $k_s$  estimates, with the distribution centering along the line of equality (median  $k_{s,CW}^*/k_{s,rc}^* = 0.96$ ). The close relationship between the two independent estimates of  $k_s$  supports the one-dimensional approach for these experiments as it indicates that the single elevation profile captures the roughness elements that contribute the greatest resistance to flow. Also, the results support the application of the Forooghi et al. (2017) roughness correlation to the A-BES experiments, which have more complex surface characteristics and far lower values of relative submergence compared to the numerical domain within which the correlation was developed.

The distribution of plane-bed experiments ( $W = 0.08$  m) overlap with the line of equality, although there is a consistent under-prediction of  $k_s$  using the roughness correlation by a factor-of-two or three (median  $k_{s,CW}^*/k_{s,rc}^* = 2.54$ ). In the case of the step-pool experiments, there is a significant under-prediction of  $k_s$  by the roughness correlation of around an order-of-magnitude (median  $k_{s,CW}^*/k_{s,rc}^* = 9.48$ ), which may be explained with the lower relative submergence (median  $h/D_{84} = 1.48$ ).

## 5.4. Results and Discussion

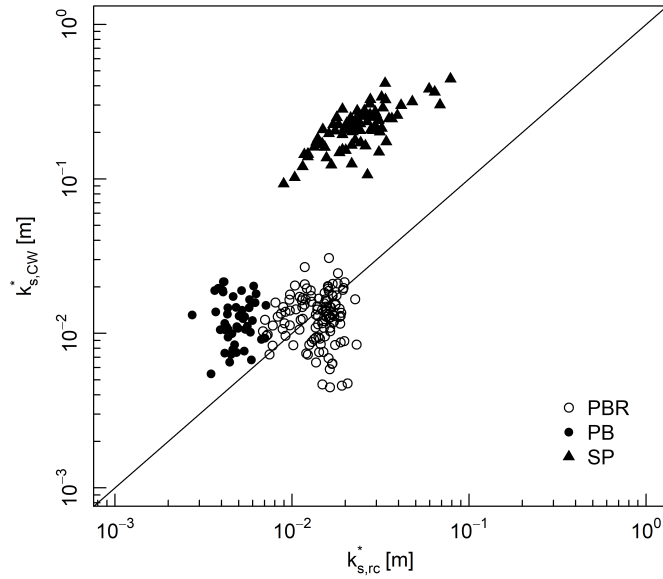


Figure 5.2: Relationship between total  $k_s$  estimated by the Forooghi et al. (2017) roughness correlation (Equation 5.3) and the Colebrook-White approach (Equation 5.1). Data is grouped by channel morphology type.

The next stage in validating the TRC approach is comparing the values of  $k_{s,rc}^*$  and  $\Sigma k_{s,rc}$ , whereby the latter is the estimate provided by applying the roughness correlation to each wavelength (giving values of  $k_{s,rc}$ ), and then taking the sum. In other words, this is comparing the values of  $k_s$  estimated by the roughness correlation with and without the wavelet transform as an intermediate stage. This comparison is important for two reasons. First, the TRC approach is an extension of the linear superposition approach, which assumes that the hydraulic effect of adding up different roughness elements is approximately linear (Millar, 1999; Wilcox and Wohl, 2006; Rickenmann and Recking, 2011). In practice, superimposing roughness elements may have nonlinear feedback effects (Yen, 2002; Li, 2009; Wilcox and Wohl, 2006), such that  $k_{s,rc}^*$  and  $\Sigma k_{s,rc}$  may potentially not be

#### 5.4. Results and Discussion

---

correlated.

Second, values of  $k_{s,rc}^*$  and  $\Sigma k_{s,rc}$  may differ as the process of signal decomposition and recombination is characterised by wave interference. For example, for each thalweg elevation profile there are two estimates of amplitude: (1) the standard deviation of elevations  $\sigma_z$ , and (2)  $\Sigma\sigma_\lambda$ , which is the sum of  $\sigma_z$  for each wavelength. However, due to positive and negative wave interference  $\sigma_z$  and  $\Sigma\sigma_\lambda$  may significantly differ. Decomposing and recombining wavelengths alters the position and magnitude of peaks and troughs in the wavelengths, and therefore, their amplitude. Similarly, wave interference may potentially confound estimates of  $k_s$  if a transform is used. For the above two reasons, it is important to demonstrate that values of  $k_{s,rc}^*$  and  $\Sigma k_{s,rc}$  are correlated, even if they are unlikely to have the same absolute value.

The transform and non-transform estimates of  $k_s$  are positively correlated with a power-law relation (Figure 5.3). It is worth noting that the two datasets are characterised by different slopes and intercepts, which may be explained with the specific characteristics of each topographic dataset (e.g. geometry, resolution) giving rise to different patterns of wave interference. However, it appears that nonlinear superposition effects and wave interference do not invalidate the TRC approach for these datasets.

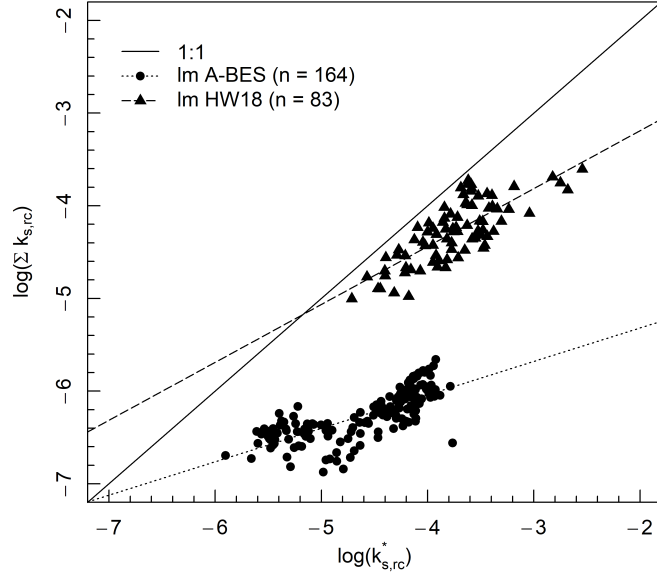


Figure 5.3: Relationship between  $k_{s,rc}^*$  and  $\Sigma k_{s,rc}$  for the A-BES and Hohermuth and Weitbrecht (2018) experiments.

### 5.4.2 Application of TRC approach

In Experiment 1a there is a general increase in the standard deviation of elevations with increasing wavelength (Figure 5.4a). Over the first ten minutes (i.e. the first two elevation profiles), there is an increase in  $\sigma_z$  at  $\lambda > 0.5$  m, with the greatest increase at  $\lambda \approx 2$  m, but smaller wavelengths remain largely unchanged. At the smallest wavelengths, the  $\sigma_z$  tends towards zero, and there is some contribution to  $\sigma_z$  at the largest wavelengths due to the slightly concave shape of the profile, evident in Figure 5.1a. Figure 5.4b presents the value of  $\sigma_z$  for each wavelength as a cumulative percentage. This type of graph is similar to the form size distribution (FSD) proposed by Nyander et al. (2003), which is the cumulative variance of each wavelength calculated using a 2D DWT. For comparison, I provide the bulk

## 5.4. Results and Discussion

grain size distribution within the same space (where wavelength is grain diameter). Grain-scale wavelengths account for less than five percent of all topographic variation, given that the arrangement of grains contribute to bed structures that usually exceed the amplitude of individual grains.

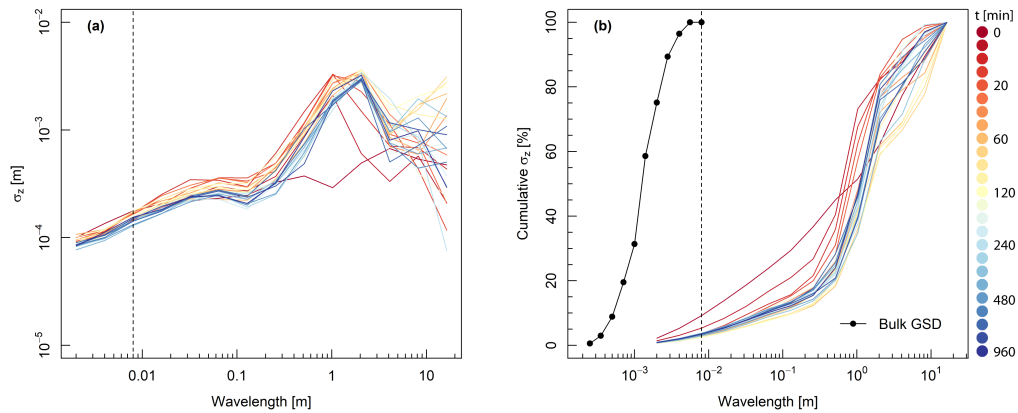


Figure 5.4: Form size distribution during Experiment 1a, where each line represents a point in time, and the initial screeded bed is included. The standard deviation of each topographic wavelength is presented as an (a) absolute, and (b) cumulative percentage, for each thalweg elevation profile. The bulk grain size distribution is included, where the wavelength corresponds to grain diameter. The vertical dashed line represents the largest grain diameter in the experiment.

The effective slope is greatest at the grain scale wavelengths ( $\lambda \leq D_{\max}$ ) where the surface is characterised by closely-bunched peaks and troughs associated with individual grains (Figure 5.5a). Values of  $ES$  decrease with increasing  $\lambda$ , due to the presence of more gently undulating roughness elements. This is evident in the example (Figure 5.1c), where the 4 mm wavelength has high  $ES$  indicated by sharp oscillations (but low  $\sigma_z$ ), and the 2 m wavelength has low  $ES$  (but high  $\sigma_z$ ). The main exception to the downwards trend of  $ES$  with increasing  $\lambda$  is the wavelength of around 2 m where there is a prominent peak in the  $ES$  distribution,

## 5.4. Results and Discussion

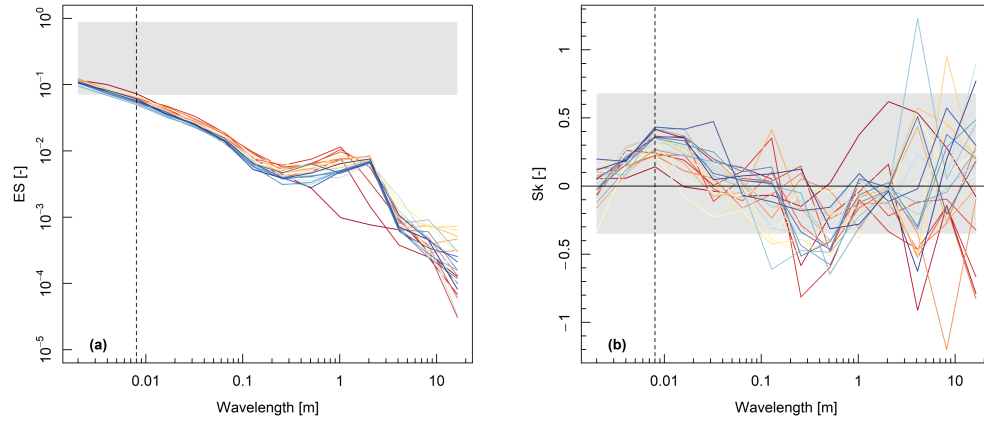


Figure 5.5: **a)** Effective slope and **b)** skewness of each topographic wavelength during Experiment 1a. The shaded area represents the range of  $ES$  and  $Sk$  values of the surfaces generated by Forooghi et al. (2017). Refer to Figure 5.4 for legend.

associated with the development of the pool-riffle-bar sequence approximately ten minutes into the experiment. Note that most of the topographic wavelengths have values of  $ES$  (and  $k_s/k$  in Equation 5.3) that are smaller than the surfaces used by Forooghi et al. (2017) to develop the roughness correlation. Short wavelengths tend to be positively skewed, moderate wavelengths ( $0.2 > \lambda > 2.0$  m) tend to be negatively skewed, and long wavelengths are either positively or negatively skewed (Figure 5.5b). There is little change in the pattern of skewness over the course of the experiment.

The distribution of  $k_{s,rc}$  values predicted for each wavelength using Equation 5.3 is presented in Figure 5.6a. Following the format of ‘grain size distribution’ and ‘form size distribution’, I term this style of plot the ‘drag size distribution’ (DSD). There is a major peak in the DSD at  $\lambda \approx 2$  m (the spacing of pools, bars, and riffles), and a minor peak at the scale of  $\lambda \approx 0.008$  m (around the size of the largest grains). At small wavelengths, and large wavelengths especially, estimated  $k_s$  tends downwards. Figure 5.6b presents the DSD as a cumulative percentage, which shows that the  $k_s$  associated with the grain scale is estimated to account

## 5.4. Results and Discussion

for approximately 30 percent of the total  $k_s$ . This proportion of grain- and form-drag is similar to estimates in gravel-bed rivers with similar morphologies (Hey, 1988; Parker and Peterson, 1980; Prestegard, 1983), which further indicates that the TRC approach provides a physically realistic decomposition of the roughness length.

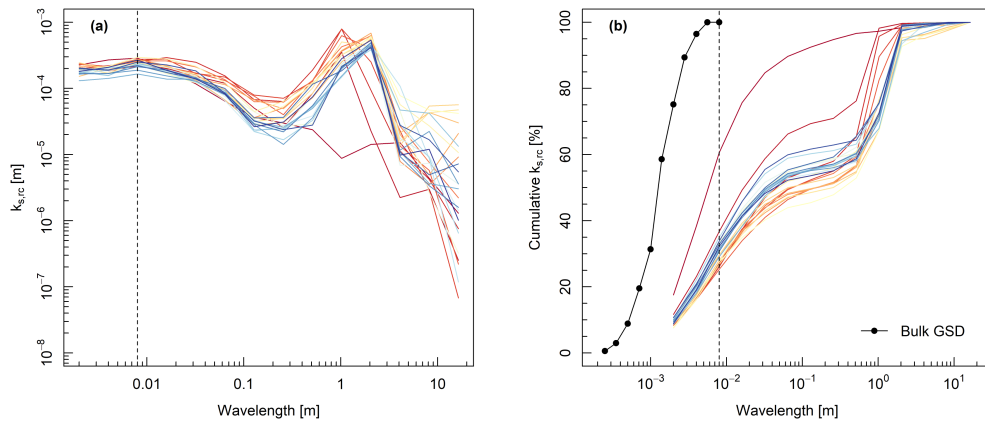


Figure 5.6: Drag size distribution over the course of Experiment 1a. The estimated roughness length of each topographic wavelength presented as an (a) absolute, and (b) cumulative percentage. Refer to Figure 5.4 for legend.

In Figure 5.7 I compare the performance of geometric ( $D_{84}$ ,  $\sigma_z$ ) and hydraulic ( $k_{s,rc}^*$ ,  $k_{s,CW}^*$ ) estimates of roughness length in estimating flow resistance, using the Ferguson (2007) variable-power equation (VPE, Equation 2.1). I provide two fitted relations for the VPE that provide baselines for comparison: 1) coefficients determined by a systematic review of  $\sigma_z$  as a roughness measure (Chen et al., 2020), and 2)  $k_{s,CW}^*$  values which are back-calculated from the hydraulic measurements. Given that these two relations represent geometric and hydraulic approaches to estimating roughness, they describe significantly different relationships between the friction factor and relative submergence.

There is a weak relationship between  $f$  and  $h/k$  if  $k$  is estimated by the bulk

#### 5.4. Results and Discussion

---

$D_{84}$  values (as an approximation of the surface GSD). Using  $\sigma_z$  as an estimate of  $k$  the step-pool experiments are consistent with the VPE relation provided by Chen et al. (2020), but  $\sigma_z$  overestimates  $k$  in the A-BES experiments. Using values of  $k_s$  from the roughness correlation, the values of relative submergence for the A-BES experiments are consistent with the Colebrook-White relation, but there is an underprediction of  $k_s$  in the step-pool experiments. These results suggest that estimates of  $k_s$  from roughness correlations may provide better estimates of flow resistance in some conditions. The results also affirm that roughness metrics derived from surface topography are superior to ones derived from the grain size distribution.

## 5.5. Implications, applications, and limitations

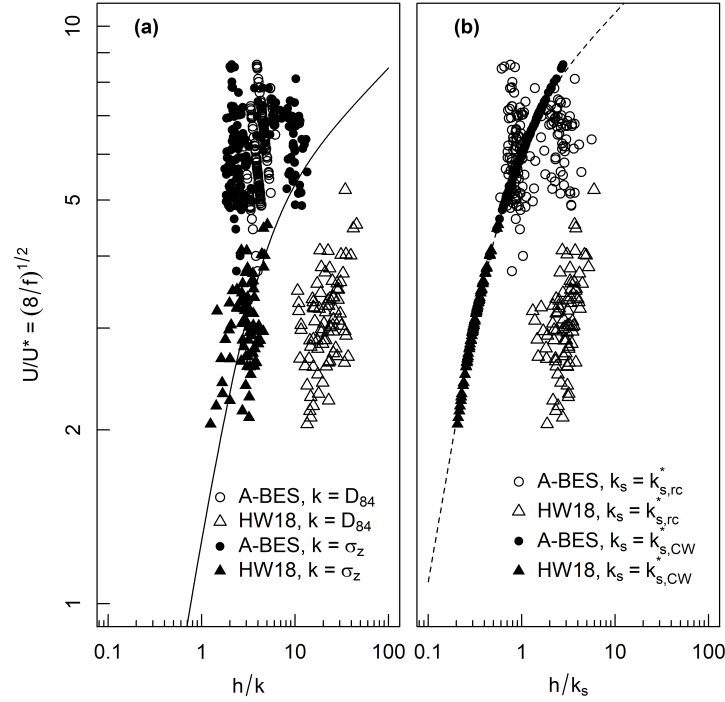


Figure 5.7: Plot of  $(8/f)^{1/2}$  against relative submergence for A-BES and Hohermuth and Weitbrecht (2018) data, using four different roughness lengths ( $D_{84}$ ,  $\sigma_z$ ,  $k_{s,rc}^*$ ,  $k_{s,CW}^*$ ). The solid line is the Ferguson (2007) VPE using coefficients  $a_1 = 3.94$  and  $a_2 = 1.36$  determined by a systematic review of  $\sigma_z$  as a roughness measure (Chen et al., 2020). The dashed line is the VPE fitted to the  $h/k_{s,CW}^*$  data, yielding coefficients of  $a_1 = 7.22$  and  $a_2 = 11.19$ .

## 5.5 Implications, applications, and limitations

Recently proposed roughness correlations in fluid dynamics (e.g. Forooghi et al., 2017; De Marchis et al., 2020) incorporate information regarding both the height of the roughness elements (a vertical roughness scale, e.g.  $\sigma_z$ ) and the arrangement or spacing of roughness elements (a horizontal roughness scale, e.g.  $ES$ ). In isolation, either one of these roughness metrics may contribute to an incom-

### 5.5. Implications, applications, and limitations

---

plete – and potentially misleading – estimate of flow resistance. It is important to recognise that, depending on the surface of interest, the total roughness length is usually a compromise between vertical and horizontal roughness scales of the bed surface.

In gravel-bed rivers, which are typically ungauged, and where measurement of hydraulic variables is subject to practical limitations (Miller, 1958), flow resistance is usually estimated using only a vertical roughness scale such as grain diameter (Hey, 1979; Ferguson, 2007). However, the relationship between grain diameter and flow resistance breaks down in natural channels for two main reasons (see Adams, 2020*b*): 1) grain diameter does not account for larger and often more dissipative roughness elements, and 2) it does not consider the horizontal spacing of these larger roughness elements, which has a systematic effect on the flow (Morris, 1955; Leonardi et al., 2007). In recent years, the increased availability of high-resolution topographic data has led to the adoption of  $\sigma_z$  as a roughness metric in gravel-bed rivers, on the basis that it includes information regarding larger-scale bed structures (Chen et al., 2020). However,  $\sigma_z$  only improves upon the first deficiency of grain-based roughness metrics and, consequently, it has inherent limitations. The roughness correlation presented by Forooghi et al. (2017) may improve upon existing roughness metrics used in gravel-bed rivers, and it may be applied to most datasets where  $\sigma_z$  is calculated.

The TRC analysis has direct applications across geomorphology. Quantification of scale-dependent patterns of channel topography and roughness length may contribute to form- and process-based classifications of channel morphology and dynamics. There have been numerous attempts to classify channels based on in-channel features and their associated processes (e.g. Montgomery and Buffington, 1997), however, analysis of bed topography is typically qualitative. One could expect that different channel types exhibit distinctive scale-based patterns of  $\sigma_z$  and  $k_s$ , which would enable a quantitative and heuristic classification index.

The scale-based decomposition of  $k_s$  may assist in identifying and forecasting the hydraulic influence of specific roughness elements in channels. For example, through the manipulation of spatial datasets by the addition or removal of features,

## 5.6. Conclusions

---

the role of natural in-channel features (e.g. large wood) and engineering designs (e.g. rock chutes) could be isolated and determined for flood conditions. Also, multiscale roughness length decomposition may contribute to an understanding of bedload transport processes, where accurate predictions rely on partitioning bed stresses between grain and form scales (Ancy, 2020b).

However, in its current form, there are some conditions in which the TRC approach is limited. The discrepancy between topographic and hydraulic estimates of  $k_s$  for step-pool channels highlights the potential limitations of the roughness correlation in steep gravel-bed rivers where slope and relative submergence have a greater hydraulic influence. In channels with significant planform resistance, the approach may require modification to account for the slope and curvature of the channel. In multi-thread channels, several profiles may need to be employed, and the results weighted according to the size of the channel. Even under such conditions, multiscale roughness length decomposition may still have considerable value with appropriate research questions.

## 5.6 Conclusions

In this chapter, I aimed to determine the relative contribution of different scales of river bed topography to the total roughness length. In a laboratory pool-riffle channel I studied these scaling patterns using a novel analysis. The transform-roughness correlation approach estimates the relative contribution of various scales of in-channel topography to the total roughness length. The channel was characterised by a bimodal distribution of roughness lengths, comprising a minor mode at the grain-scale and a major mode corresponding to the bar wavelength. The estimated contributions of these modes to the total flow resistance conforms to empirical disaggregations of grain-and-form roughness.

By modifying the roughness correlation to suit the hydraulic conditions, multiscale roughness length decomposition may be achieved in virtually any type of river or numerical model, and perhaps boundary-layers in other environments. The only requirement is that the topographic data is of a sufficient resolution and

## 5.6. Conclusions

---

spatial extent to capture the scales over which the roughness elements occur, and data of this quality is only becoming more available to geomorphologists. In particular, one can expect that given the continual advances in methods for collecting bathymetric data in both shallow (Kasvi et al., 2019) and deep channels (Dietrich, 2017), applying the TRC approach will become increasingly practical in natural rivers.

Given that the TRC approach provides novel and detailed information regarding the spatial interaction between surface topography and fluid dynamics, it may contribute to advances in hydraulics, bedload transport, and channel behaviour. Estimates of  $k_s$  from roughness correlations may provide more immediate benefits by improving upon representative roughness values in estimating flow resistance. In the following chapter, I examine the spatial distribution of shear stress and test its effect on bedload transport.

# Chapter 6

## A comparison of 1D and 2D bedload transport functions under high excess shear stress conditions

### 6.1 Introduction

The adjustment of rivers to the imposed valley gradient, sediment supply, and discharge is of central interest to geomorphology and has implications for understanding and managing natural hazards and ecological habitats. In alluvial channels, the adjustment is facilitated by the movement of sediment, arising via the interaction between the flow and deformable boundary (Bridge and Jarvis, 1982; Dietrich and Smith, 1983; Church, 2010; Church and Ferguson, 2015). Despite there being no strict relationship between the magnitudes of perturbation and geomorphic effect (Lisenby et al., 2018), larger-than-average flows (i.e. floods) are typically associated with channel adjustment and relatively large volumes of geomorphic work (Wolman and Miller, 1960). Extreme events may exert disproportionate control over the channel planform (Eaton and Lapointe, 2001). The study of sediment transport processes under these relatively high discharge events is central to understanding river behaviour.

Researchers have dedicated considerable effort to deriving mechanistic bedload transport functions – typically empirically-calibrated – that relate the rate of movement to a force-balance between the flow and individual particles (a threshold). Other approaches exist, for example, non-threshold approaches that do not utilise a critical shear stress (Recking, 2013a). One of the most simple and widely

## 6.1. Introduction

---

used threshold relations is the Meyer-Peter and Müller (1948) equation that estimates bedload transport as a function of mean excess bed shear stress ( $\bar{\tau} - \tau_c$ , where  $\tau_c$  is critical shear stress) for a given grain diameter, typically the median (i.e.  $\tau_{c50}$  for the  $D_{50}$  grain). The extension of 1D bedload transport functions to gravel-bed rivers, typically characterised by a wide range of grain sizes, necessitated several modifications that accounted for the differential mobility of grain sizes, hiding and exposure (Parker and Klingeman, 1982; Parker, 1990; Recking, 2013b; Wilcock and Crowe, 2003). Further research emphasised that at conditions where  $\bar{\tau} \approx \tau_{c50}$ , bedload transport is affected by the spatial variance in shear stress (Paola and Seal, 1995; Paola, 1996; Nicholas, 2000; Ferguson, 2003; Bertoldi et al., 2009; Francalanci et al., 2012; Recking et al., 2016). More recently, Monsalve et al. (2020) proposed a 2D bedload transport function that integrates across the distribution of shear stresses and can predict transport at lower flow conditions where  $\bar{\tau} < \tau_{c50}$ . In concert, these advances suggest a consistent trend: with decreasing excess shear stress more information regarding grain size and shear stress (i.e. resisting and driving forces) is required to predict bedload transport.

Considerably less is known about rivers under high relative shear stress conditions  $\bar{\tau} \gg \tau_{c50}$ , where most channel change occurs. This is primarily due to practical limitations. Dangers associated with floods and erosion mean that researchers may collect data before and after an event, but not during. Large-scale laboratory experiments (flumes) typically do not incorporate key degrees-of-freedom for morphologic adjustment that are available to alluvial channels, and thus do not model the full range of feedbacks between bedload transport and the deformable boundary. The notion that bedload transport in rivers collapses to a more simple function (i.e. with mean shear stress and median grain size) under high excess shear stress conditions is yet to be conclusively demonstrated. If verified, it would serve as a highly convenient assumption in understanding landscape evolution and river management. Smaller-scale laboratory experiments provide an opportunity to test this hypothesis as they model larger bed and ideally bank adjustments.

In this chapter, I answer two research questions using a Froude-scaled physical model of a gravel-bed river:

- What is the relative effectiveness of 1D and 2D bedload transport functions under high relative shear stress conditions?
- What is the conceptual difference between 1D and 2D conceptualisations of excess shear stress and bedload transport?

The experiments have a widely-graded sediment mixture and develop alternate bars under pseudo-recirculating conditions at a range of widths and discharges. Total bedload volumes, bathymetry are recorded and 2D hydraulic modelling is conducted to apply several transport functions akin to Meyer-Peter and Müller (1948) (i.e. based on median grain size) that capture different levels of information regarding shear stress. The results highlight the effectiveness of simple threshold-based bedload transport functions under high relative shear stress in laterally constrained channels, as well as differences between 1D and 2D conceptualisations of excess shear stress and bedload transport.

## 6.2 Data analysis

### 6.2.1 Determining a representative sediment transport rate

To investigate these questions, I utilised a generic Froude-scaled model of a steep gravel-bed river. This model was selected as it reproduced channel-scale processes and maintained the Froude regime of the generic field prototype, whilst flow varied between transitional and turbulent. I used all available runs besides run 2 ( $W = 0.08$  m), which were excluded due to them having a different morphology (plane-bed), as well as sidewall effects on the shear stress (energy losses to the channel boundary) (Section 3.3, Table 3.3).

These runs are characterised by an alternate bar morphology formed under constant discharge conditions for 4–16 hours, beginning from either a screeded

## 6.2. Data analysis

---

bed or a morphology developed at a lower discharge. Each experimental phase comprises an initial adjustment period during which morphology, hydraulics, and sediment transport are non-stationary. This adjustment period, which may vary from minutes to an hour, is followed by a steady-state period where these characteristics fluctuate around a mean value (see Adams, 2020*b*; Adams and Zampiron, 2020). Under recirculating conditions, the stationarity of bedload transport represents a condition in which there is no net aggradation or degradation over time. In Figure 6.1 I present two typical examples of sediment transport fluctuations under constant conditions for 16 hours. In both examples, there is a brief adjustment period with less sediment transport, followed by fluctuations around a mean value. These fluctuations are associated with second-order processes such as bar reshaping and sediment waves (e.g. Dhont and Ancy, 2018), which are outside the scope of this study.

I determined a representative sediment transport rate for each experimental phase by averaging output over the final three-hour period (Table 6.1), thus removing the initial adjustment period. There is little difference between averaging over the final hour versus the final three hours, with almost all average values being  $\pm 12.5$  percent. There were three instances where these two averaging windows yielded values differing by 15–25 percent due to high-magnitude fluctuations around an otherwise stationary bedload transport rate.

## 6.2. Data analysis

---

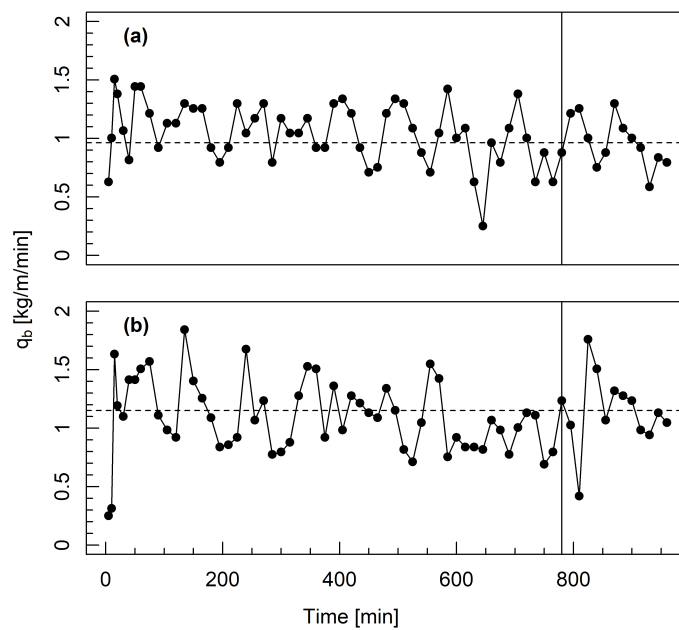


Figure 6.1: Width-averaged bedload transport over time in two runs with different widths but similar reach-averaged shear stress: a) run 1b ( $W = 0.30$  m,  $\bar{\tau} = 2.34$  Pa), and b) run 4b ( $W = 0.60$  m,  $\bar{\tau} = 2.28$  Pa). The beginning of the time window over which bedload transport is averaged is indicated by the solid vertical line, and mean transport over this period is indicated by a horizontal dashed line.

## 6.2. Data analysis

Table 6.1: Summary of mean experimental and flow model results. Parameters  $w$  = wetted width [m],  $d$  = flow depth [m],  $\bar{\tau}$  = mean shear stress [Pa],  $q_b$  = unit bedload transport [kg/m/min],  $\sigma_\tau$  is the standard deviation of shear stress,  $\alpha$  and  $\beta$  parameters describe the fitted gamma distribution of shear stress. The parameters A1, A2, B1, B2 refer to the four approaches outlined in Table 6.2.

Exp	$w$	$d$	$\bar{\tau}$	$q_b$	A1	A2	A3	A4	$\sigma_\tau$	$\alpha$	$\beta$
1a	0.26	0.015	2.65	1.8	1.67	1.13	1.56	0.84	0.46	3.8	0.26
1b	0.21	0.013	2.34	1.11	1.12	0.81	0.96	0.61	0.5	3.15	0.32
1c(1)	0.18	0.012	2.04	0.62	0.67	0.44	0.55	0.3	0.49	3.04	0.33
1c(2)	0.21	0.013	2.25	1.27	0.98	0.74	0.85	0.79	0.53	2.41	0.42
1c(3)	0.26	0.016	2.81	2.06	1.99	1.4	1.77	1.03	0.46	3.6	0.28
1c(4)	0.28	0.018	3.36	3.75	3.25	2.2	2.96	1.3	0.39	5.79	0.17
3a	0.37	0.015	2.69	2.97	1.76	1.32	1.45	1.1	0.49	2.79	0.36
3b	0.28	0.014	2.45	2.14	1.3	0.88	1.24	0.87	0.47	3.09	0.32
3c(1)	0.23	0.013	2.17	1.04	0.85	0.52	0.92	0.4	0.46	3.24	0.31
3c(2)	0.29	0.013	2.35	1.7	1.14	0.81	0.96	0.82	0.49	3.04	0.33
3c(3)	0.36	0.015	2.69	2.68	1.76	1.35	1.59	1.27	0.5	2.54	0.39
3c(4)	0.4	0.017	3.21	4.7	2.9	2.24	2.44	1.82	0.47	3.3	0.3
4a	0.48	0.015	2.74	3.13	1.85	1.42	1.46	1.19	0.5	2.9	0.34
4b	0.4	0.013	2.28	1.54	1.02	0.77	1.02	0.95	0.53	2.15	0.46
4c(1)	0.31	0.013	2.11	1.2	0.76	0.48	0.95	0.5	0.49	2.45	0.41
4c(2)	0.39	0.014	2.33	1.9	1.1	0.8	1.11	0.91	0.5	2.94	0.34
4c(3)	0.46	0.015	2.8	3.48	1.98	1.37	1.7	1.18	0.45	2.82	0.35
4c(4)	0.57	0.018	3.15	4.47	2.76	1.86	2.68	1.9	0.4	5.15	0.19

### 6.2.2 1D and 2D excess shear stress

Based on goodness-of-fit, I examined the relationship between the observed representative sediment transport rate and two formulations of excess shear stress

## 6.2. Data analysis

---

based on the Meyer-Peter and Müller (1948) equation

$$q_b = k(\bar{\tau} - \tau_c)^{1.6} \quad (6.1)$$

where  $q_b$  is width-averaged bedload transport,  $k$  accounts for flow resistance and the relative density of sediment, and the exponent 1.6 is based on Wong and Parker (2006). The value of  $k$  is highly variable across empirical datasets, whereas the exponent is relatively consistent (Gomez and Church, 1989). The critical shear stress value for the  $D_{50}$  ( $\tau_{c50}$ ) is estimated by  $\tau_c^* g(\rho_s - \rho)D$ , where  $\tau_c^*$  is the dimensionless critical shear stress,  $g$  is gravity,  $\rho$  is the density of water,  $\rho_s$  is the density of sediment. This force-balance approach is fairly typical across bedload transport equations, and the particular formulation is of no consequence in this analysis.

I aimed to investigate the concepts underlying 1D and 2D bedload transport equations, rather than refine them. Consequently, I ignored the parameter  $k$  that typically varies across channels and simplify Equation 6.1 to express the relationship between observed sediment transport and mean excess shear stress (raised to the exponent):

$$q_b \propto (\bar{\tau} - \tau_{c50})^{1.6} \quad (6.2)$$

This equation was modified to integrate across the distribution of local shear stresses

$$q_b \propto \int (\tau_{(x)} - \tau_{c50})^{1.6} dx/A \quad (6.3)$$

where  $\tau_{(x)}$  is local bed shear stress and  $A$  is the total bed area. Equations 6.2 and 6.3 are 1D and 2D approaches to correlating observed transport capacity with excess shear stress. I applied both equations using shear stress values calculated in two ways: 1) depth-slope product ( $\tau = \rho g d S$ ), and 2) 2D flow modelling, thus yielding four different approaches (Table 6.2). The former intentionally does not account for sinuosity or side-wall effects. In the case of the 1D depth-slope approach, depth was calculated using the mean depth and mean channel gradient, whereas

### 6.3. Results

in the 2D depth-slope depth was varied but the gradient remained constant. For each approach, I back-calculated the optimal value of  $\tau_c^*$  by systematically varying it and finding the strongest relationship (least-squares linear fit) between  $q_b$  and excess shear stress (i.e.  $[\bar{\tau} - \tau_{c50}]^{1.6}$  or  $\Sigma[\tau_x - \tau_{c50}]^{1.6}/A$ ), indexed by root-mean-square-error (RMSE), which is shown in Figure 6.2. I report optimised values of  $\tau_c^*$  and least-squares goodness-of-fit statistics in Table 6.2, and also include values obtained using the exponent 1.5 in each equation.

Table 6.2: Optimised values of  $\tau_c^*$  and goodness-of-fit statistics for excess shear stress and observed bedload transport using four different approaches. Values obtaining using the exponent 1.5 are presented in parentheses, and  $\bar{\tau}/\tau_{c50}$  represents the range of relative shear stress values across the experiments.

Approach	Equation	$\tau$ method	$\tau_c^*$	$r^2$	RMSE	$\bar{\tau}/\tau_{c50}$
A1	6.2 (1D)	d/S	0.066 (0.069)	0.96	0.51 (0.50)	1.36–2.11
A2	6.3 (2D)	d/S	0.098 (0.101)	0.98	0.41 (0.40)	0.30–1.90
B1	6.2 (1D)	modelled	0.050 (0.053)	0.97	0.44 (0.43)	1.56–2.53
B2	6.3 (2D)	modelled	0.086 (0.090)	0.98	0.38 (0.37)	0.36–2.00

## 6.3 Results

Under the imposed channel widths (0.30–0.60 m) and unit discharges (2.22–7.50 L/m/s) all channels developed an alternate bar morphology with pools, bars, and riffles (see Figure 6.3 for an example). Especially at low unit discharges, wetted areas ( $d > 2D_{84}$ ) on average occupied only a portion of the total available width, between 52 and 95 percent. When unit discharge was calculated using the wetted width, it was closely correlated with mean shear stress based on least-squares linear regression (Figure 6.4a), indicating a coupled adjustment between active width and shear stress.

The depth-slope method of calculating mean shear stress estimated higher values compared to the numerical model (7–23 percent higher), and also higher val-

### 6.3. Results

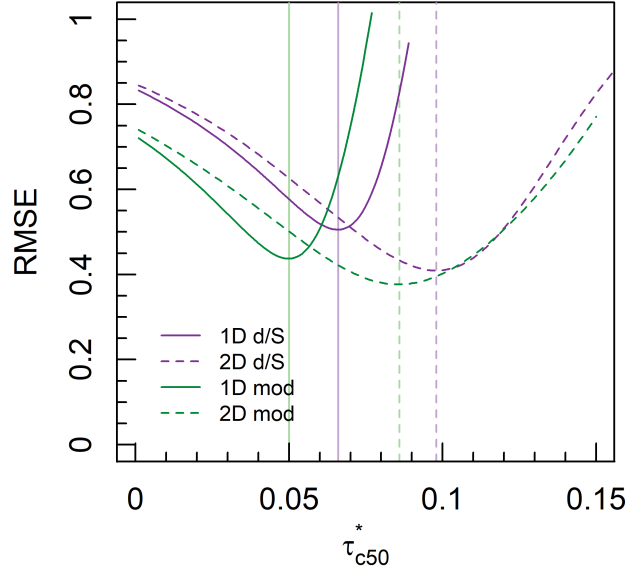


Figure 6.2: The goodness-of-fit for  $q_b$  and excess shear stress (indexed by RMSE) with varying critical dimensionless shear stress for each approach. Back-calculated critical dimensionless value is indicated where RMSE is lowest (Table 6.2).

ues of critical dimensionless shear stress in the corresponding transport functions ( $\tau_c^* = 0.066$  and  $0.050$ , respectively, Table 6.2). Both methods yielded similar estimates of excess shear stress ( $\bar{\tau} / \tau_{c50} = 1.36\text{--}2.11$  and  $1.56\text{--}2.53$ , respectively). The strong positive correlation between the two estimates of shear stress supports the assumption that at the reach-scale  $\bar{\tau} \approx \rho g d S$ .

Estimated values of  $\tau_c^*$  using the 2D approaches were consistently higher than the values obtained using the 1D approaches, but were slightly less sensitive to how shear stress was calculated ( $\tau_c^* \approx 0.095$  for both methods). Based on the 2D approach, the proportion of the wetted bed area experiencing excess shear

### 6.3. Results

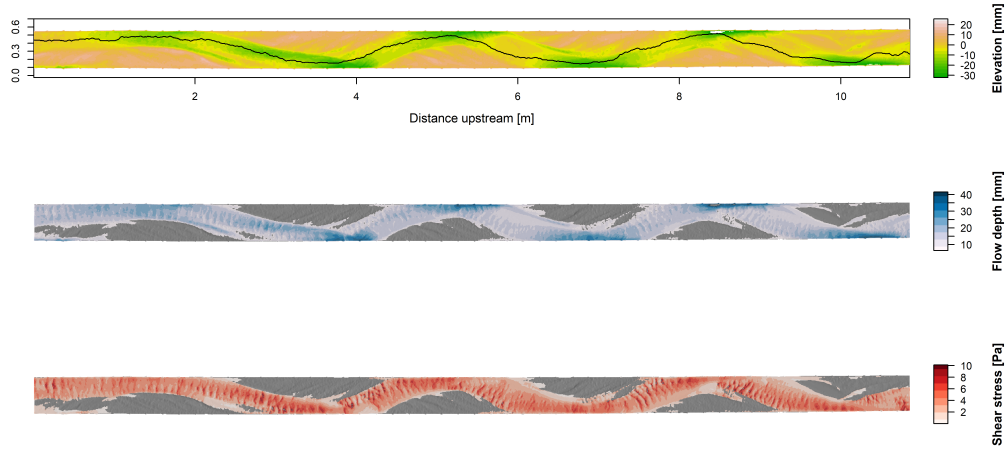


Figure 6.3: Channel area at the conclusion of Experiment 3b ( $W = 0.45$  m,  $\bar{\tau} = 2.41$  Pa) displaying characteristics (top to bottom): a) elevation, b) flow depth, and c) shear stress from flow model. Cells where  $d < 2D_{84}$  are not shown. Transect along path of highest bed shear stress is displayed as a black line.

stress was linearly related to unit discharge and ranged between 37–84 percent (Figure 6.4b). In several experiments 2D estimates of  $\tau_{c50}$  were higher than  $\bar{\tau}$ .

Local shear stresses at or below the mean were estimated to exceed  $\tau_{c50}$  only at unit discharges exceeding approximately 5 L/m/s (Figure 6.4). This range of shear stresses (i.e.  $\tau_{c50} < \tau < \bar{\tau}$ ) accounted for up to 37 percent of the total bed area at the highest flows. These results indicate considerable shear stress concentration, and the relative insignificance of moderate shear stresses in bedload transport. Shear stress distributions and estimated critical values are further visualised using examples in Figure 6.5b.

Frequency distributions of mean-normalised flow depth and shear stress (over each 5x5 mm grid cell) followed both Gaussian and gamma distributions (Figure 6.5a), confirmed by both Kolmogorov-Smirnov and Anderson-Darling tests ( $p < 0.1$ ). These distributions are qualitatively similar based on their cumulative distributions following the removal of shallow depths, which contribute a second mode of flow depths corresponding to dispersive flow or stagnant water at

### 6.3. Results

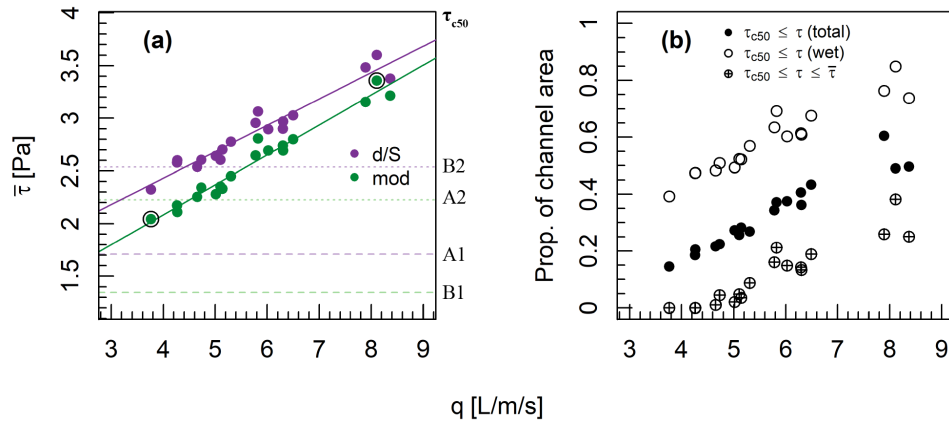


Figure 6.4: a) Relationship between unit discharge  $q$  (calculated using wetted width) and mean shear stress  $\bar{\tau}$  using depth-slope product (RMSE = 0.097,  $r^2 = 0.93$ ,  $p < 0.001$ ) and modelled shear stresses (RMSE = 0.073,  $r^2 = 0.96$ ,  $p < 0.001$ ). Horizontal lines indicate fitted values of  $\tau_{c50}$ , and circled points indicate channels with the highest and lowest shear stress used in Figure 6.5b. (b) Relationship between unit discharge and the proportion of the wetted channel area ( $d > 2D_{84}$ ) where  $\tau > \tau_{c50}$  using modelled shear stresses (i.e. approach B2), as well as the proportion of channel area where  $\tau_{c50} < \tau \leq \bar{\tau}$ .

### 6.3. Results

---

the channel margins. In the case of the shear stress distributions, the shape parameter  $\alpha$  was linearly related to unit discharge based on least-squares regression (RMSE = 0.69,  $r^2 = 0.39$ ,  $p < 0.01$ ), and the scale parameter  $\beta$  was negatively correlated (RMSE = 0.58,  $r^2 = 0.32$ ,  $p < 0.01$ ). The parameters of the gamma distribution indicate that with increasing unit discharge the distribution of shear stress became more concentrated and less positively skewed.

Despite following similar frequency distributions, modelled local flow depth and shear stress were not strongly coupled spatially (Figure 6.6). These two parameters are roughly correlated but with considerable scatter, whereby for a given grid cell mean-normalised shear stress is commonly more than a factor-of-two greater or less than normalised flow depth (i.e. high shear stress and deep flows are close but not at exactly the same locations). The spatial decoupling of flow depth and shear stress is also evident in Figure 6.3, especially where areas of high shear stress are estimated to occur immediately downstream of pools where flow is deepest.

I present the relationship between bedload transport and the four different representations of excess shear stress in Figure 6.7. These represent combinations of two different methods of calculating bed shear stress, depth-slope product and numerically modelled, against 1D and 2D representations of excess shear stress (Table 6.2). All four methods yield similar relationships between excess shear stress and observed bedload transport, indicated by RMSE values between 0.38 and 0.51, where these end-values correspond to the 2D modelled shear stress (B2) and 1D depth-slope product approach (A1), respectively. Changing the exponent from 1.6 to 1.5 in Equations 6.2 and 6.3 had almost no effect on the estimated values of  $\tau_c^*$  or the prediction errors. Altering the representative grain size from  $D_{50}$  to  $D_{84}$  has no effect on the goodness-of-fit between  $q_b$  and excess shear stress (i.e. identical RMSE), and merely reduces the back-calculated estimates of  $\tau_c^*$ .

### 6.3. Results

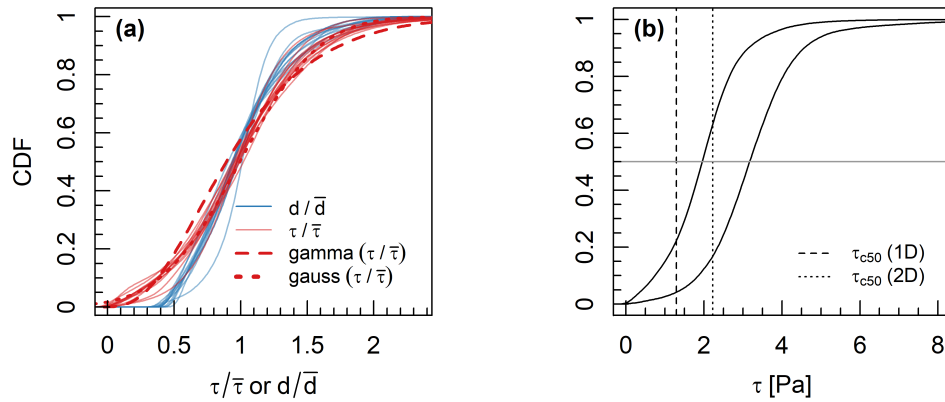


Figure 6.5: a) Cumulative distribution functions of mean-normalised modelled flow depth and shear stress at the end of each experimental phase, where the upper end of the kernel density distribution has been truncated to approximately the 99<sup>th</sup> percentile to remove outliers. Note the absence of shallow depths ( $d < 2D_{84}$ ). The average gamma distribution fit for the normalised shear stress distribution is included ( $\alpha = 3.30$ ,  $\beta = 0.30$ ), as well as the average Gaussian fitted distribution ( $\sigma = 0.47$ ). b) cumulative distribution function of non-normalised modelled shear stresses in experimental phases with highest (run 1c(4)) and lowest (run 1c(1)) mean shear stress (circled points in Figure 6.4). Estimates of  $\tau_{c50}$  using 1D and 2D approaches (B1 and B2, respectively) are indicated by dashed lines, and the horizontal line is the median shear stress, which closely corresponds to the mean.

### 6.3. Results

---

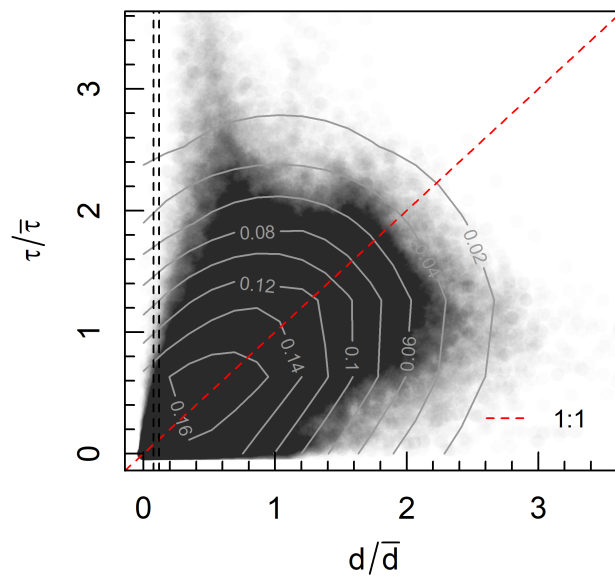


Figure 6.6: Relationship between local mean-normalised flow depth and shear stress across all experiments, produced by randomly sampling 10 percent of cells from each flow model. Contour lines represent 2D kernel density estimation, and vertical dashed lines indicate the range of flow depths that were used to threshold the flow model.

### 6.3. Results

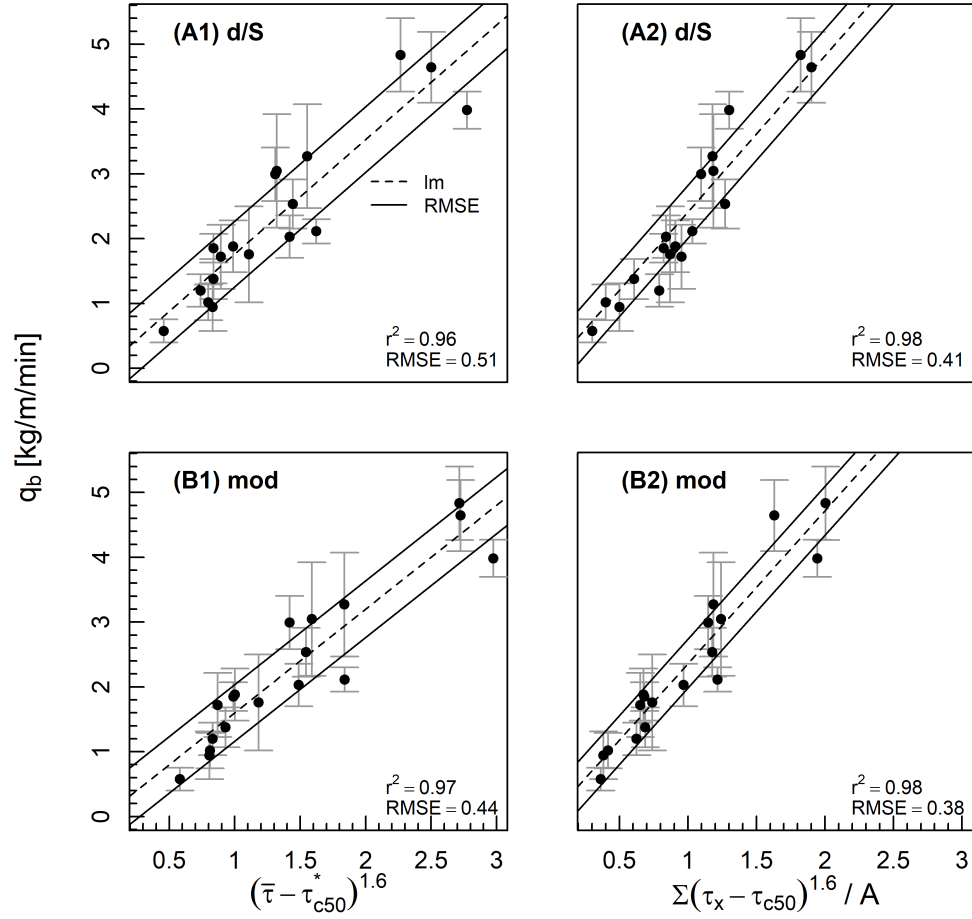


Figure 6.7: Regression of excess shear stress and observed bedload transport (averaged over final 3 hours of each experiment) using the four approaches outlined in Table 6.2. The dashed black line is the least-squares best fit, and solid black lines indicate  $\pm 1$  RMSE, and whiskers indicate  $\pm 1$  standard deviation over final 3 hours of sediment output measurements.

## 6.4 Discussion

These experiments have several advantages over traditional field and flume datasets. Although the experiments do not model lateral adjustment, the smaller scale-ratio (1:25) means they incorporate morphology and processes at a larger scale compared to most flumes with width-depth ratios between approximately 15 and 40. The bulk mixture comprises a wide range of grain sizes (0.5–8.0 mm) that have been demonstrated to modulate channel adjustment, especially under conditions where the larger-than-average grain size is only partially mobile (MacKenzie and Eaton, 2017; MacKenzie et al., 2018; Booker and Eaton, 2020; Adams, 2021). I measured total bedload volumes and adjustments to bed topography during flood stages, which is not possible in the field or in many recirculating experiments. The applied flows are longer and more constant than floods typically observed in nature (4–16 hours experimental time or 20–80 hours in the field prototype), which allows the experiments to reach an idealised steady-state whereby morphology, hydraulics, and bedload fluctuate around a mean condition (Figure 6.1). These characteristics make the experimental dataset appropriate for investigating the effectiveness of bedload transport equations in laterally-constrained gravel-bed rivers under high relative shear stress conditions.

I evaluated four different bedload transport functions based on the goodness-of-fit between excess shear stress and observed volumes of bedload transport, averaged over the final three hours of each experimental phase. I first focus our discussion on three of these approaches in increasing order of sophistication (A1, B1, then B2), and then explain their relative effectiveness. Finally, I discuss the conceptual differences between 1D and 2D bedload transport functions.

### 6.4.1 Comparison between prediction errors

Most bedload transport functions index the applied excess shear stress using the mean depth-slope product as this data is relatively easy to collect in field contexts (Gomez and Church, 1989; Barry et al., 2004; Recking, 2013*b*). This approach relies on the assumption that local variations in channel gradient and flow

#### 6.4. Discussion

---

depth cancel out, such that mean flow depth is proportional to mean shear stress (Nicholas, 2000; Ferguson, 2003). This condition was observed herein, whereby mean-normalised flow depth and shear stress followed similar frequency distributions (Figure 6.5a), despite being decoupled spatially (Figure 6.6). The approach A1 (1D depth-slope product) in our analysis was the most simplistic, and in addition, did not account for sinuosity (note the slight sinuosity in Figure 6.3 that reduces the mean channel gradient), flow resistance, or energy losses to the channel banks. The goodness-of-fit between excess shear stress and bedload transport (RMSE = 0.51) provides an approximate reference point for other approaches.

In recent decades, technological advancements in remote sensing and hydraulic modelling have allowed researchers to directly model bed shear stress, thus providing a potentially more accurate estimate. This advancement is utilised in the B1 approach (1D modelled shear stress), which accounts for the effect of both sinuosity, flow resistance, and energy losses to the channel banks. Accounting for these additional factors may explain the 13 percent reduction in RMSE (0.44) compared to approach A1. Further advancements have led to the proliferation of 2D hydraulic models and some 2D bedload transport equations, which aim to account for the proportion of the bed participating in transport and the spatial variation in shear stress (Monsalve et al., 2020). The B2 approach (2D modelled shear stress) that integrates across the frequency distribution of shear stresses did not significantly improve upon approach A1, with a similar RMSE (0.38) to approach B1.

Numerical modelling of shear stress and accounting for its frequency distribution led to similarly strong goodness-of-fit between bedload transport and excess shear stress, compared to the mean depth-slope product method. The ability of the mean shear stress to effectively capture variation in bedload transport is consistent with empirical evidence. In a re-analysis of data from Oak Creek, OR, Monsalve et al. (2020) compared the Parker and Klingeman (1982) equation to a modified 2D version and found that accounting for the distribution of shear stresses reduced prediction error by only 13 percent. Their study modelled a range of flows to the same bathymetry, and there was a similar result here when the bed was allowed to

fully adjust to the imposed flow. Using numerical and analytical models, several studies have predicted that variance in shear stress may enhance bedload transport but that this effect rapidly diminishes when  $\bar{\tau} \gg \tau_c$  (Ferguson, 2003; Francalanci et al., 2012; Recking, 2013a). The most probable reason for this sensitivity is the nonlinearity of the bedload transport law, which means that around  $\bar{\tau} \approx \tau_c$  small increases in  $\tau$  produce relatively large increases in bedload transport. The similar effectiveness of 1D and 2D functions herein provides empirical evidence that bedload transport is less sensitive to the shape of the shear stress distribution under high relative shear stress conditions.

### 6.4.2 Comparison between 1D and 2D approaches

The four approaches demonstrated key differences based on how shear stress was calculated (depth-slope product vs numerically modelled) and more importantly the formulation (1D vs 2D). Both estimates of mean shear stress were linearly related to unit discharge but those based on the depth-slope product were 7–23 percent higher (Figure 6.4), which is consistent with findings by Monsalve et al. (2020). These differences in estimated shear stress led to approximately commensurate differences in the estimated 1D values of  $\tau_c^*$  (32 percent higher). Both 1D estimates of  $\tau_c^*$  were relatively high for gravel-bed rivers but were within the range of reported estimates from both field and laboratory channels (Buffington and Montgomery, 1997).

Despite having similar prediction errors, the 1D and 2D functions provided considerably different estimates of critical dimensionless shear stress. Using the 2D approach, estimates of  $\tau_c^*$  were 48 and 72 percent higher than the 1D depth-slope and modelled shear stress methods, respectively. In several channels, the estimated critical shear stress was greater than the mean shear stress but bedload transport was observed and well predicted by the model (Figure 6.4), which in the case of a threshold-based 1D equation, would correspond to zero estimated transport. This is a distinct advantage of 2D equations at low flows, as they can account for flows where excess shear stress occupies only a fraction of the bed

## 6.4. Discussion

---

(Monsalve et al., 2020).

The differences between estimates of  $\tau_c^*$  arise from differences in how the equations conceptualise excess shear stress. In a 1D equation, when bedload transport data is available,  $\tau_c$  may be back-calculated from the mean shear stress, as is done herein. The value of  $\tau_c^*$  is adjusted until excess shear stress explains the observed bedload transport, assuming that  $\bar{\tau}$  is responsible for all entrainment. In contrast, the 2D equation does not assume that the mean shear stress participates in bedload entrainment. Based on the 2D approach, it is estimated that the mean shear stress did not exceed the estimated critical value for the  $D_{50}$  until a certain discharge threshold (5 L/m/s), and even under the highest flows these areas (i.e.  $\tau_{c50} < \tau < \bar{\tau}$ ) characterised a maximum of 37 percent of the wetted area. These values were not validated quantitatively as I did not anticipate the need for observation, although the estimates appear reasonable compared to visual observations of the experiments. This result suggests that the mean shear stress is far less significant for bedload transport compared to the larger-than-average stresses, which is intuitive especially given that these are the first stresses to entrain bed material as the flow is increased.

By conceptualising transport as a function of mean shear stress, 1D equations may inflate the importance of relatively moderate shear stresses and deflate values of  $\tau_c^*$ . This insight is based on back-calculated values rather than measurements of incipient motion, although it is important to note that studies measuring incipient motion have also been based on the mean shear stress and therefore this 1D paradigm is subsumed within the results (Gilbert, 1914; Kramer, 1935; Neill and Yalin, 1969; Wilcock, 1988). I also relied on spatio-temporally integrated rather than instantaneous local shear stresses that promote entrainment (e.g. Nelson et al., 1995a). Nevertheless, the higher estimates of critical dimensionless shear stress using the 2D approach, evaluated by considering the relative importance of shear stresses across the frequency distribution, may have a stronger conceptual basis. More broadly, the results highlight that as long as  $\tau_c$  is back-calculated, its value will be highly dependent on how shear stress is estimated, and whether its distribution is treated one- or two-dimensionally.

#### 6.4. Discussion

---

The results may have implications for non-threshold approaches to predicting bedload transport in natural gravel-bed rivers (Parker et al., 1982; Parker, 1990; Wilcock and Crowe, 2003; Recking, 2013a). These approaches recognise that usage of a single critical shear stress is ineffective at low flows and is always an approximation, especially in the case of partial transport conditions where not all grain sizes (or even grains of a given size) are equally mobile (Wilcock and McArdell, 1993). The effectiveness of threshold-based approaches under high excess shear stresses suggests that in channels with fully-developed morphology and a wide range of grain sizes, non-threshold-based approaches may not render an improvement. Also, the results challenge recent critiques of bedload transport predictions based on mean shear stress, and particularly the depth-slope assumption (Yager et al., 2018). There is indeed a poor mechanistic link between shear stress bedload transport (e.g. Nelson et al., 1995a), which means that most conventional transport functions are not fully mechanistic and are rather correlations between quantities. Despite being a poor mechanistic characterization of the transport process, the 1D approximation may be unreasonably effective when applied at a sufficiently large spatio-temporal scale or excess shear stress. I discuss this further in Chapter 7.

Further work is required to investigate differences in 1D and 2D estimates of  $\tau_c^*$  under lower excess shear stress conditions. If broadly applicable, the effectiveness of highly reductionist bedload transport functions based only on median grain size and mean shear stress would present a convenient assumption for researchers and practitioners interested in channel-forming flows. More research is required to substantiate this approach under supply-limited conditions and realistic hydrographs that enable both upward and downward adjustments with inherited channel conditions. Given that our experiments do not allow for significant lateral adjustment and meandering, the results are most applicable to channels confined by bedrock, or with cohesive or highly vegetated banks. Fully alluvial channels comprise additional feedbacks that are worthy of investigation, and the extent to which these affect reach-averaged bedload transport remains poorly understood.

## 6.5 Conclusions

I investigated the performance of 1D and 2D bedload transport functions under high relative shear stress conditions in a Froude-scaled physical model. The results support the hypothesis that under these conditions, highly reductionist bedload transport functions based only on median grain size and mean shear stress (calculated using the depth-slope product) are effective relative to 2D functions. Numerically modelling shear stress to account for flow resistance and energy losses from the channel planform and banks did not substantially reduce prediction error, nor did accounting for the relative importance of shear stresses across the frequency distribution. The results suggest that bedload transport may collapse to a more simple function (i.e. with average shear stress and grain size) under high excess shear stress conditions. Given the channels herein have limited lateral mobility, our conclusions are most applicable to channels where lateral adjustment is suppressed. Further work is required to examine the effect of planform adjustments (widening, meandering), where small-scale laboratory experiments serve as an effective research tool.

The 1D and 2D approaches provided substantially different estimates of critical dimensionless shear stress, reflecting differences in how these approaches conceptualise excess shear stress. Estimates of  $\tau_c^*$  from 2D functions may have a stronger conceptual basis, as they are derived by considering the relative importance of shear stresses across the frequency distribution, and do not assume that the mean shear stress is sufficient to mobilise the median grain size. This answers the second research question concerned with the conceptual difference between the transport functions.

# Chapter 7

## The trinity, emergence, and river behaviour

### 7.1 Introduction

The form and functioning of geomorphic systems is the end product of processes interacting across a range of spatial and temporal scales, from instantaneous sediment entrainment to landscape denudation occurring over geological timescales (Schumm and Lichty, 1965; Church, 1996; Phillips, 2016). Researchers have concentrated their efforts on individual scales, developing conceptual frameworks that explain their dynamics. At the bedform- or reach-scale, perhaps the simplest and most intuitive concept is the fluvial trinity, which describes the feedbacks between hydraulics, morphology, and sediment transport (Ashworth and Ferguson, 1986; Best, 1986; Leeder, 1983). However, reconciling the processes operating at different superimposed spatio-temporal scales is a considerable challenge, which has ultimately driven the discipline to specialisation whereby research sub-fields are often delimited by their scale (Douglas, 1982; Baker and Twidale, 1991; Harrison, 2001; Rhoads, 2006). The recognition of multiple scales leads to some fundamental questions. How do different scales of processes interact with each other? Are all scales equally important (i.e. symmetry), or do certain scales exert control over others (asymmetry)?

The challenge of multiple scales is not unique to geomorphology but is in fact characteristic of physical and biological sciences concerned with non-linear systems. In the second half of the 20<sup>th</sup> Century, researchers became increasingly aware of the limitations of the ‘reductionist’ approach in theoretical physics. As

## 7.1. Introduction

---

Anderson asserted in his 1972 article titled *More is different*, ‘The ability to reduce everything to simple fundamental laws does not imply the ability to start from those laws and reconstruct the universe.’ The properties of nature not readily apparent from so-called fundamental laws, instead arising through self-organisation of elementary particles at larger scales, are then termed ‘emergent’ phenomena. In the following decades, researchers have increasingly recognised that nature is comprised of a hierarchy of emergent scales, largely decoupled from one another and with their own fundamental laws and ontology (Haken, 1983; Schweber, 1993; Goldenfeld and Kadanoff, 1999). These hierarchies are often mirrored in the division of work across academia, whereby researchers have organised themselves into groups corresponding to these scales (Anderson, 1972).

Based on the apparent similarity between geomorphic and ecologic (or other complex) systems (Allen and Starr, 1982; Graf, 1988; Haken, 1983; Schweber, 1993; Goldenfeld and Kadanoff, 1999), several contributions have developed and promoted nested, hierarchical representations of geomorphic systems (Sugden and Hamilton, 1971; Trudgill, 1976; Allen and Starr, 1982; Werner, 1999, 2003; Murray, 2003; Harrison, 2001; Phillips, 2016), including a comprehensive review and synthesis of earlier contributions by de Boer (1992). Most of this work is predicated upon the notion that scales of form and process are connected (Jackson, 1975; Douglas, 1976), and that spatial and temporal scales of process are linked (Haigh, 1987; Graf, 1988; Schumm and Lichty, 1965). The most central proposition across these studies is that processes and forms at a given scale emerge from those at a finer scale but are constrained by processes and forms at a coarser scale (Schumm and Lichty, 1965; Walsh et al., 1998; de Boer, 1992; Werner, 2003).

The existing literature on hierarchical perspectives of geomorphic systems, however, has been rather general in scope (Werner, 1999, 2003; Harrison, 2001; Murray, 2003; Murray et al., 2014). This work has been instrumental in providing a conceptual basis for numerical models such as cellular automata and reduced complexity approaches (Murray and Paola, 1994; Wolfram, 2002). Such modelling approaches remain relatively uncommon and have even been met with resistance from proponents of the reductionist perspective, who remain sceptical

## 7.1. Introduction

---

of the presence of self-organised behaviour in rivers and the need for ‘fashionable new paradigms’ (Seminara and Pittaluga, 2012). In practice, geomorphology as a whole continues to embrace a broadly reductionist perspective that assumes linear behaviour (see Rhoads, 2006; Preston et al., 2011). However, the variation of fluvial processes across various scales, the prevalence of non-linear dynamics, and the ubiquity of self-organised phenomena limit the effectiveness of reductionist approaches to explain river behaviour (Murray et al., 2009; Church and Ferguson, 2015), just as they have in other physical sciences (Schweber, 1993). However, the dichotomy of reductionist and hierarchical viewpoints may not be necessarily useful, and rather, there may be a space within which these respective ideas may be most effective. There is an opportunity to explore the application of concepts such as emergence targeting areas of geomorphology more specifically.

In this chapter, I aim to develop hypotheses and experimental methodologies by translating the hierarchical perspective of non-linear systems from physical sciences to fluvial geomorphology. I focus on alluvial rivers where the process of emergence is most apparent, as these systems are maintained by the continuous flux of energy and matter through them (Haken, 1983). To this end, I aim to answer three questions:

- How do fluvial trinity and emergence perspectives intersect?
- What are the potential implications for understanding sediment transport and morphodynamics?
- What are the potential implications for how we physically model rivers?

As a concept that embraces scale, emergence may complement the fluvial trinity to potentially better explain the scale-dependent process interactions that drive river behaviour. The integration of these two concepts provides three primary opportunities in that: 1) the emergence perspective encompasses a language and conceptual framework distinctively suited to understanding river behaviour, 2) the conceptual intersection of these two perspectives define a set of novel hypotheses that may stimulate further research, and 3) the emergence perspective itself guides

the development of tests for these hypotheses based on a hierarchical modelling approach.

## 7.2 Fluvial trinity

The notion that rivers arise via feedbacks between morphology, hydraulics, and sediment transport (Figure 1.1) is a foundational idea in fluvial geomorphology (e.g. Gilbert, 1876), and was later formalised as the ‘fluvial trinity’ (Leeder, 1983; Ashworth and Ferguson, 1986; Best, 1986). It is central to an understanding of channel adjustment, (Lane and Richards, 1997), bedform dynamics, (Rhoads and Welford, 1991), bedload transport (Church and Ferguson, 2015), and biogeomorphic interactions (Tal and Paola, 2010). The fluvial trinity is traditionally applied within a relatively discrete range of spatial and temporal scales, which must first be defined. The achievement of Schumm and Licity’s (1965) seminal paper ‘Time, space, and causality in geomorphology’ has been the resolution of ostensible contradictions between contemporary and historical approaches to studying the landscape, re-framing spatial and temporal dimensions as fundamental to geomorphology. The latter theme, ‘causality’, has had less impact despite having significant implications for understanding basic river processes. Schumm and Licity (1965, p. 117) highlight that there are

...conflicting conclusions that could result from studying fluvial processes in the hydraulic laboratory and in a natural stream. The measured quantity of sediment transported in a flume is dependent on the velocity and depth of the flowing water and on flume shape and slope. An increase in sediment transport will result from an increase in the slope of the flume or an increase in discharge. In a natural stream, however, over longer periods of time, it is apparent that mean water and sediment discharge are independent variables, which determine the morphologic characteristics of the stream and, therefore, the flow characteristics.

## 7.2. Fluvial trinity

---

Here, Schumm and Lichty (1965) use the notion of causality to describe how system variables may be dependent or independent as the scope of geomorphological inquiry changes (see Figure 7.1 for an example of these scales). At the grain-scale, corresponding to instantaneous timescales in nature (and in the quote a highly constrained system), sediment transport is only dependent on the flow characteristics. At the landscape scale, which correspond to timescales spanning the geological cycle, discharge and sediment transport are independent variables associated with geology and climate. It is at intermediate scales where feedbacks<sup>1</sup> between channel flow, morphology, and the movement of sediment are strongest as there are fewer constraints (Ashworth and Ferguson, 1986; Best, 1986; Church, 2010; Church and Ferguson, 2015). The scale-dependence of processes implies that the fluvial trinity is a gross simplification of the processes that drive river behaviour (i.e. it is agnostic to scale).

---

<sup>1</sup>Feedbacks may be defined as mechanisms capable of reinforcing themselves, and can act as fundamental drivers of dynamics as they connect, modify, and control system evolution (Murray et al., 2014). They may be termed ‘positive’ if they loop back into the system so that initial perturbations grow, creating at least a temporary accelerating run-away reaction (e.g. bank erosion leading to removal of vegetation and reduction of effective cohesion). ‘Negative’ feedbacks tend to dampen the growth of a perturbation (potentially acting against a positive feedback).

## 7.2. Fluvial trinity

---

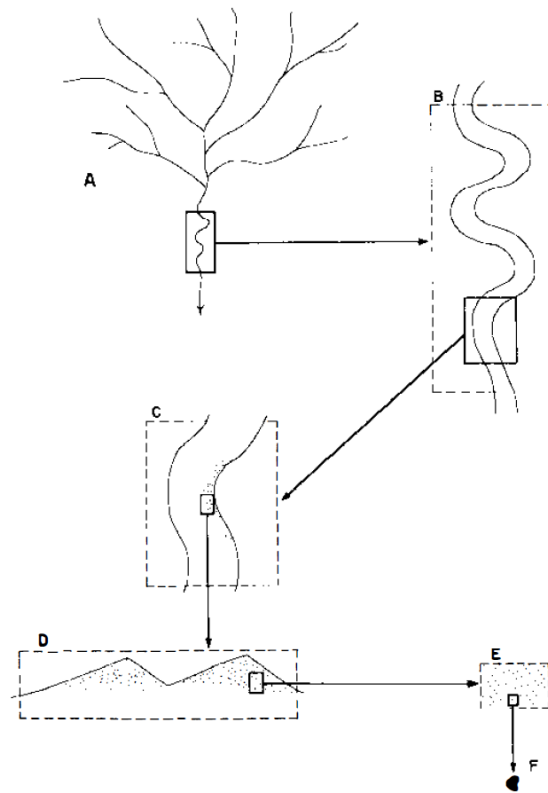


Figure 7.1: Components of the fluvial system (A - catchment, B - planform, C - bend, D - bedform, E - patch, and F - grain), from Schumm (1985)

Grains, bedforms, planforms, and catchments (or other intermediate scales) provide a convenient description of the spatio-temporal scales over which fluvial processes operate, as well as the division of labour across fluvial geomorphology (Rhoads, 2006). Fragmentation is perhaps unsurprising given the order-of-magnitude differences between these delimited scales, which for practical reasons favour isolated rather than integrated study. In addition to appropriate data and methodologies, researchers require theoretical frameworks that may inform methods and hypothesis generation. To address this, I explore how the concept of emergence may provide an effective framework to elucidate interactions between different and superimposed spatio-temporal scales of process.

## 7.3 Emergence

Emergence is a common characteristic of thermodynamically open and dissipative systems that allow for a variable exchange of energy and matter (Katchalsky and Curan, 1967; Nicolis and Prigogine, 1977). Geomorphic systems are excellent examples of these systems as they are characteristically open and highly dissipative, which can be observed in the conversion of coherent mechanical energy to heat through grain contact or fluid shear (Werner, 1995). They are increasingly recognised as nonlinear in that their dynamics depend in a nonlinear manner on external environmental parameters or internal characteristics of the system, the characteristics of the system modify the environment determining their dynamics, and the constituents of the system are strongly coupled (Werner, 2003). I now introduce the conceptual framework and terms surrounding emergence using examples of alluvial systems.

In their most simple mereological (i.e. part-whole) form, self-organised systems may be described as having two sets of spatio-temporally defined components; small-scale constituent variables and large-scale emergent variables. These components may correspond to either a process (e.g. sediment transport), a physical form (i.e. bedform), or a form-process interaction (e.g. dune migration). To communicate concepts surrounding emergence, the reader may imagine a two-tiered geomorphic system that they are familiar with, for example, gravel particles comprising an alternate bar or a stream channel atop an alluvial fan. In a natural system, however, there may be a hierarchy comprising  $n$  levels of variables, each associated with a different scale. Every system scale may be described by a phase space that contains repellor and attractor states, the latter representing sets of points that system trajectories tend to converge on (Phillips, 1992; Werner, 1995). In the case of an alluvial fan, the large-scale phase space may comprise the overall fan morphometry (e.g. gradient), whereas smaller-scale phase spaces may comprise the properties of the active channel. Werner (2003) describes the dynamics of self-organised systems by outlining three aspects of the relationship between constituent and emergent variables.

### 7.3. Emergence

---

1. The development of order, whereby the correlated, coherent time-evolution of constituent variables results in the dynamics of an ordered state, termed emergent (or autogenic) behaviour, that is decoupled from the behaviour of the constituents. The concepts of emergence and feedback are strongly related as it is the latter that facilitates the development of emerging patterns (Murray et al., 2014). This is the defining characteristic of alluvial channels, in which the channel form (emergent state) arises from the behaviour of individual grains (constituents).
2. Time-scale separation, defined by the intrinsic time-scale of adjustment (the exponential decay time for the system evolving towards an attractor state (Graf, 1977)) that determines how a landform responds to perturbation. Emergent dynamics have a longer intrinsic time-scale than constituent dynamics (and may be termed slow- and fast-scale variables, respectively), and in this sense the interaction between the two is indirect, i.e. they are ‘dynamically decoupled’. For example, in the case of meander migration, the time-scale over which individual grains are entrained and deposited is far slower than the overall movement of the channel boundary, and thus the two processes are dependent yet dynamically decoupled.
3. Dynamical asymmetry, in which there is an asymmetrical relationship between fast- and slow-scale variables, which is characterised by two reciprocal attributes:
  - (a) Abstraction, whereby the dynamics of emergent variables is not a direct reflection of constituent dynamics (Werner, 1995, 1999).
  - (b) Slaving, whereby the dynamics of constituent variables are determined directly by the dynamics at the emergent scale (Haken, 1983). For example, in rivers, at the scale of individual grains sediment transport appears independent, although at larger scales this fast process is slaved to the slower motion of bedforms (e.g. dunes, pools, bars, riffles), which are themselves confined to the path and pattern of the

### 7.3. Emergence

---

channel. Subsequently, although the propagation of cause and effect may occur upward through the scales, it may more commonly occur in a downwards direction (Werner, 1999; Murray et al., 2014).

These concepts may be further distilled into two central ideas:

1. Spatial and temporal scales are dynamically linked (large components adjust slowly relative to small ones), but there exist relatively distinct spatio-temporal scales that are dynamically decoupled from each other; and
2. this decoupling is dynamically asymmetrical, whereby small-scale constituent dynamics are enslaved by large-scale emergent dynamics

A key implication of these ideas is that the abstracted dynamics of emergent scales may not be derived from the sum of its constituents (or the laws that describe them), given that the constituent dynamics may be itself determined by emergent scales (Werner, 2003; Murray, 2007; Murray et al., 2014). Based on this reasoning several researchers have proposed that the dynamics of emergent scales are as ‘fundamental’ as the processes that concern the basic sciences (Anderson, 1972; Haken, 1983; Werner, 2003).

The concept of emergence contributes to a hierarchical description of alluvial systems, comprising a series of hypotheses surrounding the relationship between grain, bedform, planform, and catchment scales (Figure 7.1). This is an explicitly scale-dependent perspective of process, which complements the fluvial trinity perspective that simplifies modes of adjustment at any given scale. This unified framework describes river behaviour as an outcome of process interactions between sediment transport, channel morphology, and hydraulics (form, flow, and flux), occurring across different spatio-temporal scales (Figure 7.2). For simplicity, I have defined these scales according to the diagram in Figure 7.1, although one could propose an additional set of intermediate scales for a given system (e.g. bedforms may be divided into ripple, dune, and bar scales). Each scale comprises a phase space defined by the form, flow, and flux, in which attractor and repeller states reside (i.e. the range of potential system states). In the following sections,

### 7.3. *Emergence*

---

I discuss the potential implications of the emergence perspective for sediment transport, morphodynamics, and physical modelling.

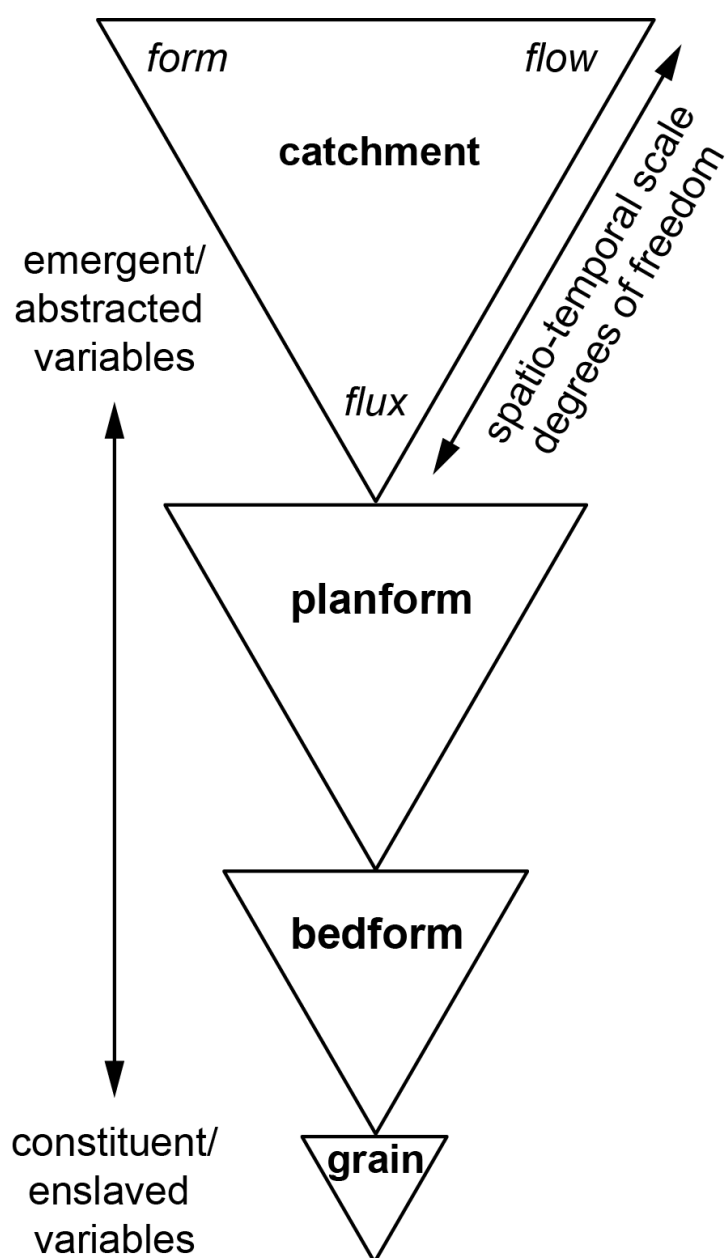


Figure 7.2: Simplified hierarchical representation of dynamically decoupled scales in fluvial systems, comprising grain, bedform, planform, and catchment variables. Form, flow, and flux variables define a phase space for each spatio-temporal scale.

## 7.4 Bedload transport

Mechanistic bedload transport equations are commonly based on the speculative analysis conducted by Du boys (1879), who conceptualised bedload transport as continuous layers of individual grains sliding against each other under the tractive force of water (Ancy, 2020a). More fundamentally, this approach is analogous to the force-balance equation describing the motion of a sliding block, whereby sediment motion is predicted when the driving force (bottom shear stress) exceeds the resisting force (critical shear stress). Thus, to estimate the volume of sediment transport of many grains, the force-balance equation has been simply integrated over the spatio-temporal scale of interest (e.g. Meyer-Peter and Müller, 1948). This approach is typically referred to as one-dimensional or 1D, although it is important to note that it is in fact 0D (i.e. representative of a single point or average condition for both shear stress and critical shear stress). As demonstrated in Chapter 6 such 0D equations may predict bedload transport accurately under certain conditions. Here lies a key question: would the high efficacy of 0D bedload transport equations at the reach-scale contradict the emergence hypothesis: i.e. whether large-scale sediment dynamics can be predicted from small-scale (grain) dynamics?

Conventional bedload transport equations are only loosely associated with grain-scale dynamics and are not truly mechanistic. Several contributions have observed a poor correlation between local shear stress and local bedload fluxes (Nelson et al., 1995b; Yager et al., 2018). This may be due to individual turbulence events or instances of flow separation which are not accounted for by shear stress, meaning that it does not fully characterise the variations in pressure that control the instantaneous lift-drag forces on the grain. Rather, conventional bedload transport equations are best described as convenient correlations between transport and fluid quantities. Consequently, such equations are not making predictions based on grain-scale processes and their efficacy would not disprove the notion of scale separation.

On the other hand, a hierarchical view of alluvial systems would suggest

#### 7.4. *Bedload transport*

---

that sediment transport is a multiscale phenomenon, where coherent (i.e. non-random) patterns emerge at relatively discrete spatial and temporal scales. For a given system, observations of bedload transport fluctuations indicate the presence of various scales with differing degrees of order. At instantaneous or quasi-instantaneous (i.e. minutes) time-scales, reviews of bedload transport formulae have found errors of around an order-of-magnitude in field and laboratory settings (Gomez and Church, 1989; Barry et al., 2004; Recking et al., 2012). This is due to short-term fluctuations in sediment transport associated with variations in local sediment supply (Leopold and Emmett, 1984), the migration of bedforms (Dhont and Ancy, 2018), and the inherently stochastic nature of physical processes that govern the entrainment and transport of grains (Einstein, 1951; Ancy, 2020*b*). For a given hydraulic condition, prediction accuracy increases as the time-scale for observations (or averaging) becomes longer (Recking et al., 2012), provided that steady-state conditions are maintained. Framed within the language of emergence, as fast-time-scale processes are integrated across time, their fluctuations give rise to emergent temporal patterns of process at slower time-scales (i.e. a reduced complexity state).

The potential practical implication of self-organisation is that larger-scale processes may be more amenable to prediction as they may exhibit a higher degree of order across time and space (Werner, 2003; Murray, 2007). In this sense, the emergence perspective appears at odds with the process approach in geomorphology. In the process approach, there is an assumption that determinism should be most apparent at smaller scales, where larger confounding processes cannot obfuscate more ‘fundamental’ interactions, which are typically framed as mechanical stresses and strains (Strahler, 1952; Rhoads, 2006). Almost a century of research in sediment transport has demonstrated that the opposite is true; noise is an intrinsic property of grain-scale processes (Ancy, 2020*b*), and patterns only emerge at larger scales (Recking et al., 2012). Thus, there appears a potential marriage of convenience between process geomorphology and emergence approaches, whereby deterministic relations may be effective provided they are developed and applied at a sufficiently large scale for the process of interest. The ability to study

sediment transport processes at emergent time-scales may be aided by the use of physical models with larger-scale ratios, where transport processes are accelerated. I discuss this opportunity further in the following section.

## **7.5 Modelling morphodynamics**

Models are tools that researchers may use to obtain observations and advance theory, although the development of models may inform and constrain theory itself. It is especially obvious to geomorphologists that all models are simplifications of reality (Baker, 1996; Beven, 1996; Kirkby, 1996). In numerical modelling, the concept of emergence has provided insight into approaches that lie between two major end-members: 1) reductionism or ‘bottom-up’ approaches, where a detailed model is built using constituent variables, and 2) universality or ‘top-down’ approaches, which employ fewer variables and attempt to model only the emergent behaviours (Werner, 2003; Murray, 2003). Here I extend these insights to physical modelling, which involve a different set of approaches and fundamental constraints, and problematise the notion of model ‘simplification’.

Physical models of geomorphic systems generally lie on a spectrum defined by two end-members of mechanical similarity: 1) 1 : 1 scale models, where all processes are replicated perfectly (e.g. Fenton and Abbott, 1977; Ancey et al., 2006), and 2) analogue or ‘toy’ models, resembling the universalist approach in which the balance of forces differ significantly from the field-scale (i.e. prototype), but illuminate the key positive and negative process feedbacks (Hooke, 1968; Peakall et al., 1996). Given the large scale of geomorphic systems, in most applications, the former serves as an idealised model, rather than one that is practical. In reality, almost all models are scaled, with some degree of mechanical dissimilarity and boundary conditions that constrain the system (Chorley, 1967; Schumm et al., 1987). Physical models can be scaled in various ways (Peakall et al., 1996), notably, based on the similarity of flow physics between model and prototype (kinematic similarity), and the ratio of vertical to horizontal scale (geometrical similarity).

## 7.5. Modelling morphodynamics

---

The perceived importance of kinematic and geometrical similarity varies across different areas of research, although their implications are often not fully realised. For example, if basic sediment transport processes are of interest kinematic similarity is typically prioritised to maintain flow properties, notably, the particle Reynolds number (Church, 2021). At the same time, the geometric similarity is relaxed, whereby a small vertical to horizontal scale ratio helps to maintain adequate flow depth (Peakall et al., 1996). The corresponding reduction in width-depth ratio suppresses emergent patterns such as bedforms, bars, and planforms, and at its most narrow states culminates in a one-dimensional or ‘1D’ river (e.g. Wilcock and McArdeall, 1993; Masteller and Finnegan, 2017).

Based on observations of self-organised geomorphic systems, Werner (2003) suggested that research surrounding short-time-scale processes such as sediment transport may not contribute to the understanding of long-time-scale properties of landforms. As Anderson (1972) described in layman’s terms, ‘the whole becomes not only more than but very different from the sum of its parts’. This notion is supported by experimental studies that embrace larger-scale processes, such as those characterising braided streams (Peirce et al., 2018). Recent findings in the study of bedload have led to a reciprocal and confirmatory insight, that 1D steady-state representations of sediment transport may be misleading because they ‘regard sediment transport as an isolated system whose variations are dictated solely by the water flow, rather than the dynamic interplay between the stream, the bed and the bedload’ (Ancy, 2020a, p. 6). If channel processes are slaved to the emergent behaviour of the system, the notion that 1D physical models are mere ‘simplifications’ may be flawed. These models may contribute to relations that have limited relevance to large-scale channel adjustment, where there are many more potential modes of adjustment.

The hierarchical view of systems calls into question whether findings in relatively constrained physical models can be up-scaled to natural systems with many more degrees-of-freedom. Indeed, both the smallest- and largest-scale processes are always misrepresented to some degree, due to the distorted fluid density in models (turbulence does not scale), truncation of grain size distributions to en-

### 7.5. Modelling morphodynamics

---

courage fully-rough flow, or space limitations that constrain the physical dimension of models. Instead, geomorphologists are forced to model a finite set of intermediate-scale processes, which is akin to the ‘hierarchical’ or ‘abstraction’ approach developed by Werner (1999, 2003). These abstraction models are constructed at levels in a hierarchy corresponding to the emergent forms, patterns, and behaviours of the landscape, isolating dynamics at different spatio-temporal scales. Consequently, the hierarchical modelling methodology may provide a useful roadmap for approaching physical modelling, which can be distilled into five steps (to visualise how this may apply to modelling rivers, imagine the hierarchy is comprised of grain, bedform, pattern, and catchment scales, wherein each scale the internal dynamical variables are hydraulics, morphology, and sediment transport):

1. Identify internal dynamical variables of the system, corresponding external environmental variables that influence the system and their intrinsic time-scales.
2. For each level  $n$  in the hierarchy, abstract the dynamics of faster (or smaller-scale) variables at level  $n+1$  into a minimal set of rules that dynamically relate the variables at level  $n$  to each other and the external environment.
3. Formulate and investigate the model at level  $n$ .
4. Test the consistency of the models by comparing the long-time-scale (time-scale of level  $n$ ) behaviour of the model at level  $n+1$  with the behaviour at level  $n$ .
5. Test the models by comparison with time-varying measurements on the natural system.

The first step is essential to any modelling approach, although the subsequent steps are particularly challenging as they involve isolating different spatio-temporal scales of process. Isolating process is inherent in some numerical approaches (e.g. reduced complexity modelling), but is not possible in physical

### 7.5. *Modelling morphodynamics*

---

models as small-scale reality cannot be truncated or eliminated. However, researchers may approximate this procedure in two ways: 1) varying boundary constraints (e.g. width-depth ratio, fixed or adjustable slope) to modify the available degrees-of-freedom for adjustment, and 2) varying model scale ratio, which has a similar effect but involves inherent distortions in the interaction between the particle and the boundary layer. Increasing disciplinary specialisation means that although geomorphologists already isolate various scales of process, it is less often conducted within the same research group or project. Also, a given research group may have access to a limited range of physical modelling infrastructure (e.g. a narrow hydraulic flume or wide stream table), meaning that they cannot achieve the steps outlined above. A more comprehensive understanding of the hierarchy of landscape processes may require a more formalised experimental approach, as well as diversification of research infrastructure.

In the short-term lies an opportunity to improve language and communication surrounding the diversity of physical models. At present, beyond mechanical similarity (e.g. Froude number etc.) there is no formalised terminology differentiating between physical models as they are commonly referred to as ‘flumes’, although models of larger-scale processes are often termed ‘stream tables’. The various segments of the hierarchical representation in Figure 7.2 provide a useful delineation of physical models that complements the distinction between 1 : 1, Froude-scale, distorted-scale, and analogue models (Peakall et al., 1996). This classification is based on the spatio-temporal scale of processes that are modelled, but critically, it encompasses the degrees-of-freedom available for adjustment and the potential for feedback and self-organisation. For example, at the narrow end of the spectrum, researchers use flumes (i.e. with fixed boundaries) to model in-channel processes such as small-scale granular physics and fluid mechanics (e.g. Fenton and Abbott, 1977; Ancy et al., 2006). At the broad end of the spectrum, researchers use stream tables (i.e. with erodible boundaries) to model large-scale channel processes at the scale of the channel pattern (e.g., Ashmore, 1982; Davies et al., 2003).

## 7.6 Conclusion

The concept of the fluvial trinity has historically served as an effective theoretical anchor point in explaining river behaviour as it simplifies modes of adjustment into three components; sediment transport, channel morphology, and hydraulics. Concepts of self-organisation and emergence may potentially complement this idea as they provide a theoretical framework predicting the interactions between different spatial and temporal scales of process. Specifically, an emergence perspective has the potential to describe several important aspects of these interactions if present, notably, dynamical asymmetry in which there is an asymmetrical relationship between processes occurring on different scales, and dynamic decoupling in which these processes only interact indirectly because they occur on different timescales. Thus, this perspective provides a hypothesis inverse to the pervasive process approach in geomorphology by highlighting the potential for large-scale system behaviour to arise from the collective behaviour of smaller-scale processes.

The concept of self-organisation may provide additional insight into observations of sediment transport, where emergent dynamics over relatively long timescales (time-averaged measurements) appear decoupled from highly variable stochastic processes on instantaneous or near-instantaneous scales. Specifically, the abstraction of slow large-scale processes from smaller faster ones in self-organised systems would mean that the study of small-scale processes surrounding grain-scale behaviour may not necessarily provide useful insights into the emergent dynamics at the scale of the channel. Also, modelling approaches would be more effective if they aimed to reproduce the emergent dynamics that are of interest, which entails replicating the appropriate degrees-of-freedom for adjustment. Further work is required to evaluate these hypotheses where hierarchical physical modeling approaches may be most effective.

# Chapter 8

## Conclusion

This thesis conducted stream table experiments of steep gravel-bed rivers to answer two general research questions:

- Does the spatial distribution of channel processes mediate river adjustment?
- What is the direction (i.e. upwards or downwards) of the relationship between channel processes that are superimposed over different spatio-temporal scales?

I first summarise the four original research chapters before outlining how they answer the primary research questions.

### 8.1 Summary

In **Chapter 4**, I physically modelled a steep gravel-bed channel and investigated the evolution of the fluvial trinity in response to successive increases in discharge. In the experiment, I identified spatially variable stage-dependent feedbacks and internal thresholds that controlled adjustments towards steady-state. At low discharges, transport capacity was likely controlled by feedbacks between morphology and sediment transport that concentrated flow and bedload within a narrow section of the bed. At moderate discharges, the selective entrainment of fine sediment from bar heads led to a concentration of larger-than-average grains which impeded further channel deformation until the discharge was increased. Each adjustment towards steady-state following perturbation involved different combinations of variables, which varied in both direction (i.e. upwards or downwards)

and magnitude. The feedbacks between hydraulics, sediment transport, morphology, and sediment texture were highly spatially dependent, which suggested more sophisticated analysis were required to interpret them.

Consequently, in the following chapters I focused on two components of the fluvial trinity and developed the analytical tools necessary to interpret their spatial variation. In **Chapter 5** I used combined recent advances in fluid dynamics, statistics, and remote sensing to estimate how roughness length varies across different physical scales in a pool-riffle channel, which provides insights into the spatial variation of hydraulics. Although this was a specific tool primarily framed around flow resistance, it provided a prototype for an intuitive representation of how channel characteristics (e.g. morphology, hydraulics) vary across different scales.

In **Chapter 6**, I evaluated the performance of 1D and 2D bedload transport functions under high relative shear stress conditions in a Froude-scaled physical model. The results suggested that bedload transport may collapse to a more simple function (i.e. with mean shear stress and median grain size) under high excess shear stress conditions. Despite being similarly accurate, the 1D and 2D approaches provided substantially different estimates of critical dimensionless shear stress, reflecting differences in how these approaches conceptualise excess shear stress.

In **Chapter 7**, I extended the hierarchical perspective of natural systems to fluvial settings, integrating the conceptual frameworks of emergence and self-organisation with the fluvial trinity. I argued that understanding the relationship between different scales of process interactions is important if we are to understand river behaviour, and discussed the potential implications for understanding sediment transport and approaching physical modelling of rivers.

## 8.2 Synthesis

The effect of the spatial distribution of channel processes on channel adjustment varied systematically with unit discharge. In Chapter 4, the adjustment of mor-

## 8.2. Synthesis

---

phology and transport capacity to imposed increases in discharge was mediated by flow concentration and surface texture patterns at relatively low discharges, but not at discharges at or above bankfull-equivalent for the experimental prototype. This result is consistent with literature roughly correlating bankfull flows with an effective discharge which re-shapes alluvial channel boundaries (Wolman and Miller, 1960), as well as models predicting partially-constrained channel adjustment when larger-than-average grain sizes are partially mobile (Wilcock and McArdell, 1997; MacKenzie et al., 2018). In Chapter 6, bedload transport was well predicted by mean shear stress across all discharges, all of which had relatively high excess shear stresses. This result is consistent with literature predicting that at a sufficiently high excess shear stress bedload is well predicted by 1D approaches due to the nonlinear shape of the transport function (Ferguson, 2003; Bertoldi et al., 2009; Francalanci et al., 2012; Recking et al., 2016). Together, these results indicate that although accounting for the spatial distribution of processes may be important for predicting channel dynamics at lower flows, they may not be necessary at higher flows.

The empirical and conceptual research contributed to an understanding of multiple scales of process and the interactions between them. In Chapter 5, I identified scaling patterns of morphology and flow resistance in a laboratory pool riffle channel based on spectral analysis. The results identified two distinct scales corresponding to the grain and bar-scale, which indicate distinct scales at which channel processes operate. This finding is consistent with previous channel classifications (Montgomery and Buffington, 1997; Hassan et al., 2007) and analyses of process (Hey, 1988; Parker and Peterson, 1980). In Chapter 7 I drew upon conceptual frameworks from other fields of natural science which may potentially explain the interaction between processes occurring on these two spatio-temporal scales, as well as larger planform and catchment scales. The integration of hierarchical frameworks in fluvial geomorphology leads to the hypothesis that dynamics at a given scale are largely controlled by dynamics at a larger scale (i.e. downwards control, de Boer, 1992; Werner, 1999). This hypothesis is supported by literature surrounding sediment transport (Ancy, 2020*b*; Recking et al., 2012),

as well as the tendency for different scales of physical models to yield different process insights (Masteller and Finnegan, 2017; Ashmore, 1982). Further work is required to evaluate these ideas in fluvial systems.

## 8.3 Future work

There are several opportunities for expanding the suite of experiments to model a wider range of conditions in gravel-bed rivers. Performing experiments with greater initial widths and lower unit discharges would extend the range of width-depth ratios and mean shear stresses, pushing the channels into different channel morphologies (e.g. braiding) and transport regimes, respectively. There are additional conditions that characterise natural channels, which could be modelled by removing the fixed banks and allowing for lateral adjustment and widening, introducing large wood, using a constant or pulsed feed (rather than recirculating), or increasing the initial channel gradient to model steeper channels. With an otherwise similar experimental setup (i.e. widths, unit discharges, data collection), these variations or treatments create a point of comparison with the runs presented herein.

The analytical tools developed in this thesis have the potential to shed light on many aspects of channel behaviour, especially if they are applied to understand periods of adjustment rather than just steady-state. The multiscale decompositions of hydraulic and topographic variables using wavelet transform can be applied to track the evolution of different scales of process (notably, grain- and bar-scale). The same technique may be applied to DEMs of difference (DODs) that record differences in topography between points in time, to describe the scales over which morphologic change occurs.

These experimental and analytical opportunities are important in answering the next set of research questions that shed light on fundamental processes and how they give rise to gravel-bed river behaviour. There are several questions that may be most fruitful and could clarify or challenge the results from this thesis:

*Under high discharges, are there conditions where 1D and 2D equations pre-*

### 8.3. Future work

---

*dict significantly different bedload transport?* It is conceivable that in natural rivers, certain conditions could suppress feedbacks that cause channels with different width-depth ratios to converge on the same transport capacity, or result in a different set of feedbacks. For example, in systems with adjustable banks, supply limitations, greater width-depth ratios, or large wood, there may be a different set of feedbacks that alter the transport capacity.

*Would predictions of bedload transport be more accurate if they accounted for the spatial distribution of shear stress, rather than just the frequency distribution? Is this even possible?* Using only the frequency distribution, proposed 2D equations (Chapter 6; Monsalve et al., 2020) remove the spatial dimension of transport and are in fact only quasi-2D. Processes of sediment entrainment, transport, and disentrainment are affected by local conditions that control the trajectories of grains downstream. Values of  $\theta_c$  cannot be measured, let alone spatially, and this is currently limiting factor in developing true 2D sediment transport equations.

*How do grain-scale phenomena such as migrating bedload sheets affect bedload transport as they interact with bar-scale processes?* In 1D physical models of rivers that lack reach-scale morphology, fluctuations in sediment transport are often attributed to migrating patches of sediment, and inputs of fine material have been shown to greatly increase transport capacity. We could expect that when larger-scale processes such as bar dynamics are allowed to emerge, the effect of grain-scale phenomena on bedload transport may be dampened. This hypothesis can be tested using a hierarchical approach in which bedload transport is compared in experiments with and without morphology (i.e. 1D and 2D).

*Do intrinsic thresholds contradict an emergence perspective in which small scales are enslaved by large scales?* Experimental results here and in the literature demonstrate that up until a certain discharge threshold larger-than-average grains can suppress bar-scale adjustments (Adams, 2021; MacKenzie and Eaton, 2017). This phenomenon could be interpreted as the reverse case in which large-scale system is controlled by smaller-scale processes, which suggests that additional conceptual development may be required to incorporate the role of intrinsic thresholds.

### 8.3. Future work

---

*How can we leverage multiscale analysis of the fluvial trinity to conceptualise and classify behaviour?* The population of rivers are typically divided into channels based on morphology, and the extent to which they change through time (i.e. steady-state/stable or adjusting/unstable), depending on the spatial or temporal scale of interest. Multiscale analyses of feedbacks between the fluvial trinity may contribute to behaviour-based river classifications as they quantify the magnitude of channel change across different spatial scales.

## 8.4 Contributions

The specific contributions and significance of each thesis chapter are outlined below:

### Chapter 4

- First study to find conclusive quantitative evidence for conceptual models describing exponential approaches towards steady-state and the potential for transiency if disturbance frequency exceeds the recovery time (Rhoads, 2020).
- Highlighted the importance of spatially dependent geomorphic thresholds (Paola and Seal, 1995; Nicholas, 2000; MacKenzie and Eaton, 2017) and found that they are most prevalent under partial transport conditions. Notably, feedbacks between morphology and sediment transport on transport capacity (associated with pools), and the effect of larger-than-average grain size fractions on channel deformations (associated with bar-heads).

### Chapter 5

- Utilised recent advances in statistics, fluid dynamics, and remote sensing to develop a transform-roughness correlation approach that estimates how roughness length varies across different spatial scales. This is the second multiscalar decomposition of roughness length in the literature (Pelletier and Field, 2016), and the first in fluvial hydraulics.
- Extended the roughness correlation developed by (Forooghi et al., 2017) to open-channel hydraulics, and demonstrated that it may improve on traditional estimates of roughness length in rivers (grain size or topography) as it incorporates a horizontal roughness scale.

### Chapter 6

#### 8.4. Contributions

---

- Provided empirical evidence to support the hypothesis that under high excess shear stress conditions 1D and 2D bedload transport functions are similarly accurate
- First study to identify that 1D and 2D approaches yield substantially different estimates of critical dimensionless shear stress, reflecting differences in how these approaches conceptualise excess shear stress.

#### Chapter 7

- Integrated conceptual frameworks of the fluvial trinity and emergence to describe how process interactions occurring at different spatio-temporal scales give rise to channel behaviour.
- Articulated the implications of the emergence perspective for physical modelling approaches in fluvial geomorphology.

# Bibliography

- Aberle, J. E. and Smart, G. M. (2003), ‘The influence of roughness structure on flow resistance on steep slopes’, *Journal of Hydraulic Research* **41**(3), 259–269.
- Adams, D. L. (2020a), ‘Code and example data for transform-roughness correlation (TRC) approach’.
- Adams, D. L. (2020b), ‘Toward bed state morphodynamics in gravel-bed rivers’, *Progress in Physical Geography* **44**(5), 700–726.
- Adams, D. L. (2021), ‘Morphodynamics of an erodible channel under varying discharge’, *Earth Surface Processes and Landforms* .
- Adams, D. L. and Zampiron, A. (2020), ‘Short communication: Multiscalar roughness length decomposition in fluvial systems using a transform-roughness correlation (TRC) approach’, *Earth Surface Dynamics* **8**, 1039–1051.
- Addison, P. S. (2018), ‘Introduction to redundancy rules: the continuous wavelet transform comes of age’, *Philosophical Transactions of the Royal Society A: Mathematical, Physical and Engineering Sciences* **376**, 1–15.
- Allen, T. and Starr, T. (1982), *Hierarchy: Perspectives for Ecological Complexity*, University of Chicago Press, Chicago, IL.
- Ancey, C. (2020a), ‘Bedload transport: a walk between randomness and determinism. Part 1. The state of the art’, *Journal of Hydraulic Research* **58**(1), 1–17.
- Ancey, C. (2020b), ‘Bedload transport: a walk between randomness and determinism. Part 2. Challenges and prospects’, *Journal of Hydraulic Research* **58**(1), 18–33.

## *Bibliography*

---

- Ancey, C., Böhm, T., Jodeau, M. and Frey, P. (2006), 'Statistical description of sediment transport experiments', *Physical Review E - Statistical, Nonlinear, and Soft Matter Physics* **74**(1), 1–14.
- Anderson, P. W. (1972), 'More Is Different', *Science* **177**(4047), 393–396.
- Ashmore, P. E. (1982), 'laboratory modelling of gravel braided stream morphology', *Earth Surface Processes and Landforms* **7**, 201–225.
- Ashworth, P. J. and Ferguson, R. I. (1986), 'Interrelationships of Channel Processes, Changes and Sediments in a Proglacial Braided River', *Geografiska Annaler* **68**(4), 361–371.
- Ashworth, P. J. and Ferguson, R. I. (1989), 'Size-selective entrainment of bed-load in gravel bed streams', *Water Resources Research* **25**(4), 627–634.
- Baker, V. R. (1996), Hypotheses and geomorphological reasoning, in B. L. Rhoads and C. E. Thorn, eds, 'The Scientific Nature of Geomorphology: Proceedings of the 27th Binghamton Symposium in Geomorphology', Wiley, Chichester, pp. 58–85.
- Baker, V. R. and Twidale, C. R. (1991), 'The reenchantment of geomorphology', *Geomorphology* **4**(2), 73–100.
- Barry, J. J., Buffington, J. M. and King, J. G. (2004), 'A general power equation for predicting bed load transport rates in gravel bed rivers', *Water Resources Research* **40**, 1–22.
- Bertoldi, W., Ashmore, P. E. and Tubino, M. (2009), 'A method for estimating the mean bed load flux in braided rivers', *Geomorphology* **103**(3), 330–340.  
**URL:** <https://linkinghub.elsevier.com/retrieve/pii/S0169555X08002936>
- Best, J. L. (1986), 'The morphology of river channel confluences', *Progress in Physical Geography* **10**(2), 157–174.

## Bibliography

---

- Beven, K. J. (1996), Equifinality and uncertainty in geomorphological modeling, in B. L. Rhoads and C. E. Thorn, eds, 'The Scientific Nature of Geomorphology: Proceedings of the 27th Binghamton Symposium in Geomorphology', Wiley, Chichester, U.K., pp. 273–288.
- Booker, W. H. and Eaton, B. C. (2020), 'Stabilising large grains in self-forming steep channels', *Earth Surface Dynamics* **8**, 51–67.
- Booker, W. H. and Eaton, B. C. (2022), 'Morphodynamic styles: Characterising the behaviour of gravel-bed rivers using a novel, quantitative index', *Earth Surface Dynamics* **10**(2), 247–260.
- Bray, D. I. (1982), Flow resistance in gravel bed rivers, in R. D. Hey, J. C. Bathurst and C. R. Thorne, eds, 'Gravel-bed rivers', John Wiley & Sons, Chichester, U.K., pp. 109–133.
- Bridge, J. S. and Jarvis, J. (1982), 'The dynamics of a river bend: a study in flow and sedimentary processes', *Sedimentology* **29**, 499–542.
- Brierley, G. J. and Fryirs, K. A. (2005), *Geomorphology and River Management*, Blackwell, Malden, MA.
- Buffington, J. M. and Montgomery, D. R. (1997), 'A systematic analysis of eight decades of incipient motion studies, with special reference to gravel-bedded rivers', *Water Resources Research* **33**(8), 1993–2029.
- Cadol, D. and Wohl, E. E. (2013), 'Variable contribution of wood to the hydraulic resistance of headwater tropical streams', *Water Resources Research* **49**(8), 4711–4723.
- Cameron, S. M., Nikora, V. I. and Stewart, M. T. (2017), 'Very-large-scale motions in rough-bed open-channel flow', *Journal of Fluid Mechanics* **814**, 416–429.

## Bibliography

---

- Chen, X., Hassan, M. A., An, C. and Fu, X. (2020), 'Rough correlations: Meta-analysis of roughness measures in gravel bed rivers', *Water Resources Research* **56**(8), 1–19.
- Chorley, R. J. (1967), Models in geomorphology, in R. J. Chorley and P. Haggett, eds, 'Models in Geography', Methuen, London, UK, pp. 59–96.
- Church, M. A. (1996), Space, time and the mountain—how do we order what we see, in B. L. Rhoads and C. E. Thorn, eds, 'The Scientific Nature of Geomorphology: Proceedings of the 27th Binghamton Symposium in Geomorphology', Wiley, Chichester, U.K., pp. 147–170.
- Church, M. A. (2006), 'Bed Material Transport and the Morphology of Alluvial River Channels', *Annual Review of Earth and Planetary Sciences* **34**(1), 325–354.
- Church, M. A. (2010), 'The trajectory of geomorphology', *Progress in Physical Geography* **34**(3), 265–286.
- Church, M. A. (2015), Channel Stability: Morphodynamics and the Morphology of Rivers, in P. Rowiński and A. Radecki-Pawlik, eds, 'Rivers—Physical, Fluvial and Environmental Processes', Springer, pp. 427–441.  
**URL:** <http://link.springer.com/10.1007/978-3-319-17719-9>
- Church, M. A. (2021), *Physical experiments in geomorphology*, The Geological Society Books.  
**URL:** <https://doi.org/10.1144/M58-2021-3>
- Church, M. A. and Ferguson, R. I. (2015), 'Morphodynamics: Rivers beyond steady state', *Water Resources Research* **51**(4), 1883–1897.  
**URL:** <https://onlinelibrary.wiley.com/doi/abs/10.1002/2014WR016862>
- Church, M. A. and Ryder, J. M. (1972), 'Paraglacial sedimentation: A consideration of fluvial processes conditioned by glaciation', *Bulletin of the Geological Society of America* **83**(10), 3059–3072.

## Bibliography

---

- Clifford, N. J., Robert, A. and Richards, K. S. (1992), 'Estimation of flow resistance in gravel-bedded rivers: A physical explanation of the multiplier of roughness length', *Earth Surface Processes and Landforms* **17**(2), 111–126.
- Collins, B. D., Montgomery, D. R., Fetherston, K. L. and Abbe, T. B. (2012), 'The floodplain large-wood cycle hypothesis: a mechanism for the physical and biotic structuring of temperate forested alluvial valleys in the North Pacific coastal ecoregion', *Geomorphology* **139**, 460–470.
- Comiti, F. and Mao, L. (2012), 'Recent Advances in the Dynamics of Steep Channels', *Gravel-Bed Rivers: Processes, Tools, Environments* pp. 351–377.
- Davies, T. R. H. and Korup, O. (2007), 'Persistent alluvial fanhead trenching resulting from large, infrequent sediment inputs', *Earth Surface Processes and Landforms* **32**(5), 725–742.  
**URL:** <https://onlinelibrary.wiley.com/doi/10.1002/esp.1410>
- Davies, T. R. H. and Sutherland, A. J. (1980), 'Resistance to flow past deformable boundaries', *Earth Surface Processes* **5**, 175–179.
- Davies, T. R., McSaveney, M. J. and Clarkson, P. J. (2003), 'Anthropic aggradation of the Waiho River, Westland, New Zealand: Microscale modelling', *Earth Surface Processes and Landforms* **28**(2), 209–218.
- Davis, W. M. (1899), 'The Geographical Cycle', *The Geographical Journal* **14**(5), 481–504.
- de Boer, D. H. (1992), 'Hierarchies and spatial scale in process geomorphology: a review', *Geomorphology* **4**(5), 303–318.
- De Marchis, M., Saccone, D., Milici, B. and Napoli, E. (2020), 'Large Eddy Simulations of Rough Turbulent Channel Flows Bounded by Irregular Roughness: Advances Toward a Universal Roughness Correlation', *Flow, Turbulence and Combustion* **105**(2), 627–648.  
**URL:** <https://doi.org/10.1007/s10494-020-00167-5>

## *Bibliography*

---

- Desloges, J. R. and Church, M. A. (1992), 'Geomorphic implications of glacier outburst flooding: Noeick River Valley, British Columbia', *Canadian Journal of Earth Sciences* **29**(3), 551–564.
- Dhont, B. and Ancey, C. (2018), 'Are Bedload Transport Pulses in Gravel Bed Rivers Created by Bar Migration or Sediment Waves?', *Geophysical Research Letters* **45**(11), 5501–5508.
- Dietrich, J. T. (2017), 'Bathymetric Structure-from-Motion: extracting shallow stream bathymetry from multi-view stereo photogrammetry', *Earth Surface Processes and Landforms* **42**(2), 355–364.  
**URL:** <http://doi.wiley.com/10.1002/esp.4060>
- Dietrich, W. E., Kirchner, J. W., Ikeda, H. and Iseya, F. (1989), 'Sediment supply and the development of the coarse surface layer in gravel-bedded rivers', *Nature* **340**(6230), 215–217.
- Dietrich, W. E. and Smith, J. D. (1983), Processes controlling the equilibrium bed morphology in river meanders., in C. Elliot, ed., 'River Meandering', American Society of Civil Engineers, New York, NY, pp. 759–769.
- Douglas, I. (1976), Lithology, landforms and climate, in E. Derbyshire, ed., 'Geomorphology and Climate', Wiley, London, pp. 345–366.
- Douglas, I. (1982), 'The unfulfilled promise: earth surface processes as a key to landform evolution', *Earth Surface Processes and Landforms* **7**(2), 101–101.
- Eaton, B. C. and Church, M. A. (2004), 'A graded stream response relation for bed load-dominated streams', *Journal of Geophysical Research* **109**, 1–18.
- Eaton, B. C., Church, M. A. and Davies, T. R. H. (2006), 'A conceptual model for meander initiation in bedload-dominated streams', *Earth Surface Processes and Landforms* **31**(7), 875–891.

## *Bibliography*

---

- Eaton, B. C., Church, M. A. and Millar, R. G. (2004), 'Rational regime model of alluvial channel morphology and response', *Earth Surface Processes and Landforms* **29**(4), 511–529.
- Eaton, B. C. and Lapointe, M. F. (2001), 'Effects of large floods on sediment transport and reach morphology in the cobble-bed Sainte Marguerite River', *Geomorphology* **40**(3-4), 291–309.
- Eckert, M. (2007), *Dawn of Fluid Dynamics: A Discipline between Science and Technology*, John Wiley & Sons.
- Einstein, H. A. (1951), Bed-load function for sediment transportation in open channel flows, in 'United States Department of Agriculture Technical Bulletin 1026', number 1026, Authority of the State of Illinois, Urbana, IL, pp. 43–49.
- Einstein, H. A. and Banks, R. B. (1950), 'Fluid resistance of composite roughness', *Transactions of the American Geophysical Union* **31**(4), 603–610.
- Fenton, J. D. and Abbott, J. E. (1977), 'Initial movement of grains on a steam bed: the effect of relative protusion', *Proceedings of the Royal Society of London* **537**, 523–537.
- Ferguson, R. I. (1981), Channel form and channel changes, in J. Lewin, ed., 'British Rivers', George Allen and Unwin, London, UK, pp. 90–125.
- Ferguson, R. I. (2003), 'The missing dimension: effects of lateral variation on 1-D calculations of fluvial bedload transport', *Geomorphology* **56**(1-2), 1–14.
- Ferguson, R. I. (2007), 'Flow resistance equations for gravel- and boulder-bed streams', *Water Resources Research* **43**(5), 1–12.
- Field, J. P. and Pelletier, J. D. (2018), 'Controls on the aerodynamic roughness length and the grain-size dependence of aeolian sediment transport', *Earth Surface Processes and Landforms* **43**(12), 2616–2626.

## *Bibliography*

---

- Forooghi, P., Stroh, A., Magagnato, F., Jakirlic, S. and Frohnapfel, B. (2017), 'Towards a Universal Roughness Correlation', *Journal of Fluids Engineering* **139**, 1–12.
- Francalanci, S., Solari, L., Toffolon, M. and Parker, G. (2012), 'Do alternate bars affect sediment transport and flow resistance in gravel-bed rivers?', *Earth Surface Processes and Landforms* **37**(8), 866–875.
- Fremier, A. K., Yanites, B. J. and Yager, E. M. (2018), 'Sex that moves mountains: The influence of spawning fish on river profiles over geologic timescales', *Geomorphology* **305**, 163–172.
- Friedkin, J. F. (1945), A laboratory study of the meandering of alluvial rivers, Technical report, War Department, US Army Corps of Engineers, Vicksburg, MS.
- Fryirs, K. A., Ralph, T. J., Larkin, Z. T., Tooth, S., Humphries, M., McCarthy, T., Hesse, P. P. and Mosimanyana, E. (2018), 'A nested hierarchical perspective to enhance interpretations and communication in fluvial geomorphology for use in water resources management: Lessons from the Okavango Delta, Botswana', *The Geographical Journal* **184**(2), 192–207.  
**URL:** <https://onlinelibrary.wiley.com/doi/10.1111/geoj.12250>
- Fryirs, K., Brierley, G. J. and Erskine, W. D. (2012), 'Use of ergodic reasoning to reconstruct the historical range of variability and evolutionary trajectory of rivers', *Earth Surface Processes and Landforms* **37**(7), 763–773.
- Furbish, D. J. (1987), 'Conditions for geometric similarity of coarse stream-bed roughness', *Mathematical Geology* **19**(4), 291–307.
- Gilbert, G. K. (1876), 'The Colorado Plateau Province as a Field for Geological Study', *The American Journal of Science and Arts* **XII**(68), 85–103.
- Gilbert, G. K. (1914), The transportation of debris by running water, Technical report, United States Geological Survey Professional Paper 86.

## *Bibliography*

---

- Goldenfeld, N. and Kadanoff, L. P. (1999), 'Simple lessons from complexity', *Science* **284**(5411), 87–89.
- Gomez, B. and Church, M. A. (1989), 'An Assessment of Bed Load Sediment Transport Formulae Bed Rivers', *Water Resources Research* **25**(6), 1161–1186.
- Graf, W. H. (1988), *Fluvial Processes in Dryland Rivers*, Springer, Berlin.
- Graf, W. L. (1977), 'The Rate Law in Fluvial Geomorphology', *American Journal of Science* **277**, 178–191.
- Grant, G. E., Swanson, F. J. and Wolman, M. G. (1990), 'Pattern and origin of stepped-bed morphology in high-gradient streams, Western Cascades, Oregon', *Geological Society of America Bulletin* **102**, 340–352.
- Green, K. C. and Westbrook, C. J. (2009), 'Changes in sediment yield, channel hydraulics and riparian area structure following loss of beaver dams', *B.C. Journal of Ecosystems and Management* **10**(68-79).
- Haigh, M. (1987), 'The holon: hierarchy theory and landscape research', *Catena: Supplement (Giessen)* **10**, 181–192.
- Hajek, E. A. and Wolinsky, M. A. (2012), 'Simplified process modeling of river avulsion and alluvial architecture: Connecting models and field data', *Sedimentary Geology* **257-260**, 1–30.  
**URL:** <https://linkinghub.elsevier.com/retrieve/pii/S0037073811002260>
- Haken, H. (1983), *Synergetics*, 3rd editio edn, Springer, New York.
- Hardy, R. J. (2012), 'The Potential of Using High-Resolution Process Models to Inform Parameterizations of Morphodynamic Models', *Gravel-Bed Rivers: Processes, Tools, Environments* pp. 116–122.
- Harrison, S. (2001), 'On reductionism and emergence in geomorphology', *Transactions of the Institute of British Geographers* **26**(3), 327–339.

## Bibliography

---

- Hassan, M. A., Smith, B. J., Hogan, D. L., Luzi, D. S., Zimmermann, A. E. and Eaton, B. C. (2007), 'Sediment storage and transport in coarse bed streams: scale considerations', *Developments in Earth Surface Processes* **11**(07), 473–496.
- Hey, R. D. (1979), 'Flow Resistance in Gravel-Bed Rivers', *Journal of the Hydraulics Division* **105**(4), 365–379.
- Hey, R. D. (1988), 'Bar Form Resistance in Gravel-Bed Rivers', *Journal of Hydraulic Engineering* **114**(12), 1498–1508.
- Hey, R. D. and Thorne, C. R. (1986), 'Stable Channels with Mobile Gravel Beds', *Journal of Hydraulic Engineering* **112**(8), 671–689.
- Hohermuth, B. and Weitbrecht, V. (2018), 'Influence of Bed-Load Transport on Flow Resistance of Step-Pool Channels', *Water Resources Research* **54**(8), 5567–5583.
- Hooke, R. L. (1968), 'Model Geology: Prototype and Laboratory Streams: Discussion', *Geological Society Of America Bulletin* **79**, 391–393.
- Howard, A. D. (1982), 'Equilibrium and time scales in geomorphology: Application to sand-bed alluvial streams', *Earth Surface Processes and Landforms* **7**(4), 303–325.
- Jackson, R. G. (1975), 'Hierarchical attributes and a unifying model of bed forms composed of cohesionless material and produced by shearing flow', *Geological Society of America Bulletin* **86**(11), 1523.  
**URL:** <https://pubs.geoscienceworld.org/gsabulletin/article/86/11/1523-1533/201706>
- James, M. R. and Robson, S. (2014), 'Mitigating systematic error in topographic models derived from UAV and ground-based image networks', *Earth Surface Processes and Landforms* **39**(20), 1413–1420.

## Bibliography

---

- Jimenez, J. (2004), 'Turbulent Flows over Rough Walls', *Annual Review of Fluid Mechanics* **36**, 173–196.
- Kasvi, E., Salmela, J., Lotsari, E., Kumpula, T. and Lane, S. N. (2019), 'Comparison of remote sensing based approaches for mapping bathymetry of shallow, clear water rivers', *Geomorphology* **333**, 180–197.  
**URL:** <https://doi.org/10.1016/j.geomorph.2019.02.017>
- Katchalsky, A. and Curan, P. F. (1967), *Nonequilibrium processes in biophysics*, Harvard University Press, Cambridge, MA.
- Keulegan, G. H. (1938), 'Laws of turbulent flow in open channels', *Journal of Research of the National Bureau of Standards* **21**, 707.
- Keylock, C. J., Singh, A. and Foufoula-Georgiou, E. (2014), 'The complexity of gravel bed river topography examined with gradual wavelet reconstruction', *Journal of Geophysical Research: Earth Surface* **119**(3), 682–700.
- Kirkby, M. J. (1996), A role for theoretical models in geomorphology, in B. L. Rhoads and C. E. Thorn, eds, 'The Scientific Nature of Geomorphology: Proceedings of the 27th Binghamton Symposium in Geomorphology', Wiley, Chichester, U.K., pp. 257–272.
- Kleinhans, M. G. (2010), 'Sorting out river channel patterns', *Progress in Physical Geography: Earth and Environment* **34**(3), 287–326.  
**URL:** <http://journals.sagepub.com/doi/10.1177/0309133310365300>
- Kramer, H. (1935), 'Sand mixtures and sand movement in fluvial model', *Transactions of the American Society of Civil Engineers* **100**(1), 798–838.
- Kumar, P. and Foufoula-Georgiou, E. (1997), 'Wavelet Analysis for geophysical applications', *Reviews of Geophysics* **34**(4), 385–412.
- Lane, S. N. and Richards, K. S. (1997), 'Linking river channel form and process: Time, space and causality revisited', *Earth Surface Processes and Landforms* **22**(3), 249–260.

## Bibliography

---

- Langbein, W. B. and Leopold, L. B. (1964), 'Quasi-equilibrium states in channel morphology', *American Journal of Science* **262**, 782–794.
- Lee, A. J. and Ferguson, R. I. (2002), 'Velocity and flow resistance in step-pool streams', *Geomorphology* **46**(1-2), 59–71.
- Leeder, M. R. (1983), On the Interactions between Turbulent Flow, Sediment Transport and Bedform Mechanics in Channelized Flows, in 'Modern and Ancient Fluvial Systems', Blackwell Publishing Ltd., Oxford, UK, pp. 3–18.  
**URL:** <https://onlinelibrary.wiley.com/doi/10.1002/9781444303773.ch1>
- Leonardi, S., Orlandi, P. and Antonia, R. A. (2007), 'Properties of d- and k-type roughness in a turbulent channel flow', *Physics of Fluids* **19**(12), 1–6.
- Leopold, L. B. and Emmett, W. W. (1984), Bedload movement and its relation to scour, in 'River Meandering', American Society of Civil Engineers, New York, NY, pp. 640–649.
- Li, G. (2009), 'Preliminary study of the interference of surface objects and rainfall in overland flow resistance', *Catena* **78**(2), 154–158.
- Limerinos, J. T. (1970), Determination of the Manning Coefficient From Measured Bed Roughness in Natural Channels, Technical report.
- Lisenby, P. E., Croke, J. and Fryirs, K. A. (2018), 'Geomorphic effectiveness: a linear concept in a non-linear world', *Earth Surface Processes and Landforms* **43**, 4–20.
- MacKenzie, L. G. and Eaton, B. C. (2017), 'Large grains matter: contrasting bed stability and morphodynamics during two nearly identical experiments', *Earth Surface Processes and Landforms* **42**(8), 1287–1295.
- MacKenzie, L. G., Eaton, B. C. and Church, M. A. (2018), 'Breaking from the average: Why large grains matter in gravel bed streams', *Earth Surface Processes and Landforms* .

## Bibliography

---

- Mackin, J. H. (1948), 'Concept of the graded river', *Bulletin of the Geological Society of America* **69**, 463–511.
- Masteller, C. C. and Finnegan, N. J. (2017), 'Interplay between grain protrusion and sediment entrainment in an experimental flume', *Journal of Geophysical Research: Earth Surface* **122**(1), 274–289.
- Meyer-Peter, E. and Müller, R. (1948), Formulas for bed-load transport, in 'Proceedings of the 3rd Meeting of the International Association for Hydraulic Structures Research', Stockholm, Sweden, pp. 1–26.
- Millar, R. G. (1999), 'Grain and form resistance in gravel-bed rivers', *Journal of Hydraulic Research* **37**(3), 303–312.
- Millar, R. G. (2000), 'Influence of bank vegetation on alluvial channel patterns', *Water Resources Research* **36**(4), 1109–1118.
- Miller, J. P. (1958), 'High mountain streams: Effects of geology on channel characteristics and bed material', *New Mexico State Bureau of Mines and Mine Resources Memoir 4* p. 51 pp.
- Monsalve, A., Segura, C., Hucke, N. and Katz, S. (2020), 'A bed load transport equation based on the spatial distribution of shear stress-Oak Creek revisit', *Earth Surface Dynamics* **8**(3), 825–839.
- Monsalve, A., Yager, E. M., Turowski, J. M. and Rickenmann, D. (2016), 'A probabilistic formulation of bed load transport to include spatial variability of flow and surface grain size distributions', *Water Resources Research* **52**(5), 3579–3598.  
**URL:** <https://onlinelibrary.wiley.com/doi/10.1002/2015WR017694>
- Montgomery, D. R. and Buffington, J. M. (1997), 'Channel-reach morphology in mountain basins', *Geological Society of America Bulletin* **109**(5), 596–611.
- Morris, H. M. (1955), 'A new concept of flow in rough conduits', *Transactions of the American Society of Civil Engineers* **120**, 373–398.

## Bibliography

---

- Murray, A. B. (2003), 'Contrasting the goals, strategies, and predictions associated with simplified numerical models and detailed simulations', *Geophysical Monograph Series* **135**(June), 151–165.
- Murray, A. B. (2007), 'Two Paradigms in Landscape Dynamics: Self-Similar Processes and Emergence', *Nonlinear Dynamics in Geosciences* pp. 17–35.
- Murray, A. B., Goldstein, E. B. and Coco, G. (2014), 'The shape of patterns to come: From initial formation to long-term evolution', *Earth Surface Processes and Landforms* **39**(1), 62–70.
- Murray, A. B., Lazarus, E., Ashton, A., Baas, A., Coco, G., Coulthard, T., Fonstad, M., Haff, P., McNamara, D., Paola, C., Pelletier, J. and Reinhardt, L. (2009), 'Geomorphology, complexity, and the emerging science of the Earth's surface', *Geomorphology* **103**(3), 496–505.  
**URL:** <http://dx.doi.org/10.1016/j.geomorph.2008.08.013>
- Murray, A. B. and Paola, C. (1994), 'A cellular model of braided rivers', *Nature* **371**(6492), 54–57.
- Nanson, G. C. and Huang, H. Q. (2017), 'Self-adjustment in rivers: Evidence for least action as the primary control of alluvial-channel form and process', *Earth Surface Processes and Landforms* **42**(4), 575–594.
- Nanson, G. C. and Huang, H. Q. (2018), 'A philosophy of rivers: Equilibrium states, channel evolution, teleomatic change and least action principle', *Geomorphology* **302**, 3–19.  
**URL:** <http://dx.doi.org/10.1016/j.geomorph.2016.07.024>
- Napoli, E., Armenio, V. and De Marchis, M. (2008), 'The effect of the slope of irregularly distributed roughness elements on turbulent wall-bounded flows', *Journal of Fluid Mechanics* **613**, 385–394.
- Neill, C. R. and Yalin, M. S. (1969), 'Quantitative definition of beginning of bed movement', *Journal of the Hydraulic Division* **95**, 585–587.

## *Bibliography*

---

- Nelson, J. M., Shimizu, Y., Abe, T., Asahi, K., Gamou, M., Inoue, T., Iwasaki, T., Kakinuma, T., Kawamura, S., Kimura, I., Kyuka, T., McDonald, R. R., Nabi, M., Nakatsugawa, M., Simões, F. R., Takebayashi, H. and Watanabe, Y. (2016), 'The international river interface cooperative: Public domain flow and morphodynamics software for education and applications', *Advances in Water Resources* **93**, 62–74.  
**URL:** <https://linkinghub.elsevier.com/retrieve/pii/S0309170815002249>
- Nelson, J. M., Shreve, R. L., McLean, S. R. and Drake, T. G. (1995a), 'Role of Near-Bed Turbulence Structure in Bed Load Transport and Bed Form Mechanics', *Water Resources Research* **31**(8), 2071–2086.
- Nelson, J. M., Shreve, R. L., McLean, S. R. and Drake, T. G. (1995b), 'Role of Near-Bed Turbulence Structure in Bed Load Transport and Bed Form Mechanics', *Water Resources Research* **31**(8), 2071–2086.
- Nezu, I. and Nakagawa, H. (1993), 'Turbulence in open-channel flows', *IAHR Monograph Series* pp. 1–281.
- Nicholas, A. P. (2000), 'Modelling bedload yield braided gravel bed rivers', *Geomorphology* **36**(1-2), 89–106.
- Nicolis, G. and Prigogine, I. (1977), *Self-organization in nonequilibrium systems*, Wiley, New York.
- Nield, J. M., King, J., Wiggs, G. F., Leyland, J., Bryant, R. G., Chiverrell, R. C., Darby, S. E., Eckardt, F. D., Thomas, D. S., Virca, L. H. and Washington, R. (2013), 'Estimating aerodynamic roughness over complex surface terrain', *Journal of Geophysical Research Atmospheres* **118**(23), 12948–12961.
- Nikuradse, J. (1933), *Laws of flow in rough pipes*, Technical report, Washington, D. C.
- Nowell, A. R. M. and Church, M. A. (1979), 'Turbulent flow in a depth-limited boundary layer', *Journal of Geophysical Research* **84**, 4816–4824.

## *Bibliography*

---

- Nyander, A. (2004), River-bed sediment surface characterisation using wavelet transform-based methods, Doctoral thesis, Napier University.
- Nyander, A., Addison, P. S., McEwan, I. and Pender, G. (2003), 'Analysis of river bed surface roughnesses using 2D wavelet transform-based methods', *Arabian Journal for Science and Engineering* **28**, 107–121.
- Paola, C. (1996), Incoherent structure: turbulence as a metaphor for stream braiding, in P. J. Ashworth, S. J. Bennett, J. L. Best and S. J. McLelland, eds, 'Coherent flow structures in open channels', Wiley, Chichester, U.K., pp. 705–723.
- Paola, C. and Seal, R. (1995), 'Grain size patchiness as a cause of selective deposition and downstream fining', *Water Resources Research* **31**(5), 1395–1407.
- Parker, G. (1990), 'Surface-based bedload transport relation for gravel rivers', *Journal of Hydraulic Research* **28**(4), 417–436.
- Parker, G. and Klingeman, P. C. (1982), 'On why gravel bed streams are paved', *Water Resources Research* **18**(5), 1409–1423.
- Parker, G., Klingeman, P. C. and McLean, D. G. (1982), 'Bedload and size distribution in paved gravel-bed streams', *Journal of the Hydraulics Division* **108**(4), 544–571.
- Parker, G. and Peterson, A. W. (1980), 'Bar Resistance of Gravel-Bed Streams', *Journal of the Hydraulics Division* **106**(10), 1159–1575.
- Peakall, J., Ashworth, P. J. and Best, J. L. (1996), Physical Modelling in Fluvial Geomorphology: Principles, Applications, and Unresolved Issues, in B. L. Rhoads and C. E. Thorn, eds, 'The Scientific Nature of Geomorphology: Proceedings of the 27th Binghamton Symposium in Geomorphology', John Wiley & Sons, pp. 27–29.

## Bibliography

---

- Peirce, S., Ashmore, P. and Leduc, P. (2018), 'The variability in the morphological active width: Results from physical models of gravel-bed braided rivers', *Earth Surface Processes and Landforms* **43**(11), 2371–2383.
- Pelletier, J. D. and Field, J. P. (2016), 'Predicting the roughness length of turbulent flows over landscapes with multi-scale microtopography', *Earth Surface Dynamics* **4**(2), 391–405.
- Phillips, J. D. (1991), 'Multiple modes of adjustment in unstable river channel cross-sections', *Journal of Hydrology* **123**, 39–49.
- Phillips, J. D. (1992), 'Nonlinear dynamical systems in geomorphology : revolution or evolution ?', *Geomorphology* **5**, 219–229.
- Phillips, J. D. (1993), 'Spatial-Domain Chaos in Landscapes', *Geographical Analysis* **25**(2).
- Phillips, J. D. (2003), 'Sources of nonlinearity and complexity in geomorphic systems', *Progress in Physical Geography* **27**(1), 1–23.
- Phillips, J. D. (2006), 'Deterministic chaos and historical geomorphology: A review and look forward', *Geomorphology* **76**, 109–121.
- Phillips, J. D. (2016), 'Vanishing point: Scale independence in geomorphological hierarchies', *Geomorphology* **266**, 66–74.  
**URL:** <http://dx.doi.org/10.1016/j.geomorph.2016.05.012>
- Polvi, L. E. and Wohl, E. E. (2012), 'The beaver meadow complex revisited — the role of beavers in post-glacial floodplain development', *Earth Surface Processes and Landforms* **37**, 332–346.
- Prestegard, K. L. (1983), 'Bar resistance in gravel bed streams at bankfull stage', *Water Resources Research* **19**(2), 472–476.
- Preston, N., Brierley, G. and Fryirs, K. (2011), 'The Geographic Basis of Geomorphic Enquiry', *Geography Compass* **5**(1), 21–34.

## Bibliography

---

- Recking, A. (2013a), 'An analysis of nonlinearity effects on bed load transport prediction', *Journal of Geophysical Research: Earth Surface* **118**(3), 1264–1281.
- Recking, A. (2013b), 'Simple Method for Calculating Reach-Averaged Bed-Load Transport Simple Method for Calculating Reach-Averaged Bed-Load Transport', *Journal of Hydraulic Engineering* **139**, 70–75.
- Recking, A., Liebault, F., Peteuil, C., Joliment, T., Etgr, U. R. and Martin, S. (2012), 'Testing bedload transport equations with consideration of time scales', *Earth Surface Processes and Landforms* **789**, 774–789.
- Recking, A., Piton, G., Vazquez-Tarrio, D. and Parker, G. (2016), 'Quantifying the Morphological Print of Bedload Transport', *Earth Surface Processes and Landforms* **41**(6), 809–822.
- Rhoads, B. L. (2006), 'The Dynamic Basis of Geomorphology Reenvisioned', *Annals of the Association of American Geographers* **96**(1), 14–30.
- Rhoads, B. L. (2020), *River dynamics: geomorphology to support management*, Cambridge University Press.
- Rhoads, B. L. and Thorn, C. E. (1993), 'Geomorphology as science : the role of theory', *Geomorphology* **6**, 287–307.
- Rhoads, B. L. and Welford, M. R. (1991), 'Initiation of river meandering', *Progress in Physical Geography* **15**(2), 127–156.
- Rickenmann, D. and Recking, A. (2011), 'Evaluation of flow resistance in gravel-bed rivers through a large field data set', *Water Resources Research* **47**(7).
- Robert, A. (1988), 'Statistical properties of sediment bed profiles in alluvial channels', *Mathematical Geology* **20**(3), 205–225.
- Rubey, W. W. (1931), 'A need for closer cooperation among students of stream-work', *Transactions of the American Geophysical Union* pp. 216–219.

## Bibliography

---

- Schlichting, V. H. (1936), 'Experimentelle untersuchungen zum Rauigkeitsproblem', *Archive of Applied Mechanics* **7**, 1–34.
- Schlichting, V. H. (1979), *Boundary-Layer Theory*, 7th edn, McGraw-Hill, New York.
- Schultz, M. P. and Flack, K. A. (2009), 'Turbulent boundary layers on a systematically varied rough wall', *Physics of Fluids* **21**(1), 1–9.
- Schumm, S. A. (1968), River adjustment to altered hydrologic regimen, Murrumbidgee River and paleochannels, Australia, Technical report, U.S. Geological Survey Professional Paper 598.
- Schumm, S. A. (1973), Geomorphic thresholds and complex response of drainage systems, in M. Morisawa, ed., 'Fluvial Geomorphology', 6 edn, State University of New York, Binghamton, pp. 299–310.
- Schumm, S. A. (1979), 'Geomorphic thresholds: the concept and its applications', *Transactions of the Institute of British Geographers* pp. 485–515.
- Schumm, S. A. (1985), 'Patterns of Alluvial Rivers', *Ann. Rev. Earth Planet. Sci.* **13**, 5–27.
- Schumm, S. A. and Khan, H. R. (1972), 'Experimental Study of Channel Patterns', *Geological Society of America Bulletin* **83**, 1775–1770.
- Schumm, S. A. and Lichty, R. W. (1965), 'Time, space, and causality in geomorphology', *American Journal of Science* **263**, 110–119.
- Schumm, S. A., Mosley, M. P. and Weaver, W. E. (1987), *Experimental Fluvial Geomorphology*, John Wiley, Hoboken, NJ.
- Schweber, S. (1993), 'Physics community and the crisis in physical theory', *Physics Today* **46**, 34–39.

## Bibliography

---

- Seminara, G. and Pittaluga, M. B. (2012), 'Reductionist versus holistic approaches to the study of river meandering: An ideal dialogue', *Geomorphology* **163-164**, 110–117.  
**URL:** <https://linkinghub.elsevier.com/retrieve/pii/S0169555X11003898>
- Smart, G. M., Duncan, M. J. and Walsh, J. M. (2002), 'Relatively Rough Flow Resistance Equations', *Journal of Hydraulic Engineering* **128**(6), 568–578.
- Strahler, A. N. (1952), 'Dynamic basis of geomorphology', *Bulletin of the Geological Society of America* **63**(September), 923–938.
- Sugden, D. and Hamilton, P. (1971), 'Scale, Systems and Regional Geography.', *Area* **3**(3), 139–144.
- Tal, M. and Paola, C. (2010), 'Effects of vegetation on channel morphodynamics: Results and insights from laboratory experiments', *Earth Surface Processes and Landforms* **35**(9), 1014–1028.
- Torrence, C. and Compo, G. P. (1998), 'A practical guide to wavelet analysis', *Bulletin of the American Meteorological society* **79**(1), 61–78.
- Trudgill, S. (1976), Rock weathering and climate: quantitative and experimental aspects, in E. Derbyshire, ed., 'Geomorphology and Climate', Wiley, London, UK, pp. 59–99.
- Walsh, S. J., Butler, D. R. and Malanson, G. P. (1998), 'An overview of scale, pattern, process relationships in geomorphology: a remote sensing and GIS perspective', *Geomorphology* **21**(3-4), 183–205.  
**URL:** <https://linkinghub.elsevier.com/retrieve/pii/S0169555X97000573>
- Werner, B. T. (1995), 'Eolian dunes: Computer simulations and attractor interpretation', *Geology* **23**(1), 107–110.
- Werner, B. T. (1999), 'Complexity in natural landform patterns', *Science* **284**(5411), 102–104.

## *Bibliography*

---

- Werner, B. T. (2003), 'Modeling landforms as self-organized, hierarchical dynamical systems', *Geophysical Monograph Series* **135**(i), 133–150.
- Wilcock, P. R. (1988), 'Methods for estimating the critical shear stress of individual fractions in mixed-size sediment', *Water Resources Research* **24**(7), 1127–1135.
- Wilcock, P. R. and Crowe, J. C. (2003), 'Surface-based Transport Model for Mixed-Size Sediment', *Journal of Hydraulic Engineering* **129**(February), 120–128.
- Wilcock, P. R. and McArdell, B. W. (1993), 'Surface-based fractional transport rates: partial transport and mobilization thresholds', *Water Resources Research* **29**(4), 1297–1312.
- Wilcock, P. R. and McArdell, B. W. (1997), 'Partial transport of a sand / gravel sediment flume', *Water Resources Research* **33**(1), 235–245.
- Wilcox, A. C. and Wohl, E. E. (2006), 'Flow resistance dynamics in step-pool stream channels: 1. Large woody debris and controls on total resistance', *Water Resources Research* **42**(5), 1–16.
- Wohl, E. (2011), 'What should these rivers look like? Historical range of variability and human impacts in the Colorado Front Range, USA', *Earth Surface Processes and Landforms* **36**(10), 1378–1390.
- Wohl, E. E. (2014), 'Time and the rivers flowing: Fluvial geomorphology since 1960', *Geomorphology* **216**, 263–282.  
**URL:** <http://dx.doi.org/10.1016/j.geomorph.2014.04.012>
- Wolfram, S. (2002), *A new kind of science*, Wolfram Media, Champaign, IL.
- Wolman, M. G. and Miller, J. P. (1960), 'Magnitude and Frequency of Forces in Geomorphic Processes', *The Journal of Geology* **68**(1), 54–74.

- Wong, M. and Parker, G. (2006), 'Reanalysis and Correction of Bed-Load Relation of Meyer-Peter and Müller Using Their Own Database', *Journal of Hydraulic Engineering* **132**(11), 1159–1168.
- Yager, E. M., Venditti, J. G., Smith, H. J. and Schmeeckle, M. W. (2018), 'The trouble with shear stress', *Geomorphology* **323**, 41–50.  
**URL:** <https://doi.org/10.1016/j.geomorph.2018.09.008>
- Yen, B. C. (2002), 'Open channel flow resistance', *Journal of Hydraulic Engineering* **128**(1), 20–39.
- Yochum, S. E., Bledsoe, B. P., Wohl, E. E. and David, G. C. L. (2014), 'Spatial characterization of roughness elements in high-gradient channels of the Fraser Experimental Forest, Colorado, USA', *Water Resources Research* **50**(7), 6015–6029.
- Zheng, S., Wu, B., Thorne, C. R. and Simon, A. (2014), 'Geomorphology Morphological evolution of the North Fork Toutle River following the eruption of Mount St . Helens , Washington', *Geomorphology* **208**, 102–116.  
**URL:** <http://dx.doi.org/10.1016/j.geomorph.2013.11.018>

# **Appendix A**

## **Publication: Chapter 2**



# Toward bed state morphodynamics in gravel-bed rivers

Progress in Physical Geography

1–27

© The Author(s) 2020

Article reuse guidelines:

[sagepub.com/journals-permissions](https://sagepub.com/journals-permissions)

DOI: 10.1177/0309133320900924

[journals.sagepub.com/home/ppg](https://journals.sagepub.com/home/ppg)**David Lawson Adams** 

The University of British Columbia, Canada; The University of Melbourne, Australia

## Abstract

In fluvial geomorphology, one of the most pervasive paradigms is that the size of the grains present in a river exercises an important effect on its character. In gravel-bed rivers, there is considerable scatter in the relations between so-called “representative grain sizes” and basic channel processes and morphologies. Under a grain size paradigm, our ability to rationalize the characteristics of a given channel and predict how it will respond to a change in conditions is limited. In this paper, I deconstruct this paradigm by exploring its historical origins in geomorphology and fluid dynamics, and identify three of its underlying premises: (1) the association between grain diameter and fluid drag derived from Nikuradse’s experiments with sand-coated surfaces; (2) the use of grain size by early process geomorphologists to describe general trends across large samples of sand-bed rivers; and (3) a classificatory approach to discerning bed structures originally developed for bed configurations found in sand-bed rivers. The conflation of sand- and gravel-bed rivers limits our ability to understand gravel-bed morphodynamics. Longstanding critique of the grain size paradigm has generated alternative ideas but, due to technological and conceptual limitations, they have remained unrealized. One such unrealized idea is the morphology-based definition of bed state – an important degree of freedom within fluvial systems, particularly in reaches where adjustments to planform are not easily achieved. By embracing recent advancements in fluid dynamics and remote sensing, I present an alternative or complementary concept of bed state based on the notion that fluvial systems act to maximize flow resistance. The proposed quantitative index represents the relative contribution of morphologic adjustments occurring at different spatial scales (discriminated using a wavelet transform) to a stable channel configuration. By explicitly acknowledging the complexity of bed adjustments we can move toward a more complete understanding of channel stability in gravel-bed rivers.

## Keywords

Gravel-bed rivers, channel stability, bed state, flow resistance, roughness correlations, wavelet transform

## 1 Introduction

As the boundaries of scientific inquiry expand, established paradigms may be retained as we approach novel yet ostensibly similar research frontiers. However, as ideas become increasingly removed from their foundational context, they may become less useful. In fluvial geomorphology, one of the most pervasive paradigms is that the size of the grains present in a river exercises an important effect on its character. This

notion was championed by the first process geomorphologists, who, amidst a quantitative revolution, derived mathematically the general relations between channel processes and the

---

### Corresponding author:

David Lawson Adams, The University of British Columbia, 1984 West Mall, Vancouver, British Columbia V6T 1Z2, Canada V6T 1Z2.

Emails: [dladams@alumni.ubc.ca](mailto:dladams@alumni.ubc.ca)

primary governing variables of valley slope, discharge, and grain size (Lane, 1957; Leopold et al., 1964; Mackin, 1948). These relations were developed using data collected by government agencies, largely from sand-bed rivers and laboratory experiments with well-sorted and fine-grained materials.

When a substantial research interest in gravel-bed rivers emerged in the 1980s, the application of existing frameworks to these relatively unstudied rivers appeared to be a natural extension. However, as several earlier authors anticipated (Rubey, 1938; Shulits, 1941), this has proven exceedingly difficult. Following the established grain size paradigm, an understanding of gravel-bed rivers requires the selection of a “representative” grain diameter from a mixture of various sizes (Shulits and Corfitzen, 1937). As a starting point, researchers sought to associate the median surface grain diameter  $D_{50}$  (i.e. 50th percentile) with flow resistance (Bray, 1982; Hey, 1979), mobility of the entire mixture (Buffington and Montgomery, 1997; Komar, 1987; Parker, 1990; Parker et al., 1982), channel stability (Diplas and Vigilar, 1992; Li, 1976; Parker, 1978), and the meandering/braiding threshold (Eaton and Giles, 2009; Eaton et al., 2010; Henderson, 1964; Millar, 2000, 2005). Averaged over a large number of samples, these relations generally hold but yield significant scatter (Barry et al., 2004; Ferguson, 2007; Gomez and Church, 1989; Recking et al., 2012), such that our ability to rationalize the characteristics of a given channel and predict how it will respond to a change in conditions is limited (Eaton et al., 2004; Leopold et al., 1964). The ability to achieve the latter is a metric by which we may measure the usefulness of our science (Leopold and Langbein, 1963).

### 1.1 The problem

The capacity to predict morphodynamic response is a contest between the apparent

disorder of rivers and theoretical frameworks that strive to elucidate order. Luna Leopold and Walter Langbein observed that the principle of indeterminacy long recognized in physics was one of geomorphology’s greatest adversaries (Langbein, 1963; Leopold and Langbein, 1963; Leopold et al., 1964). They acknowledged that given a large number of interacting factors, seemingly insignificant differences in initial conditions beyond measurement capability would give rise to vastly different outcomes. The role of non-linear system dynamics such as chaos has been more formally recognized in geomorphology since the 1990s (Malanson et al., 1990, 1992; Phillips, 1993, 2006). An implication is that, for practical purposes, geomorphic processes are best conceptualized as stochastic rather than physically deterministic. However, mainstream models of channel behavior continue to embrace deterministic foundations.

On top of the irreducible uncertainty associated with non-linear systems lies a significant degree of error associated with the state of theory. The failure of existing theory to fully capture the morphodynamics of gravel-bed rivers partly stems from the wide range of grain sizes (Bathurst, 1985; Bray, 1979) and shapes (Ibbeken and Schleyer, 2013). The unequal mobility of grain sizes inherent in poorly sorted beds (*sensu* Wilcock and McArdell, 1993, 1997) enables more complex adjustments in the form of various structural features (Grant et al., 1990; Hassan et al., 2007; Montgomery and Buffington, 1997; Venditti et al., 2017), which are necessitated by the steep nature of gravel-bed rivers. Thus, the representative grain size is arbitrary<sup>1</sup> and too reductionist to capture the full range of processes that may occur. Fundamentally, it is *not* representative, yet the grain size paradigm carries great inertia in river research and practice.

Researchers have been aware of this for some time. Early investigations found<sup>135</sup> compelling evidence contradicting the notion that *any* grain size could be representative in the context of

basic channel processes, except in the case of the most simple bed configurations (Bathurst, 1978; van Rijn, 1982). This line of critique<sup>2</sup> continues given that an alternative approach is yet to emerge (Aberle and Smart, 2003; Lane, 2005; Morvan et al., 2008; Nikora et al., 1998). As a result, researchers have spent decades modifying the existing frameworks applied to describe flow resistance, sediment entrainment, and channel stability, incorporating additional parameters to account for hiding/exposure (Einstein, 1950; Fenton and Abbott, 1977), sorting (Wilcock, 1988), the proportion of fine sediment (Venditti et al., 2010; Wilcock et al., 2001), and the importance of larger-than-average grains (MacKenzie et al., 2018; Recking, 2013), among others. However, given the fundamental limitations of the underlying theory, a complete understanding of channel behavior is currently out of reach. It follows that models of channel behavior could be enhanced by reconceptualizing the characteristics of the bed that control basic channel processes (referred to collectively as “bed state”) outside of the grain size paradigm.

## 1.2 A potential solution

Maximization of flow resistance has long been considered a stability-inducing condition in rivers (Leopold et al., 1964; Rubey, 1952), and has recently been placed within more mechanistic frameworks (Eaton and Church, 2004, 2009; Millar, 2005). In contrast to models of sediment transport, an understanding of flow resistance does not require consideration of any grain characteristics (*sensu* Einstein and Banks, 1950). The action of bedload transport contributes little to the total drag (Whiting and Dietrich, 1991), so therefore, to estimate flow resistance the channel boundary may be treated as rigid as it is in other fields of fluid research (Schlichting, 1936).

It is important to recognize that the use of grain size to predict flow resistance is a

historical contingency given that Wolman counts were, until recently, far more practicable than topographic surveys. Indeed, recent investigations have shown that in steep mountain streams even the most simple statistical analyses of gravel-bed surface topography yield superior estimates of flow resistance than grain-based ones (Aberle and Smart, 2003; Cadol and Wohl, 2013; Smart et al., 2002; Yochum et al., 2014). The maximum flow resistance approach to understanding channel stability is attractive because, in theory, it obviates the need for a priori selection of a representative grain size. A key question here is, in practice, how much can we understand about channel morphodynamics without any consideration of grains?

This is not a new line of thought. Arthur Nowell and Michael Church (1979) suggested a novel paradigm of bed state morphodynamics, remarking that understanding the relationship between bed surface geometry and near-bed fluid drag is important for understanding morphologic stability. Several contemporary studies suggested a similar approach (Davies and Sutherland, 1980; Furbish, 1987), but further development of these ideas was impeded by a range of technological and conceptual limitations.

At the time, flows within the fully rough regime<sup>3</sup> – characteristic of gravel-bed rivers (Buffington and Montgomery, 1997) – were poorly understood. Quantitative models predicting the fluid drag generated by a surface, based purely on its geometric characteristics (known as “roughness correlations”), had only been developed for simple surfaces. Collecting topographic data in rivers was an arduous, manual process, and data was limited in both resolution and spatial extent (Furbish, 1987; Robert, 1988). Analysis of irregular and aperiodic signals using transforms was hindered by the necessary number of Fourier components required to represent non-sinusoidal shapes (Engelund and Fredsoe, 1982; Plate, 1971).

Advances over the last three decades have largely overcome these limitations. The characteristics of flows within the fully rough regime are now relatively well understood, culminating in two major reviews (Jimenez, 2004; Raupach et al., 1991). Roughness correlations developed for relatively simple surfaces have been extended to irregular surfaces (e.g. Barros et al., 2018; Foroughi et al., 2017, 2018; Napoli et al., 2008) due to improvements in experimental techniques and numerical models (notably, direct numerical simulations and large-eddy simulations), alongside significant increases in computing power. Recent advances in laser scanning and structure-from-motion photogrammetry now enable the rapid and relatively inexpensive collection of high-resolution topographic data (Westoby et al., 2012). To capitalize on these new data, geomorphologists must develop theory-driven analytical tools that supersede the time-honored but crude cross-sectional analyses and qualitative descriptions of channel morphology, which are relicts of previous surveying technology. Also, the wavelet transform has emerged as a technique suited to analyzing the underlying structure of complex geophysical signals (Kumar and Foufoula-Georgiou, 1997).

Drawing from each of the advancements listed above, this paper adapts Nowell and Church's (1979) proposal into a quantitative, physically based index of bed state. This idea is progressively developed through discussion of three key areas: (1) the role of bed state resistance in channel morphodynamics; (2) the physical structure of gravel-bed surfaces; and (3) roughness correlations developed in complementary fields of fluid research that may be suitable for use in gravel-bed rivers. In doing so, I also clarify seemingly contradictory ideas within the literature regarding gravel beds: (1) the presence of distinctive and self-organized particle clusters (Cin, 1968); (2) that gravel-bed surfaces have fractal characteristics (Robert, 1988); and (3) that large, periodic

structures often contribute the most to flow resistance (Parker and Peterson, 1980).

The relative contribution of different physical scales of roughness to the total drag associated with the bed can be estimated by isolating modes of topographic variation using the wavelet transform and then applying a roughness correlation to each. Thus, it is not the total resistance that is of interest here, but rather, the spatial scales of physical feedbacks by which channels achieve stability. Endowed with the bed state analysis developed herein, future investigations may better evaluate morphologic responses to disturbance (e.g. landslides and storms) and longer-term system changes (e.g. climate change). By correlating channel-forming processes with theory-driven descriptions of channel morphology, geomorphologists may build toward morphodynamic models that are more representative, and ultimately, the ability to forecast channel responses.

## II Channel morphodynamics

A quantitative understanding of alluvial channel form and response to changes in primary governing conditions (discharge, sediment supply, and valley slope) remains an important yet elusive goal in fluvial geomorphology (Eaton et al., 2004). Arguably, the nearest approach so far is embodied in the various so-called "rational regime models" (Ferguson, 1986), which formalize the relations among governing equations traditionally applied to predict the geometry of mobile-bed canals. To close the regime description of alluvial channels, researchers have resorted to applying extremal hypotheses, i.e. states that the fluvial system will optimize to (Chang, 1979; Davies and Sutherland, 1983; Eaton et al., 2004; Kirkby, 1977; White et al., 1982; Yang, 1976). In some cases, these extremal hypotheses are equivalent (Davies and Sutherland, 1983; Millar, 2005; White et al., 1982), but in some circumstances optimality criteria such as minimum slope (Chang, 1979)

and maximum transport capacity (White et al., 1982) are limited in the range of adjustments that they embrace (Eaton and Church, 2009).

Recently there has been a movement toward more general statements of optimality that can accommodate complex morphodynamic responses, as they acknowledge more completely the degrees of freedom that alluvial systems have (Eaton et al., 2004; Millar, 2005). Eaton et al. (2004) proposed that channels tend toward a state of greatest relative stability, achieved by maximizing resistance to flow across the entire fluvial system. This is physically explained by the concept of excess kinetic energy that can act to further deform the system until it happens by chance to achieve a form that has a higher resistance to flow and is, therefore, more stable (Rubey, 1931). This aspect of system behavior has been ascribed by Huang and Nanson (2000) to a principle of least action, whereby stability is achieved by minimizing the potential for further deformation of the system.<sup>4</sup>

Eaton et al. (2004) propose that the total resistance to flow in the system  $f_{\text{sys}}$  can be indexed by substituting the valley slope  $S_v$  for the channel slope  $S$  in a flow resistance equation

$$f_{\text{sys}} = \frac{8gRS_v}{u^2} \quad (1)$$

where  $g$  is gravity,  $u$  is mean velocity, and  $R$  is the hydraulic radius, which replaces flow depth  $h$  for narrow channels with rough banks and higher relative roughness (the ratio of roughness height to flow depth). This transforms the friction parameter from a property of the stream channel ( $f$ ) to a property of the alluvial system ( $f_{\text{sys}}$ ) that incorporates various sources of resistance. Thus,  $f_{\text{sys}}$  is made up of the components

$$f_{\text{sys}} = f' + f'' + f''' \quad (2)$$

where  $f'$  is bed state resistance (grains and grain structures),  $f''$  is within-channel resistance (bars, pools, riffles), and  $f'''$  is reach-scale resistance (planform shape and gradient).<sup>5</sup> This representation explicitly states that a stable state

may be approached in multiple ways, which is consistent with observations and models of channel response (Kellerhals and Church, 1989; Montgomery and Buffington, 1998; Schumm, 1969, 1971).

As a first-order approximation, one could assume that the spatial scale at which the morphologic adjustment occurs is simply a function of the magnitude of the imposed change in conditions. Rather, the nature of channel adjustments is more complex due to physical constraints. Modification of channel gradient (i.e. through lateral migration) typically occurs on a decadal scale,<sup>6</sup> as it requires the shifting of substantial volumes of bed material. Thus, on the scale of an individual event, channel slope may be relatively constant and stability tends to be achieved through other degrees of freedom. Eaton and Church (2009) demonstrated that modulation of bed state (as well as scour<sup>7</sup>) represents the most rapid type of adjustment, as it requires the least amount of geomorphic work. Adjustments to bed state resistance represent the only independent degree of freedom in laterally confined reaches (Eaton and Church, 2009), indicating that this mode of adjustment is common where lateral migration is hindered by root-reinforced banks (Abernethy and Rutherford, 2000, 2001; Andrews, 1984; Hey and Thorne, 1986). Thus, it can be inferred that adjustments to bed state resistance are particularly important in humid and tropical regions that are well-vegetated, and in mountain rivers, which tend to be laterally confined. It follows that a physically based description of bed state is an essential component of a complete morphodynamic model.

## 2.1 Proposed definitions of bed state

The term “bed state” has been used to refer to various physical properties of gravel beds, but it is yet to be explicitly linked to fluid drag following the maximum flow resistance hypothesis. In flume experiments using sand–gravel

mixtures, Iseya and Ikeda (1987) described three types of bed state (congested, transitional, smooth) associated with the concentration and mobility of each size fraction on the bed surface. Church and Kellerhals (1978) defined bed state as the packing characteristics on the bed surface (over-loose, normally loose, under-loose), which are associated with sediment supply. The most widely adopted definition of bed state is, however, more general (e.g. Eaton and Church, 2009; Johnson, 2016; Johnson et al., 2009). For example, Eaton and Church (2009) refer to bed state as the adjustment of surface texture by armoring, the occurrence of sediment patches, and the development of sediment structures. This definition of bed state is not a quantitative index, but a mélange of grain and structural characteristics, and thus any inference regarding channel stability can only be qualitative.

Church (2006) proposed a more mechanistic definition of bed state based on the dimensionless critical shear stress  $\tau_c^*$  (or critical Shields number) associated with the bed (Shields, 1936). This parameter is typically used as a grain mobility index, representing the threshold condition at which individual grains begin to be entrained or, in practice, the state beyond which rare entrainment events rapidly become more common (Church, 2011). The critical Shields number approach has considerable advantages over other proposed definitions of bed state as it may be interpreted as a direct measure of the structural properties of the granular surface that resist grain entrainment (e.g. hiding, imbrication, packing, bed structures) (Church, 2006). How to assign a particular critical Shields number to a given bed is, however, by no means clear (Church, 2011). This is a problem because, if a definition of bed state is to be of any value, it must be measurable.

Moreover,  $\tau_c^*$  is limited as an analytical tool because it is a reach-averaged dimensionless representation of many different structural features, the influence of which is relatively

unknown. In a study of step-pool systems, Zimmermann et al. (2010) found that the critical Shields number was unsatisfactory as an indicator of bed stability as it could not account for the effect of localized bed structures. Therefore, even if  $\tau_c^*$  could be reliably estimated or measured it would be difficult to relate it to physical changes or conditions on the bed. Given that no existing definition of bed state is conducive to the maximum flow resistance approach, I identify and evaluate two potential approaches to discerning the structural qualities of gravel beds.

### III Gravel-bed structure

#### 3.1 Classificatory approach

Scientific classifications are useful simplifying devices. Leopold and Langbein (1963) framed geomorphology as a pursuit that is first interested in classifying observed forms, from which generalizations are drawn (an inductive approach). The scientific study of rivers has led to the development of many morphological classifications, the most famous being the tripartite division of river planform into braided, meandering, and straight (Leopold and Wolman, 1957). The classificatory approach has been met with several critiques from within the discipline (Goodwin, 1999a, 1999b; Juracek and Fitzpatrick, 2003). Philosophical treatments of classification and taxonomy (Collier, 1996; James, 1907; Kripke, 1972), as well as perspectives from other disciplines (Haslam, 2002; Zachar, 2015), may be enlightening as we seek to describe rivers.

Linnaeus, in his iconic *Systema Naturae* (1735), pioneered the natural classification of “kinds,” using a binomial ranking system of genera and species. Darwin (1859) and Wallace (1869) continued the “natural” classifications, explained by the process of natural selection, reflecting relationships between organisms over geological time. In practice, natural sciences benefit greatly from the recognition of natural

kinds (Collier, 1996; Kripke, 1972), notably, chemical elements and biological species. Natural kinds may: (1) be naturally occurring as opposed to artificial; (2) have clearly demarcated boundaries separating members of the natural kind from non-members; and (3) possess observable features that are causally produced by internal properties. Given that these criteria are unrealistic in the case of many branches of science, researchers have been forced to embrace pragmatist theories of classification (James, 1907) not based on reproducible observations. For example, in psychopathology, a range of models for classifying psychiatric disorders have been proposed, including practical, functional, fuzzy, and discrete kinds (Haslam, 2002; Zachar, 2000, 2002, 2015).

Albeit without explicitly describing them as such,<sup>8</sup> these are types of models that geomorphologists frequently employ. An example of fuzzy kinds may be found in the various sand-bed morphologies that have been reproduced in laboratory settings (i.e. lower-stage plane bed, ripples, dunes, upper-stage plane bed, antidunes, chutes-and-pools, cyclic steps). These morphologies may be distinguished by their clustering in phase diagrams defined by various combinations of flow and sediment variables (Allen, 1984; Cartigny et al., 2014; Southard, 1971, 1991; Venditti, 2013).

On the other hand, classificatory approaches to describing bed morphology in gravel settings have been far less effective. Researchers have reported a miscellany of features, primarily based on physical characteristics such as grain size and morphology, which have been placed within loose qualitative frameworks described by Grant et al. (1990: 341) as “perplexing and imprecise.” It is worth noting that classificatory approaches are an inevitable consequence of an emphasis on grain size, because if one acknowledges the presence of grains, they must also acknowledge the presence of forms. At best, morphological classifications are fuzzy due to

the natural variability encountered in the field (e.g. channel reach morphologies (Helm, 2019; Tamminga and Eaton, 2018)), and at worst, they are rather arbitrary (see Section 3.1.1). There have been recent advances in qualitative, process-based classifications of channel features (Hassan et al., 2007; Montgomery and Buffington, 1997; Venditti et al., 2017). However, quantifying the association between morphologic kinds and basic channel processes is difficult given that sediment entrainment and fluid dynamics in gravel-bed rivers are themselves poorly understood (Barry et al., 2004; Ferguson, 2007; Gomez and Church, 1989; Recking et al., 2012).

The various morphologic kinds that have been described are often superimposed; for example, imbricated grains occurring within a pool-riffle structure. The co-occurrence of different types under the same conditions indicates that the suite of features described in gravel-bed rivers cannot all neatly be classified as the same kind of thing (and are often differentiated by the terms “units,” “bedforms,” “structures,” etc.), unlike their sand-bed counterparts. This is perhaps why a progressive sequence of bed configurations (each associated with a unique combination of slope, flow, or sediment variables) has not yet been identified (Venditti et al., 2017). Also, the common distinction between “grains” (the particle size distribution) and “forms” (the features made up of particles) is a false dichotomy, given that accumulations of small particles can have the same hydraulic effect as a single large particle (Figure 1).

A classification of gravel-bed structures, let alone one that is both process-based and quantitative, is at present only an aspirational ideal. It follows that this approach cannot currently be used to define bed state. To further demonstrate the potential problems associated with the classificatory approach, I will briefly<sup>140</sup> critique one proposed morphologic kind that has been the topic of considerable study.

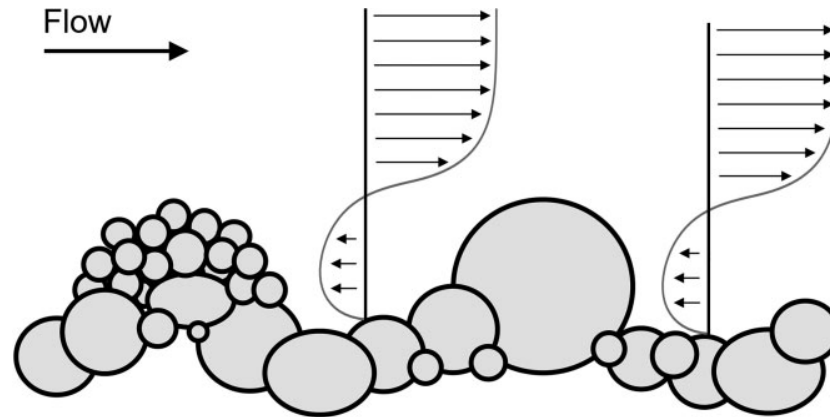


**Figure 1.** Schematic gravel bed with simplified velocity profiles where an accumulation of smaller particles has the same hydraulic effect as a single large particle.

*3.1.1 The example of particle clusters.* One of the most pervasive ideas regarding the structure of gravel beds is that of “particle clusters,” a term describing the accumulation of relatively small particles around larger ones, sitting above the average elevation of the surrounding bed (Brayshaw, 1985; Cin, 1968; Strom and Papanicolaou, 2008). It was noted early on that understanding the role of these features is hindered by difficulties in recognizing and identifying them (Naden and Brayshaw, 1987). Subsequently, research has been dedicated to detecting these features using increasingly sophisticated techniques, most recently, fractals (Curran and Tan, 2014; Papanicolaou et al., 2012; Tsakiris and Papanicolaou, 2008) and factorial kriging (Wu et al., 2018). The relatively unsatisfactory performance of statistical techniques in identifying clusters has been interpreted as a shortcoming of the algorithms, rather than the concept of clusters itself. This violates an important principle: that classifications should be treated as hypotheses and not paradigms, whereby each use of the classification should be a test either verifying or nullifying their explanatory capability (Goodwin, 1999a, 1999b). Moreover, most studies have opted to identify clusters by hand (Entwistle et al., 2008; Hendrick et al., 2010; L’Amoreaux and Gibson, 2013; Strom and Papanicolaou,

2008), which introduces a series of potential issues where complex surfaces and cognition collide.

First, the reliance on visual identification increases the potential for cognitive errors leading to false positives (or type I errors). Various forms of erroneous pattern recognition are well recognized; for example, “clustering illusion” is a logical fallacy describing the tendency to overestimate the importance of runs, streaks, or clusters in large samples of random or semi-random data (Iverson et al., 2008). These illusions are known as “phantom patterns,” and are caused by a human tendency to underpredict the amount of variability likely to appear in such data<sup>9</sup> (Gilovich, 1991). For instance, Figure 2 consists of 10,000 randomly distributed points of log-normal size distribution, consistent with the approximate size distribution of most fluvial gravels (Folk, 1966; Folk and Ward, 1957; Krumbein, 1938). Here, clusters and streaks of points are visually obvious, such that an observer may attempt to rationalize the pattern. However, these features arise through random chance rather than some specific formative process. The physical structure of gravel beds and the processes that produce them, particularly at the grain-scale, may be random enough to allow for such cognitive errors (further discussion in Section 3.2). This notion is

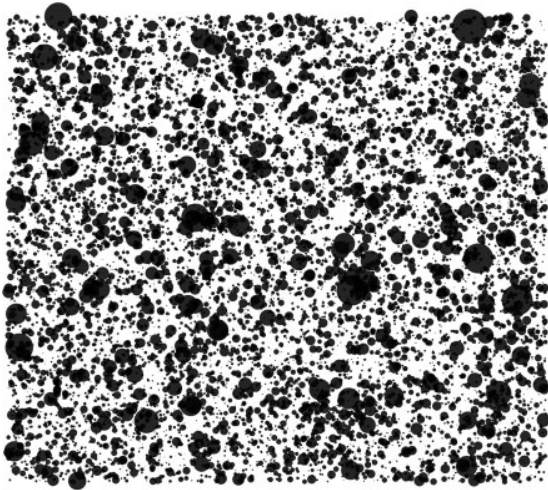


**Figure 2.** Ten thousand randomly distributed points with a log-normal size distribution.

supported by Nikora et al. (1998), who, in a study of six river reaches, found no spatial correlation between particles and were able to reject spatial particle clustering.

Second, the concept of a cluster is essentially arbitrary given that agglomerations of particles of varying size, and variation in bed elevations, are inherent characteristics of poorly sorted river beds at many scales and locations. On any given bed, a keen observer could locate a series of features matching the classical description of clusters. However, continued observation would yield features of diminishing resemblance to the description, which is perhaps why studies have been led to describe so many types of clusters, such as “pebble,” “line,” “comet,” “ring,” and “heap” (Strom and Papanicolaou, 2008).

The investigation of clusters has confirmed more general findings from other lines of research, notably, that groups of particles contribute to drag more than individual particles (Clifford et al., 1992; Leopold et al., 1964; Nikora et al., 1998; Robert, 1988), that larger-than-average particles decrease grain mobility through grain hiding (Einstein, 1950; Kirchner et al., 1990; Wilberg and Smith, 1987), and that therefore larger-than-average particles exert a

disproportionately large influence on channel stability (MacKenzie and Eaton, 2017; MacKenzie et al., 2018). Clusters are an effective concept that encapsulates these effects, but their role as distinctive structural features that arise through clear formative processes has probably been over-emphasized. The simplified, schematic representations of gravel-bed structures are exactly that. They belie a more profound quality at the grain-scale: deterministic chaos.

### 3.2 Statistical approach

For systems lacking easily discernible kinds, statistics can offer a powerful alternative. Following advances in surveying and statistics in the 1980s, researchers were granted a range of new techniques for analyzing the structure of river beds. Mirroring developments in fluid dynamics earlier in the decade (Musker, 1980), several researchers (primarily European graduate students) proposed that, to understand flow resistance, gravel beds should be treated as a random field of elevations rather than a size distribution of grains (Aberle et al., 1999; Bergeron, 1996; Butler et al., 2001; Clifford et al., 1992; Furbish, 1987; Robert, 1988, 1991). This obviates the heuristic distinction between grain and form components of resistance, and their often-presumed equivalence with frictional drag (arising due to friction between the fluid and the surface) and pressure drag (arising due to the shape of the roughness element), respectively (Furbish, 1987). A range of techniques has since been applied to centimeter- or millimeter-scale gravel-bed topography, usually in laboratory flumes. Techniques include structure functions (Butler et al., 2001; Clifford et al., 1992; Robert, 1988, 1991), filtering (Bergeron, 1996), transforms (Aberle et al., 2010), as well as simple analyses of the probability density function of elevations (moments) (Bertin and Friedrich, 2018; Ockelford and Haynes, 2013<sup>142</sup>).

Although these studies have not explicitly linked bed statistics to channel stability, some

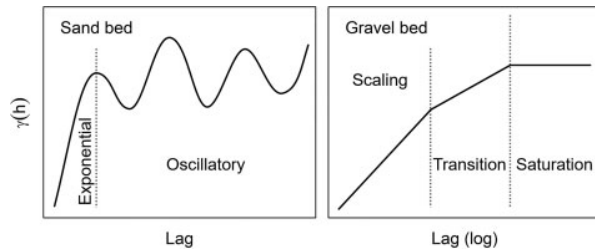


**Figure 3.** Schematic of sand- and gravel-bed variograms. Note the use of different axis scales.

Source: Robert (1988, Figure 1), adapted with permission from Springer Nature.

of these analyses may inform how we can best approach a statistical description of bed state. Notably, the scaling characteristics of gravel beds, relative to sand-bed rivers, may be illuminating. For three decades, the scaling characteristics of gravel-bed topography have been considered fundamentally different from those of sand-bed topography, as represented by variograms (Figure 3). Variograms show the amount of variability in elevation  $\gamma(h)$  between pairs of points at various distances (lags), and the general forms shown in Figure 3 have been confirmed by numerous investigations (Butler et al., 2001; Clifford et al., 1992; Furbish, 1987; Nikora and Walsh, 2004; Powell et al., 2016; Qin and Ng, 2011; Robert, 1988, 1991).

Published sand-bed variograms are typically characterized by an exponential component and an oscillatory component, which can be interpreted as small-scale stochastic and large-scale periodic bed structures, respectively. Published variograms of gravel beds have been restricted to the grain-scale (often due to practical limitations associated with past surveying techniques), within which there are three relatively distinct zones. The exponential component may be divided into two parts, the scaling and transition regions, which plot as two straight lines. The position of the inflection point at around the size of the largest grains indicates that these regions loosely correspond to individual grains and arrangements of grains, respectively. The

third zone is known as the saturation region, at which variance reaches a constant value with distance.

The power-law trend of the scaling and transition regions represent fractal behavior, whereby the slope  $b$  is inversely related to the Hausdorff or fractal dimension  $D$ . Thus, the most pervasive structural quality of gravel-bed topography has been reported to be statistical self-similarity<sup>10</sup> or scale invariance, whereby smaller scales are statistically similar to larger parts when magnified (Xu et al., 1993). The self-similar structure indicates that the formative processes (i.e. grain deposition) are characterized by deterministic chaos.

The restriction of gravel-bed variograms to the grain-scale (and perhaps the use of different axis scales in Robert's (1988) original schematic) has obscured the fact that sand- and gravel-beds can have very similar overall scaling characteristics. Figure 4 reproduces two published sand-bed variograms and compares them to gravel-bed variograms based on stream table data with well developed pool-riffle sequences. When the length of the dataset spans the reach scale (i.e. many channel widths), gravel-bed variograms exhibit both exponential and oscillatory scaling components, similar to sand-bed variograms.

It is not the overall scaling characteristics, but the position of the inflection point separating the exponential and oscillatory components, that best distinguishes sand- and gravel-bed topography. The lag at which the inflection point is located, relative to the channel width, is probably much smaller in sand-bed rivers compared to gravel-bed rivers. Periodic features on sandy beds may be observed at very small scales relative to channel widths (e.g. ripples), whereas periodic features on gravelly beds are generally found at scales much greater than the channel width (e.g. riffles). This is explained by the fact that grains in sand-bed channels are very small relative to the channel size and

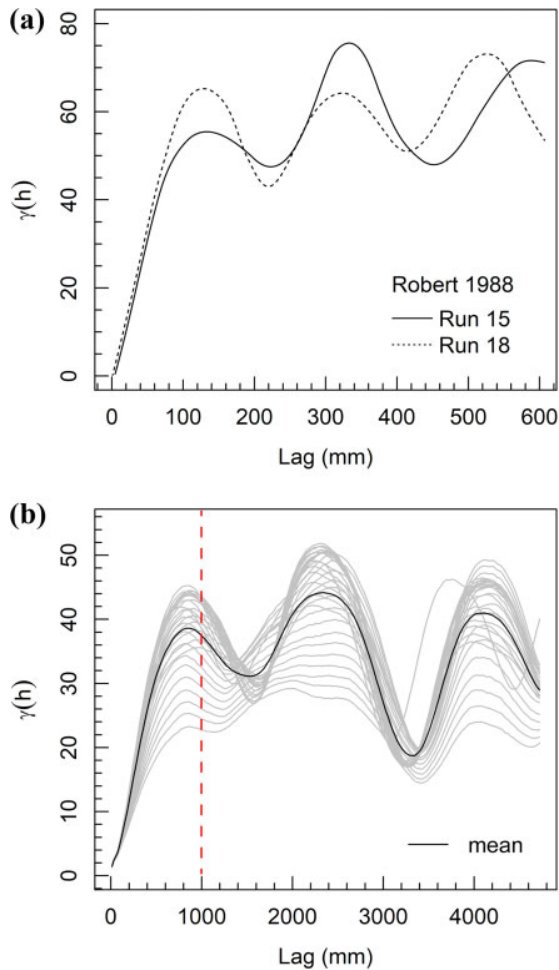


**Figure 4.** (a) Variograms based on sand-bed data (Source: Robert (1988, Figure 2), adapted with permission from Springer Nature), and (b) variograms based on gravel-bed stream table data published by MacKenzie and Eaton (2017), which contain well developed pool-riffle sequences. Each gray line represents one longitudinal profile parallel to the thalweg. Dashed line represents typical maximum lag of published gravel-bed variograms.

therefore are more easily mobilized and deposited into coherent structures.

The inflection point is important when considering how we can best define bed state because it indicates the threshold above which structural features are geometrically coherent or periodic (and therefore identifiable), and below which the bed is relatively scale-invariant and structural features are less identifiable (in which case the surface is best described with  $D$ ). In the

latter, various types of particle clustering described by researchers represent a subset of outcomes arising from a stochastic deposition of grains, but fail to characterize the surface en masse. The scale invariance of gravel beds up to the length scale of multiple channel widths partly explains why classificatory approaches to understanding bed structure have been less successful. It follows that it may be more fruitful to describe bed state with reference to bed surface geometry rather than grain characteristics or morphologic kinds.

## IV Roughness correlations

The ability to predict a priori the drag generated by a surface, based purely on its geometric characteristics, is of great interest to fluid research and practice. It is particularly important in gravel-bed rivers where the measurement of hydraulic variables is subject to practical limitations. It is through the incorporation of roughness correlations into statistical representations of bed structure that we can extend the general concept of “bed state” to the bed state *resistance* of channel morphodynamics (in other words, extending geometric roughness to hydraulic roughness). To this end, I first critique the grain-based roughness correlations currently used in fluvial geomorphology and explore their origin in the field of fluid dynamics, then turn to modern fluid dynamics, where we may find potential solutions.

### 4.1 In fluvial geomorphology

The foundational knowledge in fluid dynamics leading to the development of roughness correlations was gained at the precipice of global conflict. Between the First and Second World Wars, the minimization of wing frictional drag was a major challenge for airplane design. The process of “drag clean-up” necessitated the development of boundary layer equations for both laminar and turbulent flow to estimate aerodynamic efficiency (Eckert, 2007). This

problem was addressed by several German engineers, physicists, and fluid dynamicists, whose work has come to pervade the study of rivers. Of particular note are the experiments of Johann Nikuradse (1933), measuring the frictional drag produced by regular arrays of uniform roughness elements on the surface of pipes. Nikuradse (1933) used sand grains because, at the time, they were the easiest way to produce (almost) geometrically identical roughness elements.

Based on these experiments, Schlichting (1936) defined the equivalent sand roughness parameter  $k_s$ , which represents the size of the uniformly distributed sand grains that would obtain the same friction coefficient as the rough surface under consideration. In 1938, American government scientist Garbis Keulegan<sup>11</sup> extended the theoretical investigations of Ludwig Prandtl and Theodore von Kármán, and the experimental work of Nikuradse, from pipes to open channel flow.

As Gilbert's process geomorphology paradigm rose to prominence over the following decades (Ritter, 1988), the leading schools were critical of grain-based roughness correlations in natural channels. Although some early work suggested the use of grain size,<sup>12</sup> most came to realize that the work of Nikuradse could not be directly extended to rivers due to the presence of additional roughness components (structural features and vegetation, for example), and to gravel-bed rivers in particular due to the wide range of grain sizes (Leopold and Wolman, 1957; Leopold et al., 1964; Meland and Norrman, 1969; Sundborg, 1956).

In their seminal work, *Fluvial Processes in Geomorphology*, Leopold et al. asserted that:

... flow resistance unfortunately cannot be quantitatively specified from the type of channel boundary and the size and forms of materials making up the channel boundaries. The relation of the computed resistance to the size and configuration of bed debris is so complex that at present no simple transition between the two can be made. (1964: 255)

Geomorphologists of the Uppsala School of Physical Geography made similar remarks. In 1956 Åke Sundborg, a student of Henning Hjulström, proposed that "if there are obstacles of some kind on the bottom—bars, ripples, scattered stones, or vegetation, the grain diameter does not constitute a representative value for the roughness" (Sundborg, 1956: 147). Meland and Norrman (1969) suggested that accurately defining the boundary layer over loose heterogeneous beds using grain size would be theoretically impossible.

When interest in gravel-bed rivers increased in the 1970s, some form of roughness correlation had to be adopted because most channels were ungauged and direct measurement of their flow was often impractical (Miller, 1958). Just as Lane suggested in the 1957s, early investigations surmised that the surface  $D_{50}$  could be used (presumably, an appeal to the notion of averages as opposed to any theoretical basis), but found that this metric underestimated the total resistance (Leopold et al., 1964). A simple comparison between Nikuradse's experiments and gravel-bed surfaces is all that is required to explain this result (Bathurst, 1982). In addition to the presence of the many additional roughness components discussed above, Nikuradse's experiments were concerned with frictional drag, whereas in rivers form drag is generally more significant. Indeed, the physical irrelevance of Nikuradse's experiments to natural or "realistic" roughness appears obvious to other fields of fluid research, where  $k_s$  is interpreted as an effective flow property rather than any physical measure of roughness (Flack, 2018).

Thus, in practice, an estimation of  $k_s$  in gravel-bed rivers first requires an estimation of how much the bed surface differs from that of "sandpaper" made up of the  $D_{50}$ , as imagined by Einstein and Banks (1950). The initial solution was to multiply the grain size by an empirical constant  $C$  (Bray, 1982; Gladki, 1979; Hey, 1979; Leopold et al., 1964; Limerinos, 1970). However, the true value of  $C$  varies by at least

an order-of-magnitude across the population of gravel-bed rivers (van Rijn, 1982), and yet this approach persists given there is still no rational method to estimate it. After almost half a century, geomorphologists and engineers have not significantly advanced on the foundational theories of Nikuradse and Keulegan. As Lane (2005) has suggested, *isn't it time for a re-evaluation?* Intuitively, if there is an answer, we should look to those who study the movement of fluids.

#### 4.2 In fluid dynamics

For fluid dynamics, the work of Nikuradse represented only the beginning of roughness correlation theory. It was Hermann Schlichting who conducted the benchmark study on roughness correlations – Nikuradse merely provided a standard of reference. Schlichting (1936) performed a series of experiments on rough plates with different arrangements of roughness elements and found that drag is dependent on the spacing or “density” of features, which can be quantified using a solidity parameter  $\Lambda$ . The experiments of Nikuradse and Schlichting give rise to fundamentally different types of roughness correlation: one a function of a single roughness height, the other a function of both the height and arrangement of roughness elements, respectively.<sup>13</sup> Schlichting laid the foundation for many future studies of drag associated with the organization of discrete roughness elements of various geometries (e.g. length, height, width, spacing, steepness, or slope).

Most importantly, it is now well known that the effect of roughness element spacing on drag is systematic (Leonardi et al., 2007; Morris, 1955). At sparse spacing, roughness elements are hydraulically isolated and their effect on near-surface flow properties is small (isolated roughness flow). At close spacing, roughness elements are tightly packed such that wakes cannot form and the wall is almost smooth (skimming flow). Thus, drag is maximized at intermediate spacing where wakes associated

with roughness elements interact with those located downstream, creating complex turbulent flow (wake-interference flow). Parallel to investigations of roughness element spacing, researchers have pursued an approach stemming from the work of Musker (1980), whereby drag can be related to the statistics of the elevation field (Anderson and Meneveau, 2011; Barros et al., 2018; De Marchis et al., 2015; Yuan and Piomelli, 2014). The two approaches were defined by Grinvald and Nikora (1988) as discrete element and random field approaches, respectively.

Until recently, roughness correlations had almost solely been developed for simplified, regular arrays of roughness elements,<sup>14</sup> which culminated in two major reviews (Flack and Schultz, 2010, 2014). Fluvial geomorphologists have been aware of these approaches for some time (Gomez, 1993; Herbich and Shulits, 1964; Nowell and Church, 1979; Sundborg, 1956); however, as Ferguson and Ashworth (1992) recognized, they are difficult to use in practice due to the irregularity and multiscalarity of gravel beds. In the last decade, tremendous progress has been made in roughness correlations for irregular surface topographies in the fully rough regime (Flack, 2018). Thus, recent developments in fluid dynamics have extended roughness correlations to hydrodynamic conditions and surface geometries similar to those of gravel beds, which may provide geomorphologists with a suite of new tools for understanding channel processes (Stewart et al., 2018).

However, as Schlichting observed in his pioneering work, the intensive and systematic exploration of roughness correlations has been frustrated by the fact that “the number of parameters describing roughness is extraordinarily large owing to the great diversity of geometric forms” (Schlichting, 1979: 615). Among the main findings of recent systematic explorations are that the predictive power of specific roughness correlations is dependent on the geometry of the surface itself, and that different

descriptions of roughness are best used in combination to account for a variety of energy dissipation mechanisms associated with different surface properties. With this in mind, a “universal” roughness correlation may be formulated for a wide range of surfaces by incorporating multiple roughness parameters, as well as conditional statements regarding certain surface characteristics. For example, using direct numerical simulation of flow in channels with systematically generated surface geometries, Forooghi et al. (2017) derived the roughness correlation for the fully rough regime

$$\frac{k_s}{k_z} = f(Sk, \Delta) \cdot f(ES) \quad (3)$$

$$f(Sk, \Delta) = \begin{cases} f(Sk), & \Delta \geq 0.35 \\ f(Sk)(1 + m(Sk) \cdot (\Delta - 0.35)), & \Delta \leq 0.35 \end{cases} \quad (4)$$

$$f(Sk) = 0.67Sk^2 + 0.93Sk + 1.3 \quad (5)$$

$$f(ES) = 1.05 \cdot (1 - e^{-3.8 \cdot ES}) \quad (6)$$

where  $k_z$  is the mean maximum peak-to-valley height (calculated over multiple subsets of the surface, for example),  $Sk$  is the skewness of the probability distribution of elevations,  $\Delta$  is a measure of the diversity of roughness peak heights, and  $m(Sk) = 1.47Sk^2 - 1.35Sk - 0.66$ . The parameter  $ES$  is the effective slope (Napoli et al., 2008), which may be interpreted as the mean gradient of the local roughness elements, and is given by

$$ES = \frac{1}{L} \int_L \left| \frac{dk(x)}{dx} \right| dx \quad (7)$$

where  $k(x)$  is the height array,  $x$  is the stream-wise direction, and  $L$  is the surface length in  $x$ .

Effective slope accounts for the arrangement of roughness elements, whereby the gradient of roughness elements is inversely related to their spacing. As a result,  $ES$  controls the relative contribution of frictional and form drag (Napoli et al., 2008). Using a relation such as Equation

3, the total drag associated with the flow (within the fully rough regime) can be estimated based on its physical properties alone. The energy loss may be expressed as  $k_s$ , or another hydraulic scale such as the Hama roughness function (Flack and Schultz, 2010; Hama, 1954). Moreover, unlike  $\Lambda$ , which requires identification of individual roughness elements, it is possible to calculate  $ES$  for complex surfaces akin to river beds (Stewart et al., 2018). In the following section, I discuss how roughness correlations can best contribute to a new index of bed state resistance in rivers.

## V Toward bed state morphodynamics

In the above discussion I have conceptualized bed state as an important mode of channel adjustment contributing to morphologic stability, whereby stability coincides with maximization of flow resistance across the entire fluvial system. To this end, I suggested how we can best conceptualize gravel beds to estimate flow resistance based on geometry alone. In this section, I draw together these insights to form a prototypical index of bed state resistance that embraces technological and conceptual innovations increasingly available to and utilized by geomorphologists.

If we are to acknowledge the degrees of freedom comprising bed state resistance, which manifest in the wide range of spatial scales over which gravel-bed surfaces vary, the modes of topographic variation and their effects on flow resistance must be isolated. There have been numerous attempts to isolate the influence of different resistance components (*sensu* Eaton et al., 2004) using linear and non-linear detrending (e.g. Prestegard, 1983; Weichert et al., 2009). Transforms are an alternative approach to the detrending process, as they are commonly used to solve problems where the intricate underlying structure of a signal is of interest. Various transforms have been employed in

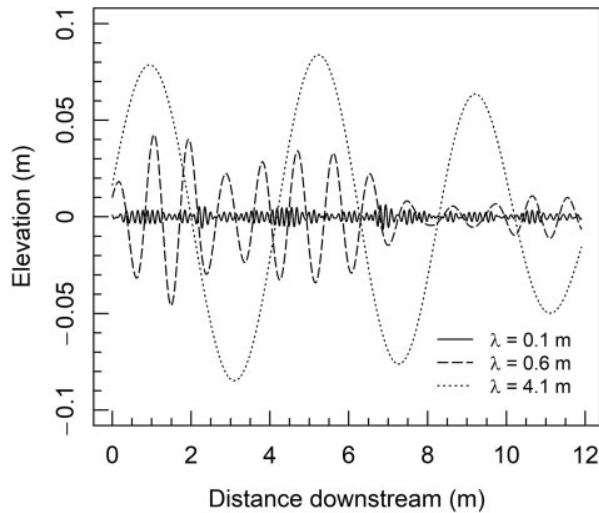


**Figure 5.** Three arbitrarily selected wavelengths that visualize long, medium, and short modes of topographic variation, which have been derived from a continuous wavelet transform of the stream table data used in Figure 4b.

more general treatments of gravel-bed surfaces, and have successfully elucidated some important structural characteristics (Keylock et al., 2014; Nyander, 2004; Qin and Ng, 2011; Singh et al., 2011; Smith, 2014). The most successful transform used in this context has been the wavelet transform, given its use of a finite analyzing function (the “wavelet”). Wavelet transform has a considerable advantage over the well-known Fourier Transform, in which the continuous analyzing function removes localized information in the case of highly irregular and aperiodic signals.

By breaking down a complex surface into a set of more simple components each at a different wavelength  $\lambda$  (Figure 5), a roughness correlation can be applied to each wavelength as if it were in isolation. This provides an estimate of the contribution of each scale of topographic variation to the total drag, rather than just a few arbitrarily selected ones (as necessitated by conventional detrending techniques). The combination of both the discrete element and random field approaches (i.e. shape and height) in Equation 3 is important, as it may differentiate the

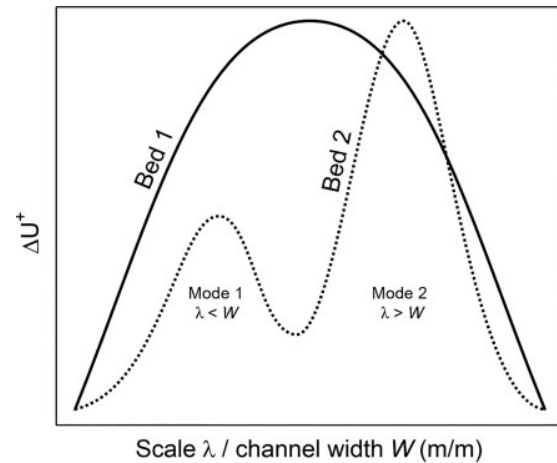


**Figure 6.** Conceptual diagram showing the distribution of drag contributions on a gravel bed. Bed one has a unimodal distribution of drag contributions, whereas bed two consists of a minor mode occurring at a small scale and a major mode occurring at a large scale.

flow resistance associated with vastly different roughness elements, ranging from individual grains (i.e. steep but small) to bars (i.e. gradual but tall). The drag contribution may be indexed by the Hama roughness function  $\Delta U^+$ , representing the downward shift in the logarithmic and outer layers of the mean streamwise velocity (Hama, 1954). Scale (i.e. wavelength) can be normalized by either bankfull depth or width following the typical treatment of bed structures such as steps and pools (Hassan et al., 2007).

We can postulate that, for any given bed, very small and very large scales would represent minima of drag contribution, and a maxima would occur at some intermediate scale (Figure 6). In many cases, the drag size distribution (DSD) would be complex. For example, large-scale bed features may comprise 10%–75% of the total drag in gravel-bed rivers (Dietrich et al., 1984; Hey, 1988; Parker and Peterson, 1980; Prestegard, 1983). Thus, we could expect skewed or even bimodal distributions, whereby the most significant mode is associated with scales greater than the channel width.

The DSD can also be presented as a cumulative distribution in the same way that grain size

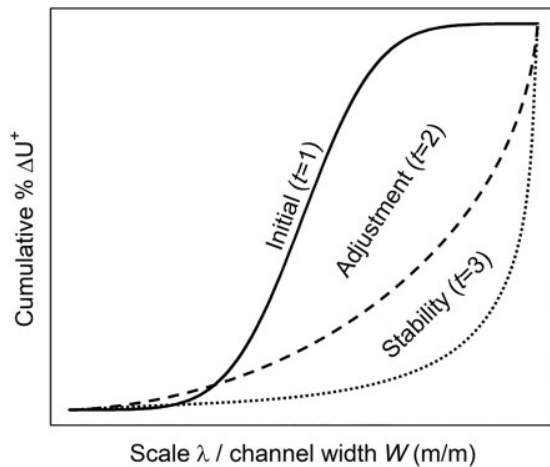


**Figure 7.** Conceptual diagram showing the cumulative distribution of drag contributions in the case where a gravel bed has adjusted to a “higher” bed state.

data is typically displayed. This presentation highlights the relative contribution of each spatial scale when different datasets are being compared. The cumulative distribution can effectively visualize trajectories of bed state adjustment over time (Figure 7), and provide a direct comparison with the evolution of surface grain size distributions. For example, Nyander (2004) developed a “form size distribution,” defined as the cumulative variance of each wavelength, and applied them to flume experiments conducted over approximately 80 hours. As the bed was subjected to increasing discharge, the relative height of large-scale bed features increased, and the adjustment to the “higher” bed state was recorded in the cumulative distribution by a shift in the inflection point toward larger scales. Nyander (2004) observed that morphologic change did not cease once a higher bed state was achieved, but rather continued within an envelope of stability. We can expect that this behavior will also be captured using the roughness correlation approach. The treatment of bed state proposed herein explicitly acknowledges the complexity of bed state adjustments, as well as the fuzzy nature of morphologic stability.

## 5.1 Assumptions and limitations

Some assumptions and limitations define a space within which the proposed index of bed state resistance is best applied, and help to clarify its interpretation. The major assumption inherent in the approach is one that is commonly used in investigations of flow resistance over surfaces with superimposed roughness elements. Components of flow resistance may be treated as linearly additive via some type of linear superposition model (Cowan, 1956; Einstein and Banks, 1950; Einstein and Barbarossa, 1952; Hey, 1988; Leopold et al., 1960; Meyer-Peter et al., 1948; Millar, 1999), but it is important to note that this is a heuristic approach (Furbish, 1987). Recent investigations have demonstrated that this assumption is, in a strict sense, invalid in gravel-bed rivers because the interaction between superimposed roughness elements may produce drag feedbacks in either direction (Li, 2009; Wilcox and Wohl, 2006). The technique developed herein may be used to discern prominent modes of bed state resistance and their relative magnitudes, but care should be taken in the interpretation of less distinctive peaks.

The major limitation of the approach is that it ignores the effect of relative roughness, or the ratio of roughness height to flow depth (Ferguson, 2007), the latter being inversely related to  $k_s$  (Knight, 1981). Most geometry-based roughness correlations have been developed in experiments with low relative roughness, whereas under most flow conditions in gravel-bed rivers the relative roughness is high. The concept of effective discharge presents a reasonable solution to these limitations, for two reasons. First, the bankfull flow is often assumed to be the “channel-forming” discharge (at which most geomorphic work is performed) and flows at and above this stage are most capable of reworking the bed surface (Ashworth and Ferguson, 1989; Wolman and Miller, 1960). Second, except in the case of the

roughest channel morphologies (notably, step-pool), the effect of relative roughness at bank-full flow is relatively low and  $k_s$  reaches a constant value with further increases in flow depth (Knight, 1981).

The Reynolds number is an important factor even within the fully rough regime; however, there have been few investigations of its specific effects on drag (e.g. Barros et al., 2018), because numerical simulations of flow over irregular boundaries at high  $Re$  are computationally intensive. Further work is required to understand the Reynolds number dependence of roughness correlations.

Another consideration is whether the roughness correlation should be applied to the entire surface (i.e. three-dimensionally) or streamwise profiles. It is now well known that the structure of gravel beds varies directionally (Butler et al., 2001), and that cross-stream structure exerts important hydraulic effects (Colombini and Parker, 1995; Forooghi et al., 2017; Kline et al., 1967). On the other hand, some studies have suggested that two-dimensional hydraulics are fairly representative of hydraulics associated with three-dimensional gravel beds and may be a reasonable simplification (e.g. Sambrook Smith and Nicholas, 2005).

## VI Conclusion

In this paper, I have deconstructed the grain size paradigm underlying the mainstream understanding of river channel morphodynamics by exploring its origins in geomorphology and related disciplines. In doing so, I have identified three ideological strands that have coalesced from a liberal, but largely unchecked, exchange of ideas between different fields of research: (1) the relations between grain diameter and fluid drag derived from Nikuradse's (1933) experiments with sand-coated surfaces; (2) the use of grain size by early process geomorphologists to describe general trends across large samples of sand-bed rivers; and (3) the classificatory

approach to discerning bed structures, originally developed for periodic bed structures found in sand-bed rivers, which is an inevitable consequence of an emphasis on grain size. The conflation of sand- and gravel-bed dynamics was largely achieved using empirical relations that now permeate the discipline. Over half a century, the grain size paradigm has shed light on many important processes associated with gravel-bed rivers. However, we must recognize that its pervasiveness limits our ability to understand channel behavior. Alternative or complementary models of understanding must be actively pursued.

The inertia of the grain size paradigm against longstanding critique highlights the influence of historical contingencies on the advancement of the discipline. At the genesis of modern process geomorphology, Sundborg (1956) and Leopold et al. (1964) emphasized the limitations of Nikuradse's relations. Keulegan (1938) recognized that the arrangement of roughness elements in a river could be more important than their heights alone. Furbish (1987) proposed that gravel beds and their hydraulic effects could be best understood using statistics rather than consideration of grains and forms as separate entities. Although some earlier authors had hinted along similar lines, Klingeman directly questioned the validity of a representative grain size in gravel-bed rivers and its association with channel morphology (Leopold, 1992, see discussion). Nowell and Church (1979) and Davies and Sutherland (1980) proposed that to formulate maximum flow resistance as a stability-inducing criterion, bed state is best defined with reference to the arrangement of features on the bed surface, akin to Schlichting's (1936) experimental relations. The sum of these notions amounts to a radical reconceptualization of bed state outside of the grain size paradigm – a stalwart of process geomorphology since its inception – that is yet to be achieved in practice.

Embracing recent advancements in complementary fields of fluid research, remote sensing,

and statistics, I have reformulated the aspirational ideas of Nowell and Church (1979) and Davies and Sutherland (1980) as a testable, physically based index of bed state. This approach not only acknowledges bed state as an important degree of freedom within the fluvial system but also recognizes the varied contribution of specific adjustments on the bed occurring at different scales and different spatial locations. The statistical representations may also be more conducive to visualizing and examining stochastic behavior. Only by explicitly acknowledging the complexity of channel adjustment can we move toward a more complete understanding of channel stability, let alone predictions of morphodynamic response.

### 6.1 Future work

In part, it is through systematic experimentation and observation, in which channel-forming processes are measured against theory-driven descriptions of channel morphology, that geomorphologists can better approach the task of building predictive morphodynamic models. Such models appear distant at this time. In the foreground lies a set of more basic questions that can be tackled forthwith.

First, how quickly does morphodynamic change occur? In the simple case of a change in discharge, the rate of morphologic adjustment to reach a new stable configuration is dependent on whether the change in energy state is upward (e.g. during a flood) or downward (e.g. following flow regulation). The former has been reported to be far more rapid (Church, 1995; Desloges and Church, 1992).

Second, how does the rate of morphologic change through time vary between the point of disturbance and the attainment of stability? We might expect that the rate of change would be rapid at first but decrease asymptotically toward zero (Graf, 1977), but there is currently a lack of concrete evidence to support this hypothesis. Third, how static is the state of morphologic

stability itself? Paintal (1971) showed that transport occurs even at sub-critical bed states (*sensu* Church, 2006), indicating that some degree of morphologic change must occur past a point usually considered to represent stable conditions. For example, using statistical representations, Nyander (2004) observed oscillations in physical bed structure around a mean value.

Fourth, how do bed state and channel planform co-evolve? Some studies have attempted to isolate the contribution of bed morphology and channel slope to a stable channel configuration (Aberle, 2000; Weichert et al., 2009), but this question remains largely unanswered due to the paucity of field data and the preponderance of flume studies in which planform is fixed. The contribution of these two primary degrees of freedom to stability is certainly not as linearly additive as the model presented by Eaton et al. (2004).

Fifth, what is the explanatory capability of the maximum flow resistance hypothesis with regard to channel stability? Recent stream table experiments involving the addition of larger-than-average grains highlight that relatively small changes in governing conditions may impose a stable state characterized by higher thresholds for grain mobility, rather than a transport-driven modification of channel boundaries (MacKenzie and Eaton, 2017). This prompts a question asked since the early geomorphologists (e.g. Rubey, 1933): how far can the concept of self-formed stability take us? Under what specific conditions is this not a useful paradigm?

Last, how much can we understand about morphodynamic behavior without consideration of grains? Stabilization by larger-than-average grains represents an extreme example where surface geometry and stability appear to be decoupled. On the other hand, it is now well understood that bedload transport models, many of which are predicated on experiments with featureless beds (e.g. Shields, 1936), also

require more careful consideration of surface structure due to its direct and indirect influences on particle mobility (Cudden and Hoey, 2003; Iseya and Ikeda, 1987; Kasprak et al., 2015; Kuhnle and Southard, 1988; Rickenmann, 2018). Thus, it is clear that morphodynamic models require simultaneous knowledge of grain and surface characteristics, and that only through the recognition of this duality can they fully represent fluvial systems. The questions outlined above have been pondered by geomorphologists for many decades but current answers are unsatisfactory or lacking entirely. Some answers are likely embedded within the types of data already available to geomorphologists. If this is the case, the conceptual framework and analytical techniques presented herein may be illuminating as we seek to model the behavior of gravel-bed rivers. We are currently conducting both fixed- and mobile-bank stream table experiments to test these ideas.

### Acknowledgements

The author would like to thank two anonymous reviewers for taking the time to review the manuscript, as well as Brett Eaton, Ian Rutherford, Marco Ghisalberti, Marwan Hassan, and Anya Leenman for reviewing the original draft. William Booker, Kevin Pierce, Lucy MacKenzie, Peter Adams, and Sheryl Lawson provided helpful comments. Lucy MacKenzie also provided the stream table data.

### Declaration of conflicting interests

The author(s) declared no potential conflicts of interest with respect to the research, authorship, and/or publication of this article.

### Funding

The author(s) disclosed receipt of the following financial support for the research, authorship, and/or publication of this article: This work was supported by a postgraduate scholarship provided by the Australian Government.

### ORCID iD

David Lawson Adams  <https://orcid.org/0000-0001-8578-8076>

### Notes

1. For example, Stelczer (1981) compiled a broad list of representative grain size percentiles used by various researchers in bed-load transport functions, ranging from  $D_{35}$  (e.g. Einstein, 1950) to  $D_{\max}$  (e.g. Gessler, 1965).
2. Nikora et al. (1998: 517) remarked that “gravel-bed roughness in natural streams can be characterized by a single size percentile, say  $D_{84}$ , only if we assume that the shape of the particle size distribution, bed arrangement, particle shape and orientation, packing, spacing and sorting, particle clusters, etc. are universal, that is, hold at all sites and flows.”
3. The fully rough regime is characterized by turbulent flows over surfaces with large roughness elements, or more precisely, when the boundary Reynolds number  $Re^* \geq 68$ , where  $Re^* = u_*k/\nu$  ( $u_*$  is the friction velocity,  $\nu$  is the kinematic viscosity, and  $k$  is the height of roughness elements making up the boundary).
4. Interestingly, these works are more formal expressions of ideas commonly held by early process geomorphologists. For example, Bagnold (1956) proposed that in the condition of bed instability brought upon by an excess in applied fluid stress, stability can only once again be attained if the grains are redeposited in a way which would increase resistance. Rubey (1952) suggested that the precise form of a graded slope with the imposed conditions of discharge, load, grain size, and degree of sorting is governed by something like the principle of least work.
5. Eaton and Church (2009) found that within-channel resistance may not be an independent, adjustable variable, most likely because bars are associated with both the bed and the channel planform. Thus,  $f''$  could be subsumed into either of the other components.
6. This period may be substantially longer. For example, Brooks (2003) found that the Red River of Manitoba has been adjusting stream gradient over the past 8000 years.
7. In practice, scour can be considered an aspect of bed state resistance due to the association between relative roughness and flow resistance (Ferguson, 2007).
8. A notable exception is Cullum et al. (2017), who suggested the use of fuzzy logic in landscape classification.
9. For example, Londoners developed specific theories about the pattern of impacts from World War II flying bombs, but Clarke (1946) showed that the impacts were a close fit to a random distribution.

10. Given that  $D$  tends to be different in downstream and cross-stream directions, gravel-bed surfaces are best described as self-affine (Butler et al., 2001).
11. At the time of Keulegan's retirement at the age of 98 he was the oldest and longest-serving (67 years) employee in federal service.
12. Upon introducing his method of sampling coarse bed material, Wolman (1954) remarked that these data could be used to estimate hydraulic roughness. Lane (1957: 41) suggested that "for streams in material coarser than sand, perhaps  $k$  [the representative roughness height] can be expressed as a function of the particle size." Rubey (1933) had questioned the underlying assumptions of this approach two decades prior.
13. Interestingly, Keulegan (1938) proposed that, in the case of "wavy" surfaces, resistance is some function of the ratio of roughness height to length (which he termed "relative waviness"). This relation was formalized by Schlichting (1936) just two years prior. It is worth noting that the distinction between rough and wavy surfaces is arbitrary. The wavy-wall equation was discarded by subsequent studies in favor of the rough-wall equation that is more conducive to the Wolman sampling approach. Thus, the importance of the arrangement of roughness elements in rivers has been recognized for almost a century but is yet to be fully embraced.
14. Typically cubes, cylinders, transverse square bars, pyramids, wedges, hemispheres, egg carton shapes, and sinusoids.

## References

- Aberle JE (2000) *Untersuchung der Rauheitsstruktur zur Bestimmung des Fließwiderstandes in Gebirgsbächen unter Klarwasserabfluß*. Doctoral thesis, University of Fridericiana at Karlsruhe.
- Aberle JE and Smart GM (2003) The influence of roughness structure on flow resistance on steep slopes. *Journal of Hydraulic Research* 41(3): 259–269.
- Aberle JE, Dittrich A and Nestmann F (1999) Description of steep stream roughness with the standard deviations. In *Proceedings of the 28th Congress of the IAHR*. Graz, Austria.
- Aberle JE, Nikora VI, Henning M, et al. (2010) Statistical characterization of bed roughness due to bed forms: A field study in the Elbe River at Aken, Germany. *Water Resources Research* 46(3): 1–11.
- Abernethy B and Rutherford ID (2000) The effect of riparian tree roots on the mass-stability of riverbanks. *Earth Surface Processes and Landforms* 25(9): 921–937.
- Abernethy B and Rutherford ID (2001) The distribution and strength of riparian tree roots in relation to riverbank reinforcement. *Hydrological Processes* 15(1): 63–79.
- Allen JRL (1984) Sedimentary structures, their character and physical basis. *Developments in Sedimentology* Amsterdam: Elsevier. p. 30.
- Anderson W and Meneveau C (2011) Dynamic roughness model for large-eddy simulation of turbulent flow over multiscale, fractal-like rough surfaces. *Journal of Fluid Mechanics* 679: 288–314.
- Andrews ED (1984) Bed-material entrainment and hydraulic geometry of gravel-bed rivers in Colorado. *Geological Society of America Annual Meeting* 95(3): 371–378.
- Ashworth PJ and Ferguson RI (1989) Size-selective entrainment of bed-load in gravel bed streams. *Water Resources Research* 25(4): 627–634.
- Bagnold RA (1956) The flow of cohesionless grains in fluids. *Philosophical Transactions of the Royal Society of London. Series A, Mathematical and Physical Sciences* 249(964): 235–297.
- Barros JM, Schultz MP and Flack KA (2018) Measurements of skin-friction of systematically generated surface roughness. *International Journal of Heat and Fluid Flow* 72: 1–7.
- Barry JJ, Buffington JM and King JG (2004) A general power equation for predicting bed load transport rates in gravel bed rivers. *Water Resources Research* 40(10): 1–22.
- Bathurst JC (1978) Flow resistance of large-scale roughness. *Journal of Hydraulic Engineering* 104(12): 1587–1603.
- Bathurst JC (1982) Flow resistance in boulder-bed streams. In: Hey RD, Bathurst JC and Thorne CR (eds) *Gravel-bed Rivers*. Chichester: John Wiley & Sons, 443–465.
- Bathurst JC (1985) Flow resistance estimation in mountain rivers. *Journal of Hydraulic Engineering* 111(4): 625–643.
- Bergeron NE (1996) Scale-space analysis of stream-bed roughness in coarse gravel-bed streams. *Mathematical Geology* 28(5): 537–561.
- Bertin S and Friedrich H (2018) Effect of surface texture and structure on the development of stable fluvial armors. *Geomorphology* 306: 64–79.

- Bray DI (1979) Estimating average velocity in gravel-bed rivers. *Journal of the Hydraulics Division* 105(9): 1103–1122.
- Bray DI (1982) Flow resistance in gravel bed rivers. In: Hey RD, Bathurst JC and Thorne CR (eds) *Gravel-bed Rivers*. Chichester: John Wiley & Sons, 109–133.
- Brayshaw AC (1985) Bed microtopography and entrainment thresholds in gravel-bed rivers. *Geological Society of America Bulletin* 96(65): 218–223.
- Brooks GR (2003) Alluvial deposits of a mud-dominated stream: The Red River, Manitoba, Canada. *Sedimentology* 50(3): 441–458.
- Buffington JM and Montgomery DR (1997) A systematic analysis of eight decades of incipient motion studies, with special reference to gravel-bedded rivers. *Water Resources Research* 33(8): 1993–2029.
- Butler JB, Lane SN and Chandler JH (2001) Characterization of the structure of river-bed gravels using two-dimensional fractal analysis. *Mathematical Geology* 33(3): 301–330.
- Cadol D and Wohl EE (2013) Variable contribution of wood to the hydraulic resistance of headwater tropical streams. *Water Resources Research* 49(8): 4711–4723.
- Cartigny MJB, Ventra D, Postma G, et al. (2014) Morphodynamics and sedimentary structures of bedforms under supercritical-flow conditions: New insights from flume experiments. *Sedimentology* 61(3): 712–748.
- Chang HH (1979) Minimum stream power and river channel patterns. *Journal of Hydrology* 41(3–4): 303–327.
- Church MA (1995) Geomorphic response to river flow regulation – Case-studies and time-scales. *Regulated Rivers-Research & Management* 11(1): 3–22.
- Church MA (2006) Bed material transport and the morphology of alluvial river channels. *Annual Review of Earth and Planetary Sciences* 34(1): 325–354.
- Church MA (2011) The Shields number is a granular bed state parameter. In: *American Geophysical Union Abstracts, Fall Meeting*, San Francisco.
- Church MA and Kellerhals R (1978) On the statistics of grain size variation along a gravel river. *Canadian Journal of Earth Sciences* 15(7): 1151–1160.
- Cin RD (1968) “Pebble clusters”: Their origin and utilization in the study of palaeocurrents. *Sedimentary Geology* 2(4): 233–241.
- Clarke RD (1946) An application of the Poisson distributions. *Journal of the Institute of Actuaries* 72(3): 481.
- Clifford NJ, Robert A and Richards KS (1992) Estimation of flow resistance in gravel-bedded rivers: A physical explanation of the multiplier of roughness length. *Earth Surface Processes and Landforms* 17(2): 111–126.
- Collier J (1996) On the necessity of natural kinds. In: Riggs P (ed.) *Natural Kinds, Laws of Nature and Scientific Reasoning*. Dordrecht: Kluwer, 1–8.
- Colombini M and Parker G (1995) Longitudinal streaks. *Journal of Fluid Mechanics* 304: 161–183.
- Cowan WL (1956) Estimating hydraulic roughness coefficients. *Agricultural Engineering* 7(7): 473–475.
- Cudden JR and Hoey TB (2003) The causes of bedload pulses in a gravel channel: The implications of bedload grain-size distributions. *Earth Surface Processes and Landforms* 28(13): 1411–1428.
- Cullum C, Brierley G, Perry GLW, et al. (2017) Landscape archetypes for ecological classification and mapping: The virtue of vagueness. *Progress in Physical Geography* 41(1): 95–123.
- Curran JC and Tan L (2014) Effect of bed sand content on the turbulent flows associated with clusters on an armored gravel bed surface. *Journal of Hydraulic Engineering* 140(2): 137–148.
- Darwin C (1859) *On the Origin of Species by Means of Natural Selection*. London: John Murray, Albemarle St.
- Davies TRH and Sutherland AJ (1980) Resistance to flow past deformable boundaries. *Earth Surface Processes* 5(2): 175–179.
- Davies TRH and Sutherland AJ (1983) Extremal hypotheses for river behavior. *Water Resources Research* 19(1): 141–148.
- De Marchis M, Milici B and Napoli E (2015) Numerical observations of turbulence structure modification in channel flow over 2D and 3D rough walls. *International Journal of Heat and Fluid Flow* 56: 108–123.
- Desloges JR and Church MA (1992) Geomorphic implications of glacier outburst flooding: Noieck River Valley, British Columbia. *Canadian Journal of Earth Sciences* 29(3): 551–564.
- Dietrich WE, Smith JD and Dunne T (1984) Boundary shear stress, sediment transport and bed morphology in a sand-bedded river meander during high and low flow. In: *River Meandering, Proceedings of the Conference Rivers '83*. New York: American Society of Civil Engineers, 632–639.
- Diplas P and Vigilar GG (1992) Hydraulic geometry of threshold channels. *Journal of Hydraulic Engineering* 118(4): 597–614.

- Eaton BC and Church MA (2004) A graded stream response relation for bed load-dominated streams. *Journal of Geophysical Research* 109(F3): 1–18.
- Eaton BC and Church MA (2009) Channel stability in bed load-dominated streams with nonerodible banks: Inferences from experiments in a sinuous flume. *Journal of Geophysical Research: Earth Surface* 114(1): 1–17.
- Eaton BC and Giles TR (2009) Assessing the effect of vegetation-related bank strength on channel morphology and stability in gravel-bed streams using numerical models. *Earth Surface Processes and Landforms* 34(5): 712–724.
- Eaton BC, Church MA and Millar RG (2004) Rational regime model of alluvial channel morphology and response. *Earth Surface Processes and Landforms* 29(4): 511–529.
- Eaton BC, Moore RD and Giles TR (2010) Forest fire, bank strength and channel instability: The ‘unusual’ response of Fishtrap Creek, British Columbia. *Earth Surface Processes and Landforms* 35(10): 1167–1183.
- Eckert M (2007) *Dawn of Fluid Dynamics: A Discipline between Science and Technology*. John Wiley & Sons.
- Einstein HA (1950) The Bed-Load function for sediment transportation in open channel flows. *Department of Agriculture Technical Bulletin* 1026.
- Einstein HA and Banks RB (1950) Fluid resistance of composite roughness. *Transactions of the American Geophysical Union* 31(4): 603–610.
- Einstein HA and Barbarossa NL (1952) River channel roughness. *Transactions of the American Society of Civil Engineers* 117: 1121–1132.
- Engelund F and Fredsoe J (1982) Sediment ripples and dunes. *Annual Review of Fluid Mechanics* 14(1): 13–37.
- Entwistle NS, Heritage GL and Johnson K (2008) Cluster detection and development using terrestrial laser scanning. *Geophysical Research Abstracts* 10. European Geosciences Union.
- Fenton JD and Abbott JE (1977) Initial movement of grains on a stream bed: The effect of relative protrusion. *Proceedings of the Royal Society of London. A. Mathematical and Physical Sciences* 352(1671): 523–553.
- Ferguson RI (1986) Hydraulics and hydraulic geometry. *Progress in Physical Geography* 10(1): 1–31.
- Ferguson RI (2007) Flow resistance equations for gravel- and boulder-bed streams. *Water Resources Research* 43(5): 1–12.
- Ferguson RI and Ashworth PJ (1992) Spatial patterns of bedload transport and channel change in braided and near-braided rivers. In: Billi P, Hey RD, Thorne CR, et al. (eds) *Dynamics of Gravel-bed Rivers*. Chichester, New York: John Wiley & Sons, Ltd, 477–496.
- Flack KA (2018) Moving beyond Moody. *Journal of Fluid Mechanics* 842: 1–4.
- Flack KA and Schultz MP (2010) Review of hydraulic roughness scales in the fully rough regime. *Journal of Fluids Engineering* 132(4): 1–10.
- Flack KA and Schultz MP (2014) Roughness effects on wall-bounded turbulent flows. *Physics of Fluids* 26(10).
- Folk RL (1966) A review of grain-size parameters. *Sedimentology* 6(2): 73–93.
- Folk RL and Ward WC (1957) Brazos River bar: A study in the significance of grain size parameters. *Journal of Sedimentary Research* 27(1): 3–26.
- Forooghi P, Stroh A, Magagnato F, et al. (2017) Towards a universal roughness correlation. *Journal of Fluids Engineering* 139(12): 1–12.
- Forooghi P, Stroh A, Schlatter P, et al. (2018) Direct numerical simulation of flow over dissimilar, randomly distributed roughness elements: A systematic study on the effect of surface morphology on turbulence. *Physical Review Fluids* 3(4): 1–27.
- Furbish DJ (1987) Conditions for geometric similarity of coarse stream-bed roughness. *Mathematical Geology* 19(4): 291–307.
- Gessler J (1965) *Der Geschiebetriebbeginn bei Mischungen untersucht an natürlichen*. PhD thesis, ETH Zurich.
- Gilovich T (1991) *How We Know What Isn't So: The Fallibility of Human Reason in Everyday Life*. New York: The Free Press.
- Gladki H (1979) Resistance to flow in alluvial channels with coarse bed materials. *Journal of Hydraulic Research* 17(2): 121–128.
- Gomez B (1993) Roughness of stable, armored gravel beds. *Water Resources Research* 29(11): 3631–3642.
- Gomez B and Church MA (1989) An assessment of bed load sediment transport formulae for gravel bed rivers. *Water Resources Research* 25(6): 1161–1186.
- Goodwin CN (1999a) Fluvial classification: neanderthal necessity or needless normalcy. In: Olsen DS and Potyondy JP (eds), *Wildland Hydrology, TPS-99-3*. American Water Resources Association, Herndon, VA, pp. 229–236.
- Goodwin CN (1999b) Improving future fluvial classification systems. *Stream Notes*.

- Graf WL (1977) The rate law in fluvial geomorphology. *American Journal of Science* 277(2): 178–191.
- Grant GE, Swanson FJ and Wolman MG (1990) Pattern and origin of stepped-bed morphology in high-gradient streams, Western Cascades, Oregon. *Geological Society of America Bulletin* 102(3): 340–352.
- Grinvald DI and Nikora VI (1988) *River Turbulence*. Leningrad: Hydrometeoizdat.
- Hama FR (1954) Boundary layer characteristics for smooth and rough surfaces. *Transactions of the Society of Naval Architects and Marine Engineers* 62: 333–358.
- Haslam N (2002) Practical, functional, and natural kinds. *Philosophy, Psychiatry, & Psychology* 9(3): 237–241.
- Hassan MA, Smith BJ, Hogan DL, et al. (2007) Sediment storage and transport in coarse bed streams: Scale considerations. *Developments in Earth Surface Processes* 11: 473–496.
- Helm C (2019) *A rapid and objective characterization of channel morphology in a small, forested channel using a remotely piloted aircraft*. Master's thesis, The University of British Columbia, Canada.
- Henderson FM (1964) Stability of alluvial channels. *Journal of the Hydraulics Division* 87(6): 109–138.
- Hendrick RR, Ely LL and Papanicolaou AN (2010) The role of hydrologic processes and geomorphology on the morphology and evolution of sediment clusters in gravel-bed rivers. *Geomorphology* 114(3): 483–496.
- Herbich JB and Shulits S (1964) Large-scale roughness in open-channel flow. *Journal of the Hydraulics Division* 90(6): 203–230.
- Hey RD (1979) Flow resistance in gravel-bed rivers. *Journal of the Hydraulics Division* 105(4): 365–379.
- Hey RD (1988) Bar form resistance in gravel-bed rivers. *Journal of Hydraulic Engineering* 114(12): 1498–1508.
- Hey RD and Thorne CR (1986) Stable channels with mobile gravel beds. *Journal of Hydraulic Engineering* 112(8): 671–689.
- Huang HEQ and Nanson GC (2000) Hydraulic geometry and maximum flow efficiency as products of the principle of least action. *Earth Surface Processes and Landforms* 16(1): 1–16.
- Ibbeken H and Schleyer R (2013) *Source and Sediment: A Case Study of Provenance and Mass Balance at an Active Plate Margin (Calabria, Southern Italy)*. Berlin: Springer.
- Iseya F and Ikeda H (1987) Pulsations in bedload transport rates induced by a longitudinal sediment sorting: A flume study using sand and gravel mixtures. *Geografiska Annaler. Series A. Physical Geography* 69(1): 15–27.
- Iverson GL, Brooks BL and Holdnack JA (2008) Misdiagnosis of cognitive impairment in forensic neuropsychology. In Heilbrunner RL (ed.) *Neuropsychology in the Courtroom: Expert Analysis of Reports and Testimony*. New York: Guildford Press, 243–266.
- James W (1907) *Pragmatism*. Cambridge, MA: Harvard University Press.
- Jimenez J (2004) Turbulent flows over rough walls. *Annual Review of Fluid Mechanics* 36: 173–196.
- Johnson JPL (2016) Gravel threshold of motion: A state function of sediment transport disequilibrium? *Earth Surface Dynamics* 4(3): 685–703.
- Johnson JPL, Whipple KX, Sklar LS, et al. (2009) Transport slopes, sediment cover, and bedrock channel incision in the Henry Mountains, Utah. *Journal of Geophysical Research* 114(F2): 1–21.
- Juracek KE and Fitzpatrick FA (2003) Limitations and implications of stream classification. *Journal of the American Water Resources Association* 3581(3): 659–670.
- Kasprak A, Wheaton JM, Ashmore PE, et al. (2015) The relationship between particle travel distance and channel morphology: Results from physical models of braided rivers. *Journal of Geophysical Research: Earth Surface* 120(1): 55–74.
- Kellerhals R and Church MA (1989) The morphology of large rivers: Characterization and management. In: Dodge DP (ed.) *Proceedings of the International Large River Symposium*, Vol. 106. Canadian Special Publication Fisheries and Aquatic Sciences, pp. 31–48.
- Keulegan GH (1938) Laws of turbulent flow in open channels. *Journal of Research of the National Bureau of Standards* 21: 707–741.
- Keylock CJ, Singh A and Fofoula-Georgiou E (2014) The complexity of gravel bed river topography examined with gradual wavelet reconstruction. *Journal of Geophysical Research: Earth Surface* 119(3): 682–700.
- Kirchner JW, Dietrich WE, Iseya F, et al. (1990) The variability of critical shear stress, friction angle, and grain protrusion in water-worked sediments. *Sedimentology* 37(4): 647–672.
- Kirkby MJ (1977) Maximum sediment efficiency as a criterion for alluvial channels. In: Gregory KJ (ed.) *River Channel Changes*. New York: John Wiley & Sons, 429–442.

- Kline BSJ, Reynolds WC, Schraub FA, et al. (1967) The structure of turbulent boundary layers. *Journal of Fluid Mechanics* 30(4): 741–773.
- Knight DW (1981) Some field measurements concerned with the behaviour of resistance coefficients in a tidal channel. *Estuarine, Coastal and Shelf Science* 12(3): 303–322.
- Komar PD (1987) Selective gravel entrainment and the empirical evaluation of flow competence. *Sedimentology* 34(6): 1165–1176.
- Kripke SA (1972) Naming and necessity. In: Harman G and Davidson D (eds) *Semantics of Natural Language*. Dordrecht: Springer, 253–355.
- Krumbein WC (1938) Size frequency distributions of sediments and the normal phi curve. *Journal of Sedimentary Research* 8(3): 84–90.
- Kuhnle RA and Southard JB (1988) Bed load transport fluctuations in a gravel bed laboratory channel. *Water Resources Research* 24(2): 247–260.
- Kumar P and Foufoula-Georgiou E (1997) Wavelet analysis for geophysical applications. *Reviews of Geophysics* 34(4): 385–412.
- L'Amoreaux P and Gibson S (2013) Quantifying the scale of gravel-bed clusters with spatial statistics. *Geomorphology* 197: 56–63.
- Lane EW (1957) A study of the shape of channels formed by natural streams flowing in erodible material. *Technical report, MRD Sediment Series No. 9*, United States Army Corps, Engineering Division.
- Lane SN (2005) Roughness – Time for a re-evaluation? *Earth Surface Processes and Landforms* 30(2): 251–253.
- Langbein WB (1963) A theory for river channel adjustment. *Transactions of the American Society of Civil Engineers*.
- Leonardi S, Orlandi P and Antonia RA (2007) Properties of d- and k-type roughness in a turbulent channel flow. *Physics of Fluids* 19(12): 1–6.
- Leopold LB (1992) Sediment size that determines channel morphology. In: Billi P, Hey RD, Thorne CR, et al. (eds) *Dynamics of Gravel-bed Rivers*. Chichester, New York: John Wiley & Sons, Ltd., pp. 297–311.
- Leopold LB and Langbein WB (1963) Association and indeterminacy in geomorphology. In: Elbritton CC (ed.) *The Fabric of Geology*. San Francisco, CA: Freeman & Cooper, 184–192.
- Leopold LB and Wolman MG (1957) River channel patterns: Braided, meandering, and straight. *Geological Survey Professional Paper 282-B*.
- Leopold LB, Bagnold RA, Wolman MG, et al. (1960) Flow resistance in sinuous or irregular channels. *United States Geological Survey Professional Paper 292-D*, 111–134.
- Leopold LB, Wolman MG and Miller JP (1964) *Fluvial Processes in Geomorphology*. San Francisco, CA: Freeman.
- Li G (2009) Preliminary study of the interference of surface objects and rainfall in overland flow resistance. *Catena* 78(2): 154–158.
- Li R-M (1976) Morphology of cobble streams in small watersheds. *Journal of Hydraulic Engineering* 102(8): 1101–1117.
- Limerinos JT (1970) Determination of the Manning coefficient from measured bed roughness in natural channels. *United States Geological Survey Water-Supply Paper 1898-B*.
- Linnaeus C (1735) *Systema naturae*. Leyden.
- MacKenzie LG and Eaton BC (2017) Large grains matter: Contrasting bed stability and morphodynamics during two nearly identical experiments. *Earth Surface Processes and Landforms* 42(8): 1287–1295.
- MacKenzie LG, Eaton BC and Church MA (2018) Breaking from the average: Why large grains matter in gravel bed streams. *Earth Surface Processes and Landforms* 43(15): 3190–3196.
- Mackin JH (1948) Concept of the graded river. *Bulletin of the Geological Society of America* 69(5): 463–511.
- Malanson GP, Butler DR and Walsh SJ (1990) Chaos theory in physical geography. *Physical Geography* 11(4): 293–304.
- Malanson GP, Butler DR and Georgakakos KP (1992) Nonequilibrium geomorphic processes and deterministic chaos. *Geomorphology* 5(3-5): 311–322.
- Meland N and Norrman J (1969) Transport velocities of individual size fractions in heterogeneous bed load. *Geografiska Annaler. Series A. Physical Geography* 51(3): 127–144.
- Meyer-Peter E, Müller R and Müller R (1948) Formulas for bed-load transport. In: *Proceedings of the 3rd Meeting of the International Association for Hydraulic Structures Research*. Stockholm, Sweden: 1–26.
- Millar RG (1999) Grain and form resistance in gravel-bed rivers. *Journal of Hydraulic Research* 37(3): 303–312.
- Millar RG (2000) Influence of bank vegetation on alluvial channel patterns. *Water Resources Research* 36(4): 1109–1118.

- Millar RG (2005) Theoretical regime equations for mobile gravel-bed rivers with stable banks. *Geomorphology* 64(3–4): 207–220.
- Miller JP (1958) High mountain streams: Effects of geology on channel characteristics and bed material. *New Mexico State Bureau of Mines and Mine Resources Memoir* 4: 51.
- Montgomery DR and Buffington JM (1997) Channel-reach morphology in mountain basins. *Geological Society of America Bulletin* 109(5): 596–611.
- Montgomery DR and Buffington JM (1998) Channel processes, classification, and response. In: Naiman R and Bilby R (eds) *River Ecology and Management: Lessons from the Pacific Coastal Ecoregion*. New York: Springer, pp. 13–42.
- Morris HM (1955) A new concept of flow in rough conduits. *Transactions of the American Society of Civil Engineers* 80(1): 1–31.
- Morvan H, Knight D, Wright N, et al. (2008) The concept of roughness in fluvial hydraulics and its formulation in 1D, 2D and 3D numerical simulation models. *Journal of Hydraulic Research* 46(2): 191–208.
- Musker AJ (1980) Universal roughness functions for naturally-occurring surfaces. *Transactions of the Canadian Society for Mechanical Engineering* 6(1): 1–6.
- Naden P and Brayshaw AC (1987) Small and medium scale bedforms in gravel-bed rivers. In: Richards KS (ed.) *River Channels: Environment and Process*. Oxford: Basil Blackwell, 249–271.
- Napoli E, Armenio V and De Marchis M (2008) The effect of the slope of irregularly distributed roughness elements on turbulent wall-bounded flows. *Journal of Fluid Mechanics* 613: 385–394.
- Nikora VI and Walsh JM (2004) Water-worked gravel surfaces: High-order structure functions at the particle scale. *Water Resources Research* 40(12): 1–7.
- Nikora VI, Goring DG and Biggs BJB (1998) On gravel-bed roughness characterization. *Water Resources Research* 34(3): 517–527.
- Nikuradse J (1933) Laws of flow in rough pipes. National Advisory Committee for Aeronautics Technical Memorandum. Report no. 1292, p. 62.
- Nowell ARM and Church MA (1979) Turbulent flow in a depth-limited boundary layer. *Journal of Geophysical Research* 84(C8): 4816–4824.
- Nyander A (2004) *River-bed sediment surface characterisation using wavelet transform-based methods*. Doctoral thesis, Napier University.
- Ockelford AM and Haynes H (2013) The impact of stress history on bed structure. *Earth Surface Processes and Landforms* 38(7): 717–727.
- Paintal AS (1971) Concept of critical shear stress in loose boundary open channels. *Journal of Hydraulic Research* 9(1): 91–113.
- Papanicolaou ANT, Tsakiris AG and Strom KB (2012) The use of fractals to quantify the morphology of cluster microforms. *Geomorphology* 139–140: 91–108.
- Parker G (1978) Self-formed straight rivers with equilibrium banks and mobile bed. Part 2. The gravel river. *Journal of Fluid Mechanics* 89(01): 127–146.
- Parker G (1990) Surface-based bedload transport relation for gravel rivers. *Journal of Hydraulic Research* 28(4): 417–436.
- Parker G and Peterson AW (1980) Bar resistance of gravel-bed streams. *Journal of the Hydraulics Division* 106(10): 1559–1575.
- Parker G, Klingeman PC and McLean DG (1982) Bedload and size distribution in paved gravel-bed streams. *Journal of the Hydraulics Division* 108(4): 544–571.
- Phillips JD (1993) Spatial-domain chaos in landscapes. *Geographical Analysis* 25(2): 101–117.
- Phillips JD (2006) Deterministic chaos and historical geomorphology: A review and look forward. *Geomorphology* 76: 109–121.
- Plate E (1971) Limitations of spectral analysis in the study of wind-generated water surface waves. In: *Proceedings of the 1st International Symposium on Stochastic Hydraulics*. Pittsburgh, PA: Pittsburgh University Press, pp. 522–539.
- Powell DM, Ockelford A, Rice SP, et al. (2016) Structural properties of mobile armors formed at different flow strengths in gravel-bed rivers. *Journal of Geophysical Research: Earth Surface* 121(8): 1494–1515.
- Prestegard KL (1983) Bar resistance in gravel bed streams at bankfull stage. *Water Resources Research* 19(2): 472–476.
- Qin J and Ng SL (2011) Multifractal characterization of water-worked gravel surfaces. *Journal of Hydraulic Research* 49(3): 345–351.
- Raupach MR, Antonia RA and Rajagopalan S (1991) Rough-wall turbulent boundary layers. *Applied Mechanics Reviews* 44(1): 1–25.
- Recking A (2013) Simple method for calculating reach-averaged bed-load transport. *Journal of Hydraulic Engineering* 139(1): 70–75.

- Recking A, Liebault F, Peteuil C, et al. (2012) Testing bedload transport equations with consideration of time scales. *Earth Surface Processes and Landforms* 37(7): 774–789.
- Rickenmann D (2018) Variability of bed load transport during six summers of continuous measurements in two Austrian mountain streams (Fischbach and Ruetz). *Water Resources Research* 54(1): 107–131.
- Ritter DF (1988) Landscape analysis and the search for geomorphic unity. *Geological Society of America Bulletin* 100(2): 160–171.
- Robert A (1988) Statistical properties of sediment bed profiles in alluvial channels. *Mathematical Geology* 20(3): 205–225.
- Robert A (1991) Fractal properties of simulated bed profiles in coarse-grained channels. *Mathematical Geology* 23(3): 367–382.
- Rubey WW (1931) A need for closer cooperation among students of stream-work. *Transactions of the American Geophysical Union* 12(1): 216–219.
- Rubey WW (1933) Equilibrium-conditions in debris-laden streams. *Transactions of the American Geophysical Union* 14(1).
- Rubey WW (1938) The force required to move particles on a stream bed. Technical report, United States Geological Survey Professional Paper 189-E.
- Rubey WW (1952) Geology and mineral resources of the Hardin and Brussels quadrangles (in Illinois). *United States Geological Survey Professional Paper* 218, pp. 179.
- Sambrook Smith GH and Nicholas AP (2005) Effect on flow structure of sand deposition on a gravel bed: Results from a two-dimensional flume experiment. *Water Resources Research* 41(10): 1–12.
- Schlichting H (1936) Experimentelle untersuchungen zum Rauheitsproblem. *Archive of Applied Mechanics* 7(1): 1–34.
- Schlichting VH *Boundary-Layer Theory*. 7th edition. New York: McGraw-Hill.
- Schumm SA (1969) River metamorphosis. *Journal of the Hydraulics Division* 95(1): 255–273.
- Schumm SA (1971) Fluvial geomorphology: Channel adjustment and river metamorphosis. In: Shen HW (ed.) *River Mechanics*. Fort Collins, CO: Water Resources Publications.
- Shields A (1936) Application of similarity principles and turbulence research to bed-load movement. Translated into English by Ott WP and van Uchelen JC. *Mitteilungen der Preussischen Versuchsanstalt für Wasserbau und Schiffbau, Berlin*, 26(5–24): 47.
- Shulits S (1941) Rational equation for river-bed profile. *Transactions of the American Geophysical Union*. 22(3): 622–631.
- Shulits S and Corfitzen WE (1937) Bed-load transportation and the stable-channel problem. *Transactions of the American Geophysical Union* 18(2): 456–467.
- Singh A, Lanzoni S, Wilcock PR, et al. (2011) Multiscale statistical characterization of migrating bed forms in gravel and sand bed rivers. *Water Resources Research* 47(12).
- Smart GM, Duncan MJ and Walsh JM (2002) Relatively rough flow resistance equations. *Journal of Hydraulic Engineering* 128(6): 568–578.
- Smith MW (2014) Roughness in the Earth sciences. *Earth-Science Reviews* 136: 202–225.
- Southard JB (1971) Representation of bed configurations in depth-velocity-size diagrams. *Journal of Sedimentary Petrology* 41(4): 903–915.
- Southard JB (1991) Experimental determination of bed-form stability. *Annual Review of Earth and Planetary Sciences* 19(1): 423–455.
- Stelczer K (1981) *Bed-Load Transport: Theory and Practice*. Littleton, CO: Water Resources Publications.
- Stewart MT, Cameron SM, Nikora VI, et al. (2018) Hydraulic resistance in open-channel flows over self-affine rough beds. *Journal of Hydraulic Research* 57(2): 1–14.
- Strom KB and Papanicolaou AN (2008) Morphological characterization of cluster microforms. *Sedimentology* 55(1): 137–153.
- Sundborg A (1956) The River Klarälven: A study of fluvial processes. *Geografiska Annaler* 38(2): 125–237.
- Tamminga A and Eaton BC (2018) Linking geomorphic change due to floods to spatial hydraulic habitat dynamics. *Ecohydrology* 11(8): 1–17.
- Tsakiris AG and Papanicolaou T (2008) A fractal approach for characterizing microroughness in gravel streams. *Archives of Hydro-Engineering and Environmental Mechanics* 55(1–2): 29–43.
- van Rijn LC (1982) The prediction of bed forms and alluvial roughness. *Mechanics of Sediment Transport*. 133–135.
- Venditti JG (2013) Bedforms in sand-bedded rivers. In: Schroder JF and Wohl E (eds) *Treatise on Geomorphology, Fluvial Geomorphology, Vol. 9*. San Diego, CA: Academic Press, pp. 137–162.

- Venditti JG, Dietrich WE, Nelson PA, et al. (2010) Mobilization of coarse surface layers in gravel-bedded rivers by finer gravel bed load. *Water Resources Research* 46(7): 1–10.
- Venditti JG, Nelson PA, Bradley RW, et al. (2017) Bedforms, structures, patches and sediment supply in gravel-bed rivers. In: Tsutsumi D and Laronne JB (eds) *Gravel-Bed Rivers: Processes and Disasters*. Wiley-Blackwell, pp. 439–466.
- Wallace AR (1869) *The Malay Archipelago: The Land of the Orang-utan, and the Bird of Paradise. A Narrative of Travel, with Studies of Man and Nature*. London: Macmillan and Co.
- Weichert RB, Bezzola GR and Minor H-E (2009) Bed erosion in steep open channels. *Journal of Hydraulic Research* 47(3): 360–371.
- Westoby MJ, Brasington J, Glasser NF, et al. (2012) ‘Structure-from-motion’ photogrammetry: A low-cost, effective tool for geoscience applications. *Geomorphology* 179: 300–314.
- White WR, Bettess R and Paris E (1982) Analytical approach to river regime. *Journal of the Hydraulic Division* 108(10): 1179–1193.
- Whiting PJ and Dietrich WE (1991) Boundary shear stress and roughness over mobile alluvial beds. *Journal of Hydraulic Engineering* 116(12): 1495–1511.
- Wilberg PL and Smith JD (1987) Calculations of the critical shear stress for motion of uniform and heterogeneous sediments. *Water Resources Research* 23(8): 1471–1480.
- Wilcock PR (1988) Methods for estimating the critical shear stress of individual fractions in mixed size sediment. *Water Resources Research* 24(7): 1127–1135.
- Wilcock PR and McArdell BW (1993) Surface-based fractional transport rates: Partial transport and mobilization thresholds. *Water Resources Research* 29(4): 1297–1312.
- Wilcock PR and McArdell BW (1997) Partial transport of a sand / gravel sediment flume. *Water Resources Research* 33(1): 235–245.
- Wilcock PR, Kenworthy ST and Crowe JC (2001) Experimental study of the transport of mixed sand and gravel. *Water Resources Research* 37(12): 3349–3358.
- Wilcox AC and Wohl EE (2006) Flow resistance dynamics in step-pool stream channels: 1. Large woody debris and controls on total resistance. *Water Resources Research* 42(5): 1–16.
- Wolman MG (1954) A method of sampling coarse riverbed material. *Transactions of the American Geophysical Union* 35(6): 951–956.
- Wolman MG and Miller JP (1960) Magnitude and frequency of forces in geomorphic processes. *The Journal of Geology* 68(1): 54–74.
- Wu FC, Wang CK and Huang GH (2018) Geomorphology delineation of gravel-bed clusters via factorial kriging. *Geomorphology* 308: 161–174.
- Xu T, Moore ID and Gallant JC (1993) Fractals, fractal dimensions and landscapes – a review. *Geomorphology* 8(4): 245–262.
- Yang CT (1976) Minimum unit stream power and fluvial hydraulics. *Journal of the Hydraulic Division* 102(7): 919–934.
- Yochum SE, Bledsoe BP, Wohl EE, et al. (2014) Spatial characterization of roughness elements in high-gradient channels of the Fraser Experimental Forest, Colorado, USA. *Water Resources Research* 50(7): 6015–6029.
- Yuan J and Piomelli U (2014) Estimation and prediction of the roughness function on realistic surfaces. *Journal of Turbulence* 15(6): 350–365.
- Zachar P (2000) Psychiatric disorders are not natural kinds. *Philosophy, Psychiatry, & Psychology* 7(3): 167–182.
- Zachar P (2002) The practical kinds model as a pragmatist theory of classification. *Philosophy, Psychiatry, & Psychology* 9(3): 219–227.
- Zachar P (2015) Psychiatric disorders: Natural kinds made by the world or practical kinds made by us? *World Psychiatry* 14(3): 22–24.
- Zimmermann A, Church MA and Hassan MA (2010) Step-pool stability: Testing the jammed state hypothesis. *Journal of Geophysical Research: Earth Surface* 115.

# **Appendix B**

## **Publication: Chapter 4**

# Morphodynamics of an erodible channel under varying discharge

David L. Adams<sup>1,2</sup> 

<sup>1</sup>Department of Geography, University of British Columbia, Vancouver, British Columbia, Canada

<sup>2</sup>School of Geography, Earth and Atmospheric Sciences, University of Melbourne, Melbourne, Victoria, Australia

## Correspondence

David L. Adams, Department of Geography, University of British Columbia, Vancouver, BC V6T 1Z2, Canada.

Email: dladams@alumni.ubc.ca

## Abstract

Alluvial channels arise through the interaction between morphology, hydraulics, and sediment transport, known as the ‘fluvial trinity’. Over relatively short timescales where climate and geology are fixed but discharge and sediment supply may vary, this process facilitates adjustments towards steady state, where the system oscillates around a mean condition. The relationship between changes in conditions and geomorphic response may be highly complex and nonlinear, especially in systems with multiple modes of adjustment. This study examines the adjustment of an erodible channel with fixed banks and a widely graded sediment mixture to successive increases in discharge. With each increase in discharge, components of the fluvial trinity adjusted towards a steady state. Particularly at relatively low discharges, adjustments were controlled by intrinsic thresholds and highlighted important morphodynamic processes. Notably, there was a strong interplay between channel morphology and sediment transport, and an effect whereby larger-than-average grains controlled channel deformation. These two processes occurred at the bar scale and were highly spatialised, which has two important implications: (1) reach-averaged representations of process provide only partial insight into morphodynamics; and (2) models of rivers that suppress these process feedbacks and size-dependent transport may not replicate morphodynamics that typically occur in field conditions. The experiments provide quantitative evidence for conceptual models describing exponential approaches towards steady state and the potential for transiency if disturbance frequency exceeds the recovery time. They also highlight how in natural rivers, particularly those with greater degrees of freedom for adjustment (notably, lateral adjustment and meandering), continuous changes in discharge may lead to nonlinear rather than steady-state behaviour. In these settings, more holistic analytical frameworks that embrace different aspects of the system are critical in understanding the direction, magnitude and timing of channel adjustments.

## KEYWORDS

alluvial channels, channel adjustment, fluvial trinity, morphodynamics, nonlinear dynamics, river behaviour, steady state

## 1 | INTRODUCTION

River behaviour varies across a wide range of temporal scales, such that the notion of system stability is intrinsically time-dependent (Lane & Richards, 1997; Phillips, 2006; Schumm & Lichty, 1965). Over relatively short timescales where climate and geology are fixed, river behaviour may be broadly classified into two conditions:

unsteady, where channel form and process are evolving; and steady, where these characteristics oscillate around a mean state (‘steady state’). Morphodynamics is concerned with adjustments to channel form and process, which are facilitated by feedbacks between morphology (form), hydraulics (flow) and sediment transport (flux), or the ‘fluvial trinity’ (Ashworth & Ferguson, 1986; Best, 1986). Recent work has emphasised how morphodynamics, and particularly the

relationship between causes (events) and the magnitude, timing and manner of geomorphic effect (response), may be highly complex and nonlinear (Lisenby et al., 2018; Phillips, 1992; Schumm, 1973). These nonlinear dynamics may be more generally prevalent in systems with multiple modes of adjustment (e.g., alluvial channels) and threshold mechanisms (Phillips, 2003)—for example, channels where bed material transport is restricted to conditions near the threshold of motion ('threshold' channels: Church, 2006).

These notions that surround morphodynamics are highly generalised but ultimately testable, although for both philosophical and methodological reasons they have not been comprehensively interrogated. A Newtonian paradigm has driven researchers to increasingly small spatiotemporal scales of inquiry and to isolate processes of hydraulics and sediment transport where conservation laws and force–balance relations may be more readily applied (Ancey, 2020; Church & Ferguson, 2015; Rhoads & Thorn, 1993). In practice, this approach has manifested in various simplifications—notably, physical and numerical models that lack degrees of freedom available for adjustment in most natural channels, and narrow grain size distributions that may not replicate important processes in prototype streams (Booker & Eaton, 2020). By reducing the modes of adjustment, and removing the potential for threshold-dependent transport (in the case of threshold channels), these simplifications may significantly reduce the potential for nonlinear behaviour that may be expected in nature (Phillips, 1993). It is also worth noting a lack of available field data and remote sensing technology, which has historically made quantitative investigations of channel behaviour difficult.

As geomorphologists become increasingly aware of philosophical blind spots and methodological oversimplifications, and have access to improved data collection techniques, there is an opportunity to examine and revise ideas surrounding channel morphodynamics. These investigations need not be exhaustive and elaborate, but rather should first seek to examine process feedbacks, steady-state conditions and nonlinear dynamics under relatively straightforward experimental scenarios. To this end, this paper analyses the adjustment of an erodible channel under varying discharge. The experiment has fixed banks but is sufficiently wide to allow for the development of alternate bars, and it has a relatively broad distribution of grain sizes. The results highlight a time-dependent interplay between

form, flow and flux towards steady state conditions, as well as the presence of nonlinear dynamics such as internal thresholds that affect channel adjustment. The findings have implications for physical and numerical modelling of rivers as well as approaches to analysing morphodynamics.

## 2 | METHODS

The analysis is of an experiment reported by Adams and Zampiron (2020, Exp1c), which models the adjustment of a steep mountain channel to successive increases in discharge under pseudo-recirculating conditions (i.e., material was recirculated at the same rate it was output, with a brief time lag). The experiment was conducted on a generic Froude-scaled stream table ( $12.2 \times 1.5$  m) that is based on field measurements from Fishtrap Creek in British Columbia, Canada. The model has a slope of 2% and a length-scale ratio of approximately 1:25, yielding a scaled channel width of 30 cm, formative discharge of 1.5 L/s and bulk material ranging from 0.25 to 8 mm. The banks were lined with interlocking bricks to make a straight 30 cm wide fixed-bank configuration (Figure 1), and the bed was screeded flat. Reach-averaged water depth and sediment flux are available throughout four successive experimental phases of increasing discharge (by 50% each time): (1) 0.67 L/s for 8 h; (2) 1 L/s for 4 h; (3) 1.5 L/s for 4 h; and (4) 2.25 L/s for 4 h. Topography and flow depth data were collected at increasingly long intervals, although sediment output was measured every 15 min at a minimum.

The fluvial trinity is indexed using reach-averaged flow resistance, topographic variation and bedload flux, which are commonly used parameters that are readily available from the experiments. Flow resistance is estimated by a variant of the Darcy–Weisbach equation  $f_{\text{sys}} = 8gRS_v/u^2$ , where  $g$  is gravity,  $R$  is the hydraulic radius (or mean hydraulic depth),  $S_v$  is the valley gradient (almost identical to channel gradient here) and  $u$  is velocity (Eaton et al., 2004). Topographic variation and bedload flux are indexed by the standard deviation of the thalweg elevation profile  $\sigma_z$  and width-averaged volumetric output rate  $q_b$ , respectively. In addition, volumetric morphological activity  $M_{\text{raw}}$  is calculated using the height difference between successive digital elevation models (DEMs). The height difference in each cell is



**FIGURE 1** Adjustable-boundary experimental system (A-BES) at the University of British Columbia, showing the 30 cm channel configuration (Adams & Zampiron, 2020, CC BY 4.0)

multiplied by cell resolution and average porosity (0.46), and summed to provide the total volumetric change.

### 3 | RESULTS

In phase 1 the channel developed a set of alternate bars over four hours, and which then rapidly rearranged in response to a shift in the bar at the upstream end, yielding seven complete bars (and a half-bar at each end). The riffles widened and bar-heads eroded in response to the first increase in flow (phase 2), although the previous morphology was largely inherited as larger-than-average grains (4.0–5.6 mm) could not be entrained from the bar-heads. The next phase almost immediately eroded the bars and rapidly deposited a set of four complete longer-wavelength alternate bars. Following the final increase in flow (phase 4), the increased discharge immediately planed off the bars to form a flat bed, and slowly redeposited a set of three complete alternate bars over four hours.

Each change in discharge yielded different combinations of adjustments between the three variables (Figure 2; see arrows). Following an initial increase during the first phase, there was a general

decrease in the system's frictional resistance with increasing discharge as flow depth increased. The standard deviation of bed elevations increased throughout the first phase, associated with the development of the pool–bar–riffle sequence. Topographic variability peaked in phases 2 and 3 as the pools deepened, but rapidly decreased in the final phase as the bed was planed. There was an exponential increase in bedload transport with increasing discharge. Bedload transport rates were typically higher at the beginning of each phase and decreased towards a relatively constant value. The notable exception is the first phase, where bedload transport was negligible prior to the development of morphology.

Morphological activity is typically presented as a volumetric change per unit time  $M$ , given that physical change is intrinsically a time-dependent process. We also present raw values that are not normalised by time ( $M_{raw}$ ), given that relatively long measurement intervals in the latter portion of each phase tend to underrepresent morphological activity (Figure 3). There was relatively little morphological activity prior to the first bar rearrangement, where there was a rapid increase (indicated by  $\alpha$ ). For the remainder of the experiment  $M_{raw}$  oscillated around a relatively constant value (annotated with a horizontal line), except for the periods at the beginning of phases

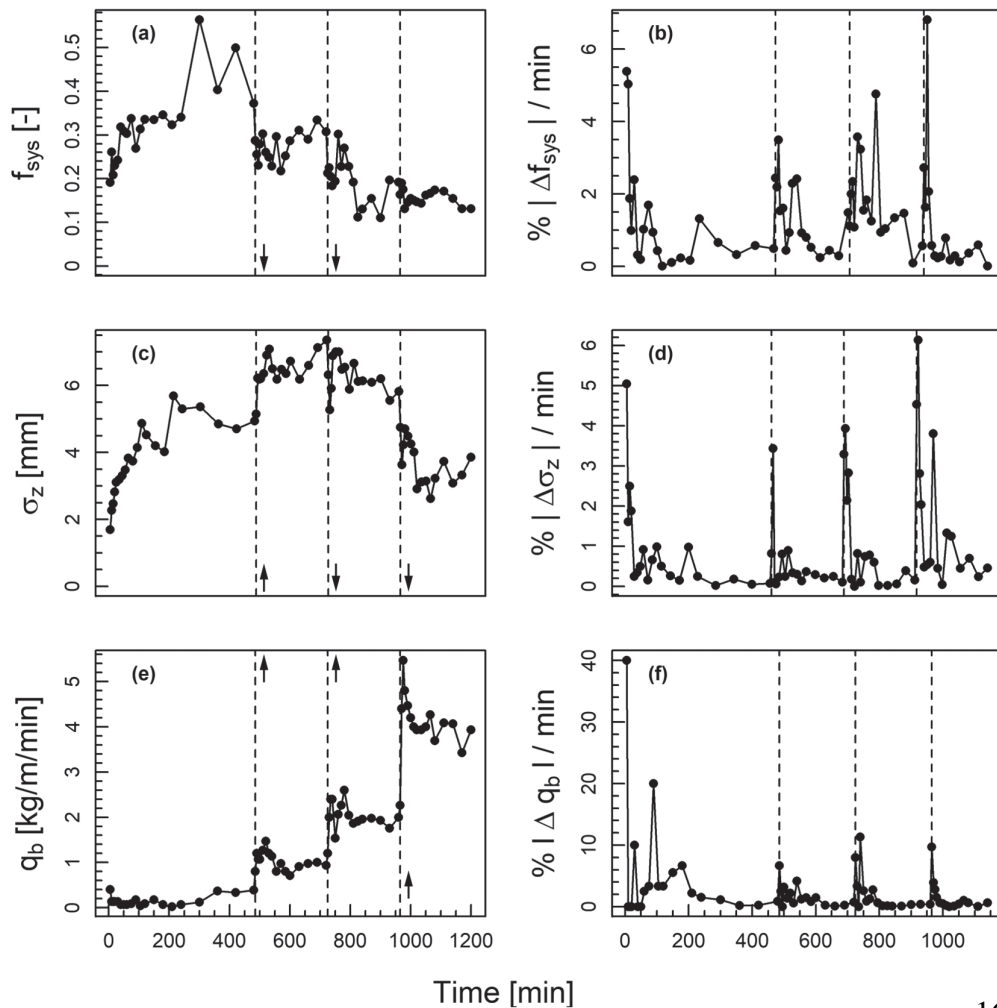


**FIGURE 2** (a,c,e) Variation in flow resistance, topographic variability and bedload transport over the duration of the multi-phase experiment, and (b,d,f) absolute percentage change in these variables over time (expressed as change per minute). Vertical dashed lines represent the beginning of each phase, and arrows indicate the direction of adjustment from the previous phase (no arrow indicates no change)

3 and 4. These two bar reorganisation events are well reflected in periods of higher morphological activity ( $\beta$  and  $\gamma$ , respectively). The rate of morphological activity  $M$  follows a similar trend to other variables, whereby change tends to be greatest immediately after each increase in discharge, before asymptoting towards zero. The relatively low rate of change at the beginning of the first phase, compared to subsequent increases in discharge, highlights the relatively small amount of volumetric change.

Flow resistance and bedload transport most effectively discriminate between the experimental phases and indicate four relatively distinct channel characters (Figure 4a). With increasing discharge, there was a stepped transition from low bedload flux and high flow resistance (phase 1) to high flux and low resistance (phase 4).

Topographic variability and bedload transport also distinguish between the four phases fairly well, although there is little difference in topographic variability between phases 2 and 3 (Figure 4b).

Changes in flow resistance, topographic variability, bedload flux and morphological activity were most rapid at the beginning of each phase (Figures 2b–f, and 3b). Bedload transport exhibited the fastest rates of change during this period. Following the initial adjustment period spanning the first few observations (the first 10–30 min), all variables reached a relatively constant rate of change. There were some exceptions to this trend;  $\Delta f_{sys}$  in phase 3 and  $\Delta q_b$  in phase 1. In the latter, the high rate of change was an artefact of the very small volumes of sediment output relative to measurement precision. In other cases, following the initial adjustment period,  $\Delta f_{sys}$  and  $\Delta q_b$

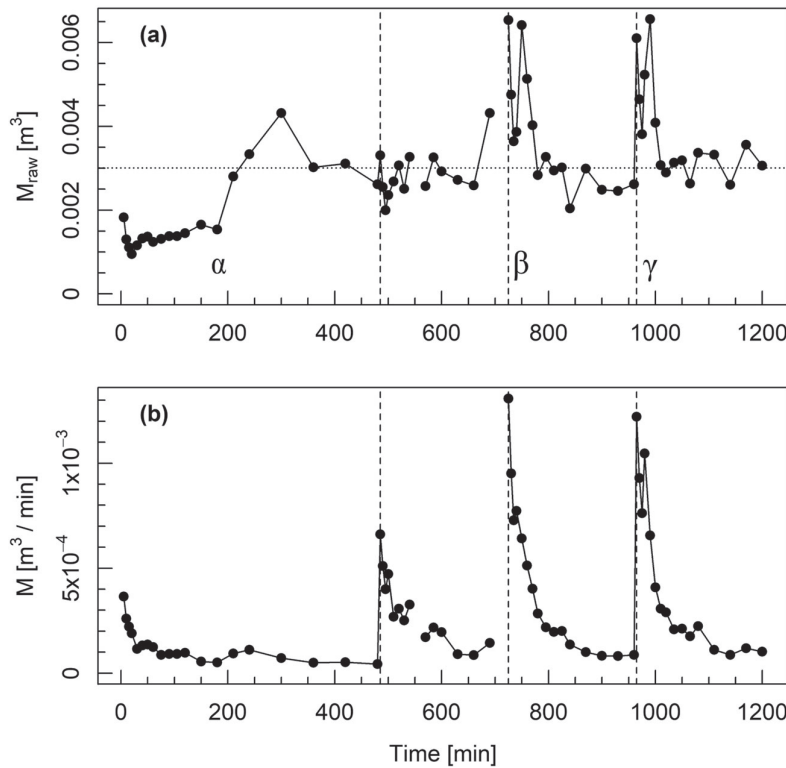


**FIGURE 3** Reach-averaged morphological activity over the duration of the multi-phase experiment, presented as both (a) raw values ( $M_{raw}$ ), and (b) normalised by time ( $M$ ). Bar reorganisation events associated with high morphological activity are indicated by Greek letters, and steady-state  $M_{raw}$  is indicated by a horizontal line

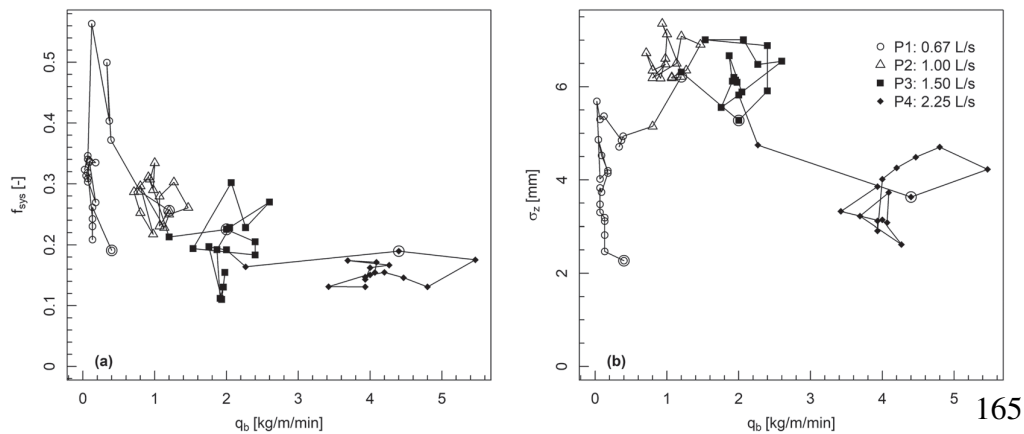


**FIGURE 4** Comparison of flow resistance, topographic variability and bedload transport values at each successive point of the experiment, combined in two different ways. Circled points represent the first measurement taken during each phase

stabilised at relatively similar values: approximately <3% change per minute. Also, the magnitude of the adjustment for each variable generally increased with increasing discharge, except for the initial change from the screeded bed in phase 1.

To further explore the patterns of adjustment towards and within steady state conditions, the rates of change in  $f_{\text{sys}}$  and  $q_b$  in each phase are presented in Figure 5. Following each successive increase in discharge, there is generally an initial period during which flow resistance and flux change at a relatively rapid rate. Following this adjustment period, there is oscillation around a more constant rate of change. These patterns vary across the different phases in two notable ways. First, there was only a relatively minor adjustment in sediment transport and flow resistance at the beginning of the second phase. Second, during the steady state period in phase 4 there was a very small rate of change, whereby sediment transport and flow resistance varied by less than 1% per minute.

## 4 | DISCUSSION

The experimental results show an adjustment to the imposed changes in discharge that involves the time-dependent evolution of flow resistance, bed morphology and bedload transport towards conditions where these characteristics become time-independent. The adjustment of these three parameters was nonlinear within each phase, such that the rate of change was rapid at first but decreased towards zero, although fluctuations continued within a finite envelope. This temporal pattern of response is consistent with general models describing the nonlinear adjustment of geomorphic systems towards a constant variance around a mean value (Graf, 1977; Langbein &

Leopold, 1964; Rhoads, 2020, fig. 6.20). Given the fluctuation in flow, form and flux variables despite constant flow conditions, the results suggest that in a real river system where discharge changes continuously the system would be considerably less steady (Howard, 1982). The system may be even more unsteady if the rate of change in external conditions is rapid relative to the adjustment time, as it may never fully adjust to the change in conditions (Rhoads, 2020, fig. 6.20). To our knowledge, the results of this study are the first to conclusively demonstrate for adjustment of river morphology the exponential approach to steady state and the potential for transiency if disturbance frequency exceeds the recovery time.

Channel adjustments (i.e., bar reorganisation events) were well reflected by changes in morphological activity, indicating the magnitude of physical change occurring between time steps. Subsequently, rapid changes in morphological activity clearly indicated points in time where the system passed intrinsic thresholds (Schumm, 1973, 1979), or where increases in discharge were geomorphically effective. The system crossed an intrinsic threshold in the first experimental phase (event *a*), where a significant morphological reorganisation (characterised by an increase in topographic variability and pool depth) led to an increase in bedload transport. Similar feedbacks between the spatial distribution of shear stress and bedload dynamics have been observed in the field and incorporated into models of sediment transport (Ferguson, 2003; Monsalve et al., 2020; Nicholas, 2000; Paola & Seal, 1995; Paola, 1996). The concentration of flow in preferential paths constitutes a fundamental feedback between channel morphology and sediment transport (Church, 2010; Church & Ferguson, 2015).

As discharge was increased, the system demonstrated a variety of adjustments. In the second phase, the previous morphology was

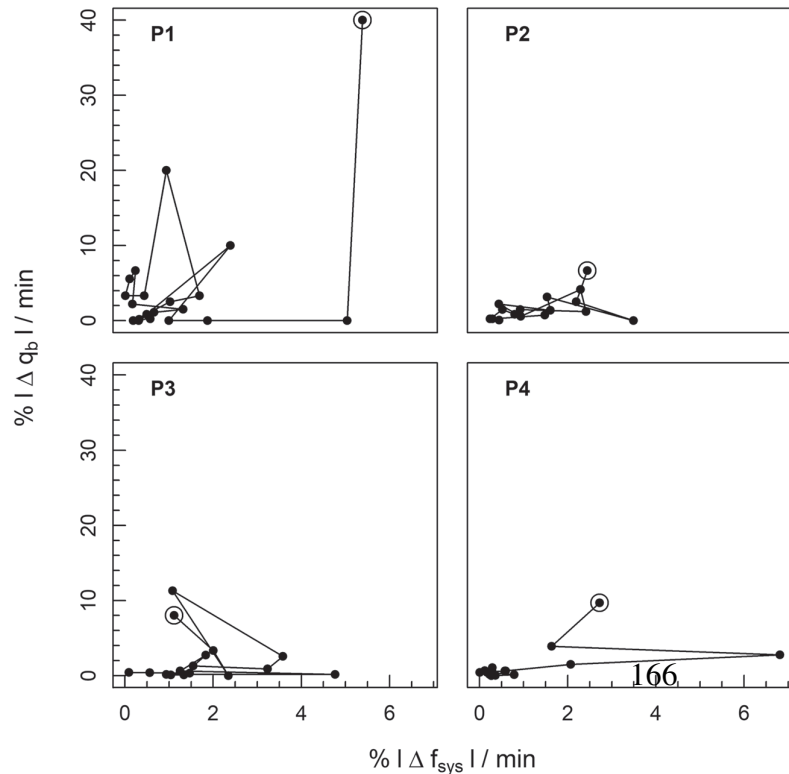


**FIGURE 5** Change in  $f_{\text{sys}}$  and  $q_b$  at each successive point of the experiment, separated by experimental phase. Circled points represent the first measurement taken during each phase

largely inherited as the increase in shear stress was not sufficient to entrain larger-than-average grains located at bar-heads. This is consistent with studies that have identified larger-than-average grains controlling sediment transport and thresholds for channel deformation, rather than the average grain size (Booker & Eaton, 2020; MacKenzie & Eaton, 2017; MacKenzie et al., 2018). The entrainment threshold for larger-than-average grains was crossed as the discharge was increased again (event  $\beta$ ), suggesting that the influence of these grain size fractions is greatest at threshold and partial transport conditions (Wilcock & McArdeell, 1993, 1997). Moreover, the lack of morphological response to the increase in discharge highlights the limitations of the geomorphic work concept in nonlinear systems (Lisenby et al., 2018; Wolman & Miller, 1960).

In the final phase, the increase in shear stress exceeded the entrainment threshold above which bars could be maintained through deposition (event  $\gamma$ ). Here, shear stress was relatively higher than what could be expected in some natural alluvial channels as the discharge was contained within fixed banks; that is, no widening or overbank spill could occur. The beginning of this phase was characterised by a rapid change in morphology and bedload transport as the pool-bar-riffle sequence was planed, and bar redevelopment occurred far more slowly than in the previous phase due to a low rate of deposition.

There was a nonlinear response of morphology and sediment transport to the regular increases in discharge throughout the experiment, and each aspect of the fluvial trinity followed strongly interrelated but differing trajectories. There was a negative parabolic trend in topographic variability and an exponential increase in bedload transport, while flow resistance decreased relatively steadily. Subsequently, combinations of these three variables distinguish between channel characters that correspond to each phase of the experiment. In other words, each steady state condition was achieved via different combinations of form, flow and flux. The diverging trajectories of these parameters represent distinct manifestations of morphodynamic interplay that facilitates the emergence of a constant variance condition for each flow regime. Interestingly, the adjustment of the fluvial trinity appeared to maintain a relatively constant level of morphological activity across the different steady state periods (i.e., even when discharge was increased).

For each discharge, each component of the fluvial trinity adjusted towards a constant variance state, suggesting that in practice system stability could be defined in various ways. Indeed, there are several definitions of channel stability that have been proposed, relating to mass balance ('grade'; e.g., Mackin, 1948), energy balance (Nanson & Huang, 2017) and a constancy of average channel morphology ('dynamic' or 'pattern' stability; e.g., Hey & Thorne, 1986; Schumm, 1985). These concepts provide a useful means of classifying channel dynamics into 'stable' and 'unstable' states by isolating a single aspect of the fluvial system. The steady state conditions observed in the experiment were characterised by different degrees of fluctuation, and there were also marginal departures from steady state conditions (secondary adjustments following the initial perturbation). These results support a spectrum of system stability that is not reflected in binary representations of behaviour and highlight the importance of determining historical patterns of variability (Brierley & Fryirs, 2005; Fryirs et al., 2012; Wohl, 2011).

## 5 | CONCLUSION

The adjustment of the channel to varying discharge highlighted several important aspects of morphodynamics. As discharge was increased, each component of the fluvial trinity exhibited a nonlinear adjustment towards a steady state characterised by fluctuations around a constant mean. Steady state conditions were achieved through the mutual adjustment between these components, suggesting that the investigation and explanation of channel behaviour require an appreciation of all three. The experiments provide quantitative evidence for conceptual models describing exponential approaches towards steady state and the potential for transiency if disturbance frequency exceeds the recovery time. They also highlight how in natural rivers, particularly those with greater degrees of freedom for adjustment, continuous changes in discharge may lead to nonlinear rather than steady state behaviour.

Particularly at relatively low discharges, the morphodynamics underscored the importance of geomorphic thresholds. Under these conditions, channel adjustments comprised feedbacks between morphology and sediment transport, and channel deformation was controlled by larger-than-average grain size fractions. These two processes occurred at the bar scale and were highly spatialised, being associated with the lateral concentration of shear stress and grain patchiness, respectively, which has two important implications. First, reach-averaged representations of process provide only partial insight into morphodynamics. Second, models of rivers that suppress morphodynamic feedbacks and size-dependent transport may not replicate morphodynamics that typically occur under field conditions.

There are, however, several challenges in studying morphodynamics in nature. Practical difficulties associated with the collection of field data often mean that only short-term or temporally sporadic data are available. These data may be misleading given the typically non-uniform rates of adjustment and relatively constant changes in channel conditions (i.e., discharge) observed in nature. Given continual advances in field methods, and in particular remote sensing (Dietrich, 2017; Kasvi et al., 2019), we can expect that historical approaches to assessing river behaviour may become increasingly realistic. Especially in natural rivers with greater degrees of freedom available (notably, lateral adjustment and meandering) and greater potential for nonlinear behaviour, more holistic assessments of channels that embrace different aspects of the system are critical in understanding the direction, magnitude and timing of adjustments. Meanwhile, laboratory experiments may provide further insights into nonlinear channel morphodynamics, where researchers may take a 'forensic' approach to identify processes both temporally and spatially.

## ACKNOWLEDGEMENTS

This work stems from discussions beside the laboratory experiments with William Booker and Shawn Chartrand, who challenged me to explore the concept of stability. I would like to thank William, Shawn, Marwan Hassan, Brett Eaton, Mike Church and Lucy MacKenzie for providing insightful feedback on the manuscript at various stages. I would also like to thank Bruce Rhoads and Gerald Nanson, whose comments stimulated considerable revisions of the manuscript. This work was supported by a postgraduate scholarship provided by the Canadian Government.

**CONFLICTS OF INTEREST**

The author declares no conflict of interest.

**DATA AVAILABILITY STATEMENT**

Data are available upon reasonable request from the author.

**ORCID**

David L. Adams  <https://orcid.org/0000-0001-8578-8076>

**REFERENCES**

- Adams, D.L. & Zampiron, A. (2020) Short communication: Multiscalar roughness length decomposition in fluvial systems using a transform-roughness correlation (TRC) approach. *Earth Surface Dynamics*, 8(4), 1039–1051.
- Ancey, C. (2020) Bedload transport: A walk between randomness and determinism. Part 2. Challenges and prospects. *Journal of Hydraulic Research*, 58(1), 18–33.
- Ashworth, P.J. & Ferguson, R.I. (1986) Interrelationships of channel processes, changes and sediments in a proglacial braided river. *Geografiska Annaler*, 68(4), 361–371.
- Best, J.L. (1986) The morphology of river channel confluences. *Progress in Physical Geography*, 10(2), 157–174.
- Booker, W.H. & Eaton, B.C. (2020) Stabilising large grains in self-forming steep channels. *Earth Surface Dynamics*, 8, 51–67.
- Brierley, G.J. & Fryirs, K.A. (2005) *Geomorphology and River Management*. Blackwell: Malden, MA.
- Church, M.A. (2006) Bed material transport and the morphology of alluvial river channels. *Annual Review of Earth and Planetary Sciences*, 34(1), 325–354.
- Church, M.A. (2010) The trajectory of geomorphology. *Progress in Physical Geography*, 34(3), 265–286.
- Church, M.A. & Ferguson, R.I. (2015) Morphodynamics: Rivers beyond steady state. *Water Resources Research*, 51(4), 1883–1897.
- Dietrich, J.T. (2017) Bathymetric structure-from-motion: Extracting shallow stream bathymetry from multi-view stereo photogrammetry. *Earth Surface Processes and Landforms*, 42(2), 355–364.
- Eaton, B.C., Church, M.A. & Millar, R.G. (2004) Rational regime model of alluvial channel morphology and response. *Earth Surface Processes and Landforms*, 29(4), 511–529.
- Ferguson, R.I. (2003) The missing dimension: Effects of lateral variation on 1-D calculations of fluvial bedload transport. *Geomorphology*, 56(1–2), 1–14.
- Fryirs, K., Brierley, G.J. & Erskine, W.D. (2012) Use of ergodic reasoning to reconstruct the historical range of variability and evolutionary trajectory of rivers. *Earth Surface Processes and Landforms*, 37(7), 763–773.
- Graf, W.L. (1977) The rate law in fluvial geomorphology. *American Journal of Science*, 277, 178–191.
- Hey, R.D. & Thorne, C.R. (1986) Stable channels with mobile gravel beds. *Journal of Hydraulic Engineering*, 112(8), 671–689.
- Howard, A.D. (1982) Equilibrium and time scales in geomorphology: Application to sand-bed alluvial streams. *Earth Surface Processes and Landforms*, 7(4), 303–325.
- Kasvi, E., Salmela, J., Lotsari, E., Kumpula, T. & Lane, S.N. (2019) Comparison of remote sensing based approaches for mapping bathymetry of shallow, clear water rivers. *Geomorphology*, 333, 180–197.
- Lane, S.N. & Richards, K.S. (1997) Linking river channel form and process: Time, space and causality revisited. *Earth Surface Processes and Landforms*, 22(3), 249–260.
- Langbein, W.B. & Leopold, L.B. (1964) Quasi-equilibrium states in channel morphology. *American Journal of Science*, 262, 782–794.
- Lisenby, P.E., Croke, J. & Fryirs, K.A. (2018) Geomorphic effectiveness: A linear concept in a non-linear world. *Earth Surface Processes and Landforms*, 43, 4–20.

- MacKenzie, L.G. & Eaton, B.C. (2017) Large grains matter: Contrasting bed stability and morphodynamics during two nearly identical experiments. *Earth Surface Processes and Landforms*, 42(8), 1287–1295.
- MacKenzie, L.G., Eaton, B.C. & Church, M.A. (2018) Breaking from the average: Why large grains matter in gravel bed streams. *Earth Surface Processes and Landforms*, 43, 3190–3196.
- Mackin, J.H. (1948) Concept of the graded river. *Bulletin of the Geological Society of America*, 69, 463–511.
- Monsalve, A., Segura, C., Hucke, N. & Katz, S. (2020) A bed load transport equation based on the spatial distribution of shear stress Oak Creek revisited. *Earth Surface Dynamics Discussions*, 8, 825–839.
- Nanson, G.C. & Huang, H.Q. (2017) Self-adjustment in rivers: Evidence for least action as the primary control of alluvial-channel form and process. *Earth Surface Processes and Landforms*, 42(4), 575–594.
- Nicholas, A.P. (2000) Modelling bedload yield braided gravel bed rivers. *Geomorphology*, 36(1–2), 89–106.
- Paola, C. (1996) Incoherent structure: Turbulence as a metaphor for stream braiding. In *Coherent flow structures in open channels*, Ashworth, P. J., Bennett, S. J., Best, J. L., McLelland, S. J. (eds), Wiley: Chichester, UK; 705–723.
- Paola, C. & Seal, R. (1995) Grain size patchiness as a cause of selective deposition and downstream fining. *Water Resources Research*, 31(5), 1395–1407.
- Phillips, J.D. (1992) Nonlinear dynamical systems in geomorphology: Revolution or evolution? *Geomorphology*, 5, 219–229.
- Phillips, J.D. (1993) Spatial-domain chaos in landscapes. *Geographical Analysis*, 25(2), 101–117.
- Phillips, J.D. (2003) Sources of nonlinearity and complexity in geomorphic systems. *Progress in Physical Geography*, 27(1), 1–23.
- Phillips, J.D. (2006) Deterministic chaos and historical geomorphology: A review and look forward. *Geomorphology*, 76, 109–121.
- Rhoads, B.L. (2020) *River dynamics: Geomorphology to support management*. Cambridge University Press: Cambridge, UK.
- Rhoads, B.L. & Thorn, C.E. (1993) Geomorphology as science: The role of theory. *Geomorphology*, 6, 287–307.
- Schumm, S.A. (1973) Geomorphic thresholds and complex response of drainage systems. In *Fluvial geomorphology*, 6th edn., Morisawa, M. (ed), State University of New York: Binghamton, NY; 299–310.
- Schumm, S.A. (1979) Geomorphic thresholds: The concept and its applications. *Transactions of the Institute of British Geographers*: 485–515.
- Schumm, S.A. (1985) Patterns of alluvial rivers. *Annual Review of Earth and Planetary Sciences*, 13, 5–27.
- Schumm, S.A. & Lichty, R.W. (1965) Time, space, and causality in geomorphology. *American Journal of Science*, 263, 110–119.
- Wilcock, P.R. & McArdell, B.W. (1993) Surface-based fractional transport rates: Partial transport and mobilization thresholds. *Water Resources Research*, 29(4), 1297–1312.
- Wilcock, P.R. & McArdell, B.W. (1997) Partial transport of a sand/gravel sediment flume. *Water Resources Research*, 33(1), 235–245.
- Wohl, E. (2011) What should these rivers look like? Historical range of variability and human impacts in the Colorado Front Range, USA. *Earth Surface Processes and Landforms*, 36(10), 1378–1390.
- Wolman, M.G. & Miller, J.P. (1960) Magnitude and frequency of forces in geomorphic processes. *Journal of Geology*, 68(1), 54–74.

**How to cite this article:** Adams, D.L. (2021) Morphodynamics of an erodible channel under varying discharge. *Earth Surface Processes and Landforms*, 1–7. Available from: <https://doi.org/10.1002/esp.5185>

# **Appendix C**

## **Publication: Chapter 5**



# Short communication: Multiscalar roughness length decomposition in fluvial systems using a transform-roughness correlation (TRC) approach

David L. Adams<sup>1,2</sup> and Andrea Zampiron<sup>3</sup>

<sup>1</sup>Department of Geography, University of British Columbia, Vancouver, BC, Canada

<sup>2</sup>School of Geography, The University of Melbourne, Melbourne, VIC, Australia

<sup>3</sup>Department of Mechanical Engineering, University of Melbourne, Melbourne, VIC, Australia

Correspondence: David L. Adams (dladams@alumni.ubc.ca)

Received: 12 June 2020 – Discussion started: 20 July 2020

Revised: 7 September 2020 – Accepted: 16 October 2020 – Published: 9 December 2020

**Abstract.** In natural open-channel flows over complex surfaces, a wide range of superimposed roughness elements may contribute to flow resistance. Gravel-bed rivers present a particularly interesting example of this kind of multiscalar flow resistance problem, as both individual grains and bedforms may contribute to the roughness length. In this paper, we propose a novel method of estimating the relative contribution of different physical scales of in-channel topography to the total roughness length, using a transform-roughness correlation (TRC) approach. The technique, which uses a longitudinal profile, consists of (1) a wavelet transform which decomposes the surface into roughness elements occurring at different wavelengths and (2) a “roughness correlation” that estimates the roughness length ( $k_s$ ) associated with each wavelength based on its geometry alone. When applied to original and published laboratory experiments with a range of channel morphologies, the roughness correlation estimates the total  $k_s$  to approximately a factor of 2 of measured values but may perform poorly in very steep channels with low relative submergence. The TRC approach provides novel and detailed information regarding the interaction between surface topography and fluid dynamics that may contribute to advances in hydraulics, bedload transport, and channel morphodynamics.

## 1 Introduction

Understanding flow resistance is of great interest to river research and practice. The estimation of flow resistance is important for determining flood magnitudes, predicting ecological habitat, estimating rates of sediment transport, and understanding channel morphodynamics. However, the hydraulics of gravel-bed channels, in particular, are relatively poorly understood (see Ferguson, 2007). Given that most of the foundational work in fluid dynamics, upon which conventional approaches to predicting flow resistance are based, was conducted using regular (e.g. Schlichting, 1936) or uniscalar (e.g. Nikuradse, 1933) bed geometry, the multiscalar topographic characteristics of these rivers present a major challenge. In particular, individual grains and assemblages of grains (“forms”) on the bed surface, spanning orders of

magnitude of scale, have variable contributions to the total flow resistance across different channel types. Thus, moving forward, mainstream empirical approaches to estimating flow resistance based solely on grain diameter would ideally be replaced by approaches that explicitly account for multiple spatial scales (see Adams, 2020a). Decomposing roughness lengths into different scales may contribute to an understanding of channel morphodynamics given that energy dissipation is increasingly recognized as a condition governing system behaviour (Eaton and Church, 2004; Nanson and Huang, 2018; Church, 2015). Also, the partitioning of bed stresses between grain and form scales is an important step in predicting bedload transport (Ancy, 2020).

Inspired by early work in fluid dynamics (Schlichting, 1936; Keulegan, 1938) and subsequent work in fluvial hydraulics (Einstein and Banks, 1950; Nowell and Church,

1979), some geomorphologists sought to disaggregate the roughness length into grain and form contributions by correlating bar geometry with flow resistance (Davies and Sutherland, 1980; Prestegard, 1983). However, further work was likely hindered by limitations associated with the collection of topographic data in rivers (Furbish, 1987; Robert, 1988). Advances in remote sensing and statistics have since allowed researchers to explore detailed scaling characteristics of gravel-bed surfaces using analyses such as variograms (Robert, 1988; Clifford et al., 1992) and transforms (Nyander et al., 2003). Topographic analyses have led to multiscalar decompositions of geometric roughness in rivers, although to our knowledge, full decompositions of hydraulic roughness have not yet been presented. The latter approach has been developed for complex aeolian surfaces using transforms (Nield et al., 2013; Pelletier and Field, 2016; Field and Pelletier, 2018), which serves as a proof of concept for a multiscalar roughness length decomposition.

In a review of flow resistance in gravel-bed rivers, Adams (2020a) identified two relatively recent advancements in the fields of statistics and fluid dynamics that could contribute to a multiscalar roughness length decomposition tool. The first advancement is the wavelet transform, which is generally superior to the Fourier transform when analysing the underlying structure of complex and aperiodic signals. This is due to the use of a finite (rather than a continuous) wavelet function, which gives rise to a family of wavelets that are dilated (stretched and compressed) and translated (shifted) along the signal (Torrence and Compo, 1998). There are now various types of wavelet transforms suited to different applications, some of which have been applied in rivers (Kumar and Foufoula-Georgiou, 1997; Nyander, 2004; Keylock et al., 2014). The second advancement is the development of roughness correlations for irregular surfaces (e.g. Forooghi et al., 2017; De Marchis et al., 2020), which estimate the roughness length of a surface based purely on its geometric characteristics.

In this study, we present a novel method of estimating the relative contribution of different physical scales of river bed topography to the total roughness length based on longitudinal profiles. The general approach consists of (1) a wavelet transform in which the channel surface is decomposed into a set of more simple components each at a different wavelength and (2) a roughness correlation that estimates the roughness length associated with each wavelength, which is expressed as the equivalent sand roughness parameter  $k_s$  (Nikuradse, 1933; Schlichting, 1936). By modifying the specific roughness correlation that is used, the transform-roughness correlation (TRC) approach may be applied across a wide range of channel types and hydraulic conditions. To demonstrate the TRC analysis, we apply it to a series of original laboratory experiments with high-resolution digital elevation models (DEMs), as well as some additional published data.

## 2 Methodological considerations

The transform-roughness correlation approach is a generic tool that should be adapted based on the hydraulic conditions and the purpose of its application. These considerations should span the dataset, the type of wavelet transform, and the specific roughness correlation that is selected. We first discuss these general considerations to provide important context for the TRC approach, prior to introducing the experimental data and the Forooghi et al. (2017) roughness correlation in Sect. 3.2.

First, the minimum resolution and spatial extent of the topographic dataset should be informed by the scale of the features of interest. The data should have a sufficiently high spatial resolution such that they can capture the range of in-channel features that produce drag. Also, to capture the characteristic geometry of bed features (notably, height and spacing) and estimate a reach-averaged roughness length, the spatial extent of the dataset should be at least the length of the largest features that influence the flow; for example, it should span a series of dune crests or pool–riffle pairs.

Second, given that the hydraulic roughness of in-channel features is of interest, the channel topography can be reduced to a one-dimensional profile extending along the thalweg, representative of the primary flow path. It is important to note here that this approach ignores resistance elements, such as channel planform, and three-dimensional interactions between flow and in-channel topography. If both hydraulic and topographic data are available, this assumption may be validated by comparing the roughness length estimated using the roughness correlation to a measured roughness length (see Sect. 3.1.2). If the range of interactions between the flow and the surface is of interest, multiple parallel elevation profiles could be analysed.

Third, the choice between discrete and continuous wavelet transforms (DWT and CWT) is a trade-off between the resolution of the decomposition and the physical resemblance to the original profile. Compared to the DWT, the CWT extracts more intricate structural characteristics from the signal and yields a greater number of wavelengths between which information is shared (Addison, 2018). However, the redundancy in the CWT generates a more abstract representation of the topographic variation at a given wavelength. In Fig. 1, we compare wavelengths extracted using a maximal overlap discrete wavelet transform (MODWT) and a CWT using the same elevation profile. At the wavelength corresponding to the spacing of a pool–bar–riffle sequence ( $\lambda \approx 2$  m), the oscillations output by the MODWT are aligned with the pool–riffle undulations (i.e. the position of peaks and the general shape are similar), but the CWT oscillations do not appear to align with the original profile. Given that they do not resemble the channel surface, it may be invalid to infer hydraulic behaviour from CWT wavelengths. 171

Fourth, the specific roughness correlation that is used should match the regime of the channel's boundary Reynolds

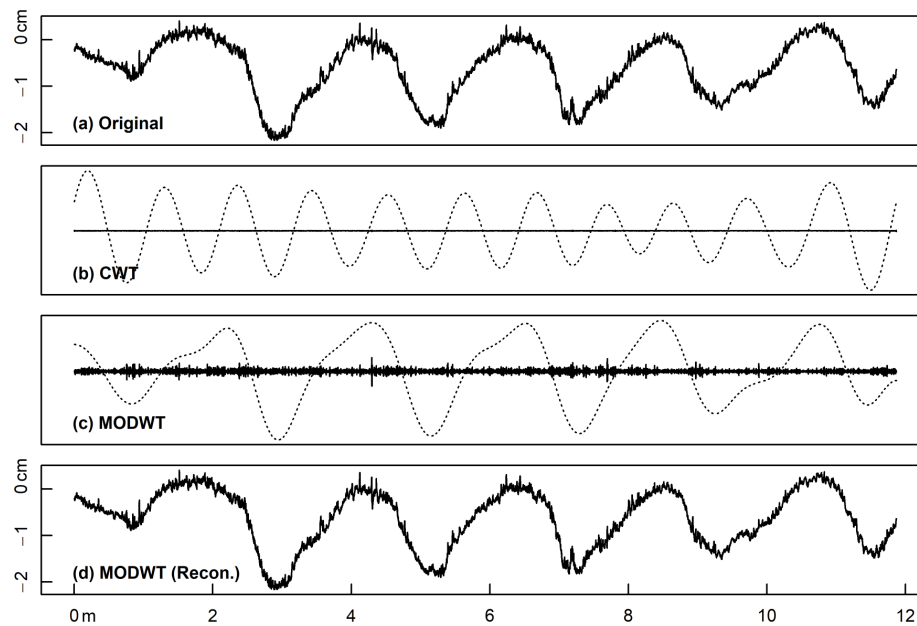


**Figure 1.** (a) Thalweg elevation profile at end of Experiment 1a (this study) featuring a prominent pool–riffle sequence, where the  $x$  axis represents distance upstream, (b) grain ( $\lambda = 4$  mm) and form ( $\lambda \approx 2$  m, dashed line) wavelengths derived from CWT, (c) the same two wavelengths derived from a MODWT, and (d) the original signal reconstructed from the MODWT by recombining wavelengths.

number  $Re^* = U^*k/v$ , where  $U^*$  is shear velocity,  $k$  is a representative roughness scale, and  $v$  is kinematic viscosity. For example, given that gravel-bed rivers tend to be within the fully rough regime where  $Re^* \geq 70$  (e.g. Buffington and Montgomery, 1997; Schlichting, 1979), it may only be valid to apply roughness correlations obtained for that regime specifically. Also, the flow should be turbulent, and it should be two-dimensional, which may be indicated (although not guaranteed) by flow aspect ratios ( $w/h$ , where  $w$  is the wetted width and  $h$  is flow depth) greater than 5 (Nezu and Nakagawa, 1993).

Last, roughness correlations in fluid dynamics tend to be developed for flows sufficiently deep to have logarithmic velocity profiles, which should be considered when they are applied to flows with less developed profiles. Jimenez (2004) suggested that logarithmic layers develop where relative submergence  $h/k$  is greater than 40, although Cameron et al. (2017) observed a logarithmic layer in rough open-channel flow at submergences as low as 1.9. During most flow conditions, it is common for gravel-bed rivers to have relative submergences of less than 10 and, in some cases, as low as 0.1 (Lee and Ferguson, 2002; Ferguson, 2007), where no logarithmic layer can develop because roughness elements are not submerged. However, if one is interested in channel-forming flows capable of reworking the bed surface (Ashworth and Ferguson, 1989; Wolman and Miller, 1960) where relative submergence may be 2 orders of magnitude higher (Limerinos, 1970; Bray, 1982), the logarithmic assumption should be satisfied for most rivers.

### 3 Application of TRC approach in gravel-bed rivers

#### 3.1 Stream table experiment

To demonstrate the TRC approach, we required a large set of DEMs and associated hydraulic data for validation and ideally straight channels where in-channel features represent the dominant source of drag. We conducted a set of experiments using the Adjustable-Boundary Experimental System (A-BES) at the University of British Columbia (Fig. 2). The A-BES comprises a 1.5 m wide by 12.2 m long tilting stream table and a recirculating water pump controlled by a digital flow meter. The experiments were run as generic Froude-scaled models with an initial bed slope of 2% and a length scale ratio of 1 : 25, based on field measurements Fishtrap Creek in British Columbia, Canada. The bulk material ranged from 0.25 to 8 mm ( $D_{\max}$ ), with a  $D_{50}$  of 1.6 mm and  $D_{84}$  of 3.2 mm (see MacKenzie and Eaton, 2017), and the grain size distribution (GSD) is included in Fig. 6.

##### 3.1.1 Experimental procedure

Roughly cast interlocking concrete bricks were configured to make two straight channels of different widths: (1) a 30 cm wide configuration that represents the scaled width of the field prototype and (2) an 8 cm wide configuration which was selected based on preliminary experiments where channel width was decreased until bar formation was suppressed entirely. Thus, the two widths yield a range of bed morphologies and hydraulic conditions.



**Figure 2.** Adjustable-Boundary Experimental System (A-BES) at the University of British Columbia, showing the camera rig and the 30 cm wide channel configuration.

A set of experiments was carried out for each configuration (Table 1), yielding two broad types of in-channel morphology: (1) pool–bar–riffle (PBR), consisting of a gently meandering, undulating thalweg with alternate bars, and (2) plane bed (PB), with no discernible morphology beyond the grain scale. The first experiment (“a”) consisted of a formative discharge (1.5 L/s for the 30 cm channel) for a duration of 16 h, where the discharge was scaled by the width of the experimental channel  $W$ . The second experiment (“b”) consisted of a flow two-thirds of the formative discharge for 16 h. The third experiment (“c”), conducted for the 30 cm wide channel only, consisted of low flow for 8 h and then three 4 h phases with discharge increasing by a factor of 1.5 each time.

Before each experiment, the bulk material was hand-mixed to minimize downstream and lateral sorting, and the channel area was screeded to the height of weirs at the upstream and downstream end. The flow was run at a low rate (at which there was little to no movement of sediment) until the bed was fully saturated and was then rapidly increased to the target flow. At the downstream end, where water free-falls over the weir, there was slight and localized lowering of the water surface due to a downdraw effect but no discernable back-water. Each period of constant discharge was divided into phases of increasing duration, between which the bed was rapidly drained (to minimize the potential for morphologic change), photographed, and re-saturated before resuming the experiment. Phases for the 16 h experiments consisted of 5, 10, 15, 30, 60, and 120 min, with four repeats of each. The 4 and 8 h periods of constant discharge followed the same sequence but did not include the longest phases. In the final 30 s of each phase, the water surface elevation was recorded at each gauge to the nearest 1 mm. Water gauges were read at an almost horizontal angle, which in conjunction with the dyed blue water, minimized systematic bias towards higher readings due to surface tension effects.

The camera rig consisted of five Canon EOS Rebel T6i DSLRs with EF-S 18–55 mm lenses, positioned at varying oblique angles in the cross-stream direction to maximize coverage of the bed, and five LED lights. Photos were taken in RAW format at 20 cm intervals, yielding a stereographic overlap of over two-thirds. Throughout the experiment, sediment collected in the trap was drained of excess water, weighed wet to the nearest 0.2 kg, placed on the conveyor belt at the upstream end, and recirculated at approximately the same rate it was output. Zero sediment was fed into the system during the first 5 min phase. For the 5 and 10 min phases, recirculation occurred at the end of the phase, and for the phases of longer duration, recirculation occurred every 15 min regardless of whether the bed was drained.

### 3.1.2 Data processing

Using the images, point clouds were produced using structure-from-motion photogrammetry in Agisoft Metashape Professional 1.6.2 at the highest resolution, yielding an average point spacing of around 0.25 mm. Twelve spatially referenced control points (and additional unreferenced ones) were distributed throughout the A-BES, which placed photogrammetric reconstructions within a local coordinate system and aided in the photo-alignment process. The point clouds were imported into RStudio where inverse distance weighting was used to produce DEMs at 1 mm horizontal resolution. Despite the use of control points, the DEMs contained a slight arch effect whereby the middle of the model was bowed upwards. This effect was first quantified by applying a quadratic function along the length of the bricks, which represent an approximately linear reference elevation (brick elevations vary by  $\pm 4$  mm). The arch was then removed by determining correction values along the length of the DEM using the residuals, which were then applied across the width of the model.

At two points in time across the experiments, Exp1a T60.1 (5 h 0 min) and Exp1c Phase 2 T30.3 (3 h 30 min), due to errors during photo collection or the photogrammetry processing, the DEMs were slightly shorter at the upstream end (9.4 and 7.9 m in length, respectively). These DEMs were still sufficiently long to include most of the bed topography and stream gauges and have been included in the following analysis.

We estimated the position of the channel thalweg in the 30 cm experiments by manually locating pool centroids and using Gaussian kernel regression to smooth the vertices between the centroids. An example of the estimated thalweg location is shown in Fig. 3. Given the absence of bars, the thalweg elevation profile of the 8 cm experiments was assumed to be the channel centreline.

By determining the position of stream gauges within the DEM, 10 wetted cross sections were reconstructed using the water surface elevation data (assuming a relatively horizontal water surface elevation), which were then used to esti-

**Table 1.** Summary of experimental conditions in the A-BES. Length refers to the median length of DEMs, which generally varies by  $\pm 0.1$  m and does not include approximately 20–30 cm of bed at the upstream end. The DEM count excludes the screeded bed which has no associated hydraulic data.

Run	Width $W$ [m] ( $\pm 0.015$ )	Length [m]	Discharge $Q$ [L/s] ( $\pm 0.03$ )	Duration [h]	DEMs	Morphology
Exp1a	0.3	10.8	1.5	16	24	PBR
Exp1b	0.3	10.7	1.0	16	24	PBR
Exp1c	0.3	11.0	0.67, 1.0, 1.5, 2.25	8, 4, 4, 4	68	PBR
Exp2a	0.08	8.7	0.4	16	24	PB
Exp2b	0.08	8.6	0.27	16	24	PB

mate reach-averaged hydraulics. Mean hydraulic depth was calculated as  $h = A/w$ , where  $A$  is cross-sectional area and  $w$  is the wetted width. Velocity was estimated using the continuity equation  $U = Q/A$ . Shear velocity is  $U^* = \sqrt{ghS}$ , where  $g$  is gravity and  $S$  is mean bed slope, and Froude number  $Fr = U/(gh)^{1/2}$ . Based on the measurement precision of stream gauge readings, errors of 6%–11% could be expected for mean hydraulic depths (relative errors are variable due to different depths), with a median of  $\pm 7.6\%$ . Accounting for the propagation of error from discharge and gauge readings, we estimate that the ratio  $U/U^*$  has a median error of  $\pm 11.5\%$ , with a maximum of  $\pm 15\%$  for the shallowest depths. A summary of reach-averaged hydraulic data is presented in Table 2.

To obtain an estimate of  $k_s$  using the hydraulic data ( $k_{s,CW}^*$ ), we used a Colebrook–White type formula defined as

$$\frac{1}{\sqrt{f}} = -K_1 \log \left( \frac{k_s}{K_2 h} + \frac{K_3}{4Re\sqrt{f}} \right), \tag{1}$$

where  $K_1 = 2.03$ ,  $K_2 = 11.09$ , and  $K_3 = 3.41$  as determined by Keulegan (1938) and  $Re$  is the Reynolds number. We neglect the second term within the logarithm as it represents the contribution of viscous forces to friction, which is likely small for hydrodynamically rough conditions. The Darcy–Weisbach friction factor  $f$  is defined as

$$\sqrt{\frac{f}{8}} = \frac{\sqrt{ghS}}{U}. \tag{2}$$

### 3.1.3 Additional experiments

In addition to the experiments conducted for this study, we obtained topographic and hydraulic data for 86 step-pool experiments published by Hohermuth and Weitbrecht (2018). The experiments were conducted in a 1 : 20 Froude-scaled model of a mountain stream, utilizing a range of bed slopes (8%–11%), channel widths (0.15–0.35 m), and unit discharges (0.019–0.167 m<sup>2</sup>/s). Four different grain size distributions were used, where  $D_{50}$  varied from 2.1–7.0 mm, and  $D_{90}$  remained around 58 mm. For a given experiment,

a range of potentially usable elevation profiles were identified based on criteria for erroneous values; then the profile closest to the channel centreline was selected. Of the 86 experiments conducted, 83 experiments are used in this study. Thus, there is a total of 247 DEMs with associated hydraulic data when combined with the A-BES experiments.

### 3.2 The transform-roughness correlation approach

Here we specifically tailor the TRC approach to the geometric and hydraulic characteristics of gravel-bed channels. First, a MODWT was applied to the thalweg elevation profiles of each DEM, yielding a set of simplified profiles representing topographic variation occurring at different wavelengths. Second, we selected a roughness correlation developed by Forooghi et al. (2017) that predicts  $k_s$  from surface geometry in the fully rough regime, which was applied to each wavelength. The relation was developed by conducting 38 direct numerical simulations in closed channels with an array of systematically varied roughness geometries, both regular and irregular. By correlating surface and flow properties, Forooghi et al. (2017) proposed the following empirical relation:

$$\frac{k_s}{k_{ref}} = F(Sk, \Delta) \cdot F(ES), \tag{3}$$

where  $k_{ref} = 4.4\sigma_z$  and  $Sk$  is the skewness of the probability distribution of elevations. The functions  $F(Sk, \Delta)$ ,  $F(Sk)$ , and  $F(ES)$  are defined, respectively, as

$$F(Sk, \Delta) = \begin{cases} F(Sk), & \Delta \geq 0.35 \\ F(Sk)(1 + m(Sk) \cdot (\Delta - \Delta_0)), & \Delta \leq 0.35 \end{cases}, \tag{4}$$

$$F(Sk) = 0.67Sk^2 + 0.93Sk + 1.3, \tag{5}$$

and

$$F(ES) = 1.05 \cdot (1 - e^{-3.8 \cdot ES}), \tag{6}$$

where  $\Delta$  is a measure of variability in the elevation of the peaks of roughness elements (height range divided by the mean;  $\Delta = 0$  if peak heights are identical),  $\Delta_0 = 0.35$  (not related to the critical ES value introduced below), and  $m(Sk) = 1.47Sk^2 - 1.35Sk - 0.66$ . The parameter ES is the

**Table 2.** Summary of A-BES experimental data collected during the final portion of each experimental phase. Values represent the mean of the last five measurements. The reported  $\sigma_z$  values were calculated following the detrending process detailed in Sect. 3.2, and  $Re^*$  was calculated with  $k = D_{84}$ . The roughness length  $k_{s,rc}^*$  is defined in Sect. 3.2. Units:  $W$  [m],  $Q$  [L/s],  $h$  [m],  $U$  [m/s],  $U^*$  [m/s],  $\sigma_z$  [m],  $k_s^*$  [m].

Exp	$W$	$Q$	$h$	$Fr$	$U$	$U^*$	$\sigma_z$	$h/D_{84}$	$h/\sigma_z$	$Re^*$	$k_{s,rc}^*$	$k_{s,CW}^*$
Exp1a	0.30	1.50	0.015	0.96	0.36	0.053	0.0055	4.09	2.67	578	0.014	0.011
Exp1b	0.30	1.00	0.012	0.86	0.30	0.049	0.0054	3.40	2.26	547	0.015	0.012
Exp1c(1)	0.30	0.67	0.012	0.61	0.21	0.048	0.0051	3.26	2.30	486	0.013	0.023
Exp1c(2)	0.30	1.00	0.014	0.72	0.26	0.051	0.0068	3.79	1.99	706	0.018	0.019
Exp1c(3)	0.30	1.50	0.015	1.01	0.38	0.054	0.0057	4.24	2.71	678	0.017	0.010
Exp1c(4)	0.30	2.25	0.018	1.03	0.44	0.060	0.0034	5.13	5.34	514	0.011	0.011
Exp2a	0.08	0.40	0.015	0.94	0.36	0.054	0.0014	4.19	10.75	196	0.005	0.012
Exp2b	0.08	0.27	0.013	0.74	0.27	0.051	0.0012	3.76	10.82	182	0.005	0.018

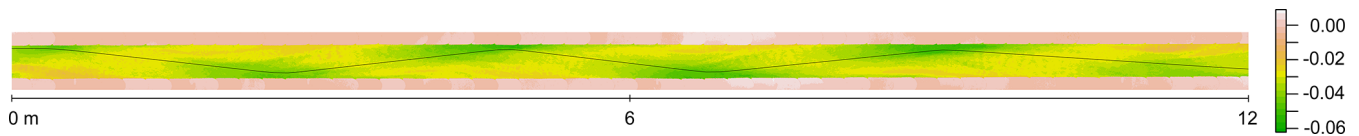


**Figure 3.** DEM of the pool–bar–riffle channel morphology at the end of Experiment 1a, with estimated position of the thalweg. Zero represents the downstream extent of the model.

effective slope, given by

$$ES = \frac{1}{L} \int_L \left| \frac{dz(x)}{dx} \right| dx, \quad (7)$$

where  $z(x)$  is the height array,  $x$  is the streamwise direction, and  $L$  is the surface length in  $x$ . Effective slope may be interpreted as the mean gradient of the local roughness elements (Napoli et al., 2008) and therefore represents the aspect ratio of roughness elements rather than their vertical height. With other surface parameters kept equal, the roughness length is strongly dependent on ES within the range  $0 < ES < 0.35$  (Napoli et al., 2008; Schultz and Flack, 2009). We calculated values of  $\Delta$  for each wavelength by identifying peaks of the oscillations and found that  $\Delta > 1$  for almost all cases. Values of  $\Delta$  could not be estimated for the longest few wavelengths as they typically contain very few (or even one) complete oscillations that could be interpreted as roughness peaks. As a result, we simply used the  $F(Sk)$  term in Eq. (4). The roughness length for each wavelength is expressed as  $k_{s,rc}$ .

In addition to applying the roughness correlation to each wavelength, we applied it to each thalweg elevation profile to obtain an estimate of  $k_s$ , expressed as  $k_{s,rc}^*$ . For this calculation, each profile was detrended using a quadratic function to remove any hydraulically irrelevant large-scale variation that  $\sigma_z$  may be sensitive to. Further detrending is not necessary with the wavelet transform as the overall trend is represented by a single wavelength and removed from all others. The experimental data and code that performs the MODWT and applies the roughness correlation are available online. In the following section, we present the results of the TRC approach applied to the experiments.

## 4 Results and discussion

In this section, we first seek to validate the TRC approach, and then focus on the multiscalar roughness length decomposition of Experiment 1a, which features a well-developed pool–bar–riffle sequence under a formative discharge. First, we compare the topographically and hydraulically based estimates of  $k_s$ . Second, we demonstrate the relationship between estimates of  $k_s$  with and without the wavelet transform. Third, we show how the key parameters of the roughness correlation (standard deviation, effective slope, skewness) vary across each wavelength. Fourth, we estimate the relative contribution of different scales of bed topography to the total roughness length and explain how the estimated values relate to the key parameters and the characteristics of the experiments. Fifth, we compare the performance of different roughness lengths in estimating flow resistance. Finally, we discuss the significance, limitations, and potential applications of the TRC approach.

### 4.1 Estimates of total $k_s$

The relationship between the estimates of  $k_s$  from the roughness correlation  $k_{s,rc}^*$  and the Colebrook–White equation  $k_{s,CW}^*$  differs between the three different channel morphologies (Fig. 4). Here, we consider  $k_{s,CW}^*$  to be a “measured” quantity which the roughness correlation may be tested against. The pool–bar–riffle experiments ( $W = 0.3$  m) exhibit the closest relationship between the two  $k_s$  estimates, with the distribution centring along the 1:1 line (median  $k_{s,CW}^*/k_{s,rc}^* = 0.96$ ). The close relationship between the two independent estimates of  $k_s$  supports the one-dimensional

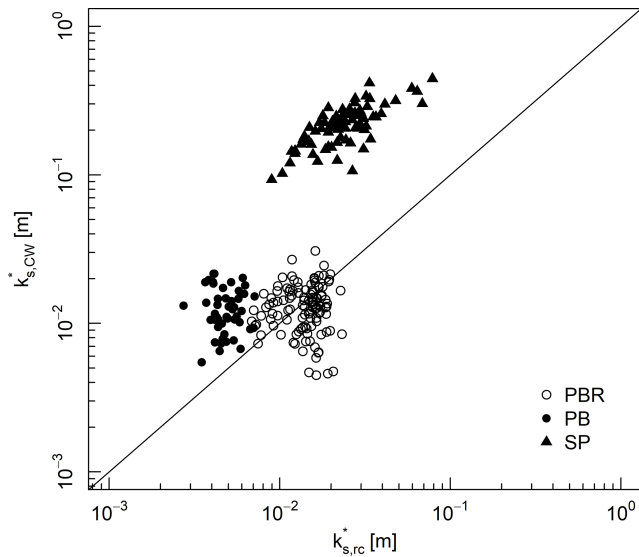


**Figure 4.** Relationship between total  $k_s$  estimated by the Forooghi et al. (2017) roughness correlation (Eq. 3) and the Colebrook–White approach (Eq. 1). Data for the A-BES experiments are grouped by channel morphology (Table 1), and the Hohermuth and Weitbrecht (2018) step–pool (SP) experiments are included.

approach for these experiments as it indicates that the single elevation profile captures the roughness elements that contribute the greatest resistance to flow. Also, the results support the application of the Forooghi et al. (2017) roughness correlation to the A-BES experiments, which have more complex surface characteristics and far lower values of relative submergence compared to the numerical domain within which the correlation was developed.

The distribution of plane-bed experiments ( $W = 0.08$  m) overlaps with the 1 : 1 line, although there is a consistent under-prediction of  $k_s$  using the roughness correlation by a factor of 2 or 3 (median  $k_{s,CW}^*/k_{s,rc}^* = 2.54$ ). In the case of the step–pool experiments, there is a significant under-prediction of  $k_s$  by the roughness correlation of around 1 order of magnitude (median  $k_{s,CW}^*/k_{s,rc}^* = 9.48$ ), which may be explained with the lower relative submergence (median  $h/D_{84} = 1.48$ ).

The next stage in validating the TRC approach is comparing the values of  $k_{s,rc}^*$  and  $\Sigma k_{s,rc}$ , whereby the latter is the estimate provided by applying the roughness correlation to each wavelength (giving values of  $k_{s,rc}$ ), and then taking the sum. In other words, this is comparing the values of  $k_s$  estimated by the roughness correlation with and without the wavelet transform as an intermediate stage. This comparison is important for two reasons. First, the TRC approach is an extension of the linear superposition approach, which assumes that the hydraulic effect of adding up different roughness elements is approximately linear (Millar, 1999; Wilcox and Wohl, 2006; Rickenmann and Recking, 2011). In practice, superimposing roughness elements may have non-linear

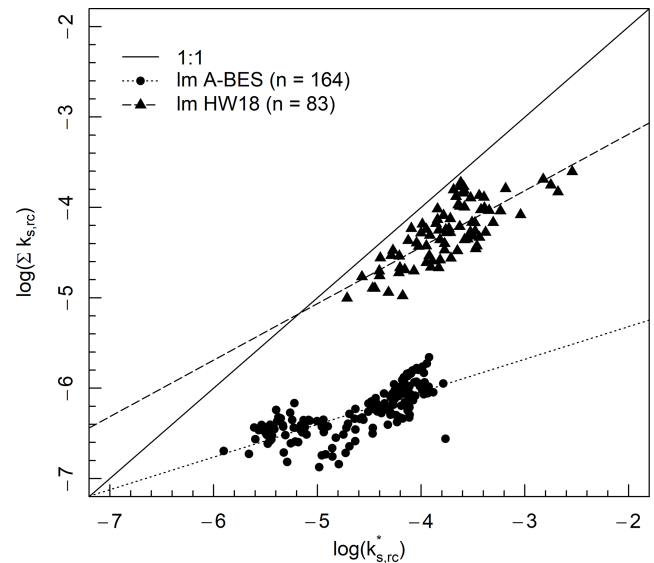


**Figure 5.** Relationship between  $k_{s,rc}^*$  and  $\Sigma k_{s,rc}$  for the A-BES and Hohermuth and Weitbrecht (2018) experiments.

feedback effects (Yen, 2002; Li, 2009; Wilcox and Wohl, 2006), such that  $k_{s,rc}^*$  and  $\Sigma k_{s,rc}$  may potentially not be correlated.

Second, values of  $k_{s,rc}^*$  and  $\Sigma k_{s,rc}$  may differ as the process of signal decomposition and recombination is characterized by wave interference. For example, for each thalweg elevation profile there are two estimates of amplitude: (1) the standard deviation of elevations  $\sigma_z$  and (2)  $\Sigma \sigma_\lambda$ , which is the sum of  $\sigma_z$  for each wavelength. However, due to positive and negative wave interference,  $\sigma_z$  and  $\Sigma \sigma_\lambda$  may significantly differ. Decomposing and recombining wavelengths alters the position and magnitude of peaks and troughs in the wavelengths and, therefore, their amplitude. Similarly, wave interference may potentially confound estimates of  $k_s$  if a transform is used. For the above two reasons, it is important to demonstrate that values of  $k_{s,rc}^*$  and  $\Sigma k_{s,rc}$  are correlated even if they are unlikely to have the same absolute value.

The transform and non-transform estimates of  $k_s$  are positively correlated with a power-law relation (Fig. 5). It is worth noting that the two datasets are characterized by different slopes and intercepts, which may be explained with the specific characteristics of each topographic dataset (e.g. geometry, resolution) giving rise to different patterns of wave interference. However, it appears that non-linear superposition effects and wave interference do not invalidate the TRC approach for these datasets.

#### 4.2 Application of TRC approach

In Experiment 1a there is a general increase in the standard deviation of elevations with increasing wavelength (Fig. 6a). Over the first 10 min (i.e. the first three elevation profiles), there is an increase in  $\sigma_z$  at  $\lambda > 0.5$  m, with the greatest in-

crease at  $\lambda \approx 2$  m, but smaller wavelengths remain largely unchanged. At the smallest wavelengths, the  $\sigma_z$  tends towards zero, and there is some contribution to  $\sigma_z$  at the largest wavelengths due to the slightly concave shape of the profile, evident in Fig. 1a. Figure 6b presents the value of  $\sigma_z$  for each wavelength as a cumulative percentage. This type of graph is similar to the form size distribution (FSD) proposed by Nyander et al. (2003), which is the cumulative variance of each wavelength calculated using a 2D DWT. For comparison, we provide the bulk grain size distribution within the same space (where wavelength is grain diameter). Grain-scale wavelengths account for less than 5% of all topographic variation, given that the arrangement of grains contribute to bed structures that usually exceed the amplitude of individual grains.

The effective slope is greatest at the grain-scale wavelengths ( $\lambda \leq D_{\max}$ ) where the surface is characterized by closely bunched peaks and troughs associated with individual grains (Fig. 7a). Values of ES decrease with increasing  $\lambda$ , due to the presence of more gently undulating roughness elements. This is evident in the example (Fig. 1c), where the 4 mm wavelength has high ES indicated by sharp oscillations (but low  $\sigma_z$ ), and the 2 m wavelength has low ES (but high  $\sigma_z$ ). The main exception to the downwards trend of ES with increasing  $\lambda$  is the wavelength of around 2 m where there is a prominent peak in the ES distribution, associated with the development of the pool–riffle–bar sequence approximately 10 min into the experiment. Note that most of the topographic wavelengths have values of ES (and  $k_s/k$  in Eq. 3) that are smaller than the surfaces used by Forooghi et al. (2017) to develop the roughness correlation. Short wavelengths tend to be positively skewed, moderate wavelengths ( $0.2 > \lambda > 2.0$  m) tend to be negatively skewed, and long wavelengths are either positively or negatively skewed (Fig. 7b). There is little change in the pattern of skewness over the course of the experiment.

The distribution of  $k_{s,rc}$  values predicted for each wavelength using Eq. (3) is presented in Fig. 8a. Following the format of “grain size distribution” and “form size distribution”, we term this style of plot the “drag size distribution” (DSD). There is a major peak in the DSD at  $\lambda \approx 2$  m (the spacing of pools, bars, and riffles) and a minor peak at the scale of  $\lambda \approx 0.008$  m (around the size of the largest grains). At small wavelengths, and large wavelengths especially, estimated  $k_s$  tends downwards. Figure 8b presents the DSD as a cumulative percentage, which shows that the  $k_s$  associated with the grain scale is estimated to account for approximately 30% of the total  $k_s$ . This proportion of grain and form drag is similar to estimates in gravel-bed rivers with similar morphologies (Hey, 1988; Parker and Peterson, 1980; Prestegard, 1983), which further indicates that the TRC approach provides a physically realistic decomposition of the roughness length.

In Fig. 9 we compare the performance of geometric ( $D_{84}$ ,  $\sigma_z$ ) and hydraulic ( $k_{s,rc}^*$ ,  $k_{s,CW}^*$ ) estimates of roughness length in estimating flow resistance, using the Ferguson (2007)

variable-power equation (VPE, Appendix A). We provide two fitted relations for the VPE that provide baselines for comparison: (1) coefficients determined by a systematic review of  $\sigma_z$  as a roughness measure (Chen et al., 2020) and (2)  $k_{s,CW}^*$  values which are back-calculated from the hydraulic measurements. Given that these two relations represent geometric and hydraulic approaches to estimating roughness, they describe significantly different relationships between the friction factor and relative submergence.

There is a weak relationship between  $f$  and  $h/k$  if  $k$  is estimated by the bulk  $D_{84}$  values (as an approximation of the surface GSD). Using  $\sigma_z$  as an estimate of  $k$ , the step–pool experiments align with the VPE relation provided by Chen et al. (2020), but  $\sigma_z$  overestimates  $k$  in the A-BES experiments. Using estimates of  $k_s$  from the roughness correlation, the values of relative submergence for the A-BES experiments are consistent with the Colebrook–White relation, but there is an under-prediction of  $k_s$  in the step–pool experiments. These results suggest that estimates of  $k_s$  from roughness correlations may provide better estimates of flow resistance in some conditions. The results also affirm that roughness metrics derived from surface topography are superior to ones derived from the grain size distribution.

## 5 Implications, applications, and limitations

Recently proposed roughness correlations in fluid dynamics (e.g. Forooghi et al., 2017; De Marchis et al., 2020) incorporate information regarding both the height of the roughness elements (a vertical roughness scale, e.g.  $\sigma_z$ ) and the arrangement or spacing of roughness elements (a horizontal roughness scale, e.g. ES). In isolation, either one of these roughness metrics may contribute to an incomplete – and potentially misleading – estimate of flow resistance. It is important to recognize that, depending on the surface of interest, the total roughness length is usually a compromise between vertical and horizontal roughness scales of the bed surface.

In gravel-bed rivers, which are typically ungauged, and where measurement of hydraulic variables is subject to practical limitations (Miller, 1958), flow resistance is usually estimated using only a vertical roughness scale such as grain diameter (Hey, 1979; Ferguson, 2007). However, the relationship between grain diameter and flow resistance breaks down in natural channels for two main reasons (see Adams, 2020a): (1) grain diameter does not account for larger and often more dissipative roughness elements, and (2) it does not consider the horizontal spacing of these larger roughness elements, which has a systematic effect on the flow (Morris, 1955; Leonardi et al., 2007). In recent years, the increased availability of high-resolution topographic data has led to the adoption of  $\sigma_z$  as a roughness metric in gravel-bed rivers, on the basis that it includes information regarding larger-scale bed structures (Chen et al., 2020). However,  $\sigma_z$  only improves upon the first deficiency of grain-based roughness

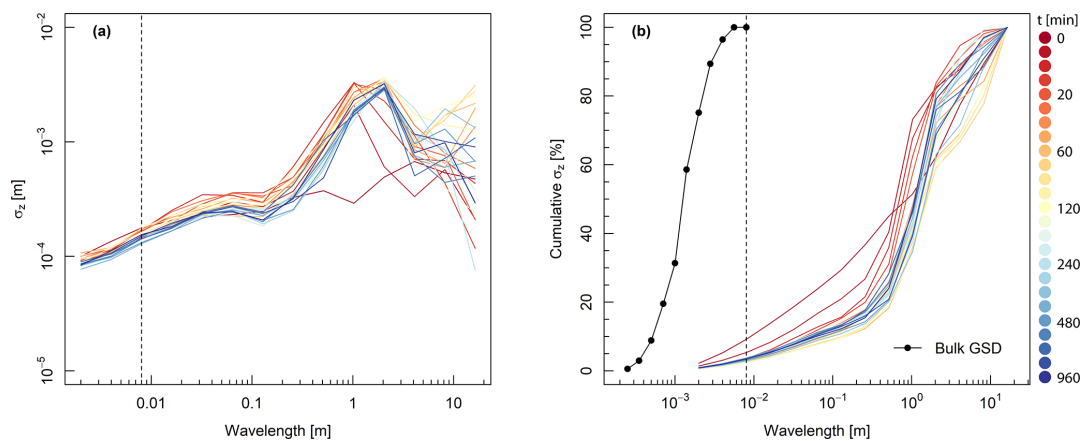


**Figure 6.** Form size distribution during Experiment 1a, where each line represents a point in time and the initial screeded bed is included. The standard deviation of each topographic wavelength is presented as an (a) absolute and (b) cumulative percentage, for each thalweg elevation profile. The bulk grain size distribution is included, where the wavelength corresponds to grain diameter. The vertical dashed line represents the largest grain diameter in the experiment.

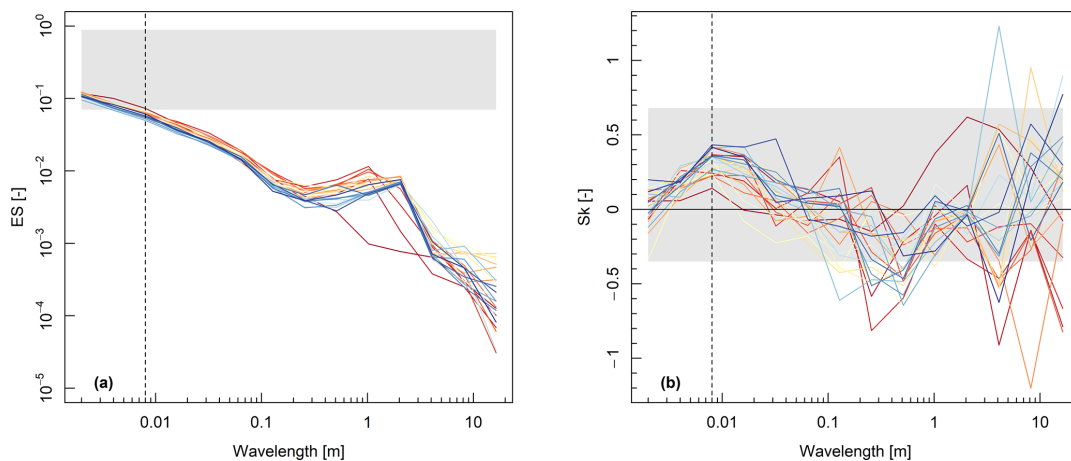


**Figure 7.** (a) Effective slope and (b) skewness of each topographic wavelength during Experiment 1a. The shaded area represents the range of ES and Sk values of the surfaces generated by Forooghi et al. (2017). Refer to Fig. 6 for legend.

metrics and, consequently, it has inherent limitations. The roughness correlation presented by Forooghi et al. (2017) may improve upon existing roughness metrics used in gravel-bed rivers, and it may be applied to most datasets where  $\sigma_z$  is calculated.

The TRC analysis has direct applications across geomorphology. Quantification of scale-dependent patterns of channel topography and roughness length may contribute to form- and process-based classifications of channel morphology and dynamics. There have been numerous attempts to classify channels based on in-channel features and their associated processes (e.g. Montgomery and Buffington, 1997); however, analysis of bed topography is typically qualitative. We expect that different channel types exhibit distinctive scale-based patterns of  $\sigma_z$  and  $k_s$ , which would enable a quantitative and heuristic classification index.

The scale-based decomposition of  $k_s$  may assist in identifying and forecasting the hydraulic influence of specific roughness elements in channels. For example, through the manipulation of spatial datasets by the addition or removal of features, the role of natural in-channel features (e.g. large wood) and engineering designs (e.g. rock chutes) could be isolated and determined for flood conditions. Also, multiscalar roughness length decomposition may contribute to an understanding of bedload transport processes, where accurate predictions rely on partitioning bed stresses between grain and form scales (Ancy, 2020).

However, in its current form, there are some conditions in which the TRC approach is limited. The discrepancy between topographic and hydraulic estimates of  $k_s$  for step-pool channels highlights the potential limitations of the roughness correlation in steep gravel-bed rivers where slope and relative submergence have a greater hydraulic influence.

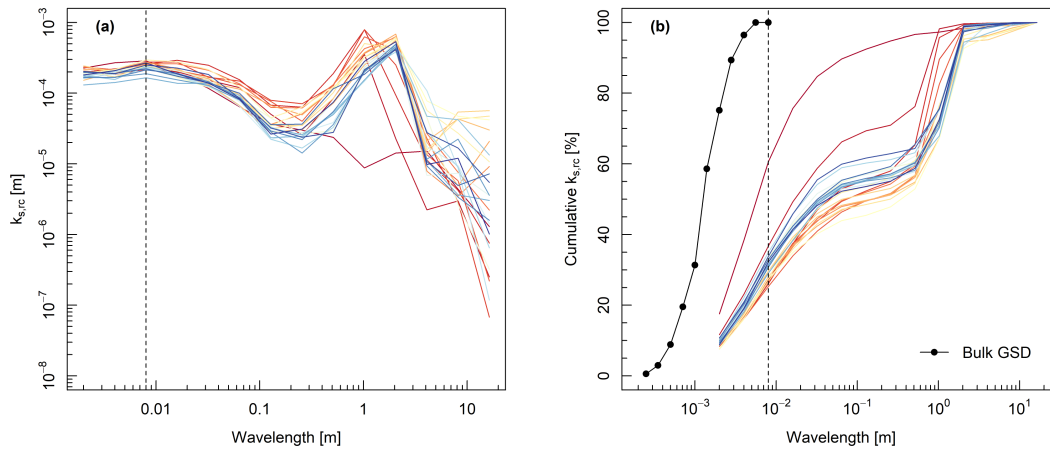


**Figure 8.** Drag size distribution over the course of Experiment 1a. The estimated roughness length of each topographic wavelength presented as an (a) absolute and (b) cumulative percentage. Refer to Fig. 6 for legend.

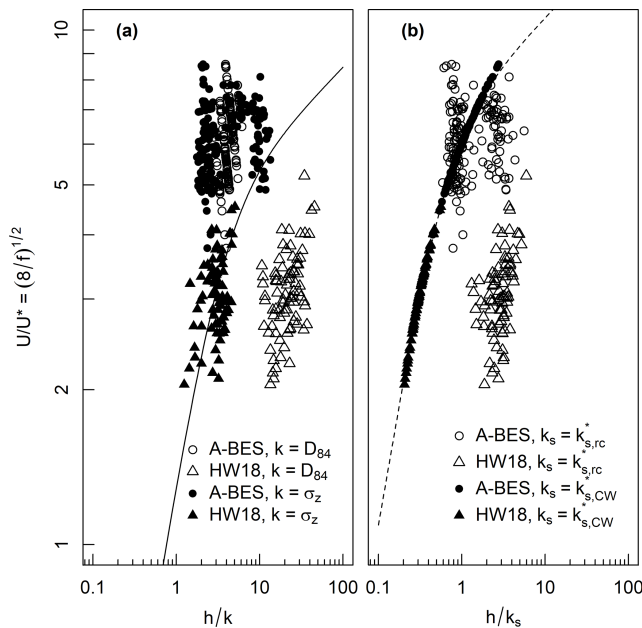


**Figure 9.** Plot of  $(8/f)^{1/2}$  against relative submergence for A-BES and Hohermuth and Weitbrecht (2018) data, using four different roughness lengths ( $D_{84}$ ,  $\sigma_z$ ,  $k_{s,rc}^*$ ,  $k_{s,CW}^*$ ). The solid line is the Ferguson (2007) VPE using coefficients  $a_1 = 3.94$  and  $a_2 = 1.36$  determined by a systematic review of  $\sigma_z$  as a roughness measure (Chen et al., 2020). The dashed line is the VPE fitted to the  $h/k_{s,CW}^*$  data, yielding coefficients of  $a_1 = 7.22$  and  $a_2 = 11.19$ .

In channels with significant planform resistance, the approach may require modification to account for the slope and curvature of the channel. In multi-thread channels, several profiles may need to be employed and the results weighted according to the size of the channel. Even under such conditions, multiscalar roughness length decomposition may still

have considerable value with appropriate research questions and interpretation.

### 6 Conclusions

The transform-roughness correlation approach estimates the relative contribution of various scales of in-channel topography to the total roughness length. By modifying the roughness correlation to suit the hydraulic conditions, multiscalar roughness length decomposition may be achieved in virtually any type of river or numerical model and perhaps boundary layers in other environments. The only requirement is that the topographic data are of a sufficient resolution and spatial extent to capture the scales over which the roughness elements occur, and data of this quality are only becoming more available to geomorphologists. In particular, we expect that given the continual advances in methods for collecting bathymetric data in both shallow (Kasvi et al., 2019) and deep channels (Dietrich, 2017), applying the TRC approach will become increasingly practical in natural rivers.

Given that the TRC approach provides novel and detailed information regarding the interaction between surface topography and fluid dynamics, it may contribute to advances in hydraulics, channel morphodynamics, and bedload transport. Estimates of  $k_s$  from roughness correlations may provide more immediate benefits by improving upon representative roughness values in estimating flow resistance. We are currently conducting experiments to further develop and apply these ideas.

**Appendix A: Ferguson (2007) variable-power equation**

Ferguson (2007) presented the variable-power flow resistance equation:

$$(8/f)^{1/2} = \frac{a_1 a_2 (h/k)}{(a_1^2 + a_2^2 (h/k)^{5/3})^{1/2}}, \quad (\text{A1})$$

where  $a_1$  and  $a_2$  are empirically derived coefficients,  $h$  is flow depth or hydraulic radius, and  $k$  is a representative roughness length.

**Code and data availability.** Data and code are available online (<https://doi.org/10.5281/zenodo.4116501>, Adams, 2020b).

**Author contributions.** DLA was responsible for conceptualization, investigation, formal analysis, and writing. AZ provided expertise in open-channel flow, contributing to the interpretation and communication of the results and the proposed technique.

**Competing interests.** The authors declare that they have no conflict of interest.

**Acknowledgements.** We would like to thank two anonymous reviewers whose comments greatly improved this paper. We also thank William Booker, Lucy MacKenzie, Brett Eaton, and Ian Rutherford for reviewing the original manuscript and Benjamin Hohermuth for providing the laboratory step-pool data. This work was supported by postgraduate scholarships provided to DLA by the Australian and Canadian governments.

**Review statement.** This paper was edited by Jens Turowski and reviewed by two anonymous referees.

## References

- Adams, D. L.: Toward bed state morphodynamics in gravel-bed rivers, *Prog. Phys. Geogr. Earth Environ.*, 44, 700–726, 2020a.
- Adams, D. L.: *adamsdl/trc* (Version v1.3), Zenodo, <https://doi.org/10.5281/zenodo.4116501>, 2020b.
- Addison, P. S.: Introduction to redundancy rules: the continuous wavelet transform comes of age, *Philosophical Transactions of the Royal Society A: Mathematical, Phys. Eng. Sci.*, 376, 1–15, 2018.
- Ancey, C.: Bedload transport: a walk between randomness and determinism. Part 2. Challenges and prospects, *J. Hydraul. Res.*, 58, 18–33, 2020.
- Ashworth, P. J. and Ferguson, R. I.: Size-selective entrainment of bed-load in gravel bed streams, *Water Resour. Res.*, 25, 627–634, 1989.
- Bray, D. I.: Flow resistance in gravel bed rivers, in: *Gravel-bed rivers*, edited by: Hey, R. D., Bathurst, J. C., and Thorne, C. R., pp. 109–133, John Wiley & Sons, Chichester, UK, 1982.
- Buffington, J. M. and Montgomery, D. R.: A systematic analysis of eight decades of incipient motion studies, with special reference to gravel-bedded rivers, *Water Resour. Res.*, 33, 1993–2029, 1997.
- Cameron, S. M., Nikora, V. I., and Stewart, M. T.: Very-large-scale motions in rough-bed open-channel flow, *J. Fluid Mech.*, 814, 416–429, 2017.
- Chen, X., Hassan, M. A., An, C., and Fu, X.: Rough correlations: Meta-analysis of roughness measures in gravel bed rivers, *Water Resour. Res.*, 56, 1–19, 2020.
- Church, M. A.: Channel Stability: Morphodynamics and the Morphology of Rivers, in: *Rivers—Physical, Fluvial and Environmental Processes*, edited by: Rowiński, P. and Radecki-Pawlik, A., pp. 427–441, Springer, 2015.
- Clifford, N. J., Robert, A., and Richards, K. S.: Estimation of flow resistance in gravel-bedded rivers: A physical explanation of the multiplier of roughness length, *Earth Surf. Proc. Land.*, 17, 111–126, 1992.
- Davies, T. R. H. and Sutherland, A. J.: Resistance to flow past deformable boundaries, *Earth Surf. Process.*, 5, 175–179, 1980.
- De Marchis, M., Saccone, D., Milici, B., and Napoli, E.: Large Eddy Simulations of Rough Turbulent Channel Flows Bounded by Irregular Roughness: Advances Toward a Universal Roughness Correlation, *Flow Turbul. Combust.*, 105, 627–648, 2020.
- Dietrich, J. T.: Bathymetric Structure-from-Motion: extracting shallow stream bathymetry from multi-view stereo photogrammetry, *Earth Surf. Proc. Land.*, 42, 355–364, 2017.
- Eaton, B. C. and Church, M. A.: A graded stream response relation for bed load-dominated streams, *J. Geophys. Res.*, 109, 1–18, 2004.
- Einstein, H. A. and Banks, R. B.: Fluid resistance of composite roughness, *Transactions of the American Geophysical Union*, 31, 603–610, 1950.
- Ferguson, R. I.: Flow resistance equations for gravel- and boulder-bed streams, *Water Resour. Res.*, 43, 1–12, 2007.
- Field, J. P. and Pelletier, J. D.: Controls on the aerodynamic roughness length and the grain-size dependence of aeolian sediment transport, *Earth Surf. Proc. Land.*, 43, 2616–2626, 2018.
- Foroghi, P., Stroh, A., Magagnato, F., Jakirlic, S., and Frohnäpfel, B.: Towards a Universal Roughness Correlation, *J. Fluids Eng.*, 139, 1–12, 2017.
- Furbish, D. J.: Conditions for geometric similarity of coarse stream-bed roughness, *Math. Geol.*, 19, 291–307, 1987.
- Hey, R. D.: Flow Resistance in Gravel-Bed Rivers, *J. Hydr. Div.*, 105, 365–379, 1979.
- Hey, R. D.: Bar Form Resistance in Gravel-Bed Rivers, *J. Hydr. Eng.*, 114, 1498–1508, 1988.
- Hohermuth, B. and Weitbrecht, V.: Influence of Bed-Load Transport on Flow Resistance of Step-Pool Channels, *Water Resour. Res.*, 54, 5567–5583, 2018.
- Jimenez, J.: Turbulent Flows over Rough Walls, *Annu. Rev. Fluid Mech.*, 36, 173–196, 2004.
- Kasvi, E., Salmela, J., Lotsari, E., Kumpula, T., and Lane, S. N.: Comparison of remote sensing based approaches for mapping bathymetry of shallow, clear water rivers, *Geomorphology*, 333, 180–197, 2019.
- Keulegan, G. H.: Laws of turbulent flow in open channels, *J. Res. Nat. Bur. Stand.*, 21, 707–741, 1938.
- Keylock, C. J., Singh, A., and Foufoula-Georgiou, E.: The complexity of gravel bed river topography examined with gradual wavelet reconstruction, *J. Geophys. Res.-Earth*, 119, 682–700, 2014.
- Kumar, P. and Foufoula-Georgiou, E.: Wavelet Analysis for geophysical applications, *Rev. Geophys.*, 34, 385–412, 1997.
- Lee, A. J. and Ferguson, R. I.: Velocity and flow resistance in step-pool streams, *Geomorphology*, 46, 59–71, 2002.
- Leonardi, S., Orlandi, P., and Antonia, R.: Properties of d- and k-type roughness in a turbulent channel flow, *Phys. Fluids*, 19, 1–6, 2007.
- Li, G.: Preliminary study of the interference of surface objects and rainfall in overland flow resistance, *Catena*, 78, 154–158, 2009.

- Limerinos, J. T.: Determination of the Manning Coefficient From Measured Bed Roughness in Natural Channels, Tech. rep., United States Geological Survey Water-Supply Paper 1898-B, 47 pp., 1970.
- MacKenzie, L. G. and Eaton, B. C.: Large grains matter: contrasting bed stability and morphodynamics during two nearly identical experiments, *Earth Surf. Proc. Land.*, 42, 1287–1295, 2017.
- Millar, R. G.: Grain and form resistance in gravel-bed rivers, *J. Hydraul. Res.*, 37, 303–312, 1999.
- Miller, J. P.: High mountain streams: Effects of geology on channel characteristics and bed material, *New Mexico State Bureau of Mines and Mine Resources Memoir* 4, 51 pp., 1958.
- Montgomery, D. R. and Buffington, J. M.: Channel-reach morphology in mountain basins, *Geol. Soc. Am. Bull.*, 109, 596–611, 1997.
- Morris, H.: A new concept of flow in rough conduits, *T. Am. Soc. Civ. Eng.*, 120, 373–398, 1955.
- Nanson, G. C. and Huang, H. Q.: A philosophy of rivers: Equilibrium states, channel evolution, teleomatic change and least action principle, *Geomorphology*, 302, 3–19, 2018.
- Napoli, E., Armenio, V., and De Marchis, M.: The effect of the slope of irregularly distributed roughness elements on turbulent wall-bounded flows, *J. Fluid Mech.*, 613, 385–394, 2008.
- Nezu, I. and Nakagawa, H.: Turbulence in open-channel flows, *IAHR Monograph Series*, pp. 1–281, 1993.
- Nield, J. M., King, J., Wiggs, G. F., Leyland, J., Bryant, R. G., Chiverrell, R. C., Darby, S. E., Eckardt, F. D., Thomas, D. S., Vircavs, L. H., and Washington, R.: Estimating aerodynamic roughness over complex surface terrain, *J. Geophys. Res.-Atmos.*, 118, 12948–12961, 2013.
- Nikuradse, J.: Laws of flow in rough pipes, Tech. rep., Washington DC, 62 pp., 1933.
- Nowell, A. R. M. and Church, M. A.: Turbulent flow in a depth-limited boundary layer, *J. Geophys. Res.*, 84, 4816–4824, 1979.
- Nyander, A.: River-bed sediment surface characterisation using wavelet transform-based methods, Doctoral thesis, Napier University, 365 pp., 2004.
- Nyander, A., Addison, P. S., McEwan, I., and Pender, G.: Analysis of river bed surface roughnesses using 2D wavelet transform-based methods, *Arab. J. Sci. Eng.*, 28, 107–121, 2003.
- Parker, G. and Peterson, A. W.: Bar Resistance of Gravel-Bed Streams, *J. Hydr. Div.*, 106, 1159–1575, 1980.
- Pelletier, J. D. and Field, J. P.: Predicting the roughness length of turbulent flows over landscapes with multi-scale microtopography, *Earth Surf. Dynam.*, 4, 391–405, <https://doi.org/10.5194/esurf-4-391-2016>, 2016.
- Prestegard, K. L.: Bar resistance in gravel bed streams at bankfull stage, *Water Resour. Res.*, 19, 472–476, 1983.
- Rickenmann, D. and Recking, A.: Evaluation of flow resistance in gravel-bed rivers through a large field data set, *Water Resour. Res.*, 47, W07538, <https://doi.org/10.1029/2010WR009793>, 2011.
- Robert, A.: Statistical properties of sediment bed profiles in alluvial channels, *Math. Geol.*, 20, 205–225, 1988.
- Schlichting, V. H.: Experimentelle untersuchungen zum Rauheitsproblem, *Arch. Appl. Mech.*, 7, 1–34, 1936.
- Schlichting, V. H.: *Boundary-Layer Theory*, McGraw-Hill, New York, 7th edn., 1979.
- Schultz, M. P. and Flack, K. A.: Turbulent boundary layers on a systematically varied rough wall, *Phys. Fluids*, 21, 1–9, 2009.
- Torrence, C. and Compo, G. P.: A practical guide to wavelet analysis, *B. Am. Meteorol. Soc.*, 79, 61–78, 1998.
- Wilcox, A. C. and Wohl, E. E.: Flow resistance dynamics in step-pool stream channels: 1. Large woody debris and controls on total resistance, *Water Resour. Res.*, 42, 1–16, 2006.
- Wolman, M. G. and Miller, J. P.: Magnitude and Frequency of Forces in Geomorphic Processes, *J. Geol.*, 68, 54–74, 1960.
- Yen, B. C.: Open channel flow resistance, *J. Hydr. Eng.*, 128, 20–39, 2002.

# **Appendix D**

## **Publication: Chapter 6**



# A comparison of 1D and 2D bedload transport functions under high excess shear stress conditions in laterally constrained gravel-bed rivers: a laboratory study

David L. Adams<sup>1,2</sup> and Brett C. Eaton<sup>1</sup>

<sup>1</sup>Department of Geography, University of British Columbia, Vancouver, BC, Canada

<sup>2</sup>School of Geography, Earth and Atmospheric Sciences, University of Melbourne, Melbourne, Australia

Correspondence: David L. Adams (dladams@alumni.ubc.ca)

Received: 15 March 2022 – Discussion started: 5 April 2022

Revised: 26 July 2022 – Accepted: 29 August 2022 – Published: 15 September 2022

**Abstract.** Channel processes under high-magnitude flow events are of central interest to river science and management as they may produce large volumes of sediment transport and geomorphic work. However, bedload transport processes under these conditions are poorly understood due to data collection limitations and the prevalence of physical models that restrict feedbacks surrounding morphologic adjustment. The extension of mechanistic bedload transport equations to gravel-bed rivers has emphasised the importance of variance in both entraining (shear stress) and resisting (grain size) forces, especially at low excess shear stresses. Using a fixed-bank laboratory model, we tested the hypothesis that bedload transport in rivers collapses to a more simple function (i.e. with mean shear stress and median grain size) under high excess shear stress conditions. Bedload transport was well explained by the mean shear stress (1D approach) calculated using the depth–slope product. Numerically modelling shear stress to account for the variance in shear stress (2D) did not substantially improve the correlation. Critical dimensionless shear stress values were back-calculated and were higher for the 2D approach compared to the 1D. This result suggests that 2D critical values account for the relatively greater influence of high shear stresses, whereas the 1D approach assumes that the mean shear stress is sufficient to mobilise the median grain size. While the 2D approach may have a stronger conceptual basis, the 1D approach performs unreasonably well under high excess shear stress conditions. Further work is required to substantiate these findings in laterally adjustable channels.

## 1 Introduction

The adjustment of rivers to the imposed valley gradient, sediment supply, and discharge is of central interest to geomorphology and has implications for understanding and managing natural hazards and ecological habitats. In alluvial channels, the adjustment is facilitated by the movement of sediment arising via the interaction between the flow and deformable boundary (Bridge and Jarvis, 1982; Dietrich and Smith, 1983; Church, 2010; Church and Ferguson, 2015). Despite there being no strict correlation between the magnitudes of perturbation and geomorphic effect (Lisenby et al.,

2018), larger-than-average flows (i.e. floods) are typically associated with channel adjustment and relatively large volumes of geomorphic work (Wolman and Miller, 1960). Extreme events may exert disproportionate control over the channel planform (Eaton and Lapointe, 2001). The study of sediment transport processes under these relatively high discharge events is central to understanding river behaviour.

Researchers have dedicated considerable effort to deriving mechanistic bedload transport functions – typically empirically calibrated – that relate the rate of movement to a force balance between the flow and individual particles. Other approaches exist: for example, non-threshold approaches that

do not utilise a critical shear stress (Recking, 2013a). One of the most simple and widely used threshold relations is the Meyer-Peter and Müller (1948) equation that estimates bedload transport as a function of mean excess bed shear stress ( $\bar{\tau} - \tau_c$ , where  $\tau_c$  is critical shear stress) for a given grain diameter, typically the median (i.e.  $\tau_{c50}$  for the  $D_{50}$  grain). The extension of 1D bedload transport functions to gravel-bed rivers, typically characterised by a wide range of grain sizes, necessitated several modifications that accounted for the differential mobility of grain sizes, hiding, and exposure (Parker and Klingeman, 1982; Parker, 1990; Recking, 2013b; Wilcock and Crowe, 2003). Further research emphasised that at conditions in which  $\bar{\tau} \approx \tau_{c50}$ , bedload transport is affected by the spatial variance in shear stress (Paola and Seal, 1995; Paola, 1996; Nicholas, 2000; Ferguson, 2003; Bertoldi et al., 2009; Francalanci et al., 2012; Recking et al., 2016). More recently, Monsalve et al. (2020) proposed a 2D bedload transport function that integrates across the distribution of shear stresses and can predict transport at lower flow conditions in which  $\bar{\tau} < \tau_{c50}$ . In concert, these advances demonstrate a consistent trend: with decreasing excess shear stress more information regarding grain size and shear stress (i.e. resisting and driving forces) is required to predict bedload transport.

Considerably less is known about rivers under high relative shear stress conditions  $\bar{\tau} \gg \tau_{c50}$ , in which most channel change occurs. This is primarily due to practical limitations. Dangers associated with floods and erosion mean that researchers may collect data before and after an event, but not during. Laboratory experiments (flumes) typically do not incorporate key degrees of freedom for morphologic adjustment that are available to alluvial channels and thus do not model the full range of feedbacks between bedload transport and the deformable boundary. Subsequently, the notion that bedload transport in rivers collapses to a more simple function (i.e. with mean shear stress and median grain size) under high excess shear stress conditions is yet to be conclusively demonstrated. If verified, it would serve as a highly convenient assumption in understanding landscape evolution and river management. Smaller-scale laboratory experiments provide an opportunity to test this hypothesis as they model larger-scale bed and ideally bank adjustments.

We test the relative performance of 1D and 2D bedload transport functions under high relative shear stress conditions in a Froude-scaled physical model. The experiments have a widely graded sediment mixture and develop alternate bars under pseudo-recirculating conditions at a range of widths and discharges. We record total bedload volumes and bathymetry, and we perform 2D hydraulic modelling to apply several transport functions akin to Meyer-Peter and Müller (1948) (i.e. based on median grain size) that capture different levels of information regarding shear stress. The results highlight the effectiveness of simple threshold-based bedload transport functions under high relative shear stress conditions in laterally constrained channels, as well as differences be-



**Figure 1.** Adjustable-Boundary Experimental System (A-BES) at the University of British Columbia, featuring camera rig (top right) and bank control system at a width of 30 cm.

tween 1D and 2D conceptualisations of excess shear stress and bedload transport.

## 2 Methodology

Experiments were performed in the Adjustable-Boundary Experimental System (A-BES) at the University of British Columbia (Fig. 1), some of which have been reported by Adams and Zampiron (2020). The A-BES comprises a 1.5 m wide by 12.2 m long tilting stream table; the experiments were run as generic Froude-scaled models based on 2003 field measurements from Fishtrap Creek in British Columbia, Canada. The channel had a gradient  $S$  of  $0.02 \text{ m m}^{-1}$ , average bankfull width of 10 m, formative discharge of approximately  $7500 \text{ L s}^{-1}$ , and bulk  $D_{50}$  of 55 mm. With a length scale ratio of 1 : 25, the A-BES was scaled to within around 30 % of the prototype, with an initial width of 0.30 m, formative discharge  $Q$  of approximately  $1.5 \text{ L s}^{-1}$ , and  $D_{50}$  of 1.6 mm ( $D_{84} = 3.2 \text{ mm}$ ,  $D_{90} = 3.9 \text{ mm}$ ; GSD2 in MacKenzie and Eaton, 2017). The sediment mixture comprised natural clasts with a density of around  $2500 \text{ kg m}^{-3}$ .

The experiments utilised interlocking landscaping bricks to constrict the channel to various widths  $W$  between approximately 0.30 and 0.60 m. In addition to the various channel widths, four different unit discharges ( $q = Q/W$ ) were used across the experiments (i.e. discharge was scaled by width) that increased by a factor of 1.5 (Table 1). Two constant-discharge runs used the middle two discharges, and one multi-discharge run consisted of the four discharge phases in increasing order. A full list of experiments is provided in Table 2.

At the beginning of each experiment the bulk mixture was mixed by hand to minimise lateral and downstream sorting, and then the in-channel area was screeded to the height of weirs at the upstream and downstream end using a tool that rolled along the brick surface. The flow was run at a low rate

**Table 1.** Summary of unit discharges  $q$  ( $Q/W$ ) used in each phase (P) of experimental runs a–c.

	Unit discharge $q$ [ $L\ m^{-1}\ s^{-1}$ ]			
	P1	P2	P3	P4
Run a	5.00			
Run b	3.33			
Run c	2.22	3.33	5.00	7.50

with little to no movement of sediment until the bed was fully saturated, and it was then rapidly increased to the target flow.

Three different types of data were collected throughout each experiment; surface photos, stream gauge measurements, and sediment output. A rolling camera rig positioned atop the A-BES consisted of five Canon EOS Rebel T6i DSLRs with EF-S 18–55 mm lenses (set at 30 mm) positioned at varying oblique angles in the cross-stream direction to maximise coverage of the bed, as well as five LED lights. Photos were taken in RAW format at 0.2 m downstream intervals, providing a stereographic overlap of over two-thirds. A total of 10 water stage gauges comprised of a measuring tape on flat boards were located along the inner edge of the bricks every 1 m. To minimise edge effects, gauges were not placed within 0.60 m of either the inlet or the outlet. The gauges were read at an almost horizontal angle, which, in conjunction with the dyed blue water, minimised systematic bias towards higher readings due to surface tension effects.

The data collection procedure was designed to maximise measurement accuracy as much as reasonably possible. Given that stream gauge data would later be paired with topographic data, the timing of gauge readings needed to closely coincide with surface photography. Every time photos were taken the bed was drained, as the surface water would distort the photos. These constraints necessitated a procedure in which manual stream gauge readings (to the nearest 1 mm) were taken 30–40 s before the bed was rapidly drained, which is around the minimum time it would take to obtain the readings. The bed was then photographed and gradually re-saturated before resuming the experiment, which took approximately 10 min.

Each discharge phase was divided into a series of segments between which the data were collected. The procedure occurred in 5, 10, 15, 30, 60, and 120 min segments with four repeats of each (i.e.  $4 \times 5$  min,  $4 \times 10$  min, and so on), which was designed to reflect the relatively rapid rate of morphologic change at the beginning of each phase. For example, in wider channels, alternate bars developed within an hour, and there was relatively little morphologic change in the following hours (Adams and Zampiron, 2020; Adams, 2021).

Throughout the experiments, sediment falling over the downstream weir was collected in a mesh bucket, drained of excess water, weighed damp to the nearest 0.2 kg, placed on the conveyor belt at the upstream end, and gradually recircu-

lated at the same rate it was output, as opposed to a “slug” (i.e. all at once) injection. Based on a range of samples collected across the experiments, we determined the weight proportion of water to be approximately 5.8 % and applied this correction factor to obtain approximate dry weights. There was no initial feed of sediment, although this no-feed period was only 5 min. The experiments are best described as pseudo-recirculating as sediment was measured and recirculated at the end of the 5 and 10 min segments and, for longer segments (i.e. 30, 60, 120 min), every 15 min.

## 2.1 Data processing

Using the images, point clouds were produced using structure-from-motion photogrammetry in Agisoft MetaShape Professional 1.6.2 at the highest resolution, yielding an average point spacing of around 0.25 mm. A total of 12 spatially referenced control points and additional unreferenced ones were distributed throughout the A-BES, which placed photogrammetric reconstructions within a local coordinate system and aided in the photo-alignment process. Using inverse distance weighting, the point clouds were converted to digital elevation models (DEMs) at 1 mm horizontal resolution.

Despite the use of control points, the DEMs contained a slight arch effect in the downstream direction whereby the middle of the model was bowed upwards, which was an artefact of the photogrammetric reconstruction (see doming: James and Robson, 2014). This effect was first quantified by applying a quadratic function (on average:  $p < 0.001$ ,  $r^2 = 0.999$ ,  $RMSE = 0.0017$  mm) along the length of the bricks, which represent an approximately linear reference elevation (brick elevations vary randomly by  $\pm 2$  mm). The arch was then removed by determining correction values along the length of the DEM using the residuals, which were then applied across the width of the model. The final least-squares linear fit along the brick surface was homoscedastic with an average root mean square error (RMSE) of 0.0018 mm (around the maximum height difference between adjacent bricks), indicating that the DEM was successfully corrected.

For each DEM, 10 wetted cross-sections were reconstructed using the water surface elevation data, which were then used to estimate reach-averaged hydraulics. For more detailed spatial analysis, the flow conditions of water depth and shear stress were reconstructed using a 2D numerical flow model (Nays2DH) to the final DEM of each discharge phase. The selection of the final DEM was arbitrary as any DEM over the steady-state portion of the experiment could have been selected. Nays2DH is a two-dimensional, depth-averaged, unsteady flow model that solves the Saint-Venant equations of free surface flow with finite differencing based on a general curvilinear coordinate system (further details can be found in Nelson et al., 2016). Notably, local shear stress is calculated using the bed friction coefficient and depth-averaged flow velocity components. Key input bound-

**Table 2.** Summary of experiments conducted in the A-BES. The DEM count excludes screeded bed. Experiment 1 is published in Adams and Zampiron (2020).

Exp.	$W$ [m]	$Q$ [ $L s^{-1}$ ]	Duration [h]	DEMs
Exp1a	0.30	1.50	16	24
Exp1b	0.30	1.00	16	24
Exp1c	0.30	0.66, 1.00, 1.50, 2.25	8, 4, 4, 4	20, 16, 16, 16
Exp3a	0.45	2.25	16	24
Exp3b	0.45	1.50	16	24
Exp3c	0.45	1.00, 1.50, 2.25, 3.37	8, 4, 4, 4	20, 16, 16, 16
Exp4a	0.60	2.00	16	24
Exp4b	0.60	3.00	16	24
Exp4c	0.60	1.33, 2.00, 3.00, 4.50	8, 4, 4, 4	20, 16, 16, 16

ary conditions are the channel DEM, an initial estimate of reach-averaged Manning's  $n$ , cell resolution, and the water discharge. We selected an  $n$  value of 0.045 based on the channel conditions, a cell resolution equivalent to 5 mm, and a flow duration of 200 s, which was sufficient to establish convergence. After an initial model run, we back-calculated a spatially variable value using the flow resistance law presented by Ferguson (2007) that accounts for the influence of relative roughness,

$$(8/f)^{1/2} = \frac{a_1 a_2 (d/k)}{(a_1^2 + a_2^2 (d/k)^{5/3})^{1/2}}, \quad (1)$$

where  $f$  is the Darcy–Weisbach friction factor,  $a_1$  and  $a_2$  are empirically derived coefficients,  $d$  is local flow depth, and the representative roughness length  $k = D_{84}$ . The spatially variable roughness value was used as an input to run the solver again.

To minimise rounding errors associated with the relatively shallow depths in our experiments, the DEM size and discharge were adjusted to the prototype scale (i.e. using a length scale ratio of 25). The estimated water depths, shear stresses, and velocities from Nays2DH were then back-transformed to the model scale (Table 3). We removed cells with relatively shallow flows defined arbitrarily as depths less than  $2D_{84}$  (6.4 mm) as they contributed a large peak in the frequency distribution of flow depths and likely account for a small proportion of bedload activity. Across the flow models, grid cells with flows less than this threshold accounted for 20%–63% of the channel area where  $d > 0$  but only 1%–21% of the total cross-sectional flow area (mean 11%). This is consistent with visual observations of dispersive and stagnant flow at the channel margins. We defined areas of the bed with flows above the  $2D_{84}$  threshold as “wetted”. The mean-normalised (i.e. local value divided by reach average) frequency distributions of flow depths and shear stresses were fitted with gamma and Gaussian distributions (coefficients in Table 3), for which the goodness of fit was assessed using both Kolmogorov–Smirnov and Anderson–Darling tests.

The results of the flow model were quantitatively validated by comparing measured reach-averaged hydraulic depths

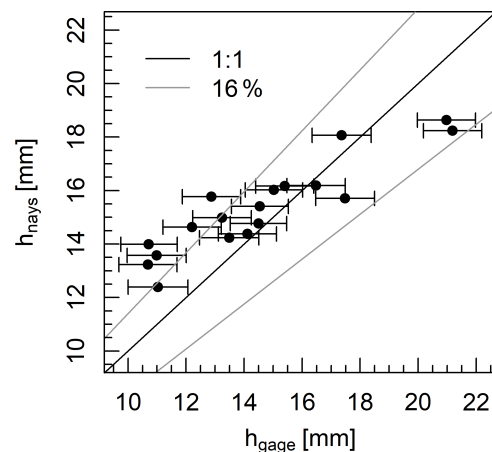


**Figure 2.** Measured versus modelled mean hydraulic depth  $h$  (i.e. reach-averaged) at the end of each experimental phase, featuring 16% bounds. Error bars are based on the measurement precision of the stream gauges.

( $h = A_c/w$ , where  $A_c$  is flow cross-sectional area and  $w$  is wetted width) to modelled ones (Fig. 2). Most estimates fell within 10%–15% of the line of equality, although the flow model estimated a narrower range (approximately 12–18 mm) of mean hydraulic depths across the experiments compared to the stream gauge measurements (11–21 mm). Stream gauges are easily biased towards deep or shallow flows due to there being only 10 fixed points, thus explaining the wider range of the estimates. The stream gauges only serve as an approximation to validate the flow model. Based on the measurement precision of the stream gauge readings (1 mm), random errors of 6%–11% could be expected for mean hydraulic depths.

## 2.2 Determining a representative sediment transport rate

The channels were formed under constant discharge conditions for 4–16 h, beginning from either a screeded bed or a morphology developed at a lower discharge. Each exper-

**Table 3.** Summary of reach-averaged hydraulics (from the 2D flow model) and sediment transport (from measurements). Parameters are as follows.  $w$ : wetted width [m],  $d$ : flow depth [m],  $U$ : velocity [ $\text{m s}^{-1}$ ],  $Fr$ : Froude number,  $Re$ : Reynolds number ( $Ud/\nu$ , where  $\nu$  is the kinematic viscosity),  $\bar{\tau}$ : mean shear stress [Pa],  $q_b$ : unit bedload transport [ $\text{kg m}^{-1} \text{min}^{-1}$ ],  $\sigma_{q_b}$  is the standard deviation of unit bedload transport,  $\sigma_{\tau}$  is the standard deviation of shear stress, and  $\alpha$  and  $\beta$  parameters describe the fitted gamma distribution of shear stress. The parameters A1, A2, B1, and B2 refer to the four approaches outlined in Table 4.

Exp.	$w$	$d$	$w/d$	$U$	$Fr$	$Re$	$\bar{\tau}$	$q_b$	$\sigma_{q_b}$	A1	A2	A3	A4	$\sigma_{\tau}$	$\alpha$	$\beta$
1a	0.26	0.015	17.2	0.36	0.92	4117	2.58	2.03	0.33	1.49	0.97	1.42	0.84	0.46	3.80	0.26
1b	0.21	0.013	15.9	0.31	0.83	3132	2.25	1.38	0.31	0.93	0.69	0.84	0.61	0.50	3.15	0.32
1(1)	0.18	0.012	15.0	0.28	0.80	2528	2.01	0.58	0.18	0.58	0.36	0.46	0.30	0.49	3.04	0.33
1(2)	0.21	0.013	16.6	0.30	0.81	2995	2.19	1.20	0.25	0.83	0.63	0.74	0.79	0.53	2.41	0.42
1(3)	0.26	0.016	16.5	0.34	0.87	4116	2.76	2.11	0.19	1.84	1.22	1.62	1.03	0.46	3.60	0.28
1(4)	0.28	0.018	15.1	0.44	1.03	6118	3.27	3.98	0.29	2.98	1.94	2.77	1.30	0.39	5.79	0.17
3a	0.37	0.015	25.3	0.34	0.87	3869	2.54	2.99	0.41	1.42	1.15	1.31	1.10	0.49	2.79	0.36
3b	0.28	0.014	20.0	0.33	0.87	3609	2.40	1.76	0.74	1.18	0.74	1.11	0.87	0.47	3.09	0.32
3c(1)	0.23	0.013	17.9	0.30	0.83	3010	2.17	1.02	0.27	0.81	0.42	0.80	0.40	0.46	3.24	0.31
3c(2)	0.29	0.013	22.1	0.31	0.83	3173	2.29	1.85	0.22	0.99	0.68	0.84	0.82	0.49	3.04	0.33
3c(3)	0.36	0.015	23.6	0.35	0.89	4083	2.61	2.53	0.38	1.54	1.18	1.44	1.27	0.50	2.54	0.39
3c(4)	0.40	0.017	23.5	0.41	0.97	5405	3.16	4.83	0.57	2.72	2.00	2.27	1.82	0.47	3.30	0.30
4a	0.48	0.015	32.2	0.35	0.89	3966	2.63	3.05	0.88	1.59	1.24	1.32	1.19	0.50	2.90	0.34
4b	0.40	0.013	29.6	0.31	0.81	3194	2.21	1.72	0.49	0.87	0.65	0.89	0.95	0.53	2.15	0.46
4c(1)	0.31	0.013	23.5	0.31	0.84	3114	2.17	0.94	0.37	0.81	0.38	0.83	0.50	0.49	2.45	0.41
4c(2)	0.39	0.014	28.2	0.32	0.85	3398	2.30	1.88	0.40	1.00	0.68	0.99	0.91	0.50	2.94	0.34
4c(3)	0.46	0.015	29.9	0.37	0.93	4390	2.76	3.27	0.80	1.84	1.19	1.55	1.18	0.45	2.82	0.35
4c(4)	0.57	0.018	32.1	0.42	0.97	5660	3.17	4.64	0.55	2.73	1.63	2.50	1.90	0.40	5.15	0.19

imental phase comprised an initial adjustment period during which morphology, hydraulics, and sediment transport were nonstationary. This adjustment period, which varied from minutes to an hour, was followed by a steady-state period during which these characteristics fluctuated around a mean value (see Adams, 2020, and Adams and Zampiron, 2020). Under recirculating conditions, the stationarity of bedload transport represents a condition in which there is no net aggradation or degradation over time. In Fig. 3 we present two typical examples of sediment transport fluctuations under constant conditions for 16 h. In both examples, there is a brief adjustment period with less sediment transport, followed by fluctuations around a mean value. These fluctuations were explained by processes such as bar reshaping and sediment waves (e.g. Dhont and Ancy, 2018), which are outside the scope of this study.

We determined a representative sediment transport rate for each experimental phase by averaging output over the final 3 h period (Table 3), thus removing the initial adjustment period. There was little difference between averaging over the final hour versus the final 3 h, with almost all average sediment output values being  $\pm 12.5\%$ . There were three instances in which these two averaging windows yielded values differing by 15%–25% due to high-magnitude fluctuations around an otherwise stationary bedload transport rate. In addition, we calculated the standard deviation of sediment output over the final 3 h period.

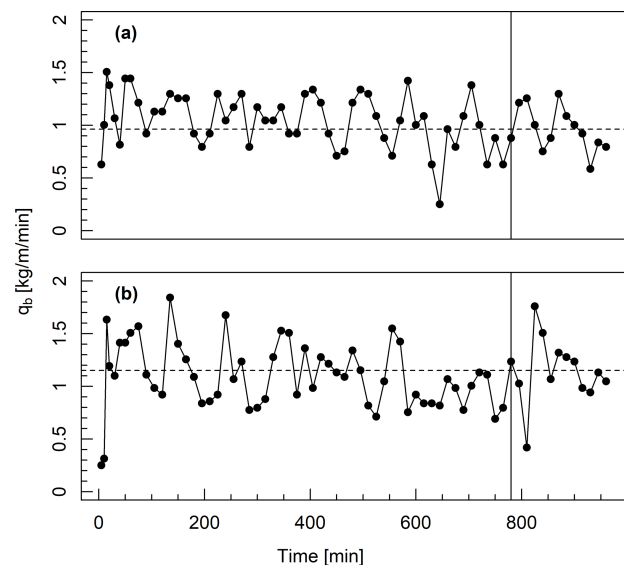


**Figure 3.** Width-averaged bedload transport over time in two experiments with different widths but similar reach-averaged shear stress: (a) experiment 1b ( $W = 0.30$  m,  $\bar{\tau} = 2.34$  Pa) and (b) experiment 4b ( $W = 0.60$  m,  $\bar{\tau} = 2.28$  Pa). The beginning of the time window over which bedload transport is averaged is indicated by the solid vertical line, and mean transport over this period is indicated by a horizontal dashed line.

### 2.3 1D and 2D excess shear stress

We examined the correlation between the observed representative sediment transport rate and two formulations of excess shear stress based on the Meyer-Peter and Müller (1948) equation,

$$q_b = k(\bar{\tau} - \tau_c)^{1.6}, \quad (2)$$

where  $q_b$  is width-averaged bedload transport,  $k$  accounts for flow resistance and the relative density of sediment, and the exponent 1.6 is based on Wong and Parker (2006). The value of  $k$  is highly variable across empirical datasets, whereas the exponent is relatively consistent (Gomez and Church, 1989). The critical shear stress value for the  $D_{50}$  ( $\tau_{c50}$ ) is estimated by  $\tau_c^* g(\rho_s - \rho)D$ , where  $\tau_c^*$  is the dimensionless critical shear stress,  $g$  is gravity,  $\rho$  is the density of water, and  $\rho_s$  is the density of sediment

We aimed to investigate the concepts underlying 1D and 2D bedload transport equations rather than to refine them. Subsequently, we ignored the parameter  $k$  that typically varies across channels and simplified Eq. (2) to express the correlation between observed sediment transport and mean excess shear stress (raised to the exponent).

$$q_b \propto (\bar{\tau} - \tau_{c50})^{1.6} \quad (3)$$

This equation was modified to integrate across the distribution of local shear stresses,

$$q_b \propto \int (\tau_{(x)} - \tau_{c50})^{1.6} dx/A, \quad (4)$$

where  $\tau_{(x)}$  is local bed shear stress and  $A$  is the total bed area. Equations (3) and (4) are 1D and 2D approaches to correlating observed transport capacity with excess shear stress. We applied both equations using shear stress values calculated in two ways: (1) the depth–slope product ( $\tau = \rho g d S$ ) based on numerically modelled flow depths and (2) numerically modelled shear stresses, thus yielding four different approaches (Table 4). Each of these approaches is summarised in Appendix A. We intentionally did not account for sinuosity or sidewall effects in the depth–slope product approach. In the case of the 1D depth–slope approach, depth was calculated using the mean depth and mean channel gradient, whereas in the 2D depth–slope we varied depth but the gradient remained constant. For each approach, we back-calculated the optimal value of  $\tau_c^*$  by systematically varying it and finding the strongest correlation (least-squares linear fit) between  $q_b$  and excess shear stress (i.e.  $[\bar{\tau} - \tau_{c50}]^{1.6}$  or  $\Sigma[\tau_x - \tau_{c50}]^{1.6}/A$ ), indexed by root mean square error (RMSE), which is shown in Fig. 4. We report optimised values of  $\tau_c^*$  and least-squares goodness-of-fit statistics in Table 4 and also include values obtained using the exponent 1.5 in each equation.

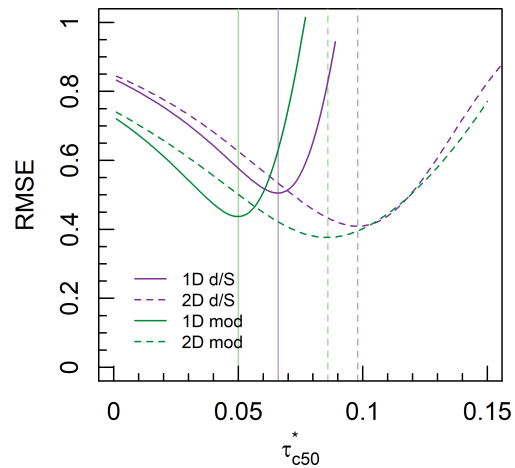


**Figure 4.** The correlation between  $q_b$  and excess shear stress (indexed by RMSE) with varying critical dimensionless shear stress for each approach. A back-calculated critical dimensionless value is indicated where RMSE is lowest (Table 4).

### 3 Results

Under the imposed channel widths (0.30–0.60 m) and unit discharges ( $2.22$ – $7.50 \text{ L m}^{-1} \text{ s}^{-1}$ ) all channels developed an alternate bar morphology with pools, bars, and riffles (see Fig. 5 for an example). Especially at low unit discharges, wetted areas ( $d > 2D_{84}$ ) on average occupied only a portion of the total available width: between 52 % and 95 %. When unit discharge was calculated using the wetted width, it was closely correlated with mean shear stress based on least-squares linear regression (Fig. 6a), indicating a coupled adjustment between active width and shear stress.

The depth–slope method of calculating mean shear stress estimated higher values compared to the numerical model (7 %–23 %) and also higher values of critical dimensionless shear stress in the corresponding transport functions ( $\tau_c^* = 0.066$  and  $0.050$ , respectively; Table 4). Both methods yielded similar estimates of excess shear stress ( $\bar{\tau}/\tau_{c50} = 1.36$ – $2.11$  and  $1.56$ – $2.53$ , respectively). The strong correlation between the two estimates of shear stress supports the assumption that at the reach scale  $\bar{\tau} \approx \rho g d S$ .

Estimated values of  $\tau_c^*$  using the 2D approaches were consistently higher than the values obtained using the 1D approaches, but they were slightly less sensitive to how shear stress was calculated ( $\tau_c^* \approx 0.095$  for both methods). Based on the 2D approach, the proportion of the wetted bed area experiencing excess shear stress was linearly related to unit discharge and ranged between 37 % and 84 % (Fig. 6b). In several experiments 2D estimates of  $\tau_{c50}$  were higher than  $\bar{\tau}$ .

Local shear stresses at or below the mean were estimated to exceed  $\tau_{c50}$  only at unit discharges exceeding approximately  $5 \text{ L m}^{-1} \text{ s}^{-1}$  (Fig. 6). This range of shear stresses (i.e.  $\tau_{c50} < \tau < \bar{\tau}$ ) accounted for up to 37 % of the total bed area at the highest flows. These results indicate considerable shear

**Table 4.** Optimised values of  $\tau_c^*$  and goodness-of-fit statistics for correlations between excess shear stress and observed bedload transport using four different approaches. Values obtained using the exponent 1.5 are presented in parentheses, and  $\bar{\tau}/\tau_{c50}$  represents the range of relative shear stress values across the experiments.

Approach	Equation	$\tau$ method	$\tau_c^*$	$r^2$	RMSE	$\bar{\tau}/\tau_{c50}$
A1	3 (1D)	$d/S$	0.066 (0.069)	0.96	0.51 (0.50)	1.36–2.11
A2	4 (2D)	$d/S$	0.098 (0.101)	0.98	0.41 (0.40)	0.30–1.90
B1	3 (1D)	modelled	0.050 (0.053)	0.97	0.44 (0.43)	1.56–2.53
B2	4 (2D)	modelled	0.086 (0.090)	0.98	0.38 (0.37)	0.36–2.00

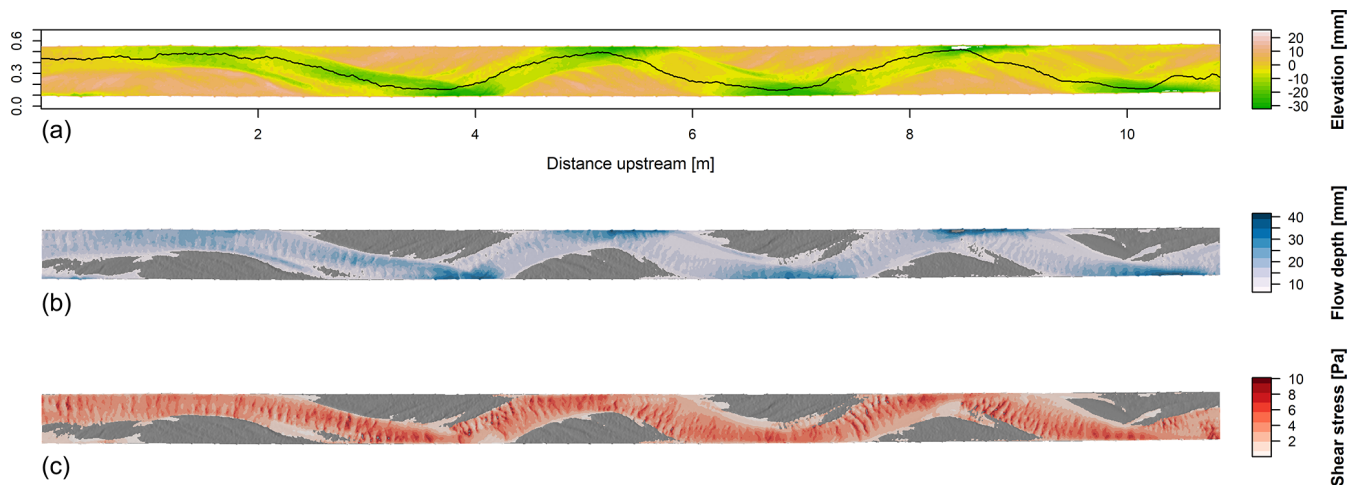


**Figure 5.** Channel area at the conclusion of experiment 3b ( $W = 0.45$  m,  $\bar{\tau} = 2.41$  Pa) displaying the following characteristics (a–c): (a) elevation, (b) flow depth, and (c) shear stress from the flow model. Cells where  $d < 2D_{84}$  are not shown. A transect along the path of the highest bed shear stress is displayed as a black line.

stress concentration and the relative insignificance of moderate shear stresses in bedload transport. We further visualise shear stress distributions and estimated critical values using examples in Fig. 7b.

Frequency distributions of mean-normalised flow depth and shear stress (over each  $5 \times 5$  mm grid cell) followed both Gaussian and gamma distributions (Fig. 7a), confirmed by both Kolmogorov–Smirnov and Anderson–Darling tests ( $p < 0.1$ ). These distributions were qualitatively similar based on their cumulative distributions following the removal of shallow depths, which contributed a second mode of flow depths corresponding to dispersive flow or stagnant water at the channel margins. In the case of the shear stress distributions, the shape parameter  $\alpha$  was linearly related to unit discharge based on least-squares regression (RMSE = 0.69,  $r^2 = 0.39$ ,  $p < 0.01$ ), and the scale parameter  $\beta$  was negatively correlated (RMSE = 0.58,  $r^2 = 0.32$ ,  $p < 0.01$ ). The parameters of the gamma distribution indicate that with increasing unit discharge the distribution of shear stress became more concentrated and less positively skewed.

Despite following similar frequency distributions, modelled local flow depth and shear stress were not strongly coupled spatially (Fig. 8). These two parameters were roughly

correlated but with considerable scatter, whereby for a given grid cell mean-normalised shear stress was commonly more than a factor of 2 greater or less than normalised flow depth (i.e. high shear stress and deep flows are close but not at exactly the same locations). The spatial decoupling of flow depth and shear stress is also evident in Fig. 5, especially where areas of high shear stress are estimated to occur immediately downstream of pools where flow is deepest.

We present the correlation between bedload transport and the four different representations of excess shear stress in Fig. 9. These represent combinations of two different methods of calculating bed shear stress – the depth–slope product and numerical modelling – against 1D and 2D representations of excess shear stress (Table 4). All four methods yielded similar correlations between excess shear stress and observed bedload transport, as indicated by RMSE values between 0.38 and 0.51; these end values correspond to the 2D modelled shear stress (B2) and 1D depth–slope product approach (A1), respectively. Changing the exponent from 1.6 to 1.5 in Eqs. (3) and (4) had almost no effect on the estimated values of  $\tau_c^*$  or the prediction errors. Altering the representative grain size from  $D_{50}$  to  $D_{84}$  had no effect on the correlation between  $q_b$  and excess shear stress (i.e. identical

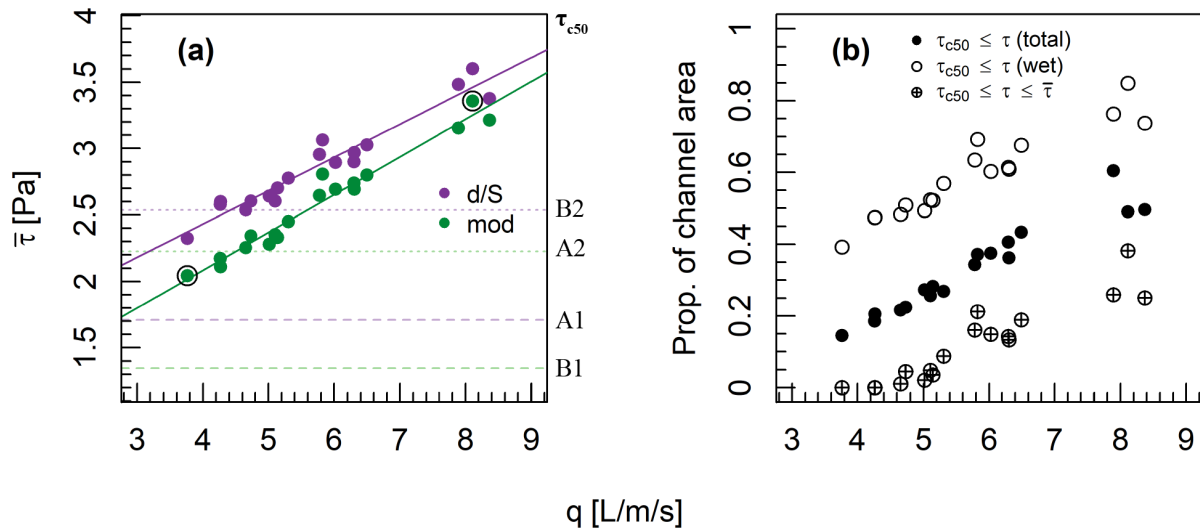


**Figure 6.** (a) Relationship between unit discharge  $q$  (calculated using wetted width) and mean shear stress  $\bar{\tau}$  using depth–slope product (RMSE = 0.097,  $r^2 = 0.93$ ,  $p < 0.001$ ) and modelled shear stresses (RMSE = 0.073,  $r^2 = 0.96$ ,  $p < 0.001$ ). Horizontal lines indicate fitted values of  $\tau_{c50}$ , and circled points indicate channels with the highest and lowest shear stress used in Fig. 7b. (b) Relationship between unit discharge and the proportion of the wetted channel area ( $d > 2D_{84}$ ) where  $\tau > \tau_{c50}$  using modelled shear stresses (i.e. approach B2), as well as the proportion of channel area where  $\tau_{c50} < \tau \leq \bar{\tau}$ .

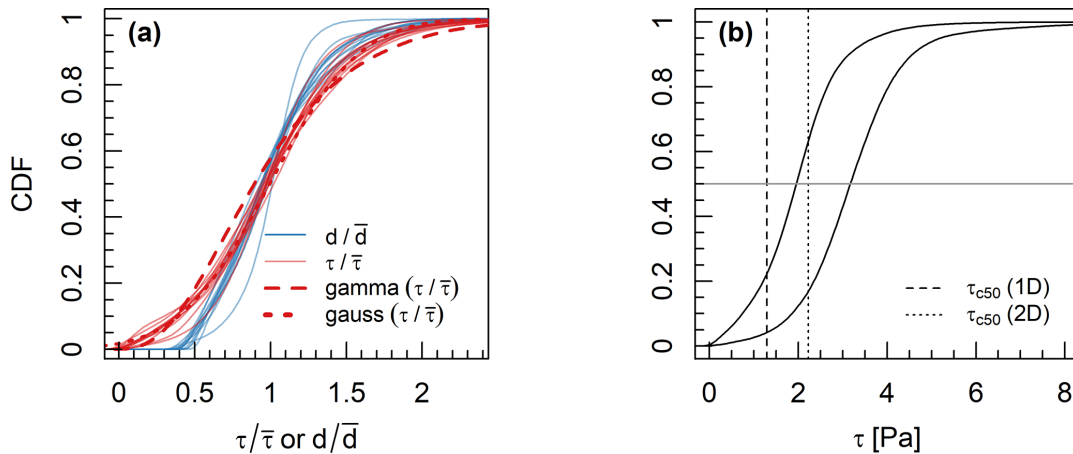


**Figure 7.** (a) Cumulative frequency distributions of mean-normalised modelled flow depth and shear stress at the end of each experimental phase, in which the upper end of the kernel density distribution has been truncated to approximately the 99th percentile to remove outliers. Note the absence of shallow depths ( $d < 2D_{84}$ ). The average gamma distribution fit for the normalised shear stress distribution is included ( $\alpha = 3.30, \beta = 0.30$ ), as is the average Gaussian fitted distribution ( $\sigma = 0.47$ ). (b) Cumulative frequency distribution of non-normalised modelled shear stresses in experimental phases with the highest (Exp1c(4)) and lowest (Exp1c(1)) mean shear stress (circled points in Fig. 6). Estimates of  $\tau_{c50}$  using 1D and 2D approaches (B1 and B2, respectively) are indicated by dashed lines, and the horizontal line is the median shear stress, which closely corresponds to the mean.

RMSE), and it merely reduced the back-calculated estimates of  $\tau_c^*$ .

#### 4 Discussion

These experiments had several advantages over traditional field and flume datasets in modelling and recording channel processes. Although the experiments did not model lat-

eral adjustment, the smaller scale ratio (1 : 25) allowed for morphology and processes at a larger scale compared to most flumes with width–depth ratios between approximately 15 and 40. The bulk mixture comprised a wide range of grain sizes (0.5–8.0 mm) that have been demonstrated to modulate channel adjustment, especially under conditions in which the larger-than-average grain size is only partially mobile (MacKenzie and Eaton, 2017; MacKenzie et al., 2018;

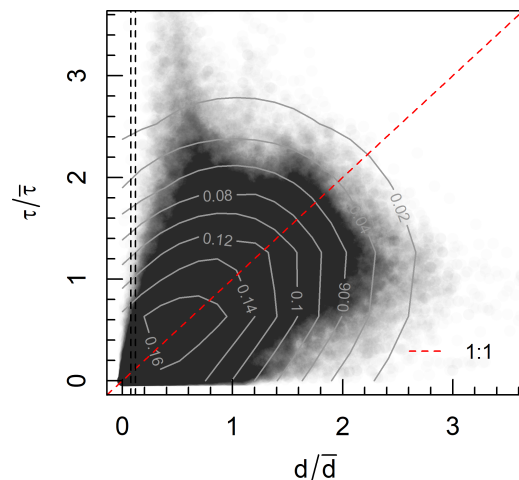


**Figure 8.** Relationship between local mean-normalised flow depth and shear stress across all experiments, produced by randomly sampling 10 % of cells from each flow model. Contour lines represent 2D kernel density estimation, and vertical dashed lines indicate the range of flow depths used to threshold the flow model.

Booker and Eaton, 2020; Adams, 2021). We measured total bedload volumes and adjustments to bed topography during flood stages, which is not possible in the field or in many recirculating experiments. The applied flows were longer and more constant than floods typically observed in nature (4–16 h experimental time or 20–80 h in the field prototype), which allowed the experiments to reach an idealised steady state whereby morphology, hydraulics, and bedload fluctuated around a mean condition (Fig. 3). These characteristics make the experimental dataset appropriate for investigating the effectiveness of bedload transport equations in laterally constrained gravel-bed rivers under high relative shear stress conditions.

We evaluated four different bedload transport functions based on the correlation between excess shear stress and observed volumes of bedload transport, averaged over the final 3 h of each experimental phase. We first focus our discussion on three of these approaches in increasing order of sophistication (A1, B1, then B2) and then explain their relative effectiveness. Finally, we discuss the conceptual differences between 1D and 2D bedload transport functions.

#### 4.1 Comparison between prediction errors

Most bedload transport functions index the applied excess shear stress using the mean depth–slope product as these data are relatively easy to collect in field contexts (Gomez and Church, 1989; Barry et al., 2004; Recking, 2013b). This approach relies on the assumption that local variations in channel gradient and flow depth cancel out such that mean flow depth is proportional to mean shear stress (Nicholas, 2000; Ferguson, 2003). We did indeed observe this condition whereby mean-normalised flow depth and shear stress fol-

lowed similar frequency distributions (Fig. 7a), despite being spatially decoupled (Fig. 8). The approach A1 (1D depth–slope product) in our analysis was the most simplistic and, in addition, did not account for sinuosity (note the slight sinuosity in Fig. 5 that reduced the mean channel gradient), flow resistance, or energy losses to the channel banks. The strength of the correlation between excess shear stress and bedload transport (RMSE = 0.51) provides an approximate reference point for other approaches.

In recent decades, technological advancements in remote sensing and hydraulic modelling have allowed researchers to directly model bed shear stress, thus providing a potentially more accurate estimate. This advancement is utilised in the B1 approach (1D modelled shear stress), which accounted for the effect of sinuosity, flow resistance, and energy losses to the channel banks. Accounting for these additional factors may explain the 13 % reduction in RMSE (0.44) compared to approach A1. Further advancements have led to the proliferation of 2D hydraulic models and some 2D bedload transport equations, which aim to account for the proportion of the bed participating in transport and the spatial variation in shear stress (Monsalve et al., 2020). The B2 approach (2D modelled shear stress) that integrates across the frequency distribution of shear stresses did not significantly improve upon approach A1, with a similar RMSE (0.38) as approach B1.

Numerical modelling of shear stress and accounting for its frequency distribution led to similarly strong correlations between bedload transport and excess shear stress compared to the mean depth–slope product method. The ability of the mean shear stress to effectively capture variation in bedload transport is consistent with empirical evidence. In a reanalysis of data from Oak Creek, OR, Monsalve et al. (2020) compared the Parker and Klingeman (1982) equation to a modified 2D version and found that accounting for the distribution of shear stresses reduced prediction error by only 13 %. Their study modelled a range of flows to the same bathymetry, and we obtained a similar result when the bed was allowed to fully adjust to the imposed flow. Using numerical and analytical models, several studies have predicted that variance in shear stress may enhance bedload transport but that this effect rapidly diminishes when  $\bar{\tau} \gg \tau_c$  (Ferguson, 2003; Francalanci et al., 2012; Recking, 2013a). The most probable reason for this sensitivity is the nonlinearity of the bedload transport law, which means that around  $\bar{\tau} \approx \tau_c$  small increases in  $\tau$  produce relatively large increases in bedload transport. The similar effectiveness of 1D and 2D functions herein provides empirical evidence that bedload transport is less sensitive to the shape of the shear stress distribution under high relative shear stress conditions.

#### 4.2 Comparison between 1D and 2D approaches

The four approaches demonstrated key differences based on how shear stress was calculated (depth–slope product vs. numerical modelling) and more importantly the formulation

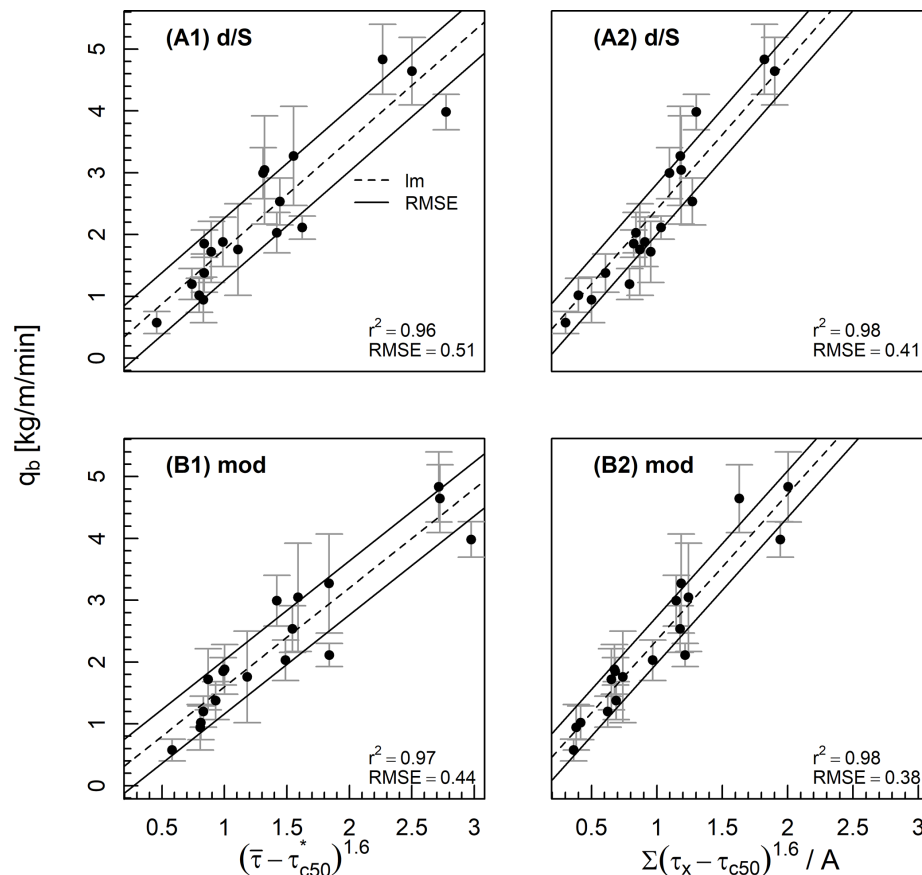


**Figure 9.** Correlation between excess shear stress and observed bedload transport (averaged over the final 3 h of each experiment) using the four approaches outlined in Table 4. The dashed black line is the least-squares best fit, solid black lines indicate  $\pm 1$  RMSE, and whiskers indicate  $\pm 1$  standard deviation over the final 3 h of sediment output measurements.

(1D vs. 2D). Both estimates of mean shear stress were linearly related to unit discharge, but those based on the depth–slope product were 7%–23% higher (Fig. 6), which is consistent with findings by Monsalve et al. (2020). These differences in estimated shear stress led to approximately commensurate differences in the estimated 1D values of  $\tau_c^*$  (32% higher). Both 1D estimates of  $\tau_c^*$  were relatively high for gravel-bed rivers but were within the range of reported estimates from both field and laboratory channels (Buffington and Montgomery, 1997).

Despite having similar prediction errors, the 1D and 2D functions provided considerably different estimates of critical dimensionless shear stress. Using the 2D approach, estimates of  $\tau_c^*$  were 48% and 72% higher than the 1D depth–slope and modelled shear stress methods, respectively. In several channels, the estimated critical shear stress was greater than the mean shear stress, but bedload transport was observed and well predicted by the model (Fig. 6), which in the case of a threshold-based 1D equation would correspond to zero estimated transport. This is a distinct advantage of 2D equations at low flows, as they can account for flows wherein

excess shear stress occupies only a fraction of the bed (Monsalve et al., 2020).

The differences between estimates of  $\tau_c^*$  arise from differences in how the equations conceptualise excess shear stress. In a 1D equation, when bedload transport data are available,  $\tau_c$  may be back-calculated from the mean shear stress, as is done herein. The value of  $\tau_c^*$  is adjusted until excess shear stress explains the observed bedload transport, assuming that  $\bar{\tau}$  is responsible for all entrainment. In contrast, the 2D equation does not assume that the mean shear stress participates in bedload entrainment. Based on the 2D approach, we estimated that the mean shear stress did not exceed the estimated critical value for the  $D_{50}$  until a certain discharge threshold ( $5 \text{ L m}^{-1} \text{ s}^{-1}$ ), and even under the highest flows these areas (i.e.  $\tau_{c50} < \tau < \bar{\tau}$ ) characterised a maximum of 37% of the wetted area. We did not validate these values as we did not anticipate the need for observation, although the estimates appear reasonable compared to our visual observations of the experiments. This result suggests that the mean shear stress is far less significant for bedload transport compared to the larger-than-average stresses, which is intuitive, especially

given that these are the first stresses to entrain bed material as the flow is increased.

By conceptualising transport as a function of mean shear stress, 1D equations may inflate the importance of relatively moderate shear stresses and deflate values of  $\tau_c^*$ . This insight is based on back-calculated values rather than measurements of incipient motion, although it is important to note that studies measuring incipient motion have also been based on the mean shear stress, and therefore this 1D paradigm is subsumed within the results (Gilbert, 1914; Kramer, 1935; Neill and Yalin, 1969; Wilcock, 1988). We also relied on spatio-temporally integrated rather than instantaneous local shear stresses that promote entrainment (e.g. Nelson et al., 1995). Nevertheless, the higher estimates of critical dimensionless shear stress using the 2D approach, evaluated by considering the relative importance of shear stresses across the frequency distribution, may have a stronger conceptual basis. More broadly, the results highlight that as long as  $\tau_c$  is back-calculated, its value will be highly dependent on how shear stress is estimated and whether its distribution is treated one- or two-dimensionally.

The results may have implications for non-threshold approaches to predicting bedload transport in natural gravel-bed rivers (Parker et al., 1982; Parker, 1990; Wilcock and Crowe, 2003; Recking, 2013a). These approaches recognise that usage of a single critical shear stress is ineffective at low flows and is always an approximation, especially in the case of partial transport conditions in which not all grain sizes (or even grains of a given size) are equally mobile (Wilcock and McArdell, 1993). The effectiveness of threshold-based approaches under high excess shear stresses suggests that in channels with fully developed morphology and a wide range of grain sizes, non-threshold-based approaches may not render an improvement. Also, the results challenge recent critiques of bedload transport predictions based on mean shear stress, particularly the depth–slope assumption (Yager et al., 2018). Although there is a poor mechanistic link between shear stress and bedload transport (e.g. Nelson et al., 1995), this approximation may be unreasonably effective when applied at a sufficiently large spatio-temporal scale or excess shear stress.

Further work is required to investigate differences in 1D and 2D estimates of  $\tau_c^*$  under lower excess shear stress conditions. If broadly applicable, the effectiveness of highly reductionist bedload transport functions based only on median grain size and mean shear stress would present a convenient assumption for researchers and practitioners interested in channel-forming flows. More research is required to substantiate this approach under supply-limited conditions and realistic hydrographs that enable both upward and downward adjustments with inherited channel conditions. Given that our experiments do not allow for significant lateral adjustment and meandering, the results are most applicable to channels confined by bedrock or with cohesive or highly vegetated banks. Fully alluvial channels comprise additional feedbacks

that are worthy of investigation, and the extent to which these affect reach-averaged bedload transport remains poorly understood.

## 5 Conclusions

We investigated the performance of 1D and 2D bedload transport functions under high relative shear stress conditions in a Froude-scaled physical model. The analysis highlights the effectiveness of highly reductionist bedload transport functions based only on median grain size and mean shear stress calculated using the depth–slope product. Numerically modelling shear stress to account for flow resistance and energy losses from the channel planform and banks did not substantially reduce prediction error, nor did accounting for the relative importance of shear stresses across the frequency distribution. The results suggest that bedload transport may collapse to a more simple function (i.e. with average shear stress and grain size) under high excess shear stress conditions. Given that the channels herein have limited lateral mobility, our conclusions are most applicable to channels where lateral adjustment is suppressed. Further work is required to examine the effect of planform adjustments (widening, meandering), for which small-scale laboratory experiments serve as an effective research tool. The 1D and 2D approaches provided substantially different estimates of critical dimensionless shear stress, reflecting differences in how these approaches conceptualise excess shear stress. Estimates of  $\tau_c^*$  from 2D functions may have a stronger conceptual basis, as they are derived by considering the relative importance of shear stresses across the frequency distribution and do not assume that the mean shear stress is sufficient to mobilise the median grain size.

## Appendix A: Four bedload transport equations

A1 Approach A1: mean shear stress assuming depth–slope product

$$q_b \propto (\bar{\tau} - \tau_{c50})^{1.6} \quad (\text{A1})$$

Here,  $q_b$  is unit bedload transport,  $\bar{\tau}$  is estimated with  $\rho g d S$  (where  $g$  is gravity,  $d$  is mean flow depth from a 2D flow model, and  $S$  is the channel gradient), and  $\tau_{c50}$  is estimated by  $\tau_c^* g (\rho_s - \rho) D$ , where  $\tau_c^*$  is the dimensionless critical shear stress chosen using the best fit (Table 4),  $\rho$  is the density of water, and  $\rho_s$  is the density of sediment.

A2 Approach A2: distribution of shear stresses assuming depth–slope product

$$q_b \propto \int (\tau_{(x)} - \tau_{c50})^{1.6} dx / A \quad (\text{A2})$$

Here,  $\tau_{(x)}$  is the local bed shear stress calculated using local depth from a 2D flow model ( $\rho g d_{(x)} S$ ), and  $A$  is the total active bed area (defined as areas where  $d > 2D_{84}$ ).

A3 Approach B1: mean shear stress based on numerical model

$$q_b \propto (\bar{\tau} - \tau_{c50})^{1.6} \quad (\text{A3})$$

Here,  $\bar{\tau}$  is estimated using a 2D flow model.

A4 Approach B2: distribution of shear stresses based on numerical model

$$q_b \propto \int (\tau_{(x)} - \tau_{c50})^{1.6} dx / A \quad (\text{A4})$$

Here,  $\tau_{(x)}$  values are based on a 2D flow model.

**Code and data availability.** Raw hydraulic and sediment transport data from Tables 3 and 4 and Figs. 2, 3, and 6–8 are available at Zenodo (<https://doi.org/10.5281/zenodo.6795606>, Adams, 2022) with an open license.

**Author contributions.** DLA was responsible for conceptualisation, data collection, formal analysis, visualisation, and writing. BCE was responsible for supervision, review, and editing.

**Competing interests.** The contact author has declared that neither of the authors has any competing interests.

**Disclaimer.** Publisher's note: Copernicus Publications remains neutral with regard to jurisdictional claims in published maps and institutional affiliations.

**Acknowledgements.** We would like to thank Rob Ferguson, Lucy MacKenzie, Will Booker, and two reviewers whose suggestions have greatly improved the paper.

**Financial support.** This work was supported by graduate scholarships provided by the Canadian and Australian governments, as well as a postgraduate writing-up award (Albert Shimmins Fund) from the University of Melbourne.

**Review statement.** This paper was edited by Rebecca Hodge and reviewed by Chenge An and one anonymous referee.

## References

- Adams, D. L.: Toward bed state morphodynamics in gravel-bed rivers, *Prog. Phys. Geog.*, 44, 700–726, <https://doi.org/10.1177/0309133320900924>, 2020.
- Adams, D. L.: Morphodynamics of an erodible channel under varying discharge, *Earth Surf. Proc. Land.*, 2021.

- Adams, D. L.: ESurf\_DA\_v1.1, Zenodo [code], <https://doi.org/10.5281/zenodo.6795606>, 2022.
- Adams, D. L. and Zampiron, A.: Short communication: Multi-scalar roughness length decomposition in fluvial systems using a transform-roughness correlation (TRC) approach, *Earth Surf. Dynam.*, 8, 1039–1051, <https://doi.org/10.5194/esurf-8-1039-2020>, 2020.
- Barry, J. J., Buffington, J. M., and King, J. G.: A general power equation for predicting bed load transport rates in gravel bed rivers, *Water Resour. Res.*, 40, 1–22, <https://doi.org/10.1029/2004WR003190>, 2004.
- Bertoldi, W., Ashmore, P. E., and Tubino, M.: A method for estimating the mean bed load flux in braided rivers, *Geomorphology*, 103, 330–340, <https://doi.org/10.1016/j.geomorph.2008.06.014>, 2009.
- Booker, W. H. and Eaton, B. C.: Stabilising large grains in self-forming steep channels, *Earth Surf. Dynam.*, 8, 51–67, <https://doi.org/10.5194/esurf-8-51-2020>, 2020.
- Bridge, J. S. and Jarvis, J.: The dynamics of a river bend: a study in flow and sedimentary processes, *Sedimentology*, 29, 499–542, 1982.
- Buffington, J. M. and Montgomery, D. R.: A systematic analysis of eight decades of incipient motion studies, with special reference to gravel-bedded rivers, *Water Resour. Res.*, 33, 1993–2029, <https://doi.org/10.1029/97WR03138>, 1997.
- Church, M. A.: The trajectory of geomorphology, *Prog. Phys. Geog.*, 34, 265–286, <https://doi.org/10.1177/0309133310363992>, 2010.
- Church, M. A. and Ferguson, R. I.: Morphodynamics: Rivers beyond steady state, *Water Resour. Res.*, 51, 1883–1897, <https://doi.org/10.1002/2014WR016862>, 2015.
- Dhont, B. and Ancey, C.: Are Bedload Transport Pulses in Gravel Bed Rivers Created by Bar Migration or Sediment Waves?, *Geophys. Res. Lett.*, 45, 5501–5508, <https://doi.org/10.1029/2018GL077792>, 2018.
- Dietrich, W. E. and Smith, J. D.: Processes controlling the equilibrium bed morphology in river meanders., in: *River Meandering*, edited by Elliot, C., American Society of Civil Engineers, New York, NY, 759–769, ISBNs: 0872623939 and 9780872623934, 1983.
- Eaton, B. C. and Lapointe, M. F.: Effects of large floods on sediment transport and reach morphology in the cobble-bed Sainte Marguerite River, *Geomorphology*, 40, 291–309, [https://doi.org/10.1016/S0169-555X\(01\)00056-3](https://doi.org/10.1016/S0169-555X(01)00056-3), 2001.
- Ferguson, R. I.: The missing dimension: effects of lateral variation on 1-D calculations of fluvial bedload transport, *Geomorphology*, 56, 1–14, 2003.
- Ferguson, R. I.: Flow resistance equations for gravel- and boulder-bed streams, *Water Resour. Res.*, 43, 1–12, <https://doi.org/10.1029/2006WR005422>, 2007.
- Francalanci, S., Solari, L., Toffolon, M., and Parker, G.: Do alternate bars affect sediment transport and flow resistance in gravel-bed rivers?, *Earth Surf. Proc. Land.*, 37, 866–875, <https://doi.org/10.1002/esp.3217>, 2012.
- Gilbert, G. K.: The transportation of debris by running water, Tech. rep., United States Geological Survey Professional Paper 86, <https://doi.org/10.3133/pp86>, 1914.

- Gomez, B. and Church, M. A.: An Assessment of Bed Load Sediment Transport Formulae Bed Rivers, *Water Resour. Res.*, 25, 1161–1186, 1989.
- James, M. R. and Robson, S.: Mitigating systematic error in topographic models derived from UAV and ground-based image networks, *Earth Surf. Proc. Land.*, 39, 1413–1420, 2014.
- Kramer, H.: Sand mixtures and sand movement in fluvial model, *T. Am. Soc. Civ. Eng.*, 100, 798–838, 1935.
- Lisenby, P. E., Croke, J., and Fryirs, K. A.: Geomorphic effectiveness: a linear concept in a non-linear world, *Earth Surf. Proc. Land.*, 43, 4–20, <https://doi.org/10.1002/esp.4096>, 2018.
- MacKenzie, L. G. and Eaton, B. C.: Large grains matter: contrasting bed stability and morphodynamics during two nearly identical experiments, *Earth S. Proc. Land.*, 42, 1287–1295, <https://doi.org/10.1002/esp.4122>, 2017.
- MacKenzie, L. G., Eaton, B. C., and Church, M. A.: Breaking from the average: Why large grains matter in gravel bed streams, *Earth Surf. Proc. Land.*, 43, 3190–3196, <https://doi.org/10.1002/esp.4465>, 2018.
- Meyer-Peter, E. and Müller, R.: Formulas for bed-load transport, in: *Proceedings of the 3rd Meeting of the International Association for Hydraulic Structures Research*, Stockholm, Sweden, June 1948, 1–26, 1948.
- Monsalve, A., Segura, C., Hucke, N., and Katz, S.: A bed load transport equation based on the spatial distribution of shear stress – Oak Creek revisited, *Earth Surf. Dynam.*, 8, 825–839, <https://doi.org/10.5194/esurf-8-825-2020>, 2020.
- Neill, C. R. and Yalin, M. S.: Quantitative definition of beginning of bed movement, *J. Hydr. Eng. Div.*, 95, 585–587, 1969.
- Nelson, J. M., Shreve, R. L., McLean, S. R., and Drake, T. G.: Role of Near-Bed Turbulence Structure in Bed Load Transport and Bed Form Mechanics, *Water Resour. Res.*, 31, 2071–2086, 1995.
- Nelson, J. M., Shimizu, Y., Abe, T., Asahi, K., Gamou, M., Inoue, T., Iwasaki, T., Kakinuma, T., Kawamura, S., Kimura, I., Kyuka, T., McDonald, R. R., Nabi, M., Nakatsugawa, M., Simões, F. R., Takebayashi, H., and Watanabe, Y.: The international river interface cooperative: Public domain flow and morphodynamics software for education and applications, *Adv. Water Res.*, 93, 62–74, <https://doi.org/10.1016/j.advwatres.2015.09.017>, 2016.
- Nicholas, A. P.: Modelling bedload yield braided gravel bed rivers, *Geomorphology*, 36, 89–106, [https://doi.org/10.1016/S0169-555X\(00\)00050-7](https://doi.org/10.1016/S0169-555X(00)00050-7), 2000.
- Paola, C.: Incoherent structure: turbulence as a metaphor for stream braiding, in: *Coherent flow structures in open channels*, edited by: Ashworth, P. J., Bennett, S. J., Best, J. L., and McLelland, S. J., Wiley, Chichester, UK, 705–723, ISBN: 978-0-471-95723-2, 1996.
- Paola, C. and Seal, R.: Grain size patchiness as a cause of selective deposition and downstream fining, *Water Resour. Res.*, 31, 1395–1407, 1995.
- Parker, G.: Surface-based bedload transport relation for gravel rivers, *J. Hydraul. Res.*, 28, 417–436, <https://doi.org/10.1080/00221689009499058>, 1990.
- Parker, G. and Klingeman, P. C.: On why gravel bed streams are paved, *Water Resour. Res.*, 18, 1409–1423, <https://doi.org/10.1029/WR018i005p01409>, 1982.
- Parker, G., Klingeman, P. C., and McLean, D. G.: Bedload and size distribution in paved gravel-bed streams, *J. Hydr. Eng. Div.*, 108, 544–571, 1982.
- Recking, A.: An analysis of nonlinearity effects on bed load transport prediction, *J. Geophys. Res.-Earth*, 118, 1264–1281, 2013a.
- Recking, A.: Simple Method for Calculating Reach-Averaged Bed-Load Transport Simple Method for Calculating Reach-Averaged Bed-Load Transport, *J. Hydraul. Eng.*, 139, 70–75, [https://doi.org/10.1061/\(ASCE\)HY.1943-7900.0000653](https://doi.org/10.1061/(ASCE)HY.1943-7900.0000653), 2013b.
- Recking, A., Piton, G., Vazquez-Tarrio, D., and Parker, G.: Quantifying the Morphological Print of Bedload Transport, *Earth Surf. Proc. Land.*, 41, 809–822, <https://doi.org/10.1002/esp.3869>, 2016.
- Wilcock, P. R.: Methods for estimating the critical shear stress of individual fractions in mixed-size sediment, *Water Resour. Res.*, 24, 1127–1135, 1988.
- Wilcock, P. R. and Crowe, J. C.: Surface-based Transport Model for Mixed-Size Sediment, *J. Hydraul. Eng.*, 129, 120–128, 2003.
- Wilcock, P. R. and McArdeell, B. W.: Surface-based fractional transport rates: partial transport and mobilization thresholds, *Water Resour. Res.*, 29, 1297–1312, 1993.
- Wolman, M. G. and Miller, J. P.: Magnitude and Frequency of Forces in Geomorphic Processes, *J. Geol.*, 68, 54–74, 1960.
- Wong, M. and Parker, G.: Reanalysis and Correction of Bed-Load Relation of Meyer-Peter and Müller Using Their Own Database, *J. Hydraul. Eng.*, 132, 1159–1168, [https://doi.org/10.1061/\(ASCE\)0733-9429\(2006\)132:11\(1159\)](https://doi.org/10.1061/(ASCE)0733-9429(2006)132:11(1159)), 2006.
- Yager, E. M., Venditti, J. G., Smith, H. J., and Schmeeckle, M. W.: The trouble with shear stress, *Geomorphology*, 323, 41–50, <https://doi.org/10.1016/j.geomorph.2018.09.008>, 2018.